AD-758 173

Advanced Engine Control Program

Chandler Evans, Inc.

prepared for

Army Air Mobility Research and
Development Laboratory
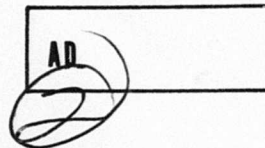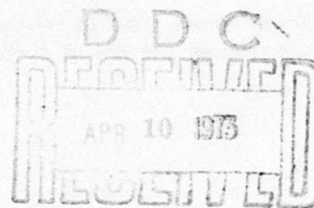
NOVEMBER 1972

USAAMRDL TECHNICAL REPORT 72-59

ADVANCED ENGINE CONTROL PROGRAM

By

A. H. White
D. F. Wills

November 1972

EUSTIS DIRECTORATE
U. S. ARMY AIR MOBILITY RESEARCH AND DEVELOPMENT LABORATORY
FORT EUSTIS, VIRGINIA

U S ARMY
MATERIEL COMMAND

DISCLAIMERS

The findings in this report are not to be construed as an official Department of the Army position unless so designated by other authorized documents.

When Government drawings, specifications, or other data are used for any purpose other than in connection with a definitely related Government procurement operation, the United States Government thereby incurs no responsibility nor any obligation whatsoever; and the fact that the Government may have formulated, furnished, or in any way supplied the said drawings, specifications, or other data is not to be regarded by implication or otherwise as in any manner licensing the holder or any other person or corporation, or conveying any rights or permission, to manufacture, use, or sell any patented invention that may in any way be related thereto.

Trade names cited in this report do not constitute an official endorsement or approval of the use of such commercial hardware or software.

DISPOSITION INSTRUCTIONS

Destroy this report when no longer needed. Do not return it to the originator.

ACCESSION for		
NTIS	White Section	☑
DDC	Buff Section	☐
UNANNOUNCED		☐
JUSTIFICATION		
BY		
DISTRIBUTION/AVAILABILITY CODES		
Dist.	AVAIL. and/or Special	
A		

DOCUMENT CONTROL DATA - R & D

(Security classification of title, body of abstract and indexing annotation must be entered when the overall report is classified)

1. ORIGINATING ACTIVITY (Corporate author)	2a. REPORT SECURITY CLASSIFICATION
Colt Industries Inc. Chandler Evans Inc. Control Systems Division West Hartford, Connecticut	Unclassified
	2b. GROUP

3. REPORT TITLE

ADVANCED ENGINE CONTROL PROGRAM

4. DESCRIPTIVE NOTES *(Type of report and inclusive dates)*

Final Report

5. AUTHOR(S) *(First name, middle initial, last name)*

A. H. White
D. F. Wills

6. REPORT DATE	7a. TOTAL NO. OF PAGES	7b. NO. OF REFS
November 1972	301 303	27

8a. CONTRACT OR GRANT NO.	9a. ORIGINATOR'S REPORT NUMBER(S)
DAAJ02-70-C-0002	
b. PROJECT NO.	USAAMRDL Technical Report 72-59
c. Task 1G162203D14416	9b. OTHER REPORT NO(S) (Any other numbers that may be assigned this report)
d.	Chandler Evans Report R-492-31

10. DISTRIBUTION STATEMENT

Approved for public release; distribution unlimited.

11. SUPPLEMENTARY NOTES	12. SPONSORING MILITARY ACTIVITY
Details of illustrations in this document may be better studied on microfiche	Eustis Directorate U.S. Army Air Mobility R&D Laboratory Fort Eustis, Virginia

13. ABSTRACT

This report summarizes the results of a 30-month program of design, fabrication, and test of an advanced electronic engine control system for small (2-to 5-lb-per-second airflow) turboshaft engines. The objective of the program was to develop engine control system technology which could be implemented in future systems to alleviate many of the problems experienced with past and present control systems.

The control system selected for development is based on the results of design trade-off studies, user surveys, and component testing. The system incorporates closed-loop control of turbine blade temperature as sensed by a radiation pyrometer for blade protection, W_F/P_{t3} scheduling for starting, acceleration and deceleration, isochronous power turbine and proportional gas producer governing, torque limiting, load sharing, start sequencing control, and compressor geometry control.

The system is comprised of three modules: a fuel-cooled hybrid electronic computer, a fluid controller with integral 37,500-rpm pump, and a remote electrohydromechanical engine geometry actuator. The system also includes the necessary engine parameter sensors. During the program, provisions for developing a regulated alternator were added to the original scope of work.

Closed-loop tests successfully demonstrated the control system performance on both a 2- and a 5-lb/sec analog computer engine simulator. Environmental temperature endurance testing and fuel contamination testing were successfully completed.

It was determined that additional redesign and development in the electronic computer and fuel pump portions of the system could result in significant improvements in reliability and efficiency. In addition, recently developed micropower electronic components offer low sensitivity to noise and voltage variations, and negligible self-heating. Although these new components were not evaluated under this program, their incorporation should improve the electronic computer design.

14. KEY WORDS	LINK A		LINK B		LINK C	
	ROLE	WT	ROLE	WT	ROLE	WT
Electronic Engine Control Design, Fabrication, Test Turboshaft Engine Fuel-Cooled Hybrid Electronic Computer Fuel Pump Alternator						

ic

Task 1G162203D14416
Contract DAAJ02-70-C-0002
USAAMRDL Technical Report 72-59
November 1972

ADVANCED ENGINE CONTROL PROGRAM

Final Report

Chandler Evans Report R-492-31

By

A. H. White
D. F. Wills

Prepared by

Colt Industries Inc.
Chandler Evans Inc. Control Systems Division
West Hartford, Connecticut

for

EUSTIS DIRECTORATE
U. S. ARMY AIR MOBILITY RESEARCH AND DEVELOPMENT LABORATORY
FORT EUSTIS, VIRGINIA

ABSTRACT

This report summarizes the results of a 30-month program of
design, fabrication, and test of an advanced electronic engine
control system for small (2-to 5-lb-per-second airflow) turbo-
shaft engines. The objective of the program was to develop
engine control system technology which could be implemented in
future systems to alleviate many of the problems experienced
with past and present control systems.

The control system selected for development is based on the
results of design trade-off studies, user surveys, and compo-
nent testing. The system incorporates closed-loop control of
turbine blade temperature as sensed by a radiation pyrometer
for blade protection, W_F/P_{t3} scheduling for starting, acceler-
ation and deceleration, isochronous power turbine and propor-
tional gas producer governing, torque limiting, load sharing,
start sequencing control, and compressor geometry control.

The system is comprised of three modules: a fuel-cooled hy-
brid electronic computer, a fluid controller with integral
37,500-rpm pump, and a remote electrohydromechanical engine
geometry actuator. The system also includes the necessary en-
gine parameter sensors. During the program, provisions for
developing a regulated alternator were added to the original
scope of work.

Closed-loop tests successfully demonstrated the control system
performance on both a 2- and a 5-lb/sec analog computer engine
simulator. Environmental temperature endurance testing and
fuel contamination testing were successfully completed.

It was determined that additional redesign and development in
the electronic computer and fuel pump portions of the system
could result in significant improvements in reliability and
efficiency. In addition, recently developed micropower elec-
tronic components offer low sensitivity to noise and voltage
variations, and negligible self-heating. Although these new
components were not evaluated under this program, their incor-
poration should improve the electronic computer design.

iii

FOREWORD

This is the final report covering work completed under Contract DAAJ02-70-C-0002 (Task 1G162203D14416). The program was conducted under the direction of Mr. Roger Furgurson, Eustis Directorate, U. S. Army Air Mobility Research and Development Laboratory, Fort Eustis, Virginia. The program work was conducted by Colt Industries Inc., Chandler Evans Inc. Control System Division under the cognizance of J. O. Nash, Vice President of Engineering and D. F. Wills, Program Manager. Acknowledgment is given to all the Chandler Evans personnel working on the program and all of the engine, airframe and sensor manufacturers who have contributed to the program.

v

Preceding page blank

TABLE OF CONTENTS

Preceding page blank

LIST OF ILLUSTRATIONS

LIST OF ILLUSTRATIONS (Cont)

LIST OF ILLUSTRATIONS (Cont)

LIST OF ILLUSTRATIONS (Cont)

LIST OF ILLUSTRATIONS (Cont)

LIST OF ILLUSTRATIONS (Cont)

LIST OF ILLUSTRATIONS (Cont)

LIST OF ILLUSTRATIONS (Cont)

LIST OF TABLES

LIST OF TABLES (Cont)

LIST OF SYMBOLS

a   turbine blade leading-edge inner radius

A_4 gas generator turbine area, ft^2

A/D   analog-to-digital

A_n power turbine stator area

b   turbine blade leading-edge outer radius

B_1 load damping coefficient, ft-lb/rad/sec

B_{pr} burner pressure ratio

B_{ft} free turbine damping coefficient, ft-lb/rad/sec

c   specific heat of turbine blade material

c_p specific heat at constant pressure, Btu-lb/°F

c_v specific heat at constant volume, Btu-lb/°F

d   impingement coolant hole diameter

3D   three dimensional

DCPW   direct current to pulse width

EMI   electromagnetic interference

FA   fuel-air ratio

FET   field effect transistor

FMEA   failure mode and effect analysis

FS   full scale

g   gravitational acceleration, 32.2 ft/sec^2

h	film coefficient, Btu/hr ft^2°F
ha	film coefficient on the cooling side
hg	film coefficient on the hot gas side
HP_{ft}	free turbine horsepower
IGV	inlet guide vane
J	mechanical equivalent of heat, 778 ft-lb/Btu
J_g	gas generator turbine inertia, slug-ft^2
J_l	load inertia, slug-ft^2
J_{ft}	free turbine rotor inertia, slug-ft^2
k	thermal conductivity of turbine blade material
K	flow coefficient, $\sqrt{°R}$/sec
Ke	engine gain, rpm/pph
K_1	turbine load gain, rad/sec/ft-lb
K_s	drive system spring rate, ft-lb/rad
ℓ	characteristic of the turbine blade dimension, ft
L	characteristic length, ft
LSI	large-scale integrated circuits
MMV	main metering valve
MSI	medium-scale integrated circuits
N_{ft}	free turbine speed, rpm

N_{ftr} free turbine reference speed, rpm

N_g gas generator speed, rpm

N_{gr} gas generator reference speed, rpm

N_u Nusselt number

P pressure, psia

P_{amb} ambient pressure, psia

P_A geometry actuator supply pressure, psia

P_B centrifugal pump outlet pressure, psia

P_E control outlet pressure, psia

P_f gear pump outlet pressure, psia

P_g gas generator power, ft-lb/sec

P_i control fuel inlet pressure, psia

P_L pump changeover valve pressure, psia

PLA   power lever angle, deg

P_m fuel metering valve upstream pressure, psia

P_n fuel metering valve downstream pressure, psia

pph   pounds per hour

pps   pounds per second

P_s bearing wash flow pressure, psia

P_{t2} compressor inlet total pressure, psia

LIST OF SYMBOLS (Cont)

P_{t3} compressor discharge total pressure, psia

P_{t4} turbine inlet total pressure, psia

P_{t5} turbine exit total pressure, psia

P_x inducer outlet pressure, psia

Q_g gas torque, ft-lb

Q_{so} output shaft torque other engine, ft-lb

Q_{st} output shaft torque this engine, ft-lb

R_e Reynolds number

ROM   read only memory

RFI   radio frequency interference

T   temperature, °R

t   time, sec

T_a turbine blade inner surface temperature, °R

T_c coolant temperature, °R

T_m average turbine blade temperature, °R

T_{t2} compressor inlet total temperature, °R

T_{t3} compressor discharge total temperature, °R

T_{t4} turbine inlet total gas temperature, °R

T_{4B} turbine blade temperature, °R

T_{4Br} turbine blade reference temperature, °R

LIST OF SYMBOLS (Cont)

V	voltage
V_g	gas velocity, ft/sec
VCO	voltage-controlled oscillator
W	impingement coolant mass flow rate/hole
W_a	airflow, pps
W_f	fuel flow, pph
W_g	gas flow = $W_a + W_f$, pps
W_1	load natural frequency, rad/sec
W_{ft}	free turbine natural frequency, rad/sec
α	thermal diffusivity of turbine blade
β	collective pitch, deg
γ	ratio of specific heats, $\frac{Cp}{Cv}$
Δ_T	increment of temperature, °F, °R
δ	relative absolute pressure $\frac{p \text{ (in. Hg)}}{29.92 \text{ in. Hg}}$
Φ	phase angle, deg
ζ_1	load damping, ratio, rad
ζ_{ft}	free turbine damping ratio, rad
λ_n	Nth eigenvalue
η	efficiency
θ	temperature correction, $\frac{T_{t2}}{519°R}$

LIST OF SYMBOLS (Cont)

θ_L load angular displacement, rad

θ_{ft} free-turbine angular displacement, rad

θ_v inlet guide vane angular displacement, deg

μ absolute viscosity, pps/ft^2

ρ density, lb/ft^3

τ time constant, sec

INTRODUCTION

Control systems for gas turbine engines are normally developed in parallel with the development of the engine. The peculiarities of each gas turbine engine and the inherent inflexibility of conventional hydromechanical controls often result in costly control system development programs. Generally, these development programs yield clever solutions, b᷑ applicable only to the problems on the particular engine being developed.

Furthermore, significant advancement has been made in gas turbine engine technology during the past decade. This technology has provided substancial reduction in the weight, size, and frontal area of the engine. Moreover, further reductions are possible if accessory gearboxes can be eliminated and if more of the engine accessory functions can be integrated within the engine control system. It is necessary, therefore, to develop a control system technology which offers flexibility for wide application potential and which incorporates control features and engine accessory functions which reduce requirements for accessory gearboxes.

In view of the recent advances that have been made in electronic sensors and computing devices, it appears reasonable that a flexible control using electronic technology can be developed for gas turbine engines. Electronic control eliminates the need for a gearbox other than for the pump drive. With a high-speed pump capable of being mounted on the engine shaft, this gearbox could also be eliminated. Other potential advantages of using electronic control are high accuracy, reduction in vulnerability, less sensitivity to fuel contamination, and smaller size and weight.

Based on current technological forecasts, the unit cost of electronic controls will be less than their hydromechanical control counterpart within the production time frame considered in this program. The total life cycle cost of an engine and control system with an electronic control can also be improved considerably. Simple diagnostic and maintenance procedures can be implemented because the engine and control variables are available to provide continuous or sampled information on the state of the engine and control. Modular construction of the control will allow simpler maintenance procedures for identification and repair of control problems.

The objective of this 30-month Advanced Technology Engine
(ATEC) Development Program was to develop the technology which
would allow incorporation of the improvements referred to
above for free turbine engines in the 2- to 5-lb/sec airflow
class beginning their formal development cycle in 1975.

Breadboard and prototype hardware for a complete system was
fabricated and tested. The system developed includes a fluid
controller module, an electronic computer module, and an IGV
actuator module.

The fluid controller module schedules fuel flow in proportion
to an electric signal from the computer. The fluid controller
incorporates an electric stepper motor-positioned metering
valve with feedback resolver, a throttling pressure regulator,
an integrated 37,500-rpm pump, and a backup manual fuel
metering controller.

The electrohydromechanical IGV actuator incorporates an elec-
tric stepper motor-controlled hydraulic servovalve, a feed-
back resolver, and integral mechanical backup control. The
backup control schedules actuator position as a function of a
speed pressure signal from the centrifugal pump. This pro-
vides coarse automatic IGV control in the event of an elec-
tronic failure.

The electronic computer module provides all of the computa-
tional and logic functions. Two prototype electronic packages
with built-in fuel cooling plate were fabricated for compre-
hensive environmental testing, and two complete breadboard
systems were made for use in developing circuit designs and
for closed-loop system testing. A radiation pyrometer was
fabricated and tested, and all the other required sensors
were selected and test evaluated.

In January 1971, the program was modified to include the dem-
onstration and evaluation of a regulated alternator as part of
the ATEC. A demonstration unit was designed, fabricated, and
tested. A design study showed that packaging the alternator
in the fluid controller was the best mounting location. How-
ever, it was not possible to integrate the alternate hardware
with the control package as a part of the current program.

2

The ATEC system will complement the technology advances being made in the 2- to 5-lb/sec airflow class of engines. It was desired to maximize the advancement in the state of the art of the engine control system and its component parts in the following areas:

1. Increased flexibility and interchangeability of components for turboshaft engines in the 2- to 5-lb/sec class.

2. Elimination of the requirements for mechanical drive input to the control or provide capability for driving control and associated components at 50% of engine speed.

3. Improved vulnerability resistance features.

4. Decreased contamination sensitivity.

5. Increased ability to accommodate various grades of fuel without adjustment.

6. More efficient packaging, allowing integration with an advanced lightweight accessory package.

7. Increased system reliability and decreased frequency of maintenance.

8. Advanced maintainability features, including quick installation and removal.

9. Provisions for engine analyzer inputs using inherent features of the control.

10. Lower unit cost potential.

11. Design life of 5,000 hours or more.

12. Minimum size and weight.

DISCUSSION

The original program to develop and evaluate the components
and system concepts was divided into the following six areas
of effort:

1. System
2. Geometry Actuator
3. Fluid Controller
4. Simulation and Control Mode
5. Sensors
6. Electronic Computer

The overall 30-month program was broken into three phases:

Phase I   - Design - 14 months
Phase II - Fabrication - 7 months
Phase III - Test - 9 months

Figures 1 and 2 are program task charts which describe the
tasks under each of the six work areas for each phase of the
program. Figure 3 summarizes the activity and time used for
each work area and also indicates the program milestones.
This shows that the program overran by two months, which was
caused by a delay during the system test phase due to problems
with the pump drive gearbox.

The addition of the regulated alternator to the program added
a seventh area of effort. The work tasks and time spent on
this effort is shown in Figure 4.

The development and accomplishments in the seven areas of
effort are discussed in the following section.
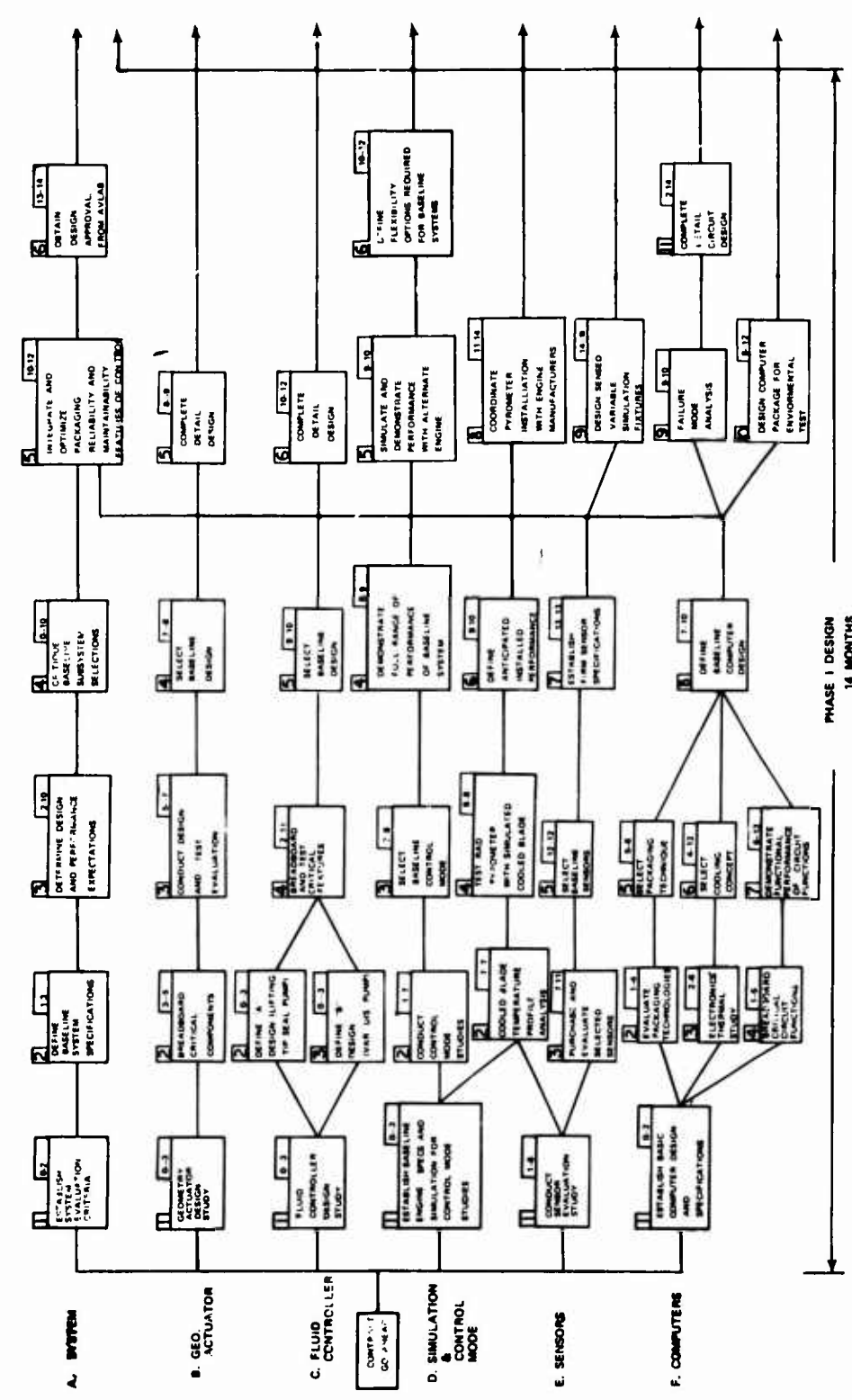
Figure 1. Program Task Chart (Phase I).

5
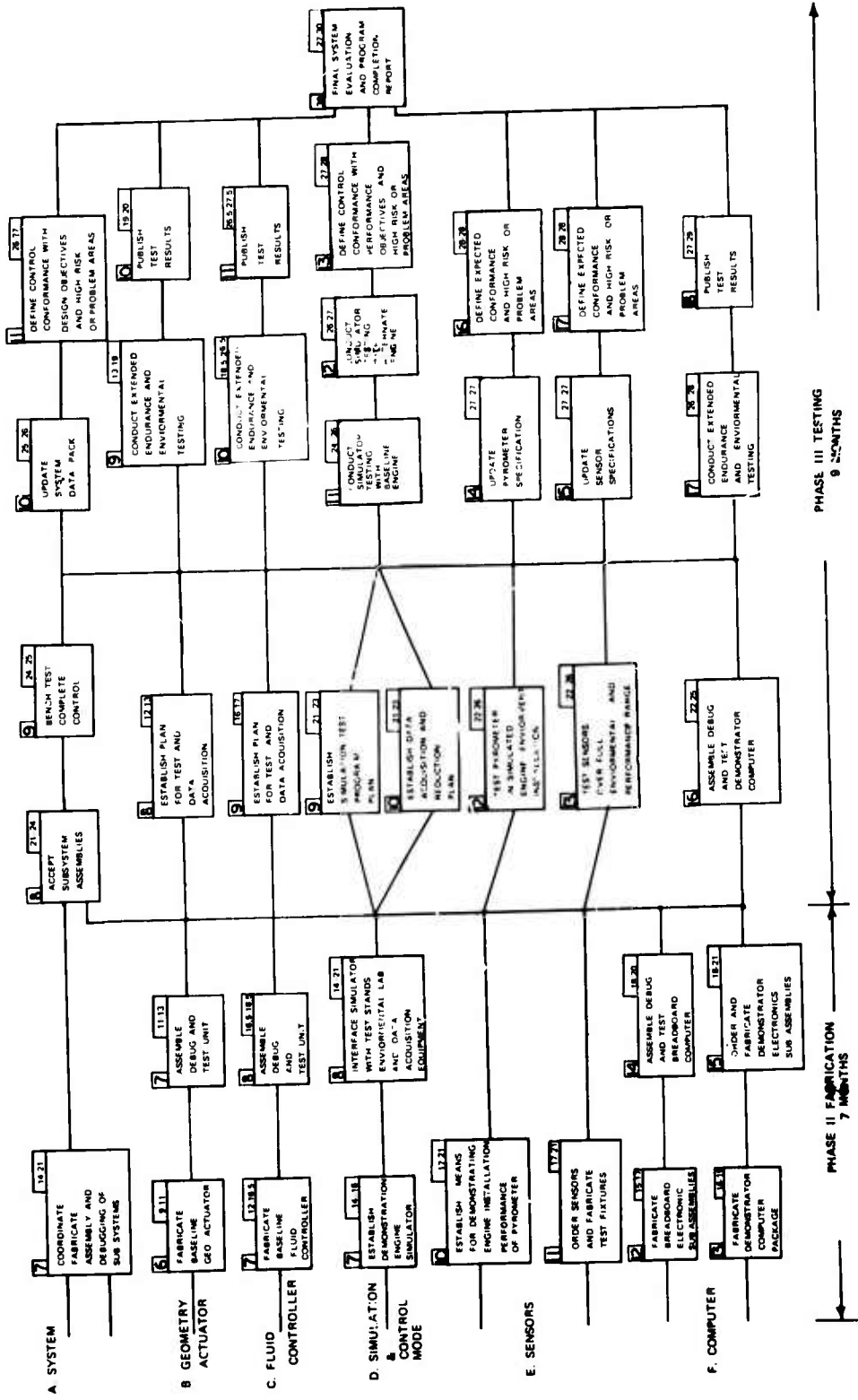
Figure 2. Program Task Chart (Phases II and III).

6
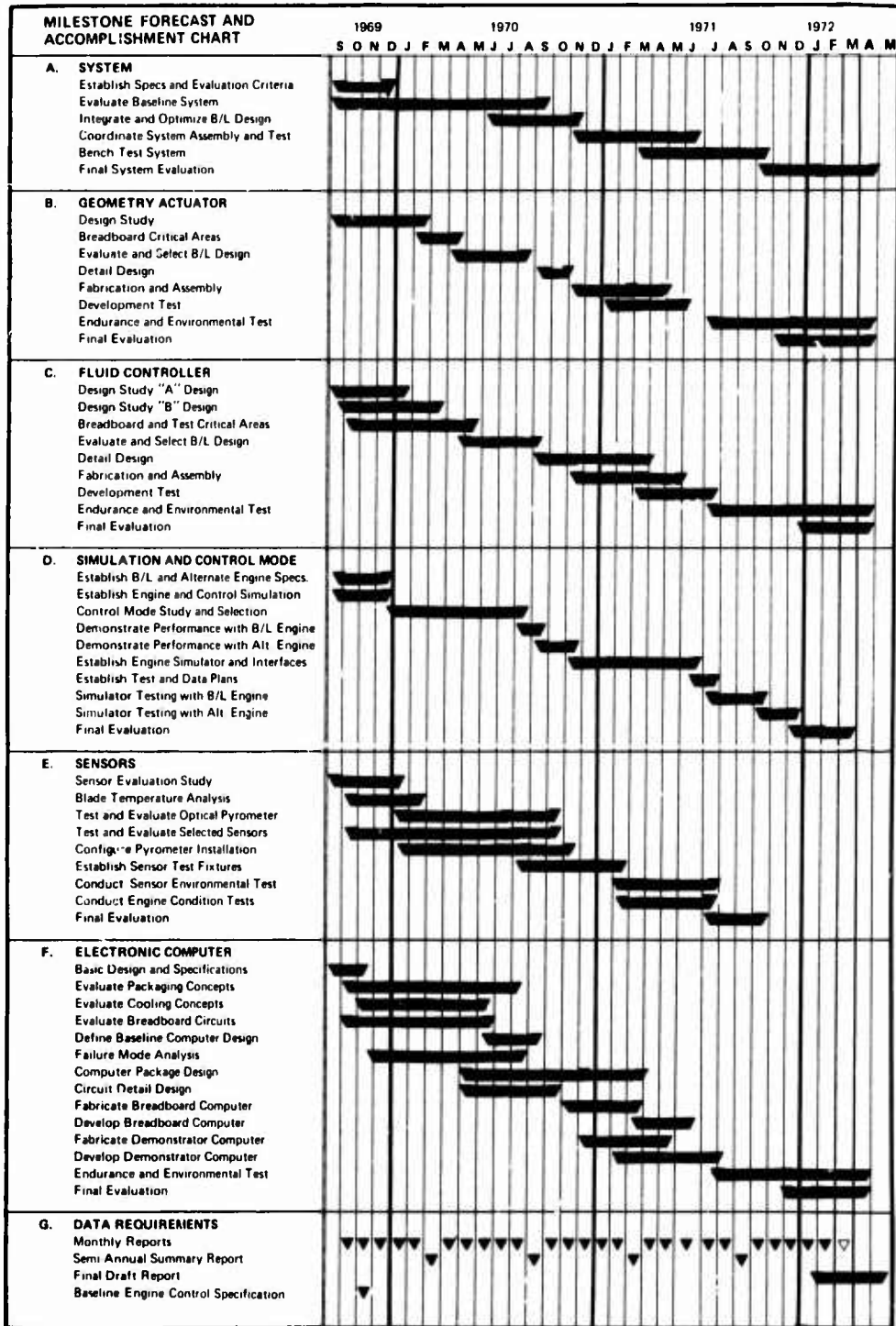
Figure 3. Program Schedule and Milestone Chart.
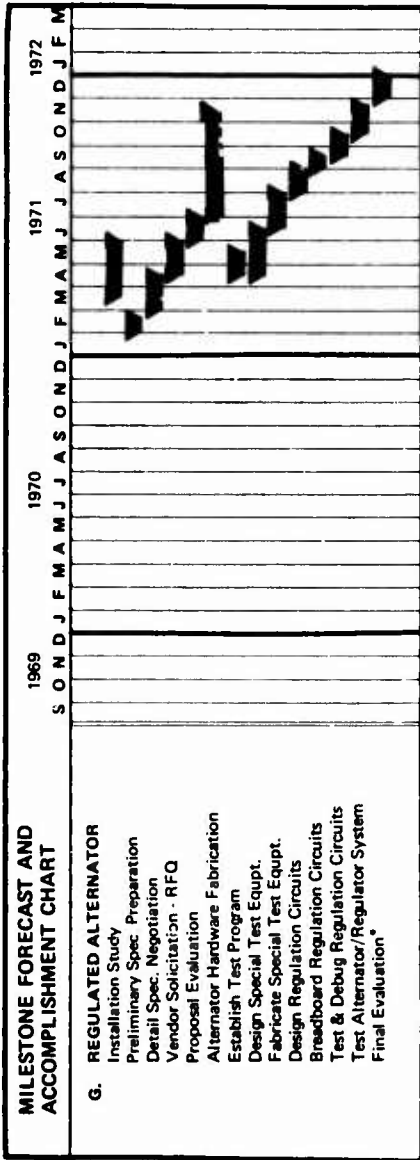
Figure 4. Alternator Program Schedule.

8

SYSTEM

The control system design goals, performance specifications, and requirements for the final design evaluation evolved from previous control system specifications, detailed discussions with USAAMRDL, and surveys of cognizant engine, airframe and Army personnel. These surveys helped to resolve questions on specific areas of the specifications which required more definition and/or expert judgment. The control system requirements were specified for an advanced free turbine engine in the 2- to 5-lb/sec airflow class for a twin-engine helicopter. This application was judged to impose the most demanding control system requirements for a free turbine engine installation.

Design Goals & Achievements

The design goals established for this program are tabulated in Table I and were directed toward:

1. Eliminating those problem areas and shortcomings experienced with current hydromechanical controls.

2. Developing the new sensors and technologies required for control of small advanced free turbine engines.

3. Having the advanced control technology ready for engine development commencing in 1975.

It is impossible to fully assess the achievements made toward all these goals because some of them can be determined only after years of operating experience. However, significant progress was made, and Table I includes a summary of what are felt to be salient achievements made toward the goals established for each item.

System Design Specification

During the design phase of the program, a detailed control system specification was prepared covering performance, design, and environmental requirements. This was updated periodically based on the results of our control mode studies and information garnered from the surveys. The actual flow schedules, gains, and dynamic requirements were established from

9

TABLE I. DESIGN GOALS AND ACHIEVEMENTS

ITEM	GOAL	COMMENTS	ACHIEVEMENTS
Flexibility/ Interchangeability	Demonstrate control of a base and an alternate engine with the same control system.	The Engine Control System Specification will define a 5#/sec base engine, a 2#/sec alternate engine. Substantial differences in engine schedules and dynamics will be specified.	Closed-loop performance was demonstrated on both engines with the same breadboard control hardware. An electrically programmable 3-D cam was demonstrated.
Eliminate Requirement for Mechanical Drive.	Pumps to operate at 50% engine speed. No other mechanical drives required.	Engine Speeds: Base 55,000 rpm. Alternate 75,000 rpm.	A 37,500-rpm fuel pumping system was successfully run on contaminated fuel. A 37,500-rpm alternator with self-regulating capabilities was demonstrated.
Decrease Vulnerability	Minimize area exposed and the effect of battle damage on the engine and control system. Decrease probability of fire, overspeed or burn up for single hit.	Vulnerability $V = A_S P$ A_S = exposed area $P_{K/N}$ = probability of A/C kill/hit	Control is 50% smaller than current controls and the pressurized fuel area is substantially reduced. High-speed capability results in smaller gearbox.
Fuel Contamination	Fuel pump and metering system to qualify per paragraph 3.4.1.3 of MIL-E-5007C.	Centrifugal pump, metering valve design and electronic computation reduce control sensitivity to dirt.	Improved contamination resistance due to use of centrifugal pump and electronic computer.
Accommodate Various Grades of Fuel.	Control system to operate without requiring fuel density or fuel type adjustments.	Requires closed-loop control on fuel flow or gas temperature.	Turbine blade temperature limiter is insensitive to fuel heating value.
Efficient Integration with Other Accessories	Provide within the control system, fuel pressurization, automatic start sequencing, electrical power supply, and engine sensed signals for diagnostics and pilot display.	Control package includes all engine control and accessory functions of engine except for providing starting power, lubrication and torque sensing.	Pump and alternator are integral with fuel controller. Start sequencing is included in electronic computer. Electrically sensed signals are available for pilot display.
Increase Reliability	MTBF = 20,000 hr	Present hydromechanical controls have MTBF = 15,000 hr. MTBF and TBO goals are applicable to assemblies which are replaceable at the operations level.	An efficient electronic cooling scheme using a fuel cooled dielectric fluid demonstrated that the densely packaged electronics can survive the engine-mounted temperature environment. Turbine blade temperature limiting and redundant power turbine overspeed protection is provided.
Advanced Maintainability Features Including Quick Installation and Removal	TBO = 2,500 hr Installation and adjustments to be minimized and require the use of only one common hand tool at a time.	Modular construction of control will simplify diagnosing problems and effecting repairs.	Control is comprised of three modules which are changeable at the operations level without need for adjustment. Electronics isochronous power turbine governor eliminates need for collective pitch coordination and therefore simplifies rigging.
Provision for Engine Analyzer Input	Electrical signal of all sensed engine states, which are required for input to an engine analyzer, will be made available.	Readily available from electronic computer.	The goal has been satisfied.
Lower Unit Cost	Cost not to exceed 15% of total engine cost.	Cost based on total production of 10,000 units at 100/month.	Forecasts on electronics production costs indicate that by 1975 electronic controls will cost less than hydromechanical controls.
Design Life	Potential of 5,000 hr or more.	This life potential is based on all parts having a wear life greater than 5,000 hr.	Electronic computer reduces the number of components that wear.
Size and Weight	Total system dry weight not to exceed 14.3 lb Weight Allocation: Pump & Fuel Metering 4.6 lb Computer Package 3.5 lb Actuator .8 lb Sensors 1.9 lb Alternator 3.5 lb Total System Volume not to exceed 155 cu. in.	Revised to include alternator. Weight of sensors does not include torque sensor. Geometry actuator specification revised, making weight of 0.8 lb unrealistic.	The total system weight and size goal can be met.

control mode studies on a 2-lb/sec and 5-lb/sec engine and in appropriate size helicopter rotor system. A summary of the baseline control system specification is given in Table II.

System Description

An overview of the engine/control system is shown in Figure 5. This figure describes the engine configuration, control inputs and sensed parameters, and the interconnections within the control components and the engine. Figure 6 shows a system component diagram which describes the various sensors, control components, input/output signals, and all of the interfaces.

As indicated by Figure 6, the electronic control system is engine mounted, fuel cooled, and self powered. The control system has an integrated fuel pump, a remote inlet guide vane actuator, and a redundant power turbine overspeed governor; it also provides for manual control of fuel metering.

The torque sensors are not included in the hardware development program because they are inherently an integral part of the engine. For purposes of demonstrating the performance of the control, a frequency signal proportional to torque was generated. Also, only one geometry actuator (IGV) was developed, whereas most advanced engines will require an interstage bleed valve and IGV actuator. It was decided that developing one actuator was sufficient to demonstrate the technology.

A functional description of the control system is shown in Figure 7.

Control System Envelope

Two separate packaging design studies were made, one with an integrated alternator and one without. The two configurations are shown in Figures 8 and 9. Figure 9 shows the design with the alternator.

The addition of the alternator is reflected in the size of the fuel controller package. The packaging study showed that a net savings of between 0.5 and 1.0 lb results from integrating the alternator as opposed to it being in a separate package. This savings did not include the weight of mounting and driving the alternator as a separate package. The alternator increases the control weight by about 2.5 lb.

11

TABLE II. BASELINE CONTROL SPECIFICATION SUMMARY
(TWIN-ENGINE HELICOPTER APPLICATION)

Turbine Blade Temperature Limiting*	±30°F
W_F/P_{t3} Start, Acceleration & Deceleration	±2pph, ±4%, ±7.5%
Isochronous Power Turbine Governing	±.25%
Proportional Gas Producer Governing	±1%
Semiautomatic Start**	$W_F = f$ (PLA)
Twin-Engine Load Sharing	±5% Torque
Torque Limiting*	115% ±5%
Engine Malfunction Protection (Twin Installation)	Pilot Indication
Variable Compressor Geometry Scheduling $f(N\sqrt{\theta})$	±1.5%
Load Anticipation	Collective Pitch
Proportional Power Turbine Overspeed Protection	.05 Sec Response
Manual Emergency System	Pilot Actuated
Ground & Flight Idle and Military Speed Set	Independently Adjustable
Fuel Inlet Temperature	-65° to 135°F
Ambient Temperature	-65° to 250°F
Vibration and Fuel Contamination	MIL-E-5007C

*Pilot can reset to higher limits for emergency PLA setting.

**Pilot initiates fuel flow on moving PLA to ground idle setting.
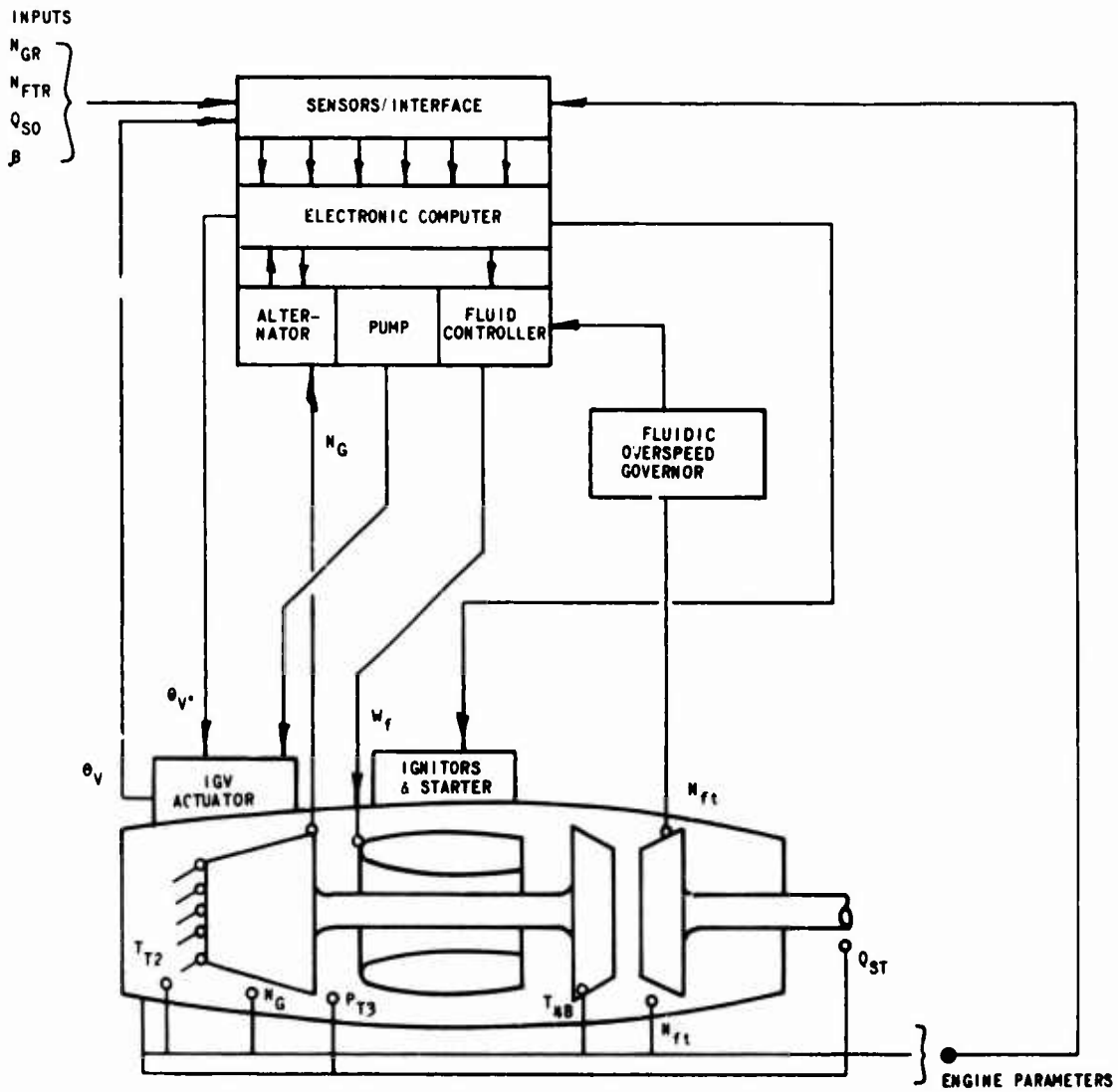
Figure 5. Engine Control System.

13
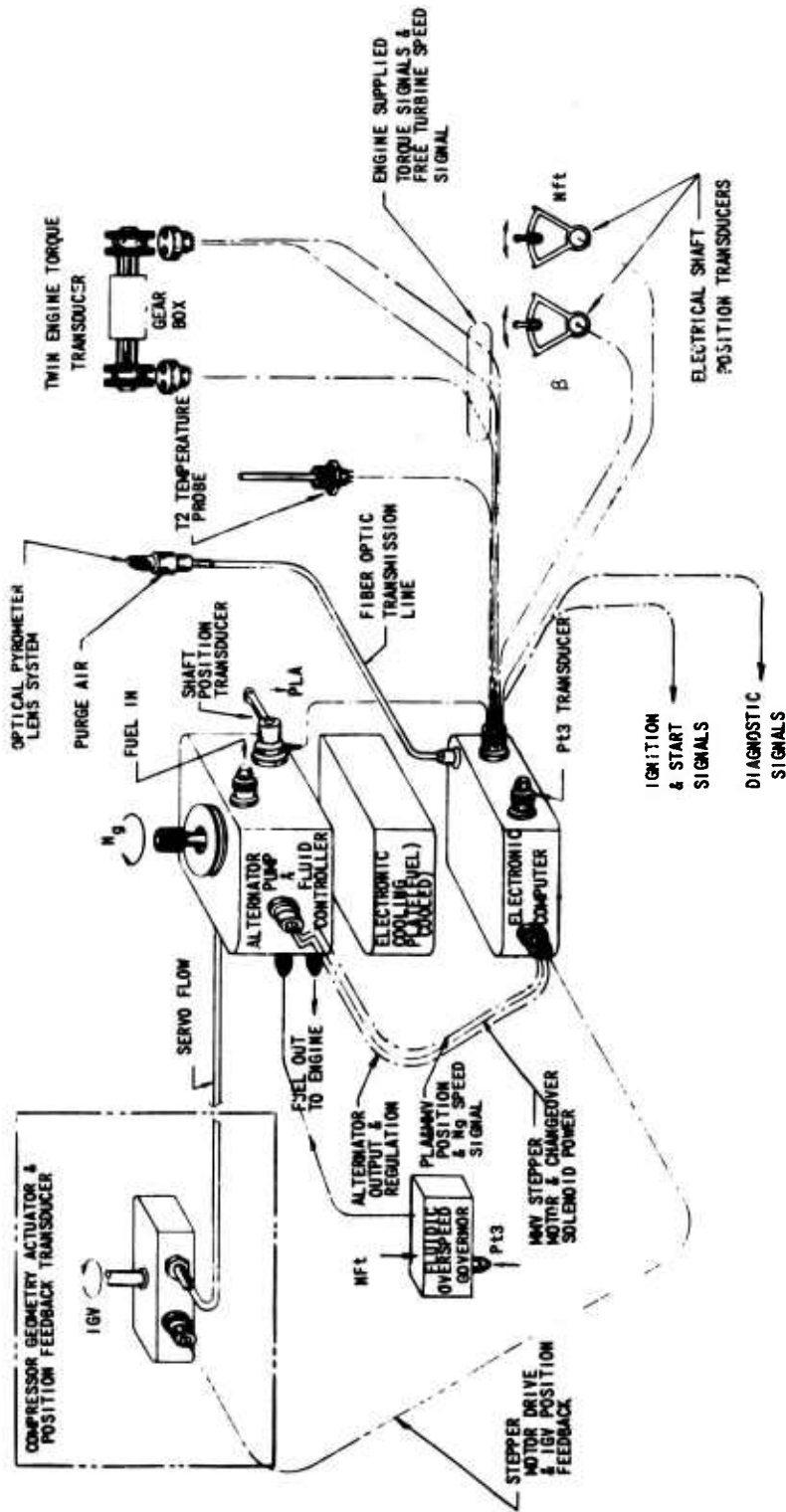
Figure 6.   System Component Diagram.
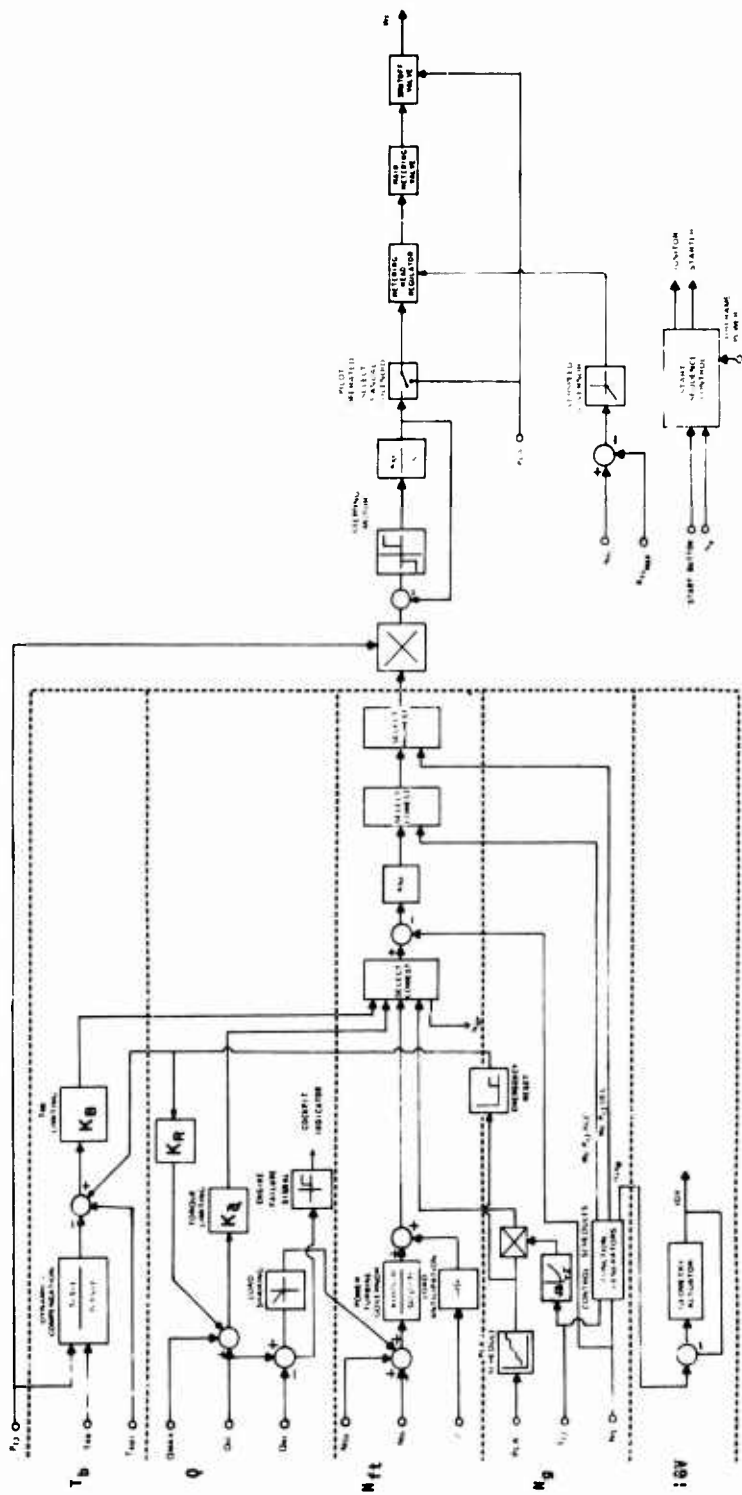
Figure 7. Functional Block Diagram.

15
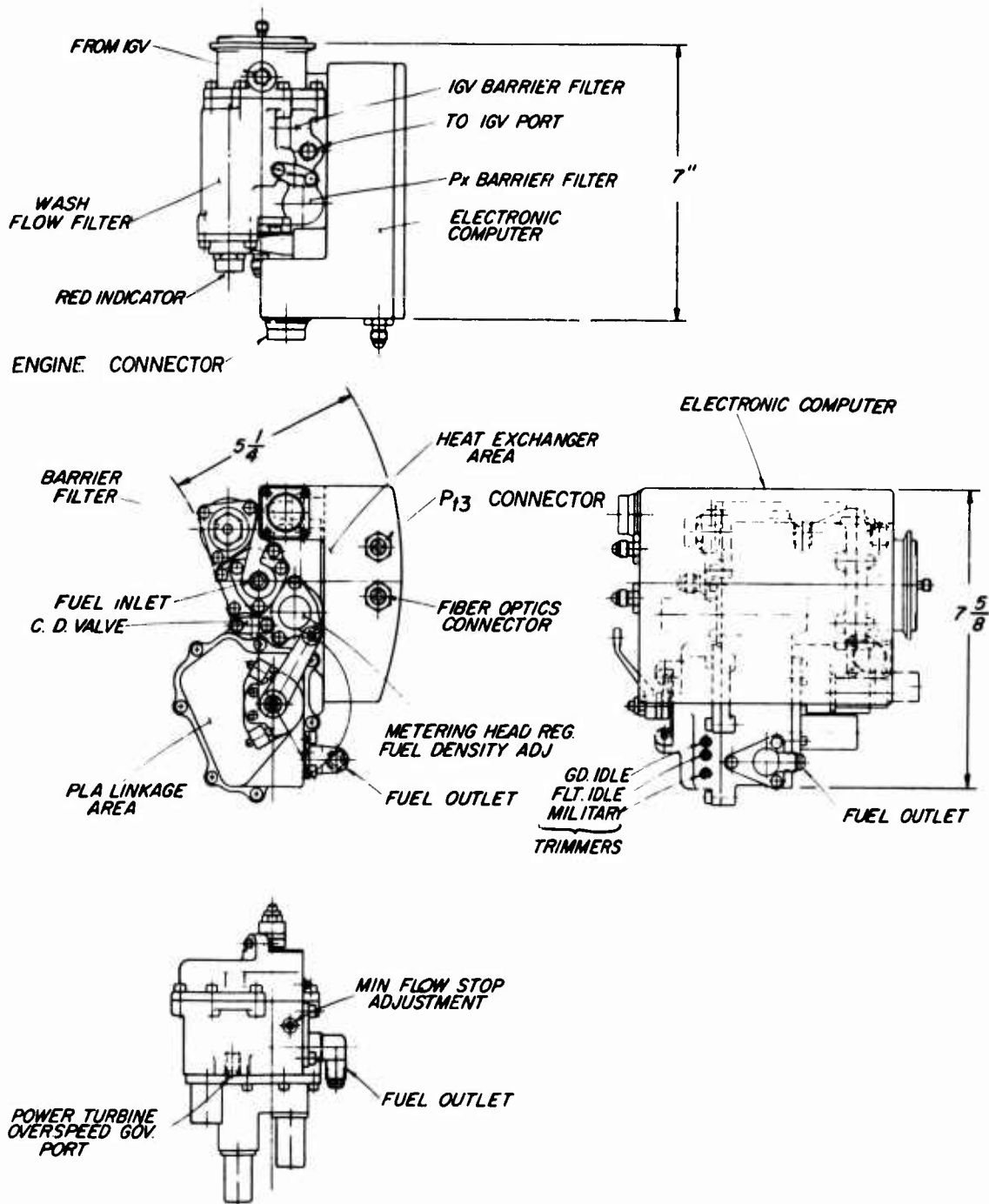
Figure 8. Installation Package Without Alternator.

16
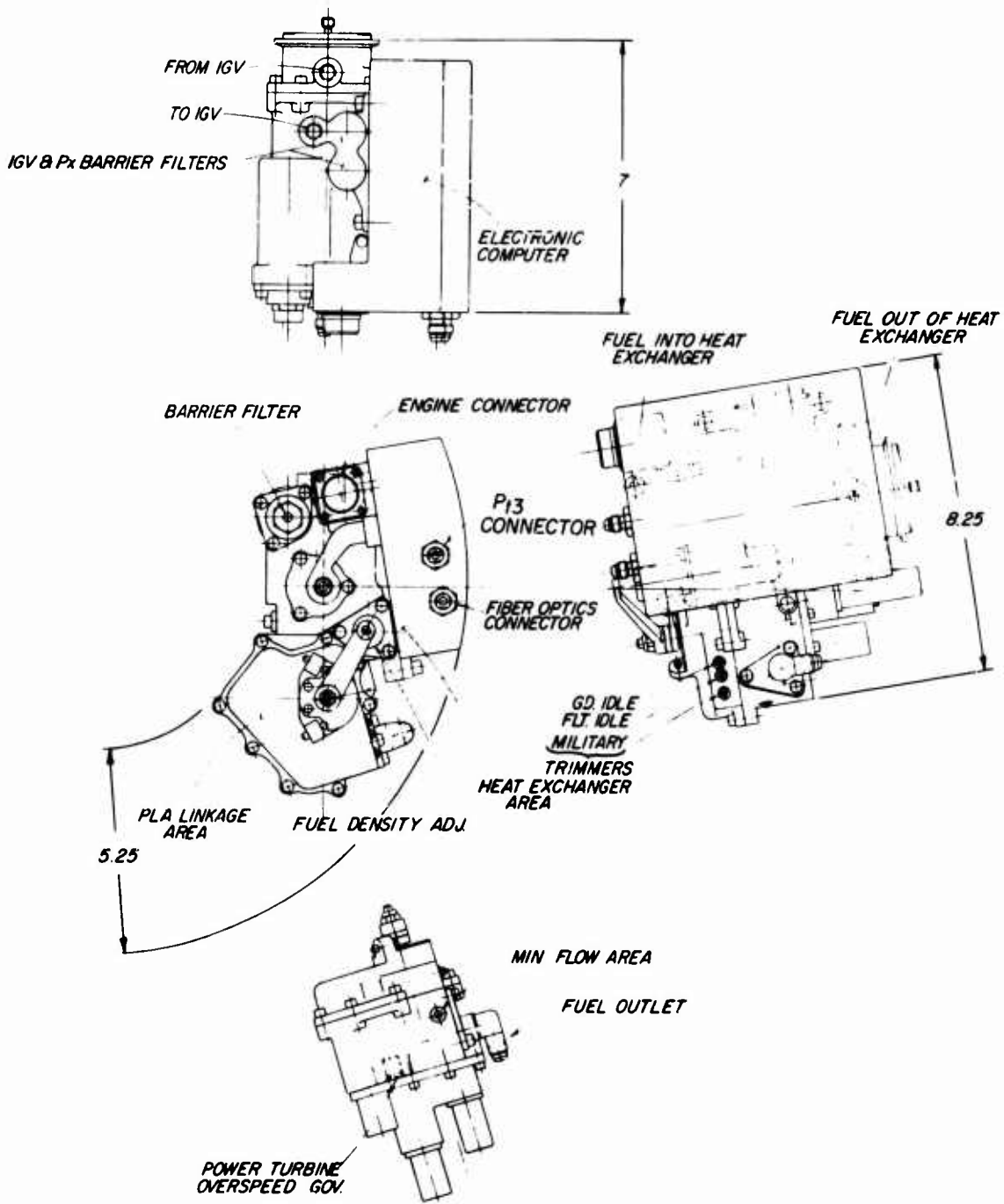
Figure 9. Installation Package With Alternator.

Control System Features

A mock-up showing the three field replaceable modules of the control system is shown in Figure 10. The fluid controller, electronic computer and geometry actuator are completely interchangeable, and no calibration is required for replacement of one unit. The combined weight of the three modules is 12.5 lb without the alternator and 15 lb with the alternator. The main features of each control module are outlined below.

Fuel Controller Module

Fuel Pump, Fuel Metering and Fuel Shutoff
Manual Fuel Flow Control
Alternator for Control and Ignition Power

Electronic Computer Module

Hybrid Electronic Computer
Turbine Blade Temperature Sensor
P_{t3} Sensor
Cooling Plate (Fuel Cooled)

Geometry Actuator Module

Electrohydromechanical Actuator
Backup Control During Manual Operation

Special Features

System Weight	15 lb
Pump/Alternator Drive Speed	37,500 rpm
Operates on Contaminated Fuel	MIL-E-5007C Dirt
Electronically Programmable 3-D Cam	
Closed-Loop Turbine Blade Temperature Limiter	

System Error Analyses

There are many potential error sources within a relatively complex system. In general, system error is caused by dynamic lags, disturbances, manufacturing tolerances, wear, and variation due to environmental changes, etc. Although error

18

ELECTRONIC COMPUTER

PCD

TB
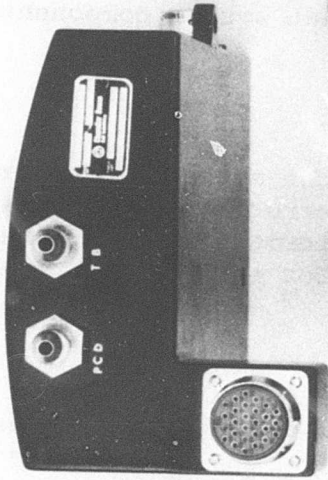
GEOMETRY ACTUATOR

FLUID CONTROLLER

1-FOOT SCALE
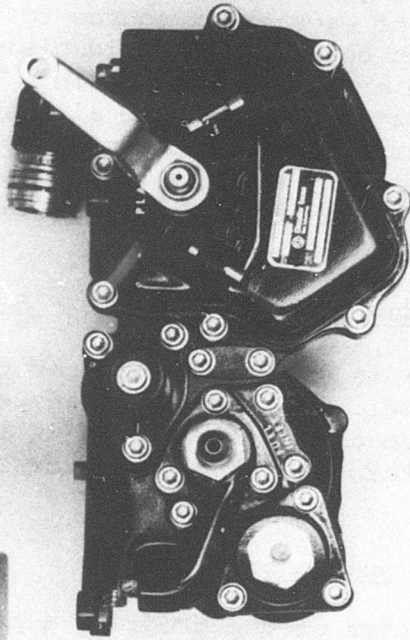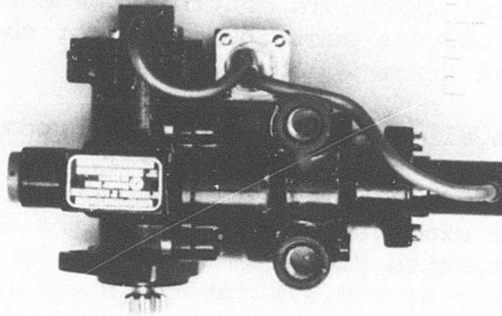
Figure 10. Advanced Engine Control Modules (Mock-Up).

19

prediction is more of an art than a science, certain error predicting techniques are recognized as offering relatively reliable trends and are a useful design tool. The error analysis method used in this study is the root square sum (RSS) error budget method. Based on the RSS estimate of the contribution of each error source to the overall allowable error for each control mode, a decision can be made as to whether these errors are tolerable. Error budgeting then allows a redistribution of the allowable control mode error to ease the accuracy specifications on system components which may have difficulty meeting requirements and tighten accuracy requirements where indications are that system components exceed requirements.

Error Model

Figure 11 is a block diagram of the engine and control error model. The effect of any error source injected into the system can be determined in terms of the resulting steady-state control mode error for each of the control modes.

Error Allocations

At the start of the program, a preliminary system error analysis was conducted based on the RSS method. As a first estimate, each component contributing error to a particular control mode was allowed an equal share of the total allowable control mode error E. If there were m components contributing error then the allowable component error would be $\pm E/\sqrt{m}$.

The allowable error for each component was compared with its estimated design error, and thereby an assessment of the adequacy of the component's performance was determined. For example, in this study the N_g speed sensor had an estimated design error of $\pm$ .1% speed and an allowable error of $\pm$ 0.33% for the starting control mode. This indicated that for this particular control mode the accuracy of the speed sensor was substantially better than the RSS error specified. More of the allowable error for this control mode could therefore be budgeted to other components.

20
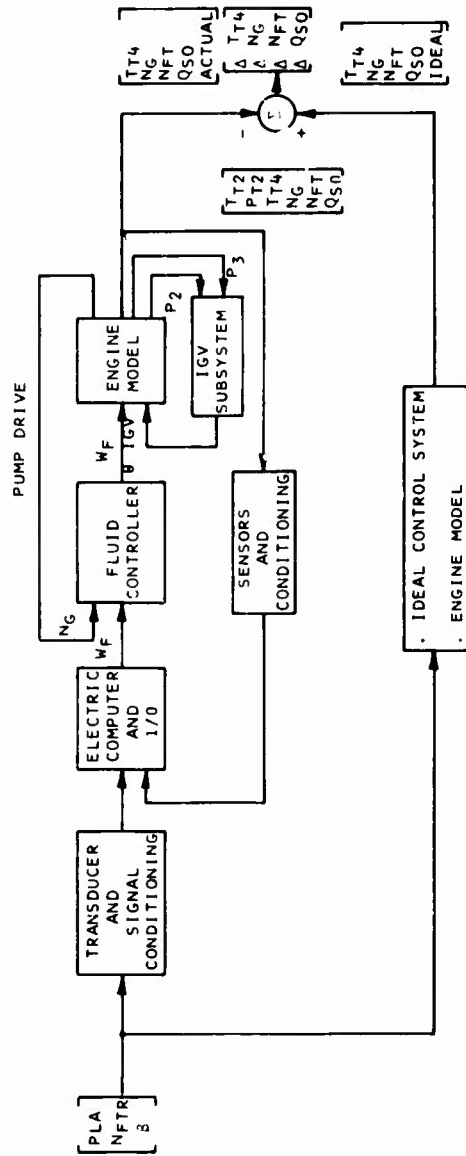
Figure 11. Control Error Analysis Model.

21

Certain deficiencies in the preliminary design were
evident when the RSS errors based on estimated design
were compared with the allowable errors. As a result of
the preliminary analysis, errors were redistributed.

The results of this study establish accuracy requirements
for the components in the control system. Table III
summarizes the results of the error analysis studies for
all of the control modes at worst-case operating conditions

System Performance

To demonstrate system design and performance compliance with
specifications, three separate phases of testing were conducted
as outlined below.

1. Open-loop steady-state and frequency response dynamic
    tests.

2. Closed-loop performance tests using an analog computer
    engine simulator.

3. Environmental/endurance qualification tests.

The results of this test evaluation program establish that the
steady-state and dynamic performance of the control system has
satisfactorily met the specified requirements. There were no
system functional or dynamic problems uncovered. In addition
to these system performance tests, separate performance and
environmental tests were conducted on each of the control
modules. The results of the component testing are included in
the corresponding sections of this report.

Open Loop System Testing

Open loop steady state and dynamic tests were conducted
to ensure that all of the flow schedules, control gains,
and system dynamic performance were within specified
requirements. These tests demonstrated the accuracy of
the electronic computer and hydro-mechanical fluid con-
troller metering system. The test results showed that the
control performance at room temperature over simulated

TABLE III. BASE LINE ENGINE CONTROL ERROR ANALYSIS

COMPONENT CONTRIBUTION TO MODE ERROR

Error Source		Units	Est. Design	Deceleration		Torque Limiting		Temp. Limiting			Load Sharing		Power Turbine Speed Governor		Gas Generator Speed Governor		Start	Accel	IGV
				Sea Level	25,000 ft	Std. Day	Cold Day	Hot Day	Std. Day	Cold Day	Std. Day	Cold Day	Sea Level	25,000 ft	Sea Level	25,000 ft	Up to 55% N_g	Above 55% N_g	
	Ng Sensor	%Ng*	±0.1	-	-	-	-	-	-	-	-	-	-	-	±0.1%	±0.1%	±0.03pph	±0.84%	±0.1%
	Nft Sensor	%Nft*	±0.1	-	-	-	-	-	-	-	-	-	±0.1%	±0.1%	-	-	-	-	-
	Pt3 Sensor	PSI	Ref. to Figure	±2.6%	±2.6%	±0.52%	±0.52%	±2.2°F	±2.0°F	-	±0.2%	±0.2%	-	-	±0.15%	±0.32%	±0.75pph	±2.5%	-
Sensors	T4B Sensor	°F	±10.0	-	-	-	-	±9.2°F	±9.03°F	-	-	-	-	-	-	-	-	-	-
	Qst Sensor	%	±3.0	-	-	±3.0%	±3.0%	-	-	-	±3.0%	±3.0%	-	-	-	-	-	-	-
	Qno Sensor	%	±3.0	-	-	-	-	-	-	-	±3.0%	±3.0%	-	-	-	-	-	-	-
	MRV Position Sensor	Degrees	±0.7	±1.75%	±1.75%	±1.2%	±1.2%	±0.91°F	±0.91°F	-	-	-	-	-	±0.08%	±0.22%	±0.4pph	±0.48%	-
	Tt2 Sensor	°F	See √θ	-	-	-	-	-	-	-	-	-	-	-	-	-	-	-	-
Function Generator	Wf/Pt3 Start	%Rated	±2.9	-	-	-	-	-	-	-	-	-	-	-	-	-	±0.45pph	-	-
	Wf/Pt3 Accel	% Rated	±2.1	-	-	-	-	-	-	-	-	-	-	-	-	-	-	±2.1%	-
	Wf/Pt3 Decel	% Rated	±0.5	±0.5%	±0.5%	-	-	-	-	-	-	-	-	-	-	-	-	-	-
	√θ (Tt2 Sensor) Includes	% Rated	±0.5	-	-	-	-	-	-	-	-	-	-	-	±0.1%	±0.07%	±0.07pph	±0.37%	±2.3%
Multipliers	√θxPLA Mult	%Ng*	Negligible	-	-	-	-	-	-	-	-	-	-	-	±0.00%	±0.00%	-	-	-
	Wf/Pt3 Mult	% FS	±0.3%	-	-	±0.25%	±0.28%	±2.7°F	±2.5°F	-	±0.2%	±0.2%	-	-	±0.06%	±0.14%	±0.1pph	±0.3%	-
Governors	PLA Resolver	Degrees	±0.7	-	-	-	-	-	-	-	-	-	-	-	±0.14%	±0.14%	-	-	-
	Nft Set Speed	%Nft*	±0.1	-	-	-	-	-	-	-	-	-	±0.1%	±0.1%	-	-	-	-	-
	T4BR Set Limit	% Value	±0.1	-	-	±0.1%	±0.1%	±2.0°F	±1.9°F	-	-	-	-	-	-	-	-	-	-
	QSTR Set Limit	% Value	±0.1	-	-	-	-	-	-	-	-	-	-	-	-	-	-	-	-
Hydro/ Mech Fluid Control	Stepper Motor	Steps	±1.0	±2.1%	±2.1%	±1.1%	±1.1%	±4.0°F	±4.0°F	-	±0.18%	±0.22%	±0.16%	±0.175%	±0.17%	±0.54%	±0.6pph	±2.3%	±0.265%
	MRV Contour	%Point	±1.4	±1.5%	±1.5%	±0.26%	±0.26%	±.85°F	±1.85°F	-	-	-	-	-	±0.14%	±0.17%	±0.4pph	±0.8%	-
	MRV Head Pres. Req.	PSI	±0.375	±1.7%	±1.7%	±0.65%	±0.65%	±5.15°F	±4.75°F	-	-	-	-	-	±0.35%	±0.14%	±0.4pph	±2.0%	-
Governor Droop Error				-	-	-1.25% +3.53% -4.75%	±1.25% +4.75% -3.53%	+7.0°F +19.1°F -12.1°F	-7.0°F	-	-	-	-	-	-	-	-	-	-
Total Estimated Error Potential				±4.7%	±4.7%	+3.53% -4.75%	+4.75% -3.53%	+19.1°F -12.1°F	+12.1°F -19.1°F	-	±4.25%	±4.26%	±0.21%	±0.22%	±0.49%	±0.74%	±1.33pph	±4.66%	±1.4%
System Specification				±7.5%		±5.0%		±30.0°F			±5.0%		±0.25%		±1.0%		±2.0pph	±5.0%	±1.6%

23

gas turbine inlet temperatures covering the specified envelope from -65°F to 135°F, from idle to emergency power, was in compliance with the specified accuracy.

The dynamic requirements of the system were also shown from frequency and transient response tests to be within the specified requirements. Each closed-loop control mode was designed for 6 db gain margin and 45° phase margin.

Closed-Loop Testing

Closed-loop tests were conducted using an analog computer simulation for the engines. Figure 12 is a block diagram description of the test layout, showing the interconnections between the fuel controller on the test stand and the breadboard electronic computer and analog engine simulator located in the computer lab about 50 ft away. Figures 13 and 14 are photographs of the setup in the computer lab. Figure 15 shows a photograph of the test stand setup. A complete evaluation of each control loop for both the 5-lb/sec baseline engine and 2-lb/sec alternate engine was made. The alternate engine required changes in gain and flow schedule, which were made using the same control hardware.

A brief summary of the results of the closed-loop test demonstration is outlined below.

1. Acceleration and Deceleration

   The transient performance requirement to accelerate the engine from idle to maximum power within 3 seconds was satisfied. However, the acceleration time is inherently an engine capability established by excess fuel flow surge and maximum temperature limits. Similarly, the deceleration capability of the system is dependent on the blowout limits. For both acceleration and deceleration, the control system does not impede performance.

2. Power Turbine Governor

   Power turbine speed error transients were held to within the specified 3% limit. This required collective pitch reset of the gas generator

24
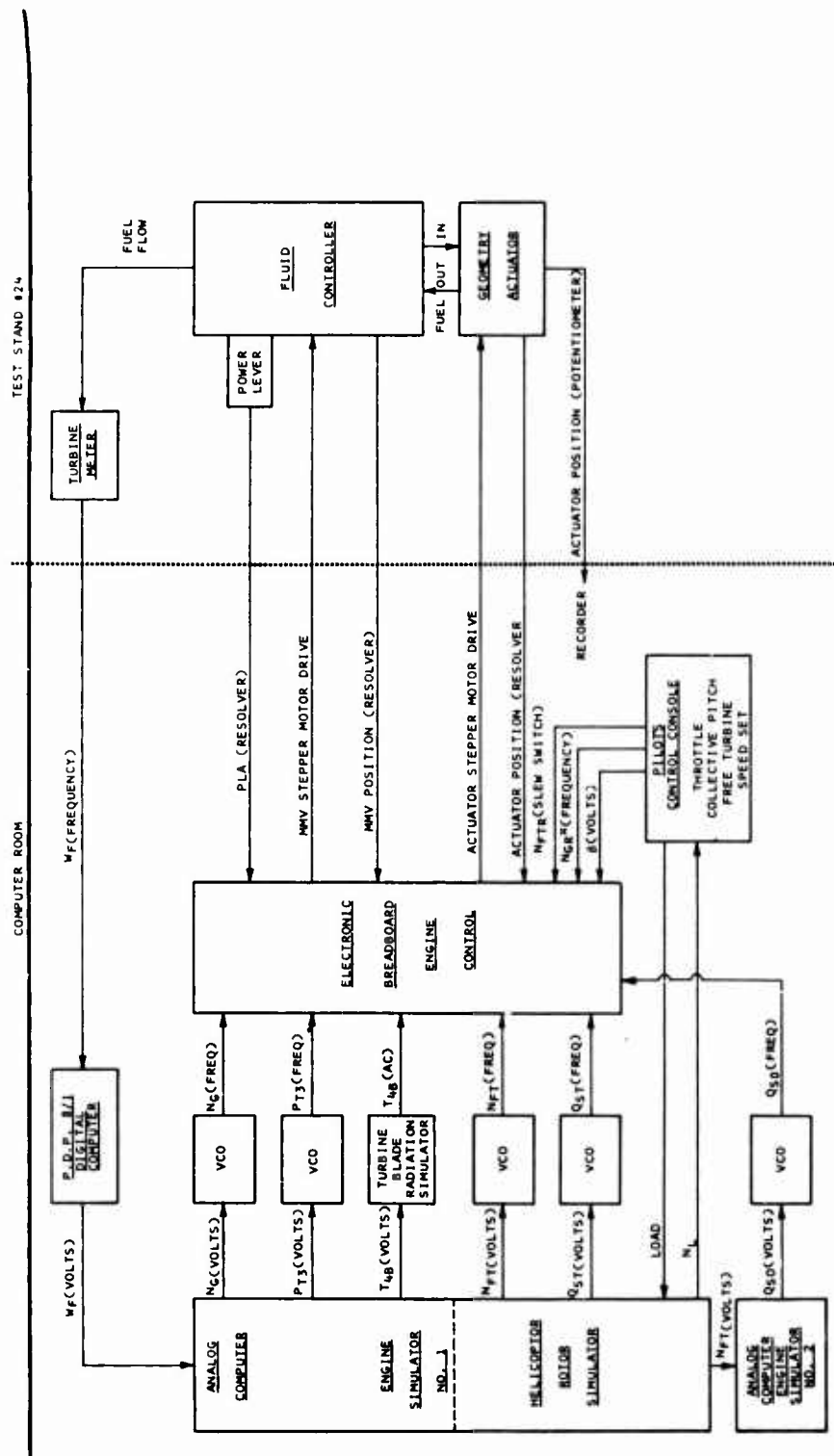
Figure 12. Test Setup for Closed-Loop Testing.

Figure 13.   Engine Simulator and Electronic Fuel Controller.

Figure 14.   Gas Turbine Engine Sensor Simulators.
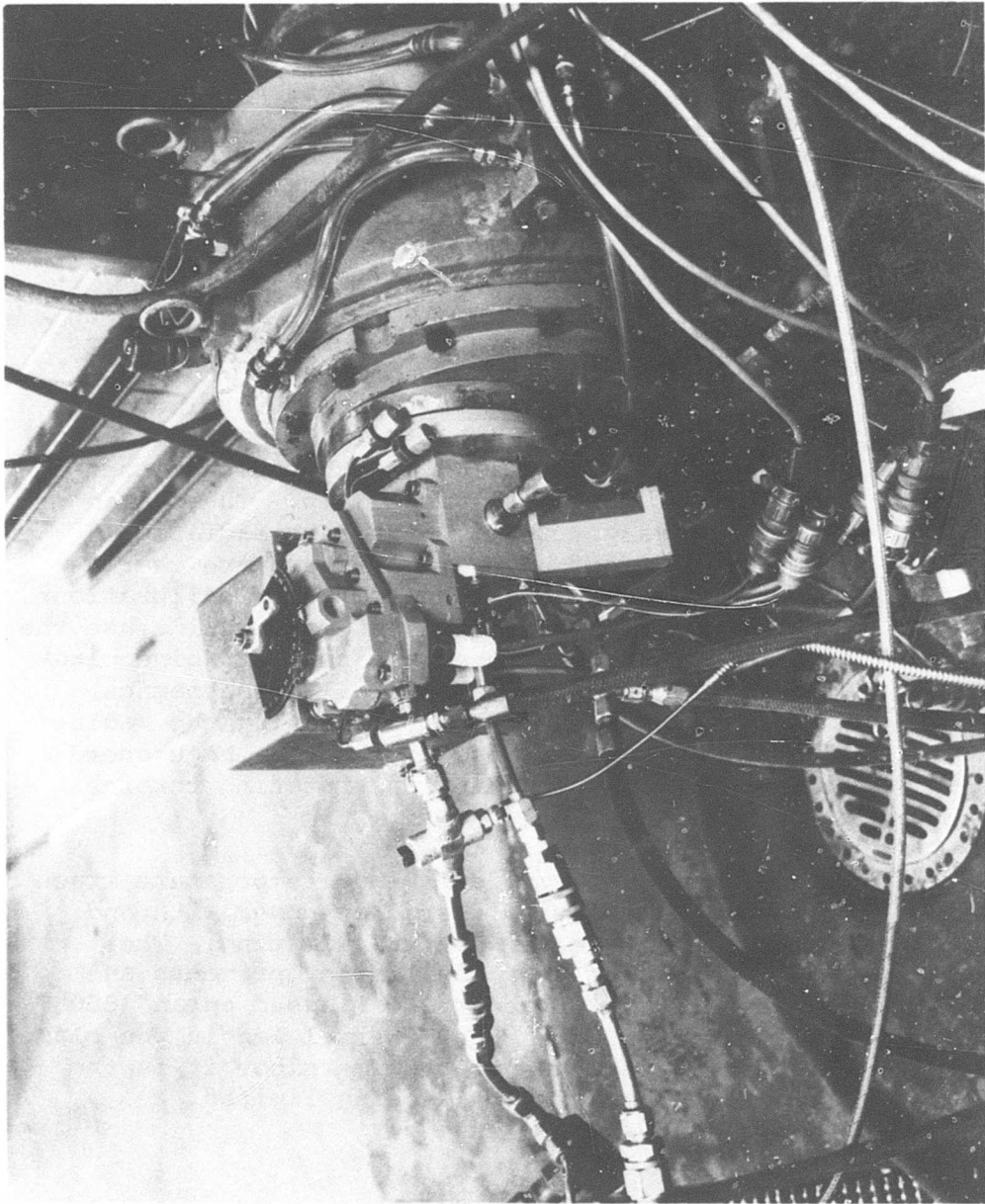
Figure 15. Fuel Control Test Stand.

governor. Transient power turbine speed errors
of up to 12% were limited to 2% with the governor
reset. Figures 16 and 17 summarize the transient
performance capability of the power turbine gover-
nor control. These traces show the performance
of the baseline engine and control system during
gross changes in collective pitch for simulated
sea level and 25,000 ft conditions. Similar
results were obtained with the alternate engine.

3. Blade Temperature Limiter

Closed-loop turbine blade temperature limiting
was demonstrated using the blade temperature
simulator shown in Figure 18. The turbine blade
temperature from the engine simulator (voltage
signal) has been rescaled and the voltage used
to drive a tungsten filament lamp. The scaling
has been arranged to give the same radiation
pyrometer output current vs temperature charac-
teristics obtained from heated strip calibrations.
In this way, the radiation detector will sense the
same radiant energy expected from a turbine blade
at that particular temperature. The dynamics
have been represented by interrupting the radia-
tion with a chopper disc fitted to a high speed
air motor which simulates the rotating turbine
blades.

Figure 19 shows a typical blade temperature trace
during a transient to emergency power with and
without the blade temperature limiting. The
results indicate that the limiter prevents an
overtemperature of about 200°F based on an 1800°F
limit. The uncompensated thermal lag in the blade
does not affect the performance since it is the
blade temperature that is being limited.

4. Torque Limiting

The transient performance of the torque limiting
loop is shown in Figure 20. These results simu-
late an acceleration from idle to high power
pulling a load of 80% collective pitch.

28
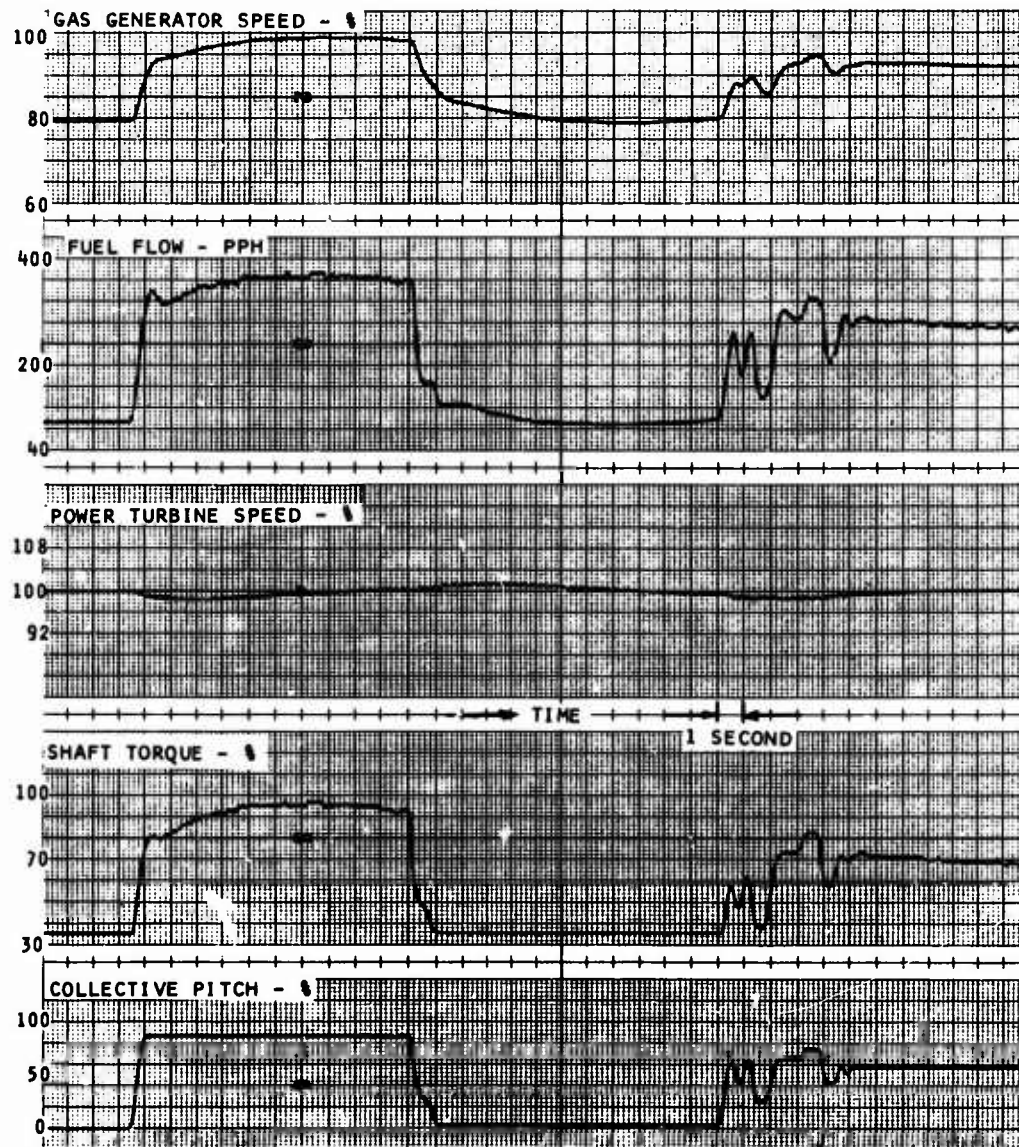
Figure 16. Power Turbine Governor Closed-Loop
Performance (Sea Level).

29
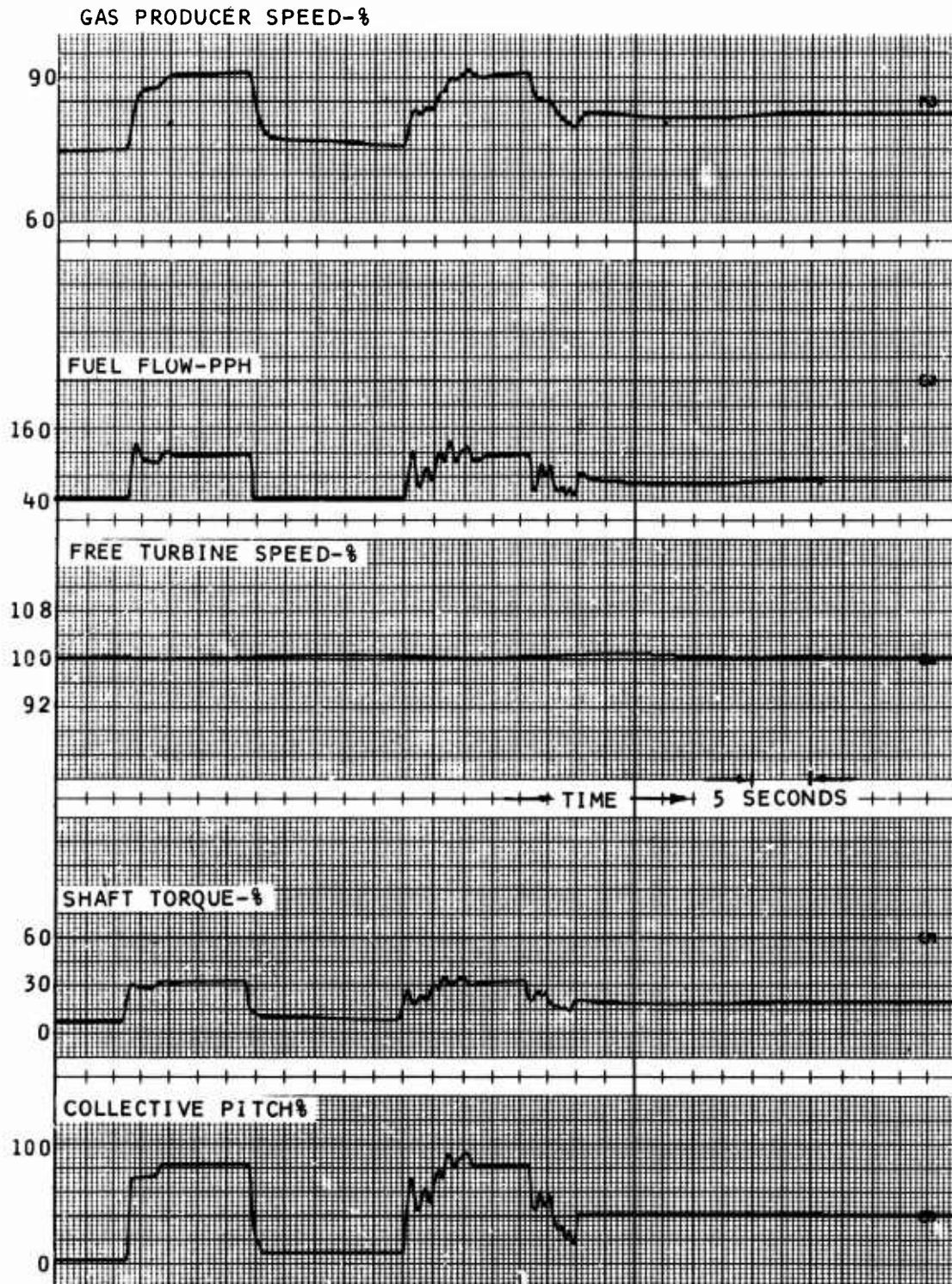
Figure 17. Power Turbine Governor Closed-Loop
Performance (25,000 Ft).

30
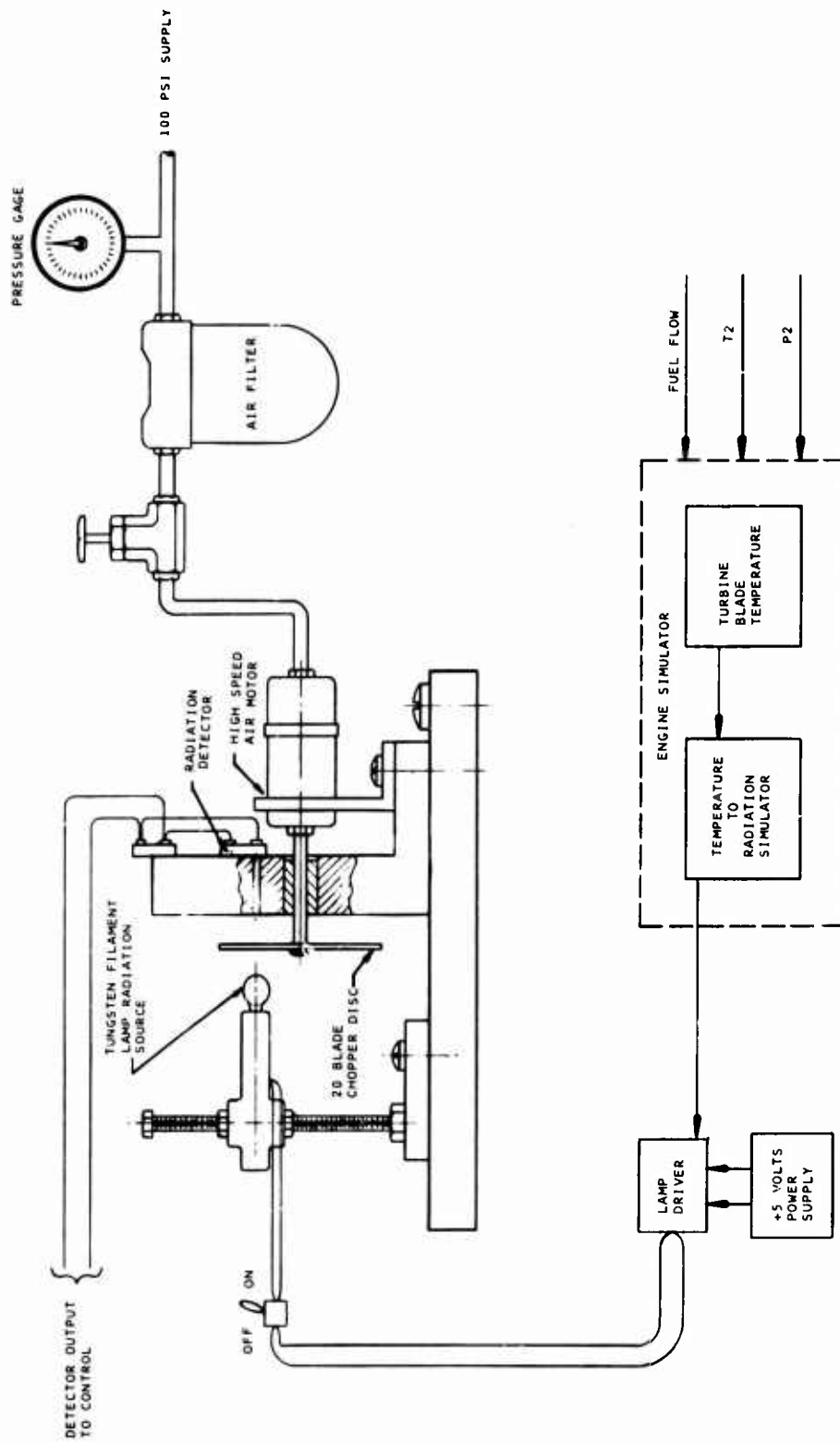
Figure 18. Turbine Blade Temperature Simulator.

31
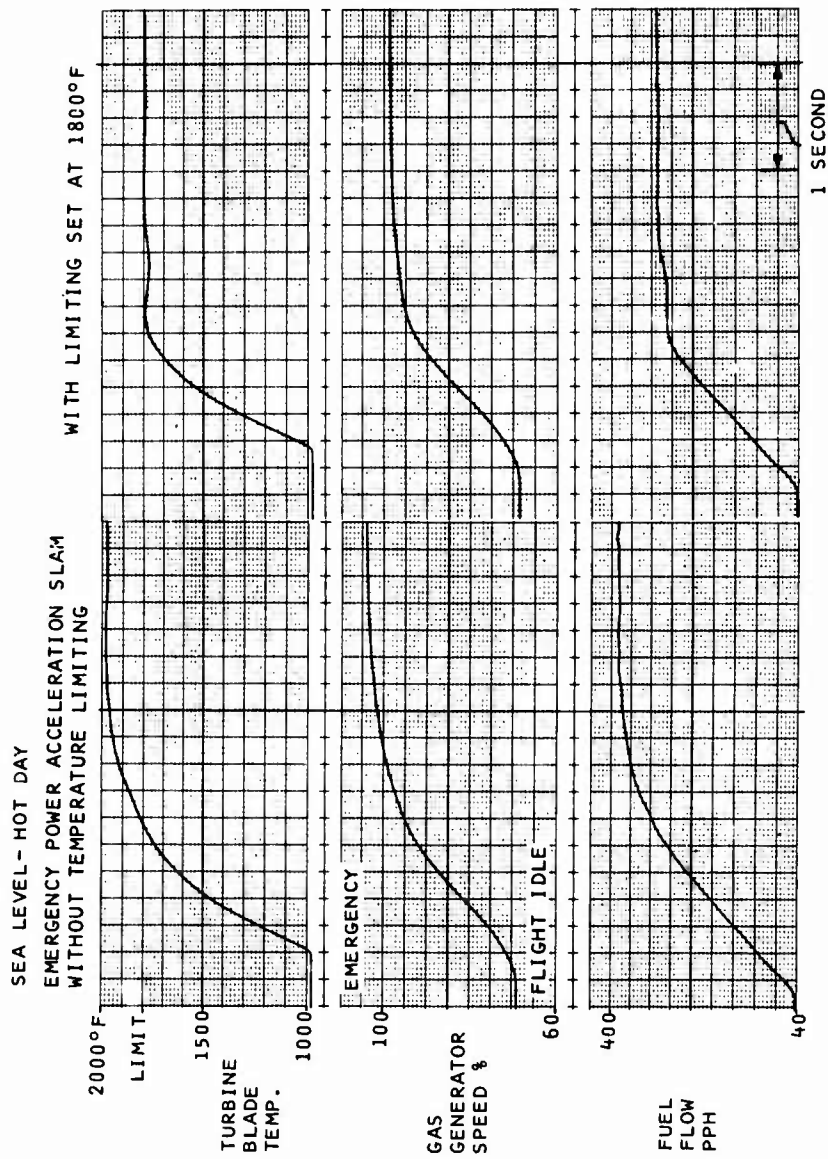
Figure 19. Blade Temperature Limiting Closed-Loop Performance.

32
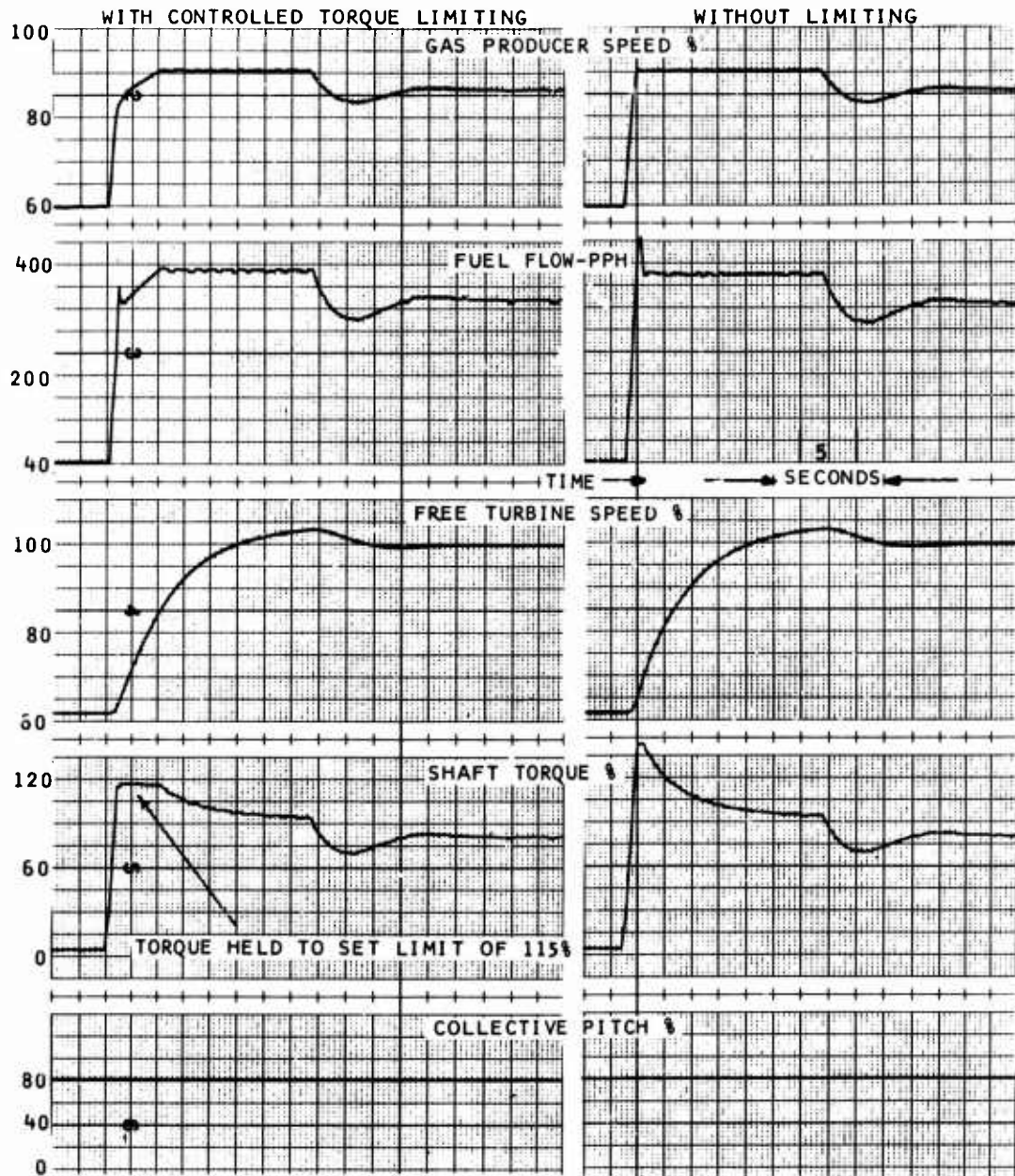
Figure 20. Torque Limiting Closed-Loop Performance.

33
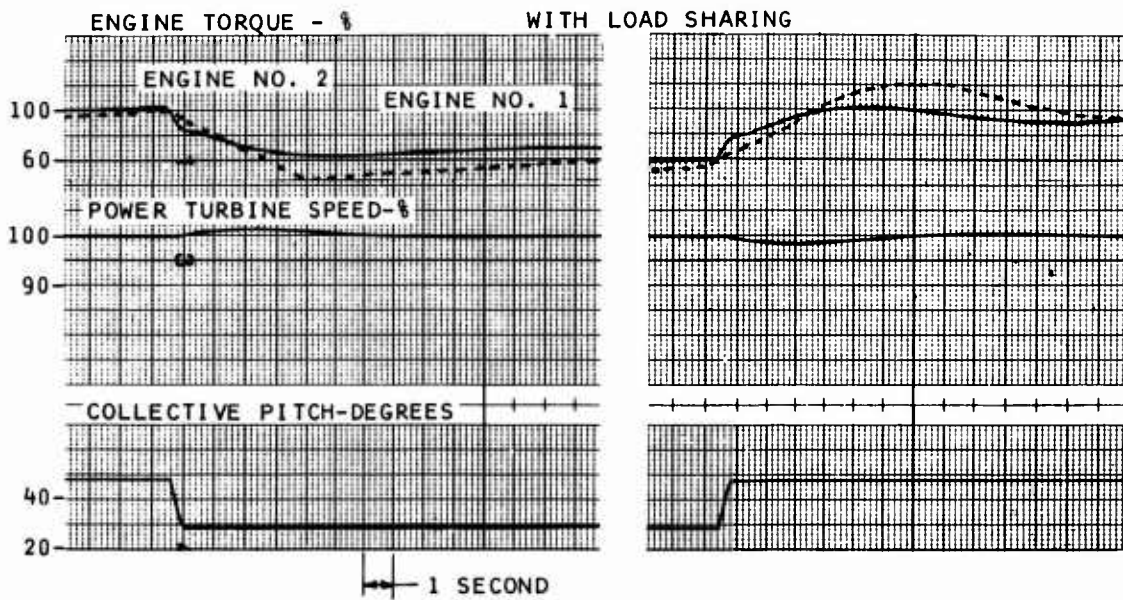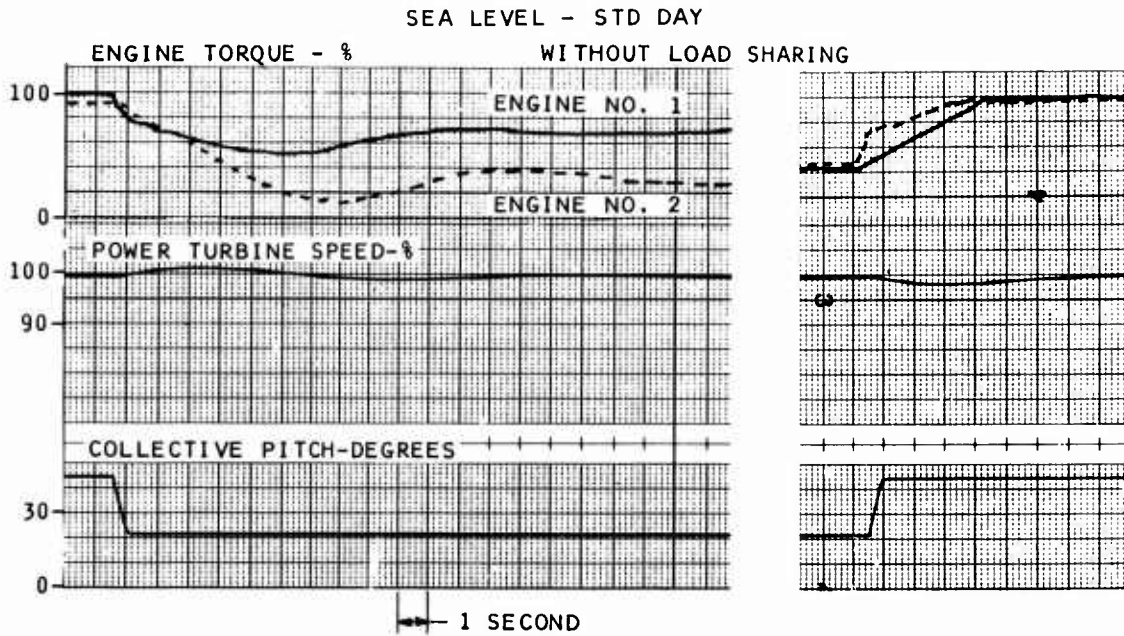
Figure 21.   Load Sharing Closed-Loop Performance.

34

The results indicate that torque is limited to within the specified 115 ± 5%.

5. Load Sharing

To demonstrate load sharing, a second analog computer engine was simulated using a simple linear model of the baseline engine. The transient dynamics of this second engine were established to be sufficiently different from the primary engine simulator to ensure that large splits would occur without load sharing control.

Figure 21 shows transient load splits with and without load sharing control. The results indicate the significant improvement in load sharing with the control. However, during large transients wherein both engines would be on the acceleration control, the system would not be responsive to load mismatches. The load-sharing control operates by increasing the torque on the low output engine. If that engine is already at the acceleration limit then it cannot respond. It is undesirable to provide load-sharing control by decreasing the high output engine because this would slow down acceleration time. Also, resetting the low power engine has undesirable failure modes. For example, if one engine is lost the load-sharing control will decrease the power of the remaining engine.

Environmental and Endurance Tests

The Demonstrator II computer and the fluid controller package was assembled, and environmental and endurance testing on the complete system was conducted. A diagram of the test setup is shown in Figure 22.

The initial environmental test consisted of 3 "Hot Day Mission Profiles", as described in Table IV. This 3-hour test cycle is meant to represent a mission profile resulting in the worst case operating conditions for the electronic computer and fuel pump due to fuel temperature rise.

TABLE IV. HOT DAY MISSION PROFILE

TIME (min)	POWER LEVEL	CONTROL SETTINGS			PHYSICAL SETTINGS			DUMMY SETTINGS				FUEL FLOW OUTPUT	AMBIENT T
		PLA	$N_{FT}*$ (rpm)	β	T_{t2} (°F)	P_{cd} (psia)	N_d (rpm)	N_{ft} (10^3 rpm)	T_b (°F)	Q_{st} (10^3 ft-lb)	Q_{so} (ft-lb)	W_F (pph)	T_{amb} (°C)
Start	0	0	34K	0	135	14.7	0	0	0	0	0	0	71
0- 10	Ground Idle (S.L.)	G.I.	34K	0	135	30	20,600	$K_1 W_f$	0	0	0	30	71
10- 15	Max Power (S.L.)	MIL	34K	Max	135	185	33,800	$K_2 W_f$	0	1	1	300	71-121 (1 minute)
15- 60	Cruise Pwr. (10,000')	MIL	34K	NOM	135	80	30,000	$K_3 W_f$	0	.5	.5±.1	100	121
60- 65	Flt. Idle (10,000')	F.I.	34K	0	135	45	25,100	$K_4 W_f$	0	0	0	60	121
65- 80	Ground Idle (10,000')	G.I.	34K	0	135	20	20,600	$K_5 W_f$	0	0	0	370	121
80- 85	Emer. Power S.L.	Emerg.	34K	Emerg.	135	235	37,500	$K_6 W_f$	+50	1±.2	1	30	121
85-130	Cruise Pwr. (S.L.)	MIL	34K	NOM	135	120	30,000	$K_7 W_f$	0	.5	.5	140	121
130-180	0	0	34K	0	135	14.7	0	0	0	0	0	0	-4° - 71 (5 minutes)

The purpose of this test is to check the system performance at critical points during a representative worst-case mission.

36
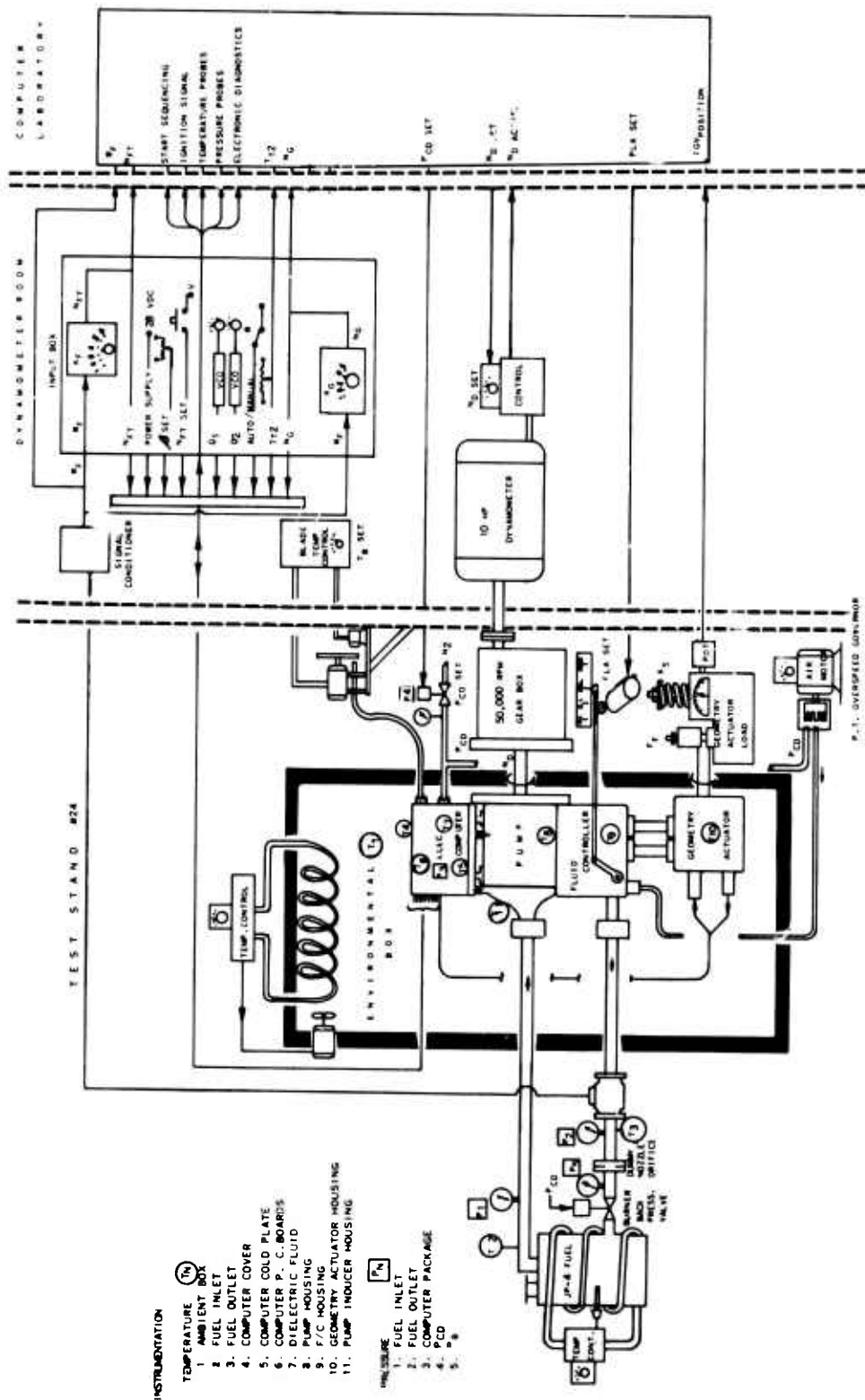
Figure 22. Environmental and Endurance Test Setup.

The system was then set up for automated testing and data acquisition, which was conducted by the Hewlett Packard Data Acquisition System, shown in Figure 23.

The environmental/endurance testing consisted of:

1. 50 hours at 121°C ambient and 57°C fuel
2. 20 hours at -54°C ambient and fuel
3. 18 hours of contamination testing per MIL-E-5007C Spec.
4. 30 hours at room temperature

The environmental/endurance test cycle is shown in Figure 24. Each cycle takes 18 minutes to complete.

The data acquisition system cycles the fuel flow, according to Figure 24, by varying the pump speed and changing the input parameters to the demonstrator computer. The voltage controlled oscillator is used to convert the dc level supplied by the data acquisition system into a frequency signal. Besides cycling the fuel flow, the acquisition system also records the following data at each fuel flow level:

Fluid Controller, Pump, & IGV Parameters

1. Automatic-to-Manual Changeover Pressure
2. Inducer Outlet Pressure
3. Centrifugal Pump Outlet Pressure
4. Gear Pump Outlet Pressure
5. Metering Valve Pressure Drop
6. Pump Changeover Valve Pressure
7. High-Speed Gearbox Temperature
8. Control Outlet Fuel Temperature
9. Pump Drive Speed
10. Pressure Inlet to Pump
11. Fuel Inlet Temperature to Pump
12. Pressure Outlet from Fluid Controller
13. Geometry Actuator Position

Thermistor locations in the demonstrator package

1. MMV Stepper Motor Driver
2. VCO
3. Multi-Layer Board Binary Rate Multiplier (BRM)
4. Function Generator ROM

38
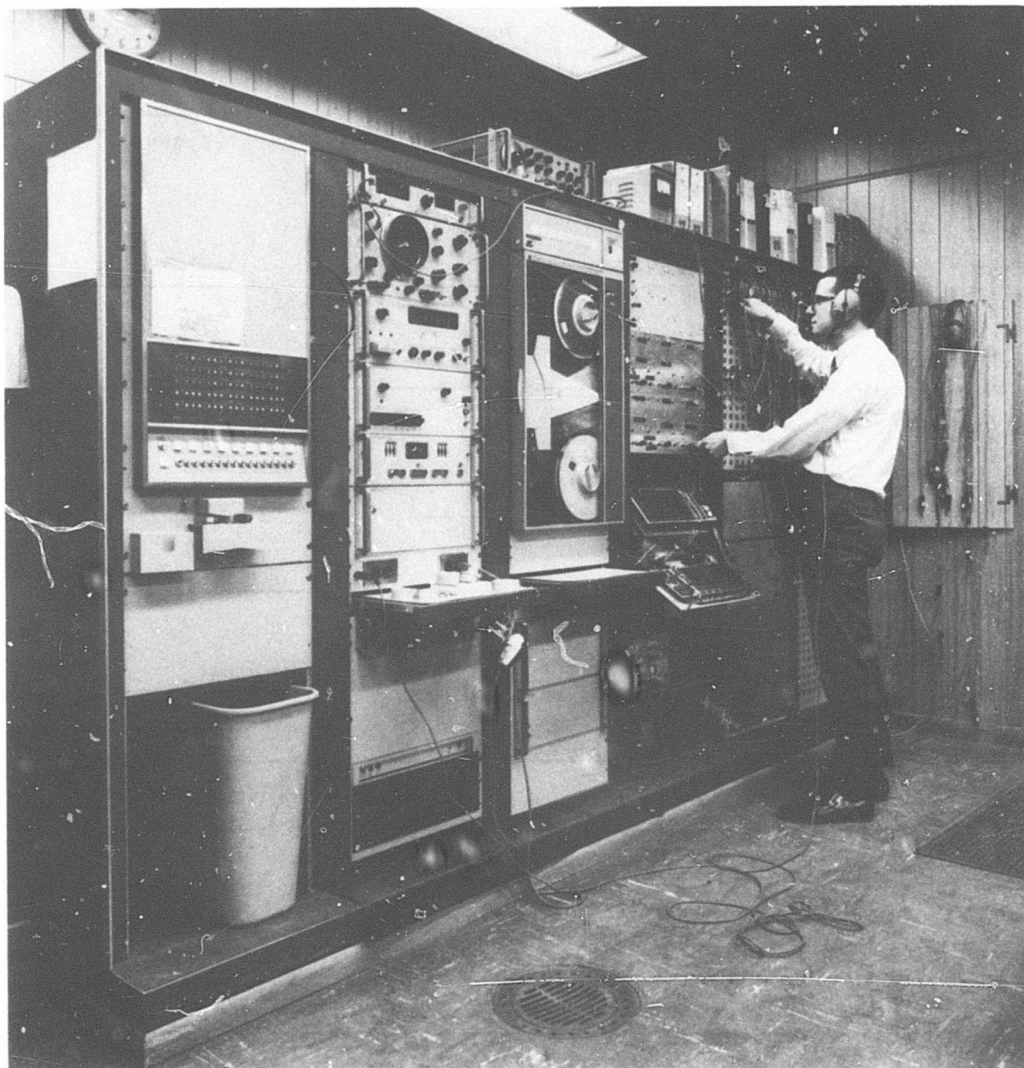
Figure 23.   Hewlett Packard Data Acquisition System.

39
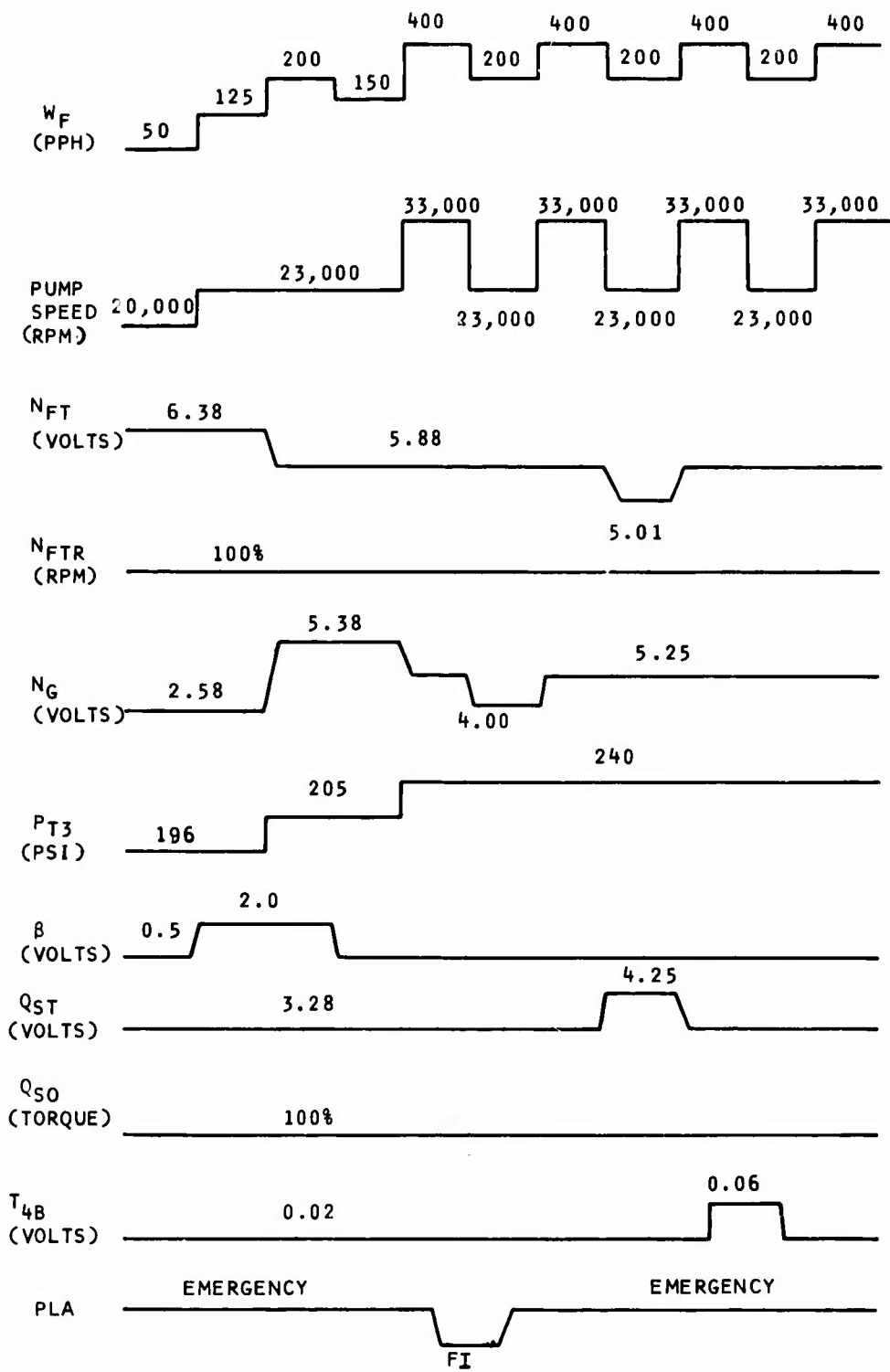
Figure 24.   Environmental/Endurance Test Cycle.

5. Power Supply +5V Regulator Power
6. Power Supply Diode Located on Cold Plate
7. Inlet Fuel to Cold Plate
8. Outlet Fuel from Cold Plate
9. Cover
10. Mounting Pad on Cold Plate

Other signals from Demonstrator Package

1. W_F/P_{t3} in control
2. N_g
3. N_{ft}
4. N_{ft}^*
5. P_{t3}
6. β
7. Q_{st}
8. Q_{so}
9. T_{4B}
10. PLA
11. +5V supply
12. -12V supply
13. N_{ft} error output after lag compensator
14. N_{gr}
15. $\sqrt{\theta}$
16. W_F

Figure 25 shows the Dynamometer Room where the $\pm$ 28 volt power supplies and the VCO were housed.

Hot Day Mission Profile

The Hot Day Mission schedule is described in Table IV. In accordance with this schedule the system was soaked at +71°C for 50 minutes. After the high temperature soak, the input parameters were manually changed to obtain the correct output fuel flows. The complete mission was run 3 times.

Figure 26 shows the approximate location of 10 thermistors which were bonded to the demonstrator package. The temperature data measured by the thermistors describes the temperature profile of the electronics as a function of the fuel flow and ambient temperature.

41

POWER SUPPLIES
FOR ± 28 VOLTS

VCO'S
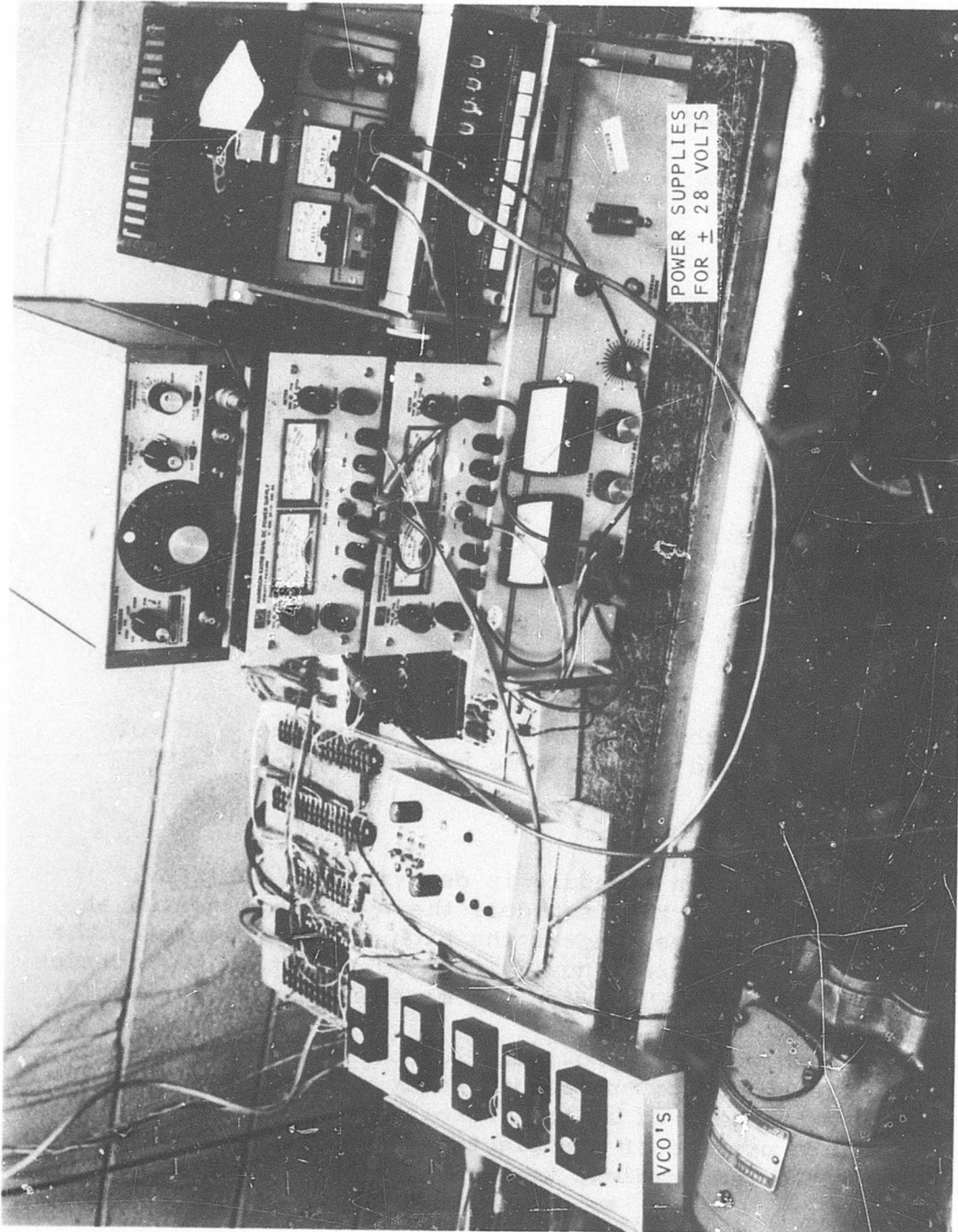
Figure 25. Dynamometer Room Test Setup.

42
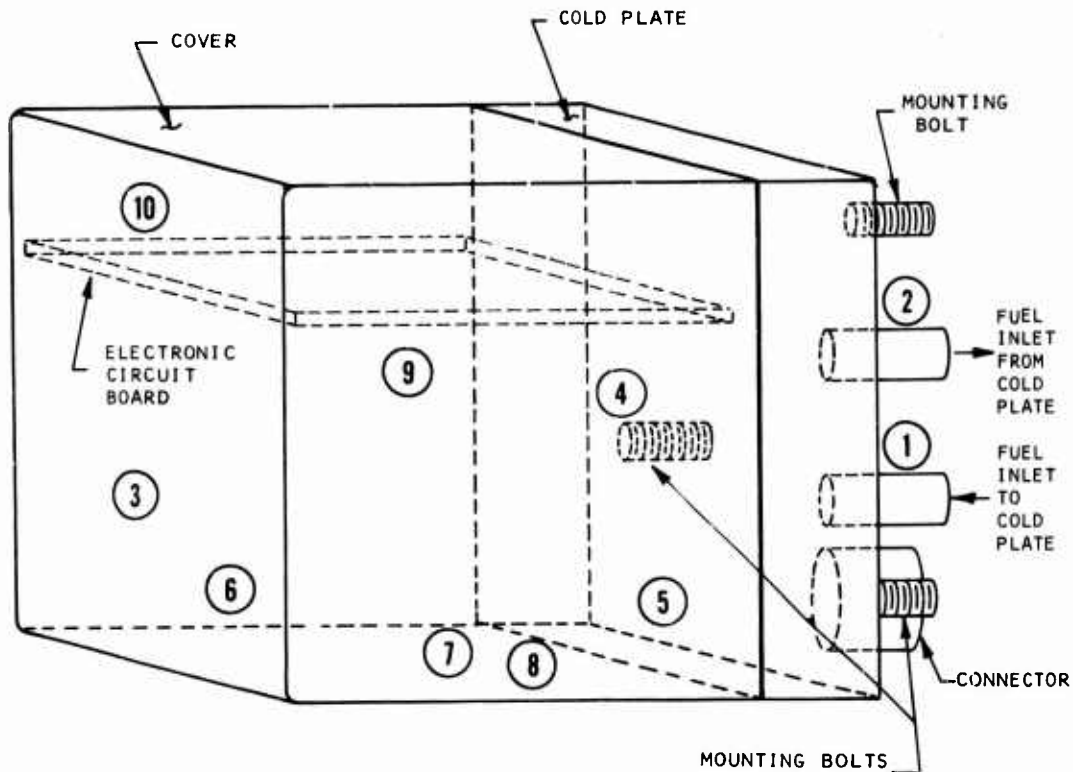
LOCATION OF THERMISTORS

THERMISTORS OUTSIDE CONTROL
① INLET FUEL TEMPERATURE
② OUTLET FUEL
③ COVER TEMPERATURE
④ COLD PLATE TEMPERATURE THERMISTER BONDED TO BASE OF MOUNTING BOLT

THERMISTORS INSIDE CONTROL
⑤ DIODE TEMPERATURE, DIODE BOLTED TO INSIDE OF COLD PLATE
⑥ β SIGNAL PROCESSOR
⑦ MMV STEPPING MOTOR DRIVE
⑧ TRANSISTOR IN +5 VOLT REGULATOR
⑨ FUNCTION GENERATOR ROM
⑩ MULTILAYER BOARD BRM

Figure 26. Thermistor Locations for Hot Day Test.

The temperature data obtained from these tests are tabulated
in Table V. The data indicate that as fuel flow drops,
the temperature rise across the cold plate increases. When
fuel flow was 100 pph the temperature drop, FO-FI, was 5°C
and increased to 9°C when the fuel flow decreased to 60 pph.
Furthermore, when the fuel flow increased to 370 pph the
temperature drop decreased to 1°C. The temperatures inside
the demonstrator package also showed a rise when fuel flow
decreases. At low fuel flows all the thermistors indicated
a rise in temperature.

The Hot Day Mission Profile presents the worst possible
operating conditions due to heat rise caused by low fuel
flows, high ambient temperatures (121°C), and high fuel
inlet temperature (57°C). The coolant fluid maintained
the temperature inside the computer below 100°C even under
worst-case operating conditions. This test demonstrated
the operation of the cooling system and the control system
under worst-case conditions.

Endurance Testing

The primary purpose of the endurance test was to establish
the capability of the control to survive repeated cycling
through several operating modes at standard, hot (121°C),
and cold (-54°C) day conditions and with contaminated fuel.
Evaluation of the control following these tests showed no
degradation in performance, evidence of excessive wear, or
component part failures.

The endurance test results were used to measure the repeat-
ability of the control at each control mode and operating
condition. The repeatability was measured by computing
the sigma of the fuel flow distribution about its mean
value for each mode and operating condition. The sigma
value is identical to the RMS error in repeatability since
an ideally repeatable control would have zero sigma dis-
tribution; i.e., the same fuel flow would be recorded
during each cycle for a given control mode and operating
condition. A high sigma value therefore indicates poor
repeatability.

The computed mean fuel flow and RMS error for each cycle
point and operating condition are listed in Table VI.
These values were computed using all of the data obtained

44

TABLE V. HOT DAY MISSION PROFILE TEST DATA

Ambient Temp. (°C)	Fuel Flow (pph)	Fuel In (°C)	Fuel Out (°C)	Cover (°C)	Cold Plate (°C)	Diode (°C)	β (°C)	Driver (°C)	Transistor (°C)	ROM (°C)	BRM (°C)
+ 71	30	86	90	83	88	85	79	79	90	83	83
+ 71	300	59	61	76	66	69	77	79	82	85	85
+122	300	63	64	77	67	71	74	76	82	80	80
+122	100	70	75	83	78	79	81	82	89	86	86
+122	100	72	77	86	79	81	84	85	91	89	89
+122	60	74	83	89	83	89	88	89	94	94	94
+122	370	64	65	81	69	74	81	87	87	88	87
+122	140	64	69	79	70	74	80	87	89	90	89
+122	140	64	69	80	72	75	80	87	89	90	89

Cycle Point	Mean Flow (pph)	RMS Error (pph)	RMS Error (% of Reading)	RMS Error (% FS)	Operating Conditions
			TABLE VI. ENDURANCE TEST DATA (All Data Points)		
1	46.4	2.5	5.4	0.6	Room temp.
2	96.4	7.3	7.6	1.8	
3	203.6	10.2	5.0	2.5	40 hours
4	135.2	14.4	10.7	3.5	cycle time
5	358.6	2.8	0.8	0.7	161 samples
6	210.5	10.8	5.1	2.6	
7	357.1	3.1	0.9	0.8	
8	190.0	8.8	4.6	2.1	
9	362.5	5.4	1.5	1.3	
1	68.8	11.6	16.8	2.8	121°C ambient
2	86.1	4.1	4.8	1.0	temp.
3	220.9	14.3	6.5	3.5	50 hours
4	163.6	21.6	13.2	5.3	cycle time
5	332.7	6.2	1.9	1.5	
6	210.2	24.7	11.8	6.0	167 samples
7	333.7	7.4	2.2	1.8	
8	185.0	4.2	2.3	1.0	
9	334.0	8.1	2.4	2.0	
1	68.9	4.7	6.8	1.1	-54°C ambient
2	76.7	4.0	5.2	1.0	temp.
3	202.1	11.0	5.4	2.7	
4	177.7	4.3	2.4	1.0	20 hours
5	302.3	9.9	3.3	2.4	cycle time
6	202.0	25.8	12.8	6.3	
7	313.8	13.4	4.3	3.3	43 samples
8	188.1	10.5	5.6	2.6	
9	295.7	16.3	5.5	4.0	
0	287.5	30.4	10.6	7.4	18 hours of contamination test

46

for each operating condition. Table VI also includes the
mean fuel flow and RMS error computed from the data ob-
tained during 18 hours of contamination testing. Contami-
nation testing is identified as cycle point "O" since the
control was not automatically cycled. During this test,
the control was left at the set point while supplied with
contaminated fuel.

1. Room and Hot Day Test Results

    The RMS errors computed from the complete test data
    are significantly higher than what should be expected
    from a properly performing control. A review of the
    test conditions indicated that these large errors are
    primarily due to improper test conditions. The large
    repeatability errors for room temperature and 121°C
    ambient result from electrical noise pickup in the
    test setup. Electrical noise filtering was provided
    about half way through the hot test. This signifi-
    cantly reduced RMS noise level in the test setup and
    thereby improved repeatability. Table VII compares
    the RMS errors computed from data obtained during the
    first 10 hours of testing at 121°C ambient (before
    noise filtering was provided), with RMS error values
    computed from data obtained during the last 10 hours
    of the hot test. The RMS error in repeatability is
    less than 2% of full scale during the last 10 noise-
    free hours, while the repeatability error during the
    first 10 hours is almost twice as large (3.9% of full
    scale).

2. Cold Day Endurance Test Results

    After the control had completed the cold day test, the
    barrier filter was inspected and found to have been
    clogged. The clogging was caused by ice due to exces-
    sive amounts of water in the fuel. The filter element
    used has completed 400 hours testing at -54°C with
    similar flow conditions in another application.
    Table VII gives data for the first 14 hours of testing
    before the filter clogged and shows that for the same
    test conditions the deviation is reduced from 12.8%
    of point to 1.6% of point.

47

Cycle Point	Mean Flow (pph)	RMS Error (pph)	RMS Error (% of Reading)	RMS Error (% FS)	Operating Conditions
			TABLE VII. ENDURANCE TEST DATA (Selected Data)		
1	48.3	1.6	3.3	0.4	121°C ambient
2	91.8	4.3	4.7	1.0	temp.
3	196.4	8.2	4.2	2.0	
4	127.2	13.6	10.7	3.3	
5	340.1	8.5	2.5	2.1	First 10 hours
6	248.6	16.0	6.4	3.9	
7	337.1	8.5	2.5	2.1	40 samples
8	181.4	6.2	3.4	1.5	
9	344.7	10.4	3.0	2.5	
1	74.9	0.9	1.2	0.2	121°C ambient
2	84.1	1.3	1.5	0.3	temp.
3	228.4	0.6	0.3	0.1	
4	174.5	1.1	0.6	0.3	
5	329.2	1.5	0.5	0.4	Last 10 hours
6	199.0	1.6	0.8	0.4	
7	332.7	7.7	2.3	1.9	43 samples
8	186.5	1.6	0.9	0.4	
9	329.8	1.8	0.5	0.4	
1	70.1	1.8	2.6	0.4	-54°C ambient
2	77.0	1.6	2.1	0.4	temp.
3	208.8	2.0	1.0	0.5	
4	175.7	2.9	1.6	0.7	First 14 hours
5	306.0	5.3	1.7	1.3	
6	202.9	3.3	1.6	0.8	30 samples
7	312.7	7.9	2.5	1.9	
8	182.3	5.2	2.8	1.3	
9	303.5	3.5	1.2	0.9	
0	302.5	2.6	0.85	0.6	First 5 hours contamination test

3. Contamination Testing

Eighteen hours of contamination testing were completed. During approximately the last 8 hours of this test the centrifugal pump was in cavitation. Table VII gives test results for the first 5 hours of testing and the results indicate a RMS error of 2.6% compared to the 10.6% error computed from the total 18 hours of testing. The problems which occurred were:

a) Worn gear pump journal bearings which induced a high flow through the barrier filter, causing the filter to clog.

b) The heat exchanger bypass valve clogged with contamination after 12 hours running; this caused the centrifugal pump to cavitate.

The wear in the pump bearing can be rectified by providing a better distribution of clean wash flow lubrication. The heat exchanger bypass valve has insufficient valve stroke; this can be remedied by a simple design change.

Examination of the components after the contamination testing showed that the main components of the system, the centrifugal impeller, the metering head regulator, and the fuel metering valve had excellent contamination resistance. Also, with the barrier filter and heat exchange bypass valve in operation, the control has the ability to accurately control contaminated fuel.

Summary of System Evaluation

A comprehensive performance and endurance test evaluation of the control system has proven design and performance compliance. No major problem areas were uncovered. Those design faults which were identified can easily be corrected through minor changes in hardware design.

GEOMETRY ACTUATOR

A geometry actuator will be required on advanced gas turbine
engines for positioning compressor stator vanes and/or operat-
ing bleed valves. The objective of this program was to develop
the best actuation system for these advanced engine require-
ments. Positioning the stator vanes was determined to be more
demanding than the operation of bleed valves in terms of accu-
racy and performance. The actuator was therefore designed spe-
cifically for the stator vane requirement. It is possible,
however, that this same actuator could serve a dual purpose,
i.e., operate both bleed valves and stator vanes from one out-
put shaft.

The detailed requirements for the actuator were obtained from
a thorough survey of the major engine manufacturers and are
summarized below.

Design Requirements

1. In consideration of pneumatic systems, engine manufac-
    turers are reluctant to allow steady-state air leakage
    from the compressor in excess of 0.1%.

2. Either compressor pressure ratio or corrected speed is
    an acceptable means for scheduling the guide vanes.

3. With a rotary actuator, 30 to 35 degrees of angular
    output is required.

4. The actuator must operate satisfactorily with maximum
    output stiction loads of 50 to 100 in./lb.

5. The actuator must maintain a scheduled accuracy of
    ± 1/2 degree during steady-state and transient opera-
    tion. A transient accuracy of ± 1 degree will prob-
    ably be acceptable.

6. In the event of an electrical failure, the actuator
    system must continue to control the guide vanes so
    that the engine can operate over its full speed range.
    Starting under this failed condition is also a require-
    ment.

7. Although not a specific requirement, a fuel pressure
    powered system is favored. Contamination, torque re-
    quirements, and high temperatures are thought to be
    serious drawbacks for a pneumatic system.

50

Selected Design

Six different systems were investigated. Two of the systems
used pneumatic computation for scheduling and actuation and
were completely independent of the fuel control system. The
other systems used electronic computation for scheduling and
considered pneumatic, electric, or hydraulic power for actu-
ation. A summary of the trade-off study conducted on these
systems is given in Table VIII. To meet the design require-
ments outlined above within a reasonable size and weight, the
electrohydraulic actuator using high pressure fuel for actu-
ation power and electronic computation for corrected speed
scheduling was determined to be the best system.

A schematic of the geometry actuator is shown in Figure 27,
and its operation is described as follows: The input from the
electronic computer drives the stepper motor which, through the
operation of the ballscrew, translates the 3-way control valve.
The valve controls P_x pressure and thereby forces the piston
to follow the position of the control valve. The piston motion
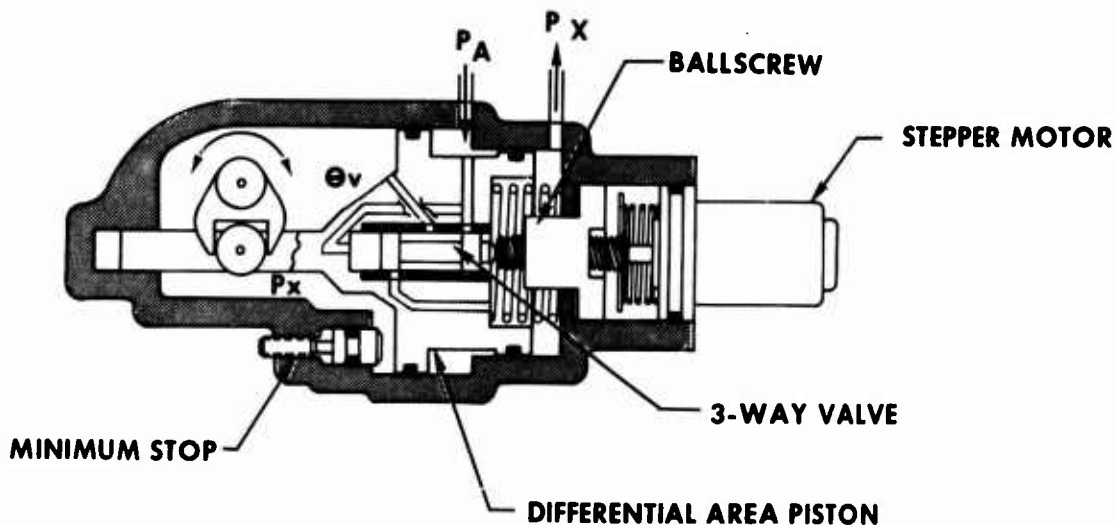
Figure 27. Geometry Actuator Schematic.

51

TABLE VIII. GEOMETRY ACTUATOR TRADE-OFF

	Type	Computation	Actuator	Accuracy	Flexibility	Vulnerability	Relative Weight	Relative Cost	Basic Limitations	Basic Advantages	Remarks
1.	Pneumatic	Flowing P3/P2	Proportional	6%	Completely independent	Good	0.8	1	Accuracy and gas consumption	Flexibility and vulnerability	Unacceptable to engine manufacturers
2.	Pneumatic	Nonflowing P3/P2	Proportional	6%	Completely independent	Good	1.25	1.5	Accuracy and size	Vulnerability	Large, expensive & can't meet accuracy
3.	Electro-pneumatic	Elect. $N/\sqrt{\theta}$	Nonlinear	2%	Requires elect. input	Good	1.25	1.3	High temp. pressure range of P_3	Meets req.	Large, and two electronic inputs required
4.	Electro-hydraulic	Elect. $N/\sqrt{\theta}$	Nonlinear	2%	Requires fuel and elect. input	Potential fire hazard	1	1.2	Vulnerability		Two electronic inputs required
5.	Electro-hydraulic	Elect. $N/\sqrt{\theta}$	Stepper with hydro follow-up	2%	Requires elect. & fuel input	Potential fire hazard	0.9	1.2	Vulnerability & servo flow	Only one elect. input	Best candidate
6.	Elect.	Elect. $N/\sqrt{\theta}$	Large stepper	2%	Requires high elect. power input	Good	2.5	0.5	Very high on weight and elect. power	Lowest cost	Too heavy

is converted to a rotary output by a crank mechanism. The output position is sensed by a resolver and fed back to the electronic computer. The feedback signal is compared to the reference signal and the error drives the stepper motor. The system thereby operates as a closed-loop position feedback servomechanism. The reference signal generated in the computer corresponds to the desired actuator position as specified by the corrected speed schedule.

In the event of an electrical failure, or if power is lost or switched off for manual fuel control, a built-in backup control operates through an internal force feedback system and schedules actuator position as a function of pump pressure rise. The fuel pressure source (PA-PX) is supplied by the fluid controller centrifugal pump. This pressure rise is a function of the pump speed and therefore is an indication of engine speed. The pressure rise is sensed by the 3-way control valve. Opposing the force which this pressure creates on the valve is a feedback spring located within the ballscrew. The force of the feedback spring is directly proportional to actuator position. Summing these two forces at the valve provides an actuator position schedule as a function of speed. During normal operation, the electronic position feedback system overrides this hydromechanical backup schedule.

To ensure that the actuator is in the correct position for engine starting, a spring is used to force the piston to the IGV closed position.

Figure 28 is a photograph of the geometry actuator hardware disassembled. The piston and housing are aluminum and the running surfaces are Martin-hardcoated to resist wear. The control valve and sleeve are AMS 5630. The output shaft, which is supported by two ball bearings, is manufactured from AMS 5620. The feedback resolver (not shown) and stepper motor are purchased items. The weight of the actuator is estimated to be 1.5 lb in flight hardware.

Shaft Seal Tests

As a part of the actuator program, rotary shaft seals were evaluated. No dynamic elastomeric seal is available that will survive the fuel temperature range (-65°F to +300°F) and abrasion for the life required of the shaft seals in this control

COVER

PISTON

SHAFT

SHAFT
HOUSING

SPRING
(ENSURES
STARTING
POSITION)

SLEEVE

SERVO
VALVE

BALL
SCREW

PISTON
HOUSING

STEPPING
MOTOR
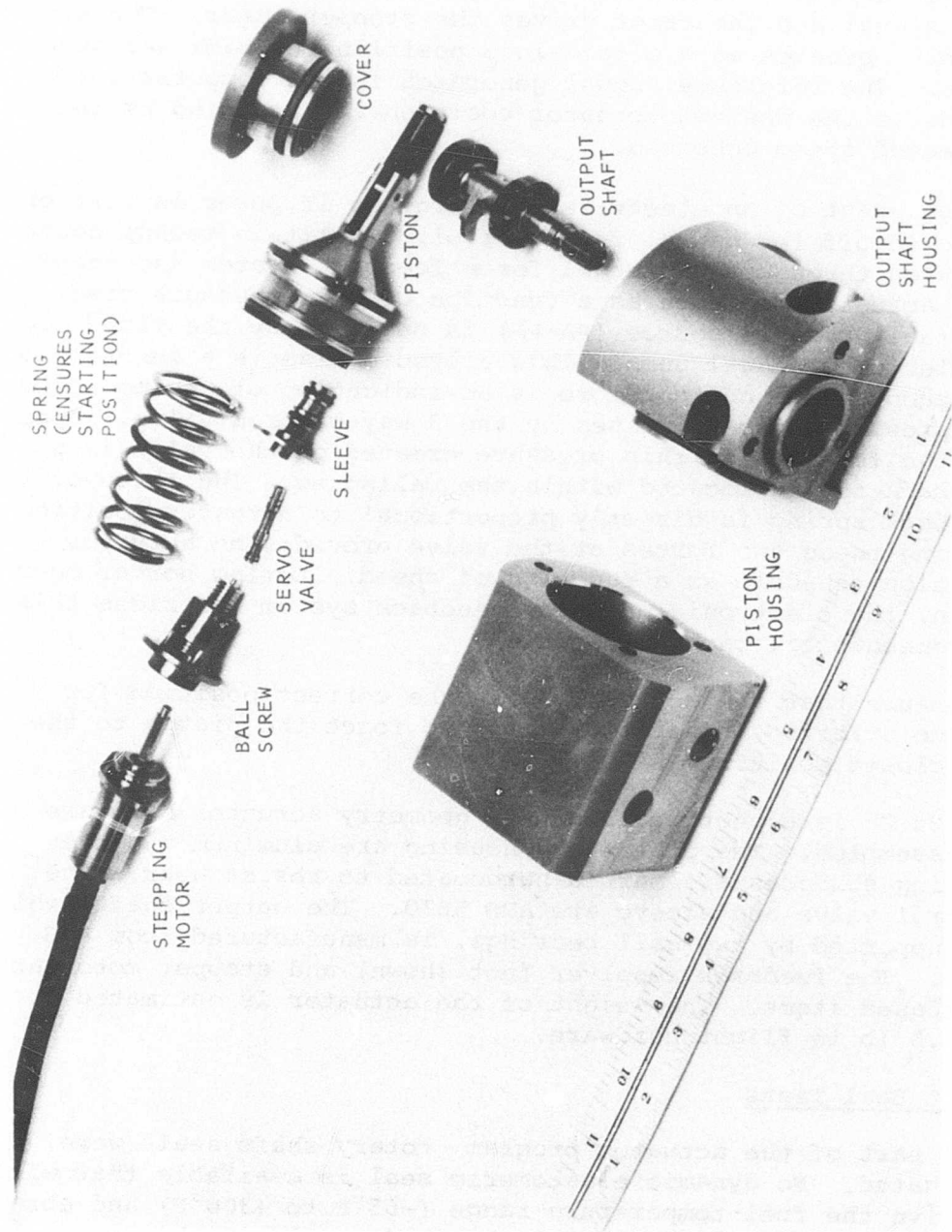
Figure 28. Geometry Actuator Hardware.

54

system. Power lever seals as well as the geometry actuator
output shaft seal were considered.

Four types of Teflon seals were all cycled for equal periods at
hot (+300°F), cold (-65°F), and room temperature conditions for
a total of 150 hrs (54,000 cycles). Fuel pressure was varied
from 20 to 800 psi during the cycling. Two of the seals tested
proved to be effective for application in this advanced control
system. Neither seal exhibited measurable leakage or excessive
wear as a result of the cycling. One of these was a graphite-
filled Teflon seal supported by a flat wire spring. The other
was a virgin Teflon seal and used a fluorosilicone o'ring for
support. Both seals were installed in the housing as opposed
to being installed on the shaft. Similar seals installed on
the shaft failed during the testing.

Each of the successful seals was used in the development units.
The flat wire spring support seal was used in the geometry act-
uator and the fluorosilicone supported version in the fluid
controller. No problems were experienced with either seal.

Actuator Performance

The geometry actuator design schedule of guide vane position
vs corrected gas generator speed is shown in Figure 29. On the
same figure is X-Y Plotter data from closed-loop steady-state
testing; Figure 30 shows closed-loop transient test data. This
data was obtained using a torsional loading fixture which pro-
vides a frictional and aerodynamic load such as will be en-
countered on an engine. The maximum load was set at 70 in./lb.
The results indicate that the accuracy meets the ± 1/2 degree
requirements. The transients test results indicate increased
hysteresis. This was determined to be caused by a loose test
fixture which supported the potentiometer used for sensing
output position in this test.

Figure 31 shows the fail-safe system design schedule along with
predicted limits of operation. Also plotted in this figure are
the high stress and stall region limits of the engine. As
shown, the fail-safe schedule will allow the engine to operate
over the full speed range without encountering high stress or
stall conditions. Test data on this system at room temperature
was within the limits shown in the figure, but hysteresis and

55
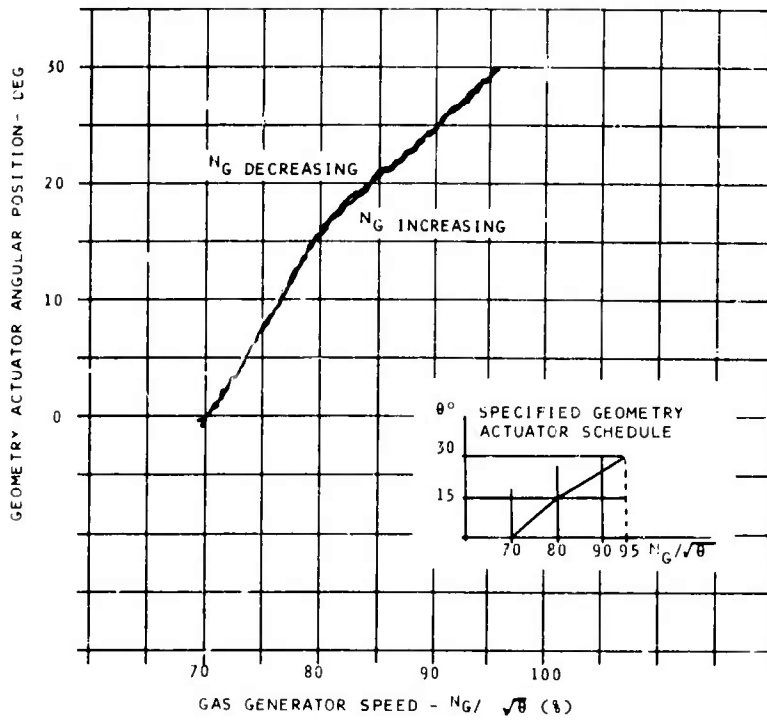
Figure 29.   Geometry Actuator Steady-State Performance.
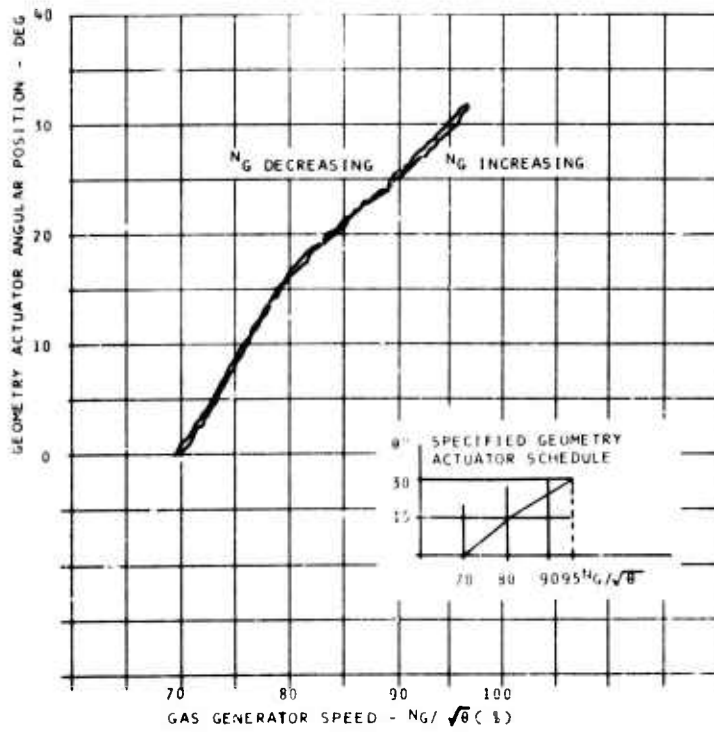
Figure 30.   Geometry Actuator Transient Performance.

56
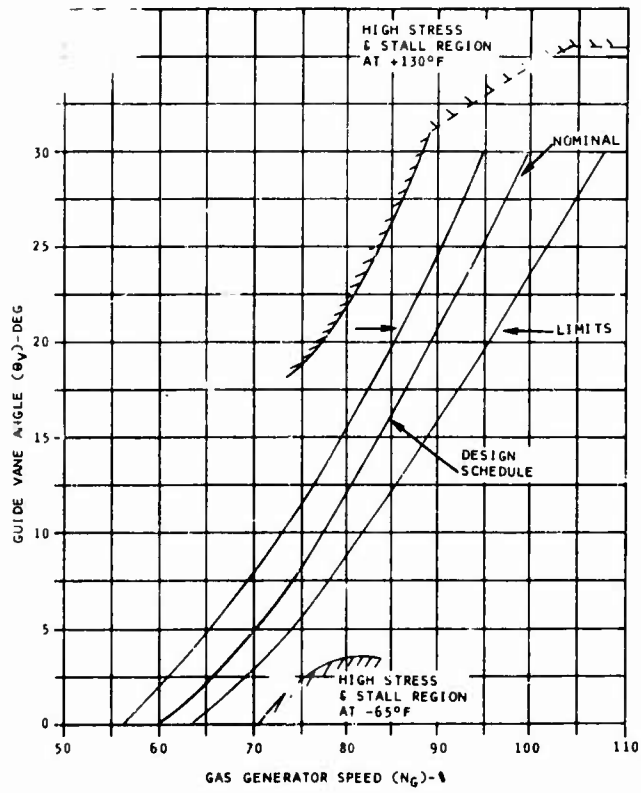
Figure 31. Geometry Actuator Backup Control Requirements.

repeatability errors were such that the actuator would not stay
within these limits over the entire operating envelope. This
condition was traced to the ballscrew. The ballscrew exhibits
a random tendency to jam at arbitrary positions under the re-
verse load it experiences in the backup mode. Increasing the
speed sufficiently would break the jam, allowing the system to
schedule properly.

The present ballscrew features an internal return mechanism for
transferring the balls from the end to the beginning of their
track. The jamming problem appears to be caused by this method
of return. An external return ballscrew would most likely
solve the problem.

Endurance Testing

During the hot day mission profile testing, the hot air nozzle
used to heat the environmental box was inadvertently located
adjacent to the IGV stepper motor electrical drive cable. To
achieve an ambient temperature of +250°F in the environmental
box, the hot air nozzle inlet temperature had to be set at
500°F. The heat from the nozzle caused a short circuit in the
IGV cable which resulted in a failure in the IGV stepper motor
driver. Due to the extensive testing still remaining to be run
on the pump and fluid controller in the time left in the pro-
gram, the IGV stepper motor driver was not repaired. The IGV
actuator was operating in the backup mode for 80 hours during
the Hot and Room Temperature Endurance Cycling. Because of the
problem with the ballscrew, the actuator did not continually
cycle. However, not much was lost because a comprehensive en-
durance test had already been conducted on the shaft seals and
a new ballscrew design was required. Also, the stepper motor
and resolver were evaluated within the fluid controller.

The geometry actuator described herein satisfies the require-
ments established for the advanced generation of gas turbine
engines. A preliminary layout of the production configuration
is shown in Figure 32. Further development on the ballscrew
is required to improve the performance of the backup system.
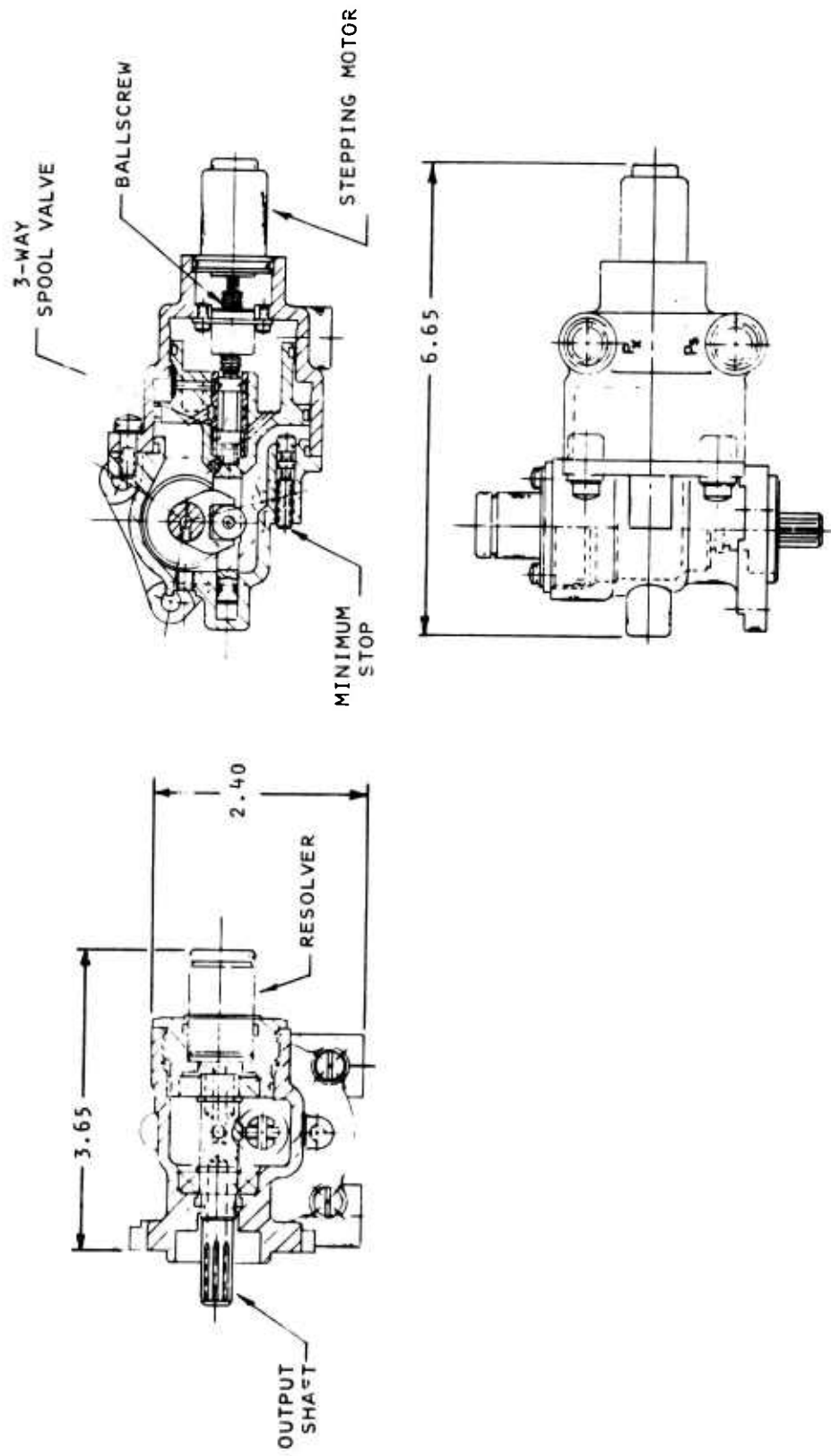
Figure 32. Geometry Actuator Layout.

59

FLUID CONTROLLER

The object of this program was to provide a control system
which could be applied to a wide range of engine sizes, and
also satisfy the requirements for reliability, maintainability,
small size, high contamination resistance, and low cost. Flex-
ibility can be achieved by providing electronic computations
and sensing. The fluid controller then has to be capable of
providing a wide range of fuel flow and pressures with only
small modification to meet requirements for various engines.

With this objective in mind, three fluid control systems
evolved for evaluation. The main component in each system is
the pump; the other systems components, which are required to
control, are fundamental and of the same type hardware. The
three systems which were evaluated include:

1. A centrifugal pump and throttling type fuel metering
    system as shown in Figure 33.

2. A variable displacement vane pump and pump control
    system as shown in Figure 34.

3. A gear pump and by-pass type metering system as shown
    in Figure 35.

Each of these systems was considered because it had advantages
in specific areas. The centrifugal pump system was expected
to have good contamination-resistance potential for very high
speed and it is relatively simple. The variable vane pump
system offers low fuel temperature rise and fewer system com-
ponents. The gear pump system was considered primarily because
it is the conventional concept. It has no known advantages in
contamination resistance or high speed.

The basis for comparison was mainly between the centrifugal
pump system and the variable displacement vane pump system,
knowing that if major problems were experienced, the gear pump
system could always be used.

Centrifugal Pump System (Figure 33)

A high speed (37,500 rpm) centrifugal pump is used to provide
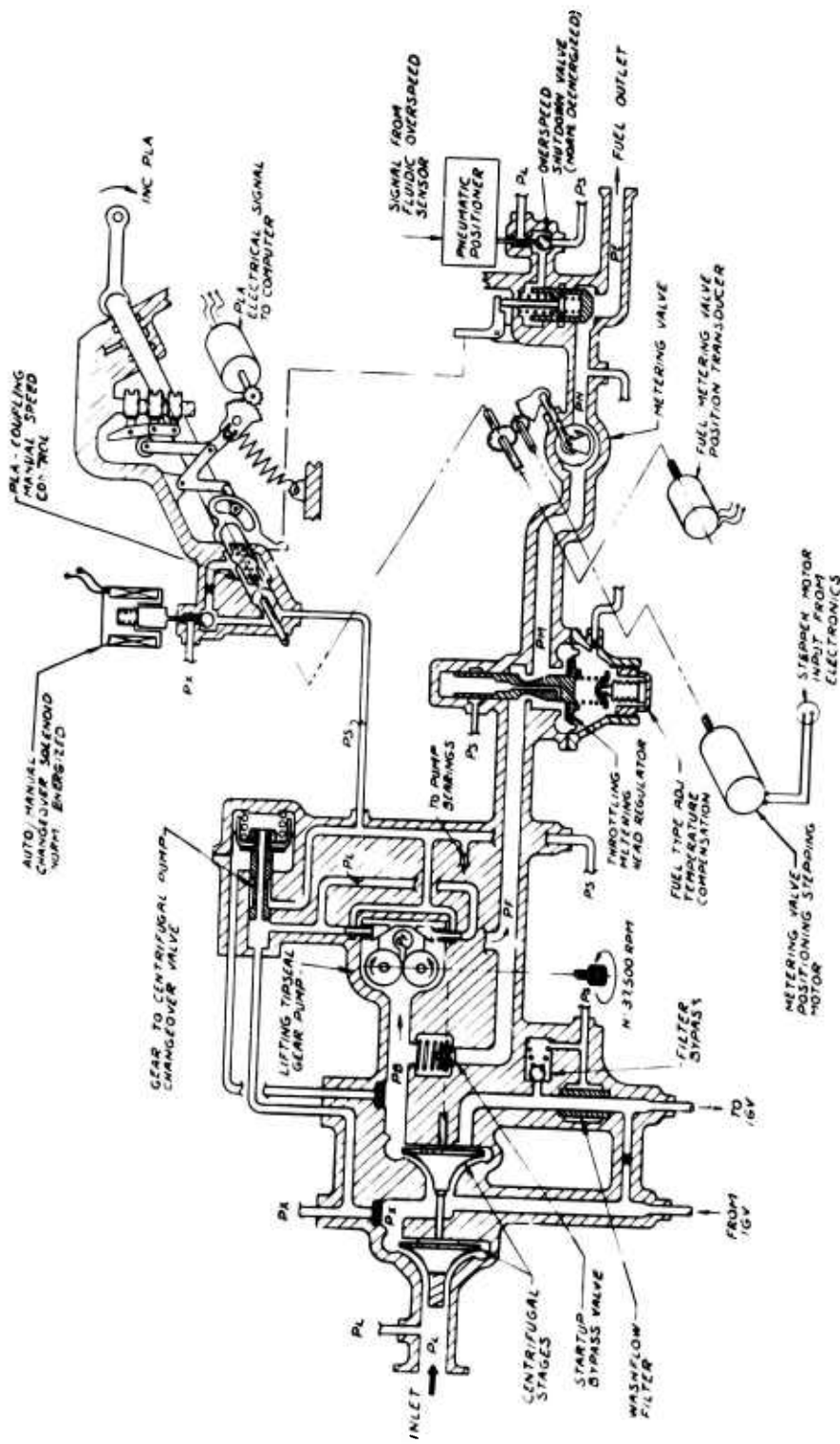
Figure 33. Centrifugal Pump System.

61
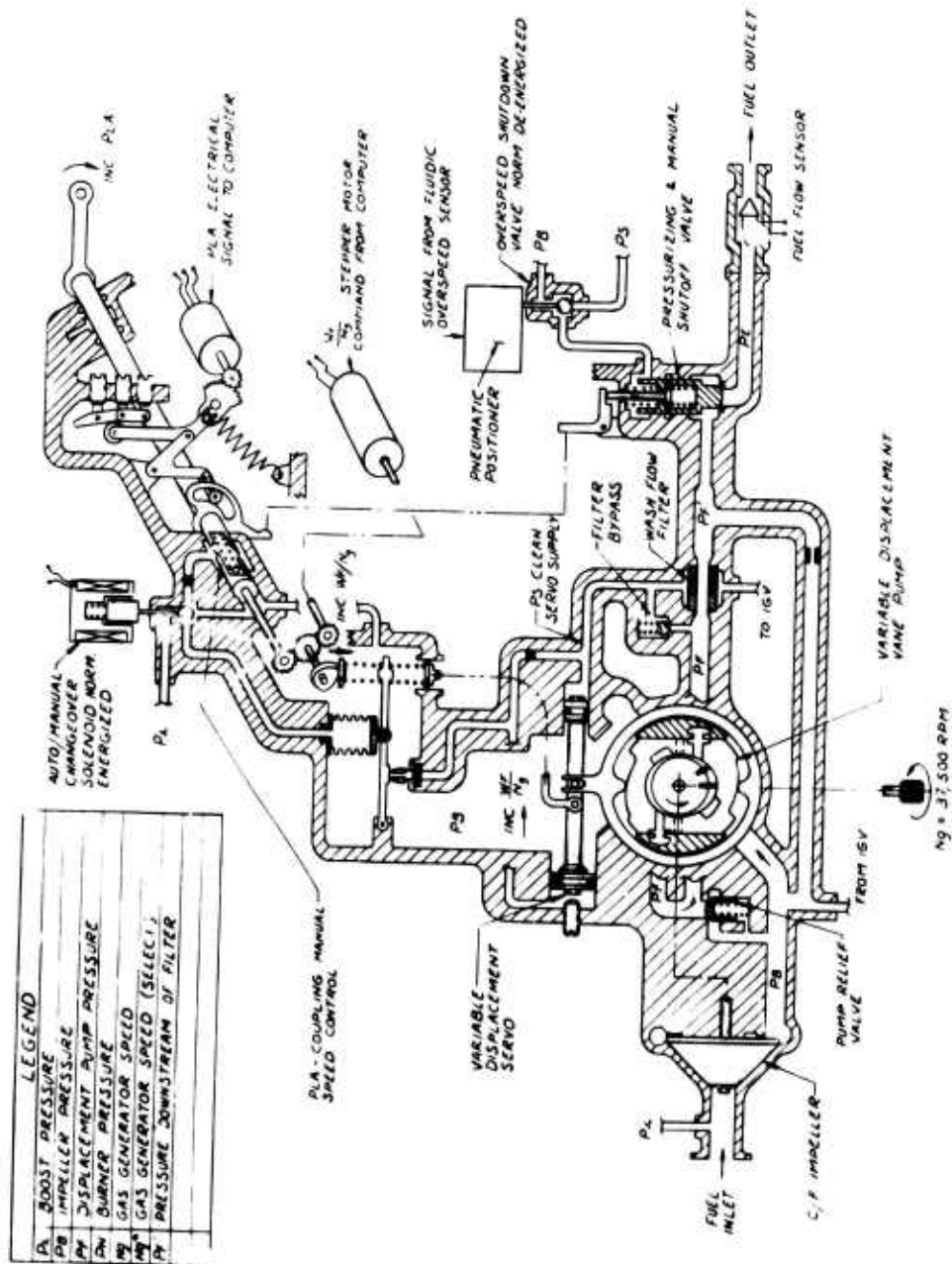
Figure 34. Variable Displacement Vane Pump System.

62

PLA LEVER DIRECTLY COUPLED TO
POTENTIOMETER ENGAGES METERING
VALVE ON MANUAL CHANGEOVER
COMMAND

PLA TRANSDUCING POTENTIOMETER
OUTPUT TO ELECTRONICS

MANUAL CHANGEOVER SOLENOID
AND DETENT MECHANISM
NORMALLY ENERGIZED
DE-ENERGIZE TO CONNECT
POWER LEVER TO METERING
VALVE

OPTIONAL
MASS FLOW SENSOR
OUTPUT TO ELECTRONICS

STEPPER MOTOR
INPUT

SHUT OFF SOLENOID
INPUT FROM COCKPIT SWITCH
AND/OR ELECTRONIC
OVERSPEED/TEMP TRIP

SHUTOFF
VALVE

METERING
VALVE

WASH FLOW
FILTER

BYPASS REGULATOR
WITH INTEGRAL RELIEF
VALVE

DISCONNECT SWITCH
NORMALLY ENERGIZED
DE-ENERGIZE TO BREAK
ON MANUAL
CHANGEOVER

N_1 = 97,500 RPM

POSITIVE DISPLACEMENT
CONTAMINANT RESISTANT
PUMP STAGE

CENTRIFUGAL
STAGE

STEPPER
MOTOR

Figure 35.   Gear Pump and Bypass System.

63

the pressure and flow to the engine for steady-state operation.
A tip sealed gear pump is provided for engine starting since a
centrifugal pump is not capable of priming itself. The block
used for sealing the tips of the gear pump is held in position
by pressure from a changeover valve. A pressure speed signal
from the centrifugal pump outlet actuates the changeover valve
so that at just below engine idling speed the gear pump tip
seal is unloaded and thereafter the system operates on the
centrifugal pump. This arrangement ensures maximum contami-
nation resistance of the pumping system since the gear pump is
windmilling during normal operation.

Metering of fuel flow is accomplished by a rotating plate valve
and a throttling head regulator. The metering valve is rotated
by a stepping motor through a gear reduction. The stepping
motor receives commands from the electronic computer.

A manual system is provided which connects the pilots input
directly to the metering valve. The connection is made by a
mechanical link when the changeover solenoid is de-energized.
Therefore, in the event of a power failure the system changes
automatically to the manual system.

Variable Displacement Vane Pump System (Figure 34)

Engine flow and pressure is provided by a high-speed variable
displacement vane pump. For a given vane displacement, flow
is proportional to pump speed. The vane displacement is con-
trolled by rotation of a ring which forces the vanes into and
out of the rotor by cam surfaces. The rotation of the ring is
determined by a force balanced electrohydraulic actuator which
is controlled by the electronic computer. Fuel mass flow is
fed back to the computer from a flow sensor in the outlet fuel
line.

A fairly sophisticated manual backup system is provided which
provides closed-loop gas generator speed control. Upon de-
energizing the changeover solenoid, the pilots input is mech-
anically linked to the flapper servo linkage and compared to a
pressure speed signal from the impeller. The resulting force
error moves the flapper valve to control the pump displacement
and thereby provides proportional gas generator governing.

A nonlinear analog simulation of the variable displacement
vane pump system was done to optimize bellows sizes and lever

64

ratios. Also it was necessary to analyze the effect of positive feedback produced through the pump speed loop with this flow control mode.

Trade-Off Studies

Based on a design layout of each fuel control system, a trade-off study was conducted. The results of this study are summarized in Table IX. The main findings were that the centrifugal pump system would weigh 29% less and be 37% lower in cost and have the potential of a much higher pump speed. The cost and weight difference is due mainly to the high machining time and weight of the variable displacement vane pump. Based on these results, it was decided to select the centrifugal pump system as the baseline fluid controller.

Barstock Testing

After the decision had been made to use the centrifugal pump system, all the fuel-metering components involving a technical risk were made in barstock form and tested.

These components were:
1. Main metering valve.
2. Metering head regulator.
3. Wash flow filter.

Main Metering Valve

A fixture was made to test the rotating plate valve concept. Various combinations of valve material were tested. The material which was best for weight and contamination resistance was aluminum with the wear surfaces hard coated. Test results showed that a rotating plate valve had very good contamination resistance, was excellent for metering low fuel flows, and required a low torque to drive it.

Metering Head Regulator

A metering head regulator was tested which represented the design required for the baseline control. The design included damping flow force compensation and force amplification by using a diaphragm. The test results are shown in Figure 36, which shows the effect of redesigning for flow force compensation. The drop in metering head with increasing fuel flow is acceptable because it can be compensated for in the main metering valve contour.

65

TABLE IX.	COMPARISON OF FLUID CONTROLLER SYSTEMS	
Parameter	Centrifugal Pump System	Variable Displacement Vane Pump System
Simplicity	More components, but requires conventional manufacturing techniques. All fluid interconnections permit dense package.	Fewer components, but requires sophisticated manufacturing techniques. Force balance servo systems create larger package.
Present-day cost ratio	1.00	1.37
Present-day weight ratio	1.00	1.29
Growth to higher engine speeds (37,500 rpm current)	May be extended higher.	Limited by available material combinations.
Overall pump efficiency (projected)	15%	40%
Fuel temperature rise	90°F at 450 pph and 850 psi.	28°F at 450 pph and 600 psi will permit greater turndown at 100% speed.
Manual system	Direct metering valve coupling.	Incorporates a simple closed-loop gas generator speed control system.
General remarks	Can be demonstrated using present-day technology. Advances directed toward improved materials and packaging for lower cost and weight.	Requires development of manufacturing techniques and a control-mounted fuel flow sensor to ensure a competitive position.
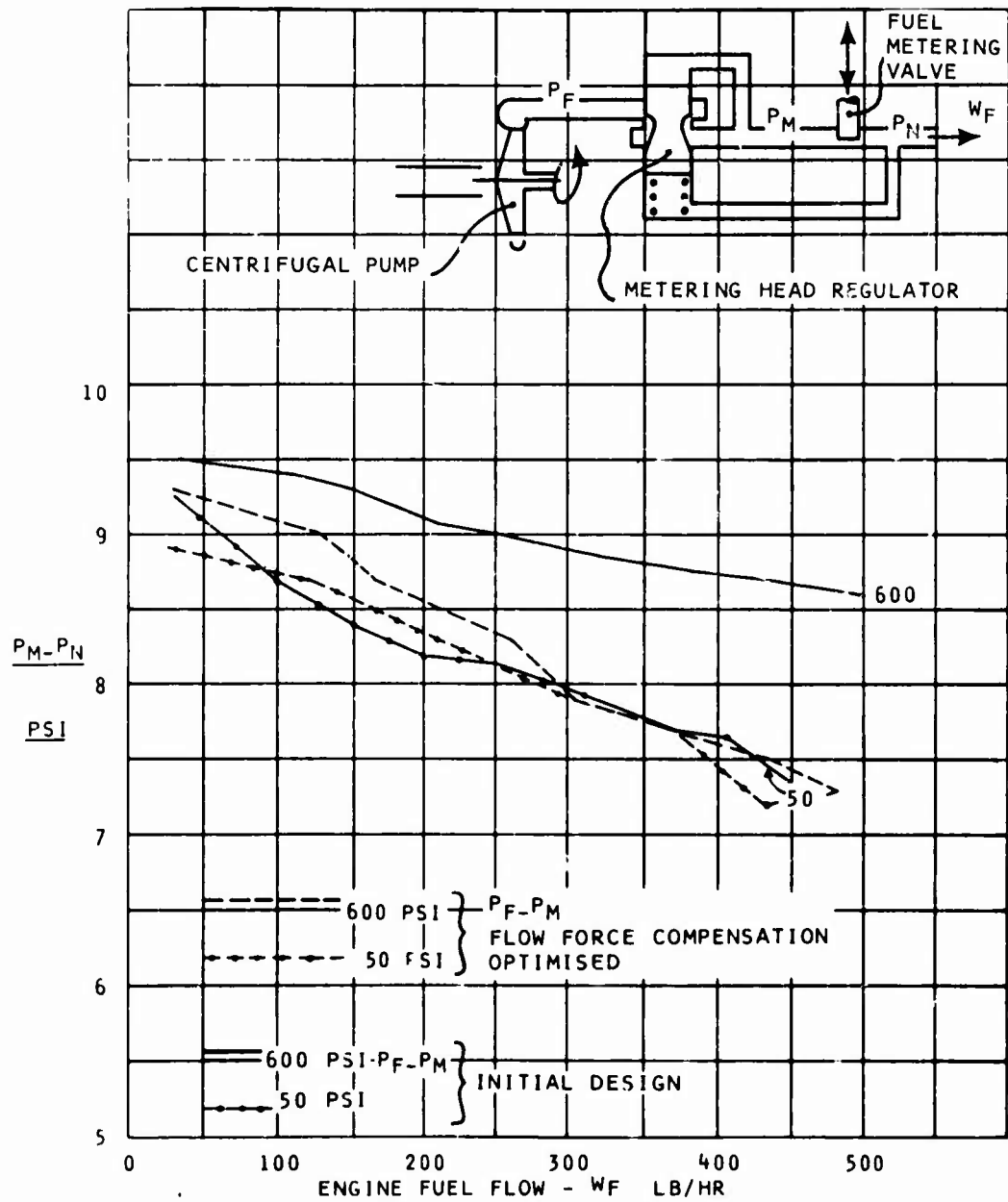
Figure 36.   Metering Head Regulator Performance.

Wash Flow Filter

Many types of filter material and different geometric configurations were evaluated in an attempt to develop a wash flow filter for the baseline control. It was found, however, that for a wash flow filter to operate effectively, the through flow must be 3 or more times greater than the filtered flow. Because of this limitation in operation, it was not possible to use a wash flow filter. Therefore, it was necessary to use a barrier filter for providing clean flow to the pump bearings and metering head regulator wash flow. The small amount of filter flow required results in a reasonably small barrier filter.

Baseline System

The baseline system resulted from in-house design studies and suggestions made by a survey of Army, airframe and engine manufacturers' requirements. The findings affecting the fluid controller design philosophy included:

It is required that the pilots input be mechanical since for an electronic control it is necessary to provide a positive mechanical fuel shutoff.

A mechanical manual system is required, and it is preferable that in the event of an electrical failure the control should automatically change smoothly to the manual system.

To protect against destructive turbine overspeed due to a sheared load shaft, an independent proportional power turbine overspeed governor is required.

System Description

A schematic of the baseline fluid controller is shown in Figure 37.

Fuel enters the control, and passes through a conical inducer. From the inducer the flow then splits, with a small amount of flow being diverted through a heat exchanger for cooling the electronic computer, the remaining flow passes through a check valve to a single-stage centrifugal impeller. The check valve maintains a constant flow through the heat exchanger. The centrifugal impeller was sized to suit a high-pressure burner

68
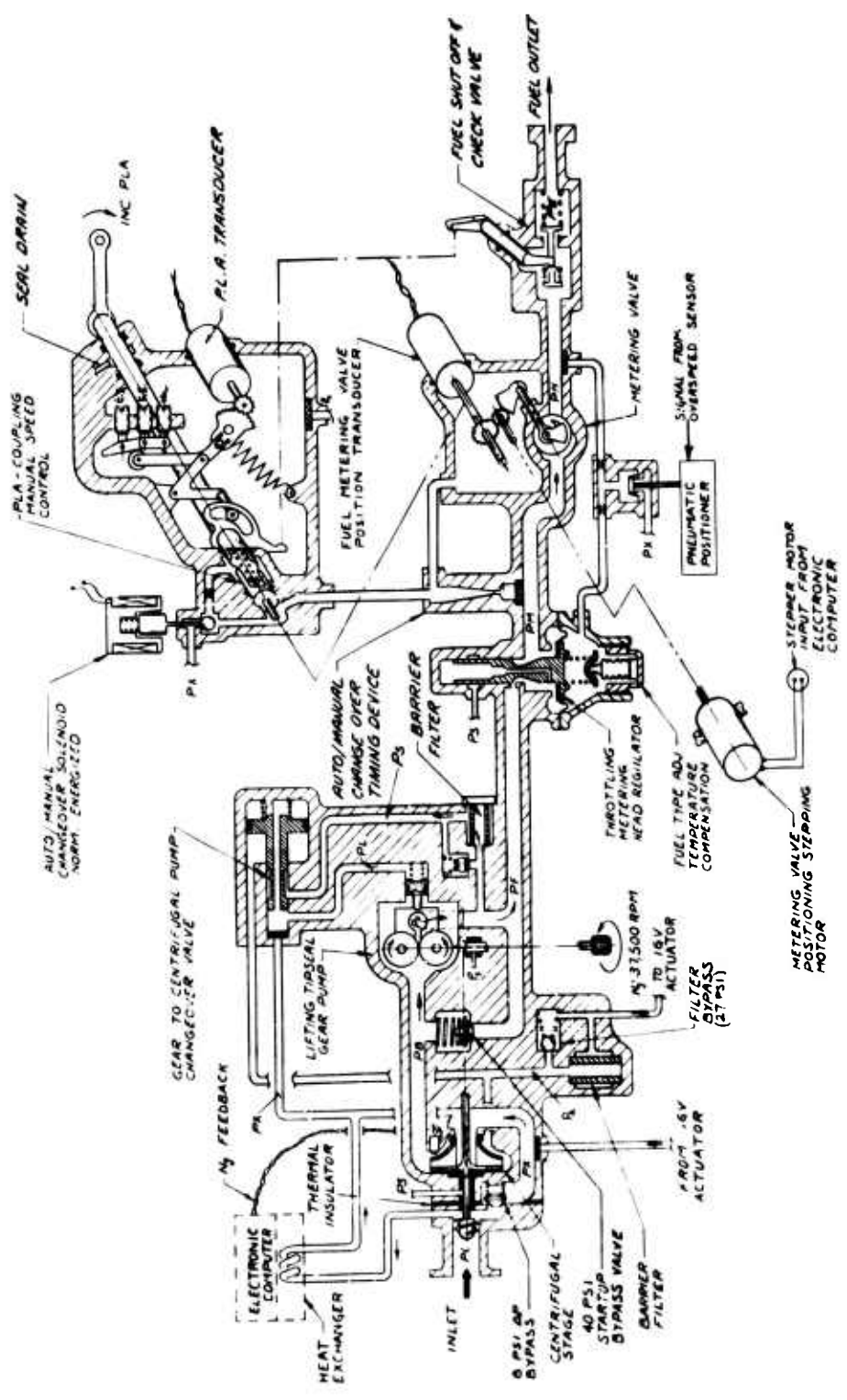
Figure 37. Baseline Fluid Controller.

system (850 psi at 37,500 rpm) since a low-pressure system is easier to achieve from packaging and fuel temperature considerations.

The fuel then enters a tip-sealed gear pump, which during normal engine operation (idling to maximum) has the tip loading block withdrawn so that the gears windmill. This allows the pump to have maximum contamination resistance. For starting, the tip loading block is held on the gears by fuel pressure which is controlled by the pump changeover valve. The changeover valve is actuated by outlet pressure from the centrifugal pump. It is arranged that the changeover from the gear pump to the centrifugal pump takes place below engine idling speed so that there is no discontinuity in pressure or flow during normal engine operation. During engine starting, fuel flow in excess of engine demand is by-passed to the gear pump inlet by a start-up by-pass valve.

Fuel mass flow is controlled by a rotating plate metering valve in conjunction with a throttling head regulator. A feature of using a throttling head regulator is that variation in pressure drop with fuel flow can be compensated for with the metering valve area. The lowest practical metering valve pressure drop was used to maximize the metering valve area. This allows maximum contamination resistance. The metering head is manually adjustable for fuel type and is compensated for fuel temperature. The area sensing the metering head was determined by considering steady-state accuracy, transient response, and contamination requirements.

The rotating plate type of metering valve provides good contamination resistance and can be made to have negligible leakage. This was demonstrated during barstock testing. The metering valve is driven through a gear reduction of 122/1 from a stepping motor; this is required to give the necessary resolution and torque amplification. The metering valve area is exponential for most of the flow range; this allows constant flow sensitivity or constant percentage of point change in fuel flow for one step of the stepping motor. To allow good transient response and accurate governing, the stepping motor is driven in 15° steps for transients and 7.5° steps for governing. Fuel flow feedback to the computer is provided by a resolver giving metering valve position.

A manual system is provided by a mechanical link between the

pilot's input and the metering valve. A solenoid controls the fuel pressure on the piston; if the solenoid is de-energized, the piston moves toward the pilot's input shaft. The end of the piston has a cam surface which, on contact with the input shaft, causes the piston to rotate. The piston is geared to the metering valve, hence rotation of the piston causes fuel flow to change. This mechanism ensures that in the event of an electrical failure, the metering valve automatically aligns itself to the pilot's demand. The rate of change of fuel flow is a function of the piston velocity and the cam contour. The baseline system was designed to have the piston velocity held constant by a cavitating venturi. The transition from automatic to manual can be made to give a compromise acceleration schedule from S.L. to 5000 ft, where failure of the computer would be most hazardous.

The pilot's input schedule is provided by rotation of a lever; the schedule is given in Figure 38. Rotation of the power lever is converted by levers and gears to rotation of a resolver, which sends the input command to the computer. Independent adjustments are provided for ground idle, flight idle and military. Emergency setting is increased or decreased by the same as adjustments made to military.
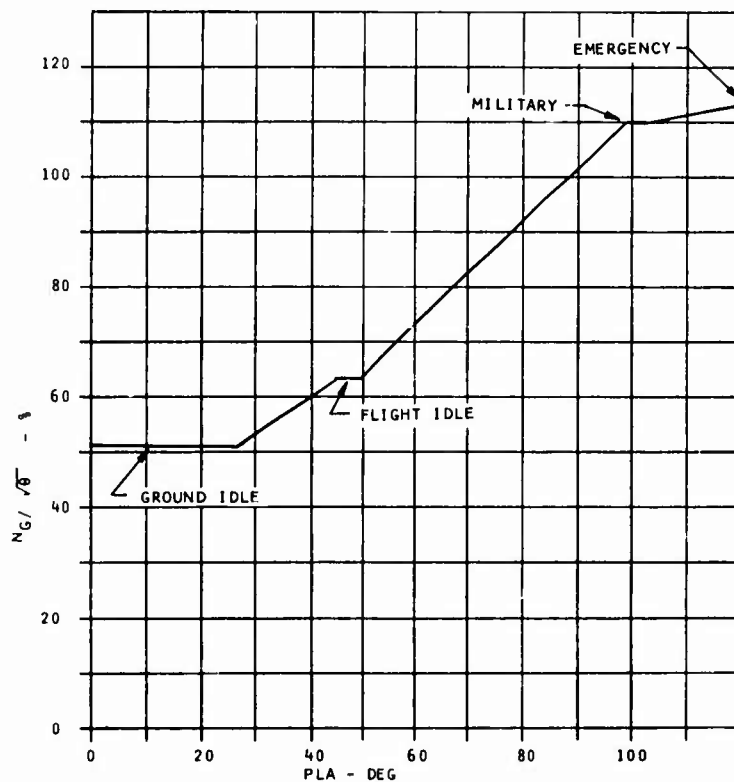
Figure 38. PLA Schedule.

71

A proportional power turbine overspeed governor is incorporated in the control. Power turbine speed error is converted to a pressure signal which is used to vary the head across the metering valve.

System Manufacturing

The baseline system was made with no particularly difficult manufacturing problems. Figures 39 and 40 show the main components of the fluid controller.

Package Design and Mock-Up

Installation designs were submitted to Army, airframe, and engine manufacturers for review. The application considered was for a twin-engine helicopter. The designs incorporate the following suggestions, which were made as the result of the review:

1. The electronic computer should be mounted on top of the fluid controller so that the accessory gearbox can be used for other accessories.

2. All adjustments should be accessible from the front of the engine (ground idle, flight idle, military and head regulator).

3. The PLA lever should be at the front of the control rotating side by side, to suit twin- or single-engine installation.

4. The fuel outlet should be directed toward the combustion chamber.

5. The barrier filter should have a "pop out" device to indicate when the element should be changed and be accessible from the front of the engine.

6. All electrical components and harnesses between these components and the computer should be between the accessory gearbox and the control to decrease vulnerability.

Figure 41 shows a front engine view of a mock-up of the control and reflects compliance with the above suggestions.

72
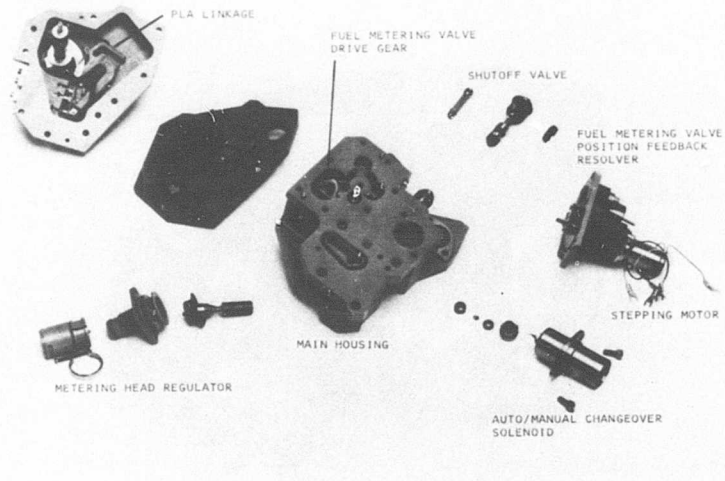
Figure 39.   Disassembled View of Fluid Controller
             (Left Side).
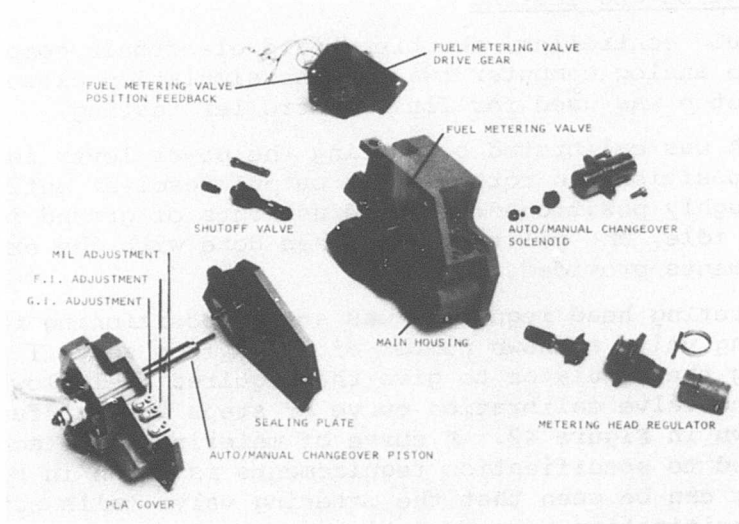
Figure 40.   Disassembled View of Fluid Controller
             (Right Side).

73

ELECTRONIC COMPUTER

METERING HEAD REGULATOR

COMPUTER/FLUID CONTROLLER
CONNECTOR

PCD   TB

ENGINE/AIRFRAME
CONNECTOR

FUEL OUTLET

PLA

FILTER CRITICAL
ΔP INDICATOR

BARRIER FILTER

FUEL INLET

G.I., F.I., MIL
ADJUSTMENTS

2 3 4 5 6 7 8 9 10 11 12

1-FOOT SCALE
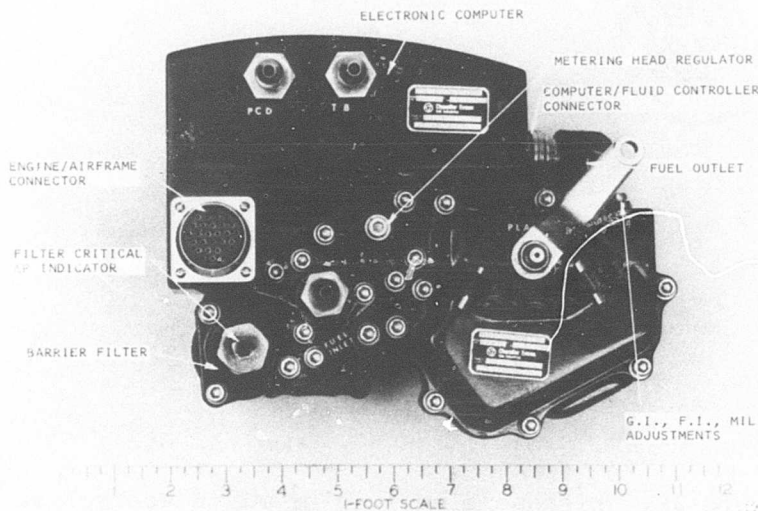
Figure 41. Advanced Engine Control Mock-Up.

Calibration and Testing

The fluid controller, the breadboard electronic computer, and the analog computer twin-engine simulation closed-loop test setup was used for fluid controller testing.

The PLA was calibrated by putting the power lever in a fixed position and rotating the output resolver until it was roughly positioned; fine adjustments of ground idle, flight idle, and military were then done with the external adjustments provided.

The metering head regulator was set by positioning the metering valve a known number of steps from shutoff and adjusting the regulator to give the required fuel flow. A metering valve calibration curve of steps against fuel flow is shown in Figure 42. A curve of metering valve accuracy compared to specification requirements is shown in Figure 43. It can be seen that the metering valve falls within the specification requirements.

74
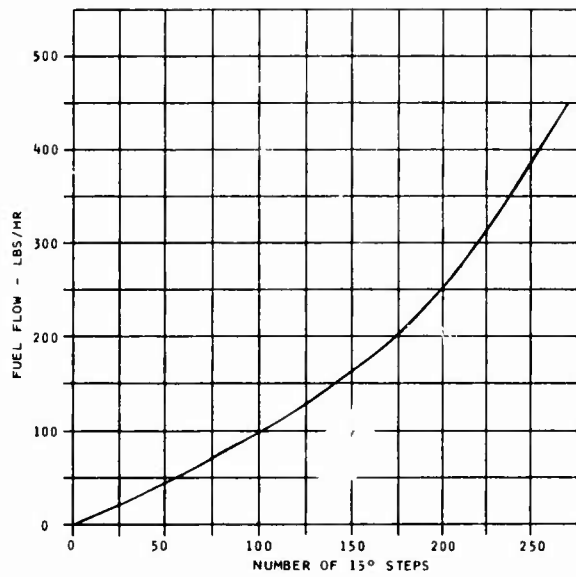
Figure 42.   Metering Valve Calibration Curve.
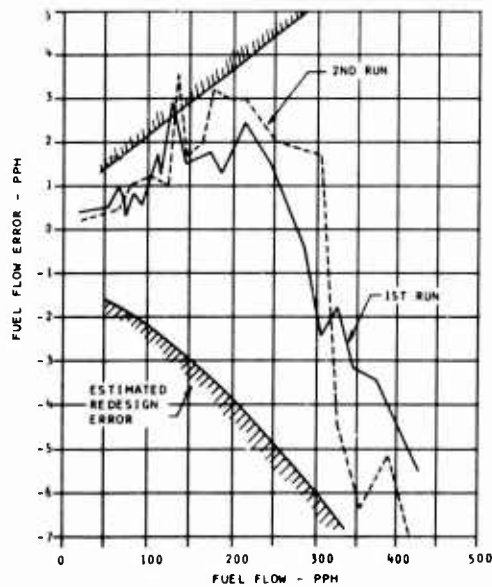
Figure 43.   Fuel Metering Accuracy.

75
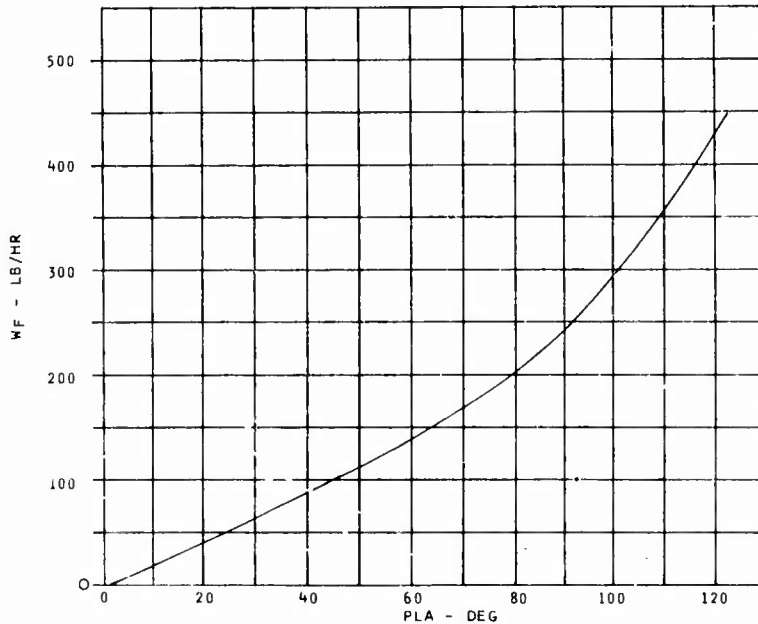
Figure 44.   Manual System Calibration.

The metering valve position is correlated with the feedback signal by rotating the resolver to give the correct output.

The system is very simple and easy to calibrate, requiring only the adjustments of two resolvers and a head regulator.

A fuel flow calibration curve for the manual system is shown in Figure 44.   This calibration is by internal components and is not externally adjustable.

The metering head regulator transient response was determined on manual flow control by a step input applied to PLA (which on manual is connected directly to fuel metering valve).   The fuel flow response for small step changes in PLA can be approximated by first order lag with a measured time constant of 25 ms. Test results are shown in Figure 45.   The 60-Hz ripple on both the input and output signals is line frequency interference. The specified response was 60 ms or less based on simulation studies.   Therefore, the transient performance of the head regulator is satisfactory.

The transient performance during a change from automatic to manual control is shown in Figure 46. This demonstrates that the time delay principle works satisfactorily. However, no attempt was made to approximate an acceleration schedule. This can be done by changing the cam surface of the changeover piston. The cam profile used to demonstrate the principle was a simple helix.
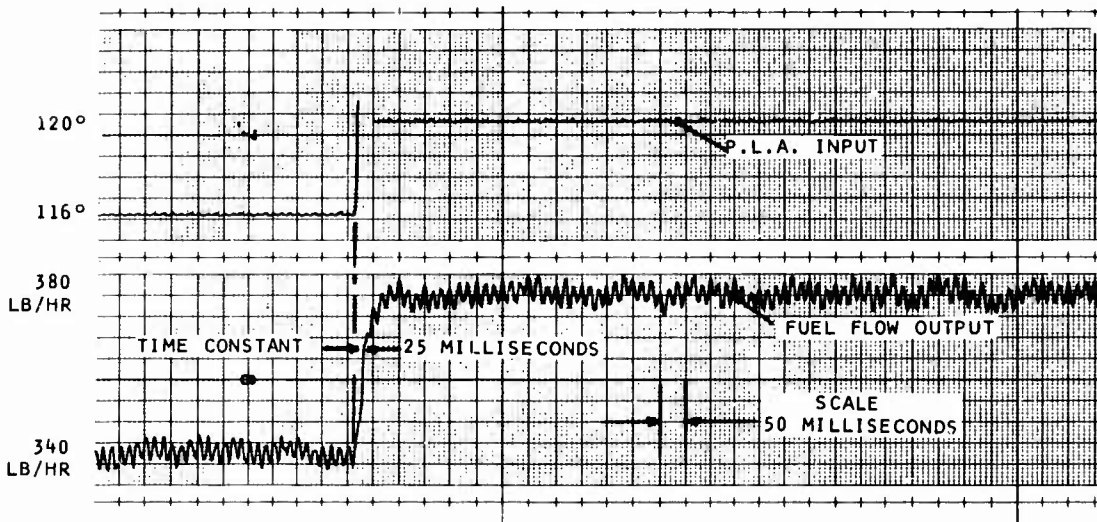
Figure 45. Metering System Transient Response.
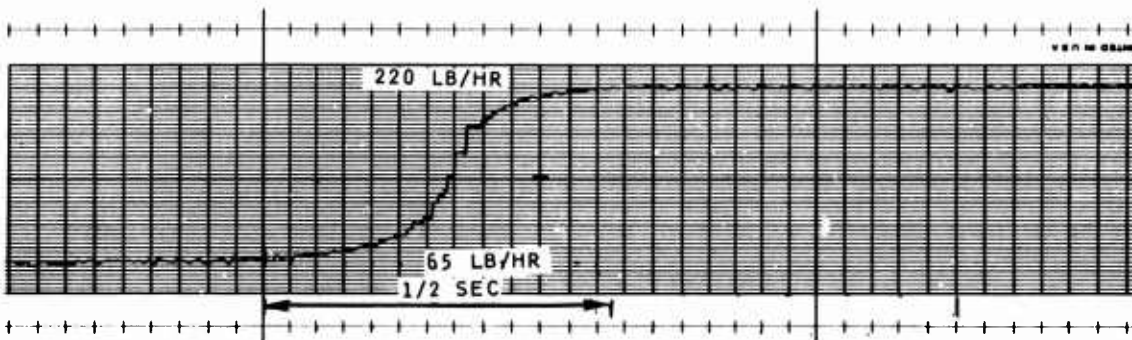
Figure 46. Automatic to Manual Changeover.

77

The system calibration was followed by closed-loop testing to
establish the steady-state and dynamic performance of the con-
trol in conjunction with the engine simulation.

Endurance Testing

The final phase of testing was to evaluate the endurance of
the fluid controller and demonstrator electronic computer by
cycling the complete system with a Hewlett Packard computer.
The endurance test setup is shown in Figures 47 and 48. The
following endurance testing was completed:

Hot Day Mission Profile   - 3 cycles completed, 3 hr/cycle

Room Temperature Endurance - 30 hr

Hot Day Endurance   - 50 hr

Cold Day Endurance   - 20 hr

Contamination Testing   - 18 hr

The total running for the program of the baseline fluid con-
troller (including pumps) was 277 hrs.

The fluid controller was disassembled after completing the en-
durance test and was found to be in good condition. The met-
ering valve and head regulator showed good resistance to wear.
Figure 49 shows the metering valve and head regulator after
contamination testing which was the last phase of testing; the
wiping action of the metering valve in removing dirt can be
seen.

Pump Selection

The requirements for an advanced fuel pumping system for a 2-
to 5-lb/sec engine size can be divided into two categories:

Category I   Requirements common to all aircraft
               fuel pumps.

V/L capability - The ability to pump with a two-phase
fluid at the pump inlet.
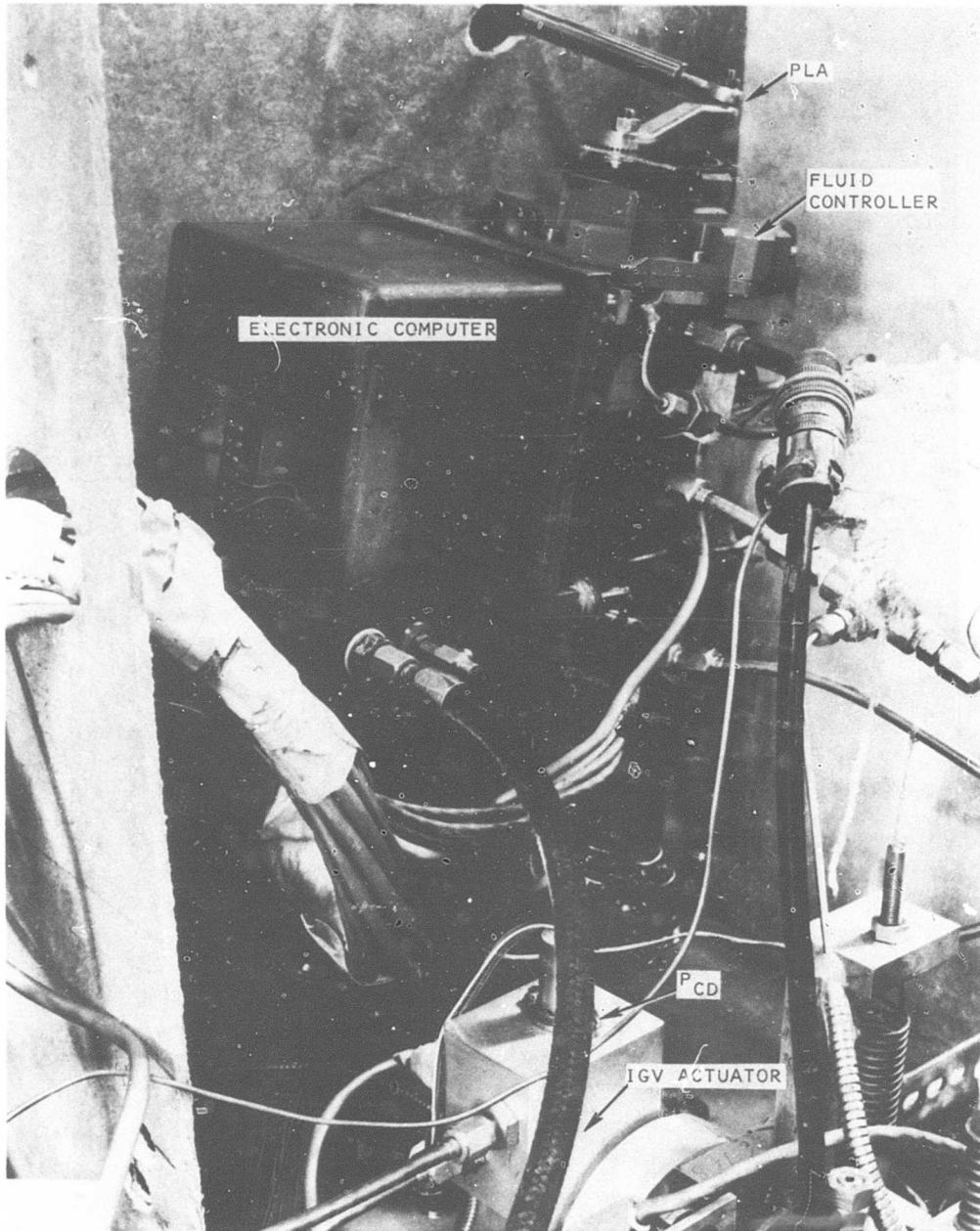
Figure 47.   Endurance Test Setup.

79
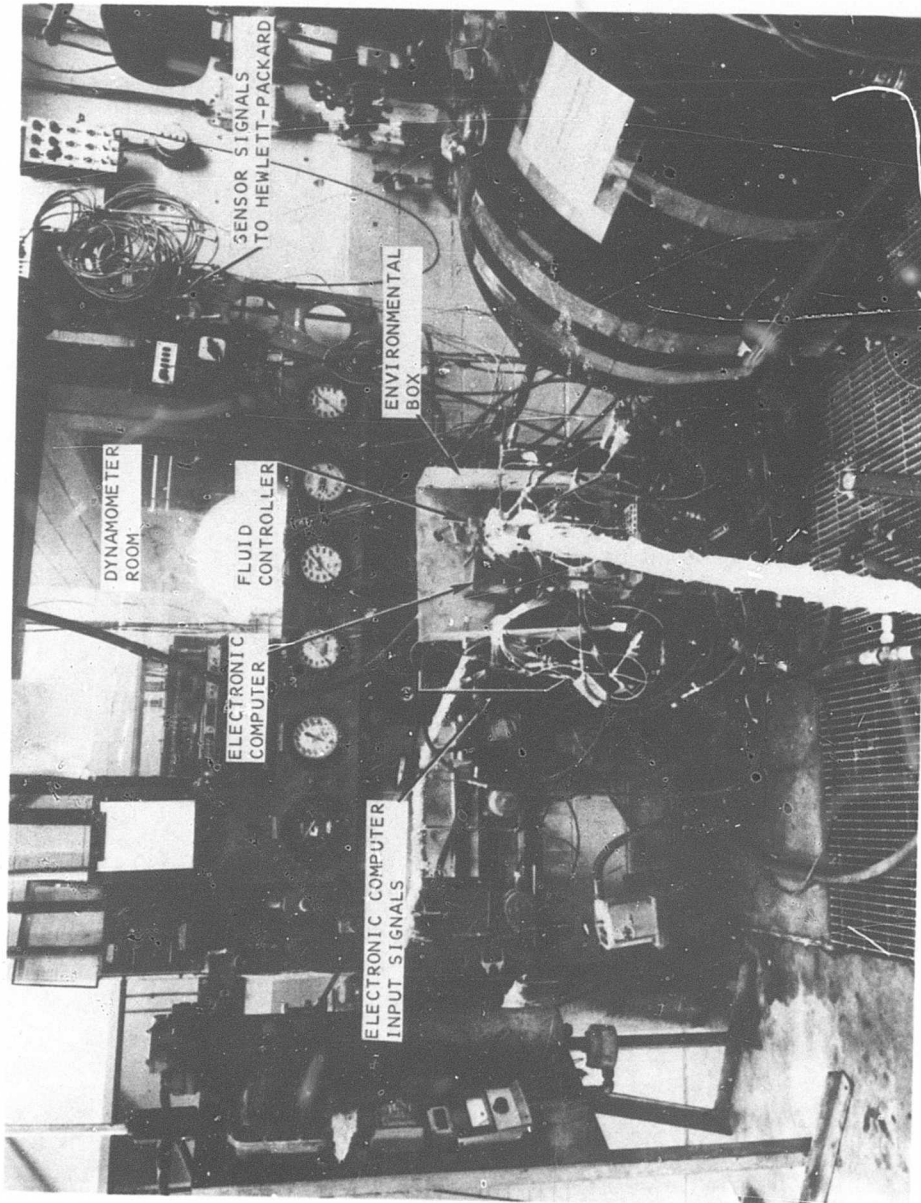
Figure 48. Endurance Test Setup.

80
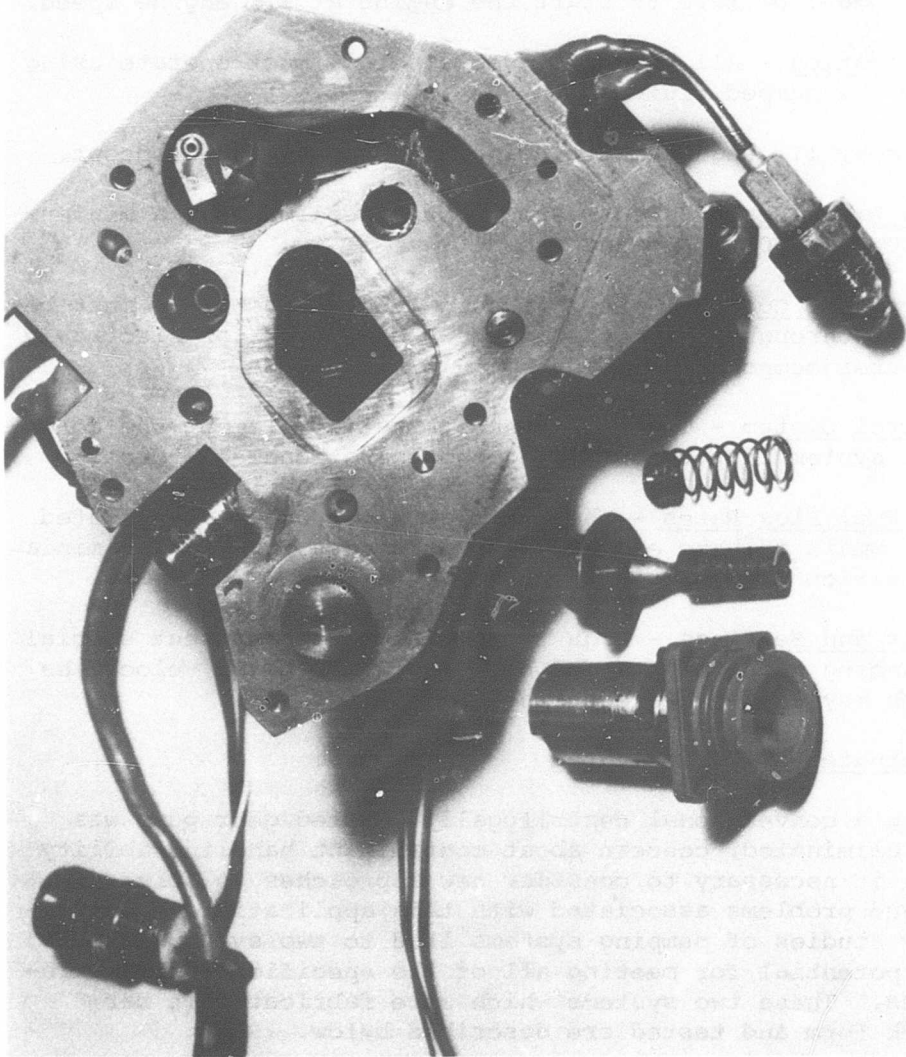
Figure 49. Control Hardware After Endurance Tests.

Contaminated Fuel - The pump must operate without excess performance degradation on contaminated fuel per MIL-E-5007C.

Dry Lift - The ability to self prime from a low fuel supply without assistance.

Starting - The pump must supply fuel at required pressure rise and flow rate to start the engine at 10% engine speed.

Lubrication - All bearings, seals, etc., must operate using only the pumped fluid.

Category II   Requirements unique to this control concept.

High Drive Shaft Speed - Pump input speed must be a minimum of 50% to 100% of engine speed.

Electronic Cooling - Fuel at pump inlet temperature must be pumped through the electronic heat exchanger for electronic computer component cooling.

Control System - The pump concept must complement the control system in both packaging and operational features.

Low Fuel Flow Rates - The low flow requirements associated with small turbine engines present unique problems of miniaturization of pumping elements.

Seals and Bearings - High rotational speeds present special balancing requirements and high surface rubbing velocities which may exceed state-of-the-art limitations.

Alternate Design Evaluated

While a conventional centrifugally boosted gear pump was not eliminated, concern about contaminant handling ability made it necessary to consider new approaches to solve the unique problems associated with this application. Preliminary studies of pumping systems lead to two systems which had potential for meeting all of the specification requirements. These two systems which were fabricated in bar stock form and tested are described below.

82

Centrifugal Pump

This pumping concept is a centrifugal main stage with a lifting tip seal gear pump for starting. Contamination handling ability is assured by the contamination resistant main stage used for all operating conditions except starting. The lifting tip seal gear pump is unloaded at idle and higher speeds and is therefore not subject to contamination under pumping conditions. An axial inducer mounted in the main stage inlet served as a boost pump and a source of cooling flow for the electronic package.

Design conditions for the pumping elements were:

	Starting Stage		Main Stage	Boost Stage
Δpsi	40		400	8
flow	35 pph		700	700
RPM	3,750		37,500	37,500

The original main pump was a two-stage concept for providing 800 psi.

Dimensions of the pumping hardware are given below:

Starting Gear Stage

No. teeth	14
Gear O.D.	.40 in.
Gear pitch	40
Gear material	M2 Tool Steel
Journal dia	.193 in.
Gear width	.261 in.

Main Centrifugal Stage

Diameter	1.67 in.
No. vanes	3
Inlet vane angle	8°
Discharge vane angle	25°
Inlet dia	.62 in.

83

Boost Stage

Type	Axial
O.D.	.500 in.
Lub. dia	.295 in.
Lead	.250 in.
Degrees wrap	360°

A schematic of the pumping concept was shown in Figure 33.

This pumping system was designed and fabricated for test evaluation.

The test program conducted disclosed the following:

1. The lifting tip seal gear type starting pump successfully produced the starting flow required.

2. The tip seal unloaded smoothly and also reloaded the gears upon system shutdown.

3. The main pumping stage met its design conditions of 700 pph, 400 psi at 37,500 rpm.

4. Overall efficiency of the main stage was limited to 12% at design conditions by disc friction.

5. The axial inducer did not meet the required V/L conditions and did not perform well at suppressed inlet conditions.

Vane Pump

A balanced variable displacement vane pump provided both starting and main fuel flow for this system. A conical boost pump was used to provide V/L capability and charge the vane stage inlet. A photograph of the pumping components is shown in Figure 50.

To make use of available hardware, design conditions for the vane pump element were:

RPM	35,000
Fuel flow	1850 pph (max)
Δp	800 psi

84

Design Parameters-Variable Displacement Vane Pump

Vane tip velocity	100 ft/sec
No. vanes	14
Vane stroke	.014 in.
Rotor width	.850 in.
Rotor dia	.60 in.

Design Parameters Conical Impeller

Type	Conical (shrouded)
Core angle	45°
Outside dia	1.035 in.
Inlet dia	.340 in.
No. vanes	3
Lead	.2844 in.
Head coefficient	.44
Material	17-4
Specific speed	556 rpm
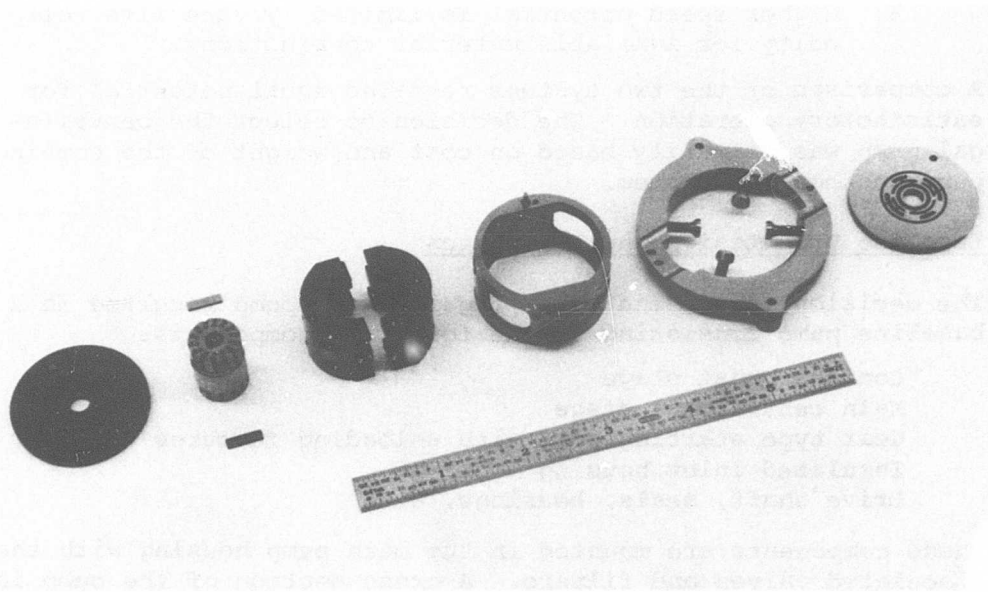
Figure 50. Variable Displacement Vane Pump.

85

Test evaluation of the vane stage demonstrated:

The variable flow capabilities of the vane stage.

Operation at 35,000 rpm.

Initially, poor volumetric efficiency was caused by vane "skip" on the pumping profiles. Increasing under vane pressure improved volumetric efficiency by reducing the vane skip.

Performance of the conical inducer demonstrated .45 V/L capabilities at 37,500 rpm.

Comparable performance with both stepped and straight vanes.

Sufficient test data was obtained to demonstrate that this pumping concept had the advantage of:

1. Higher overall efficiency.
2. Lower temperature rise.

The pump had the following disadvantages:

1. 37% more costly to manufacture.
2. 29% heavier.
3. Higher speed potential is limited by vane life velocity for available material combinations.

A comparison of the two systems revealed equal potential for satisfactory operation. The decision to select the centrifugal pump was primarily based on cost and weight of the combined pump and control system.

Baseline Pump Design and Evaluation

The decision to use the centrifugal system pump resulted in a baseline pump consisting of the following components:

Conical boost stage
Main centrifugal stage
Gear type starting pump with unloading features
Insulated inlet housing
Drive shaft, seals, bearings, etc.

These components are mounted in the main pump housing with the associated valves and filters. A cross section of the pump is shown in Figure 51.

86
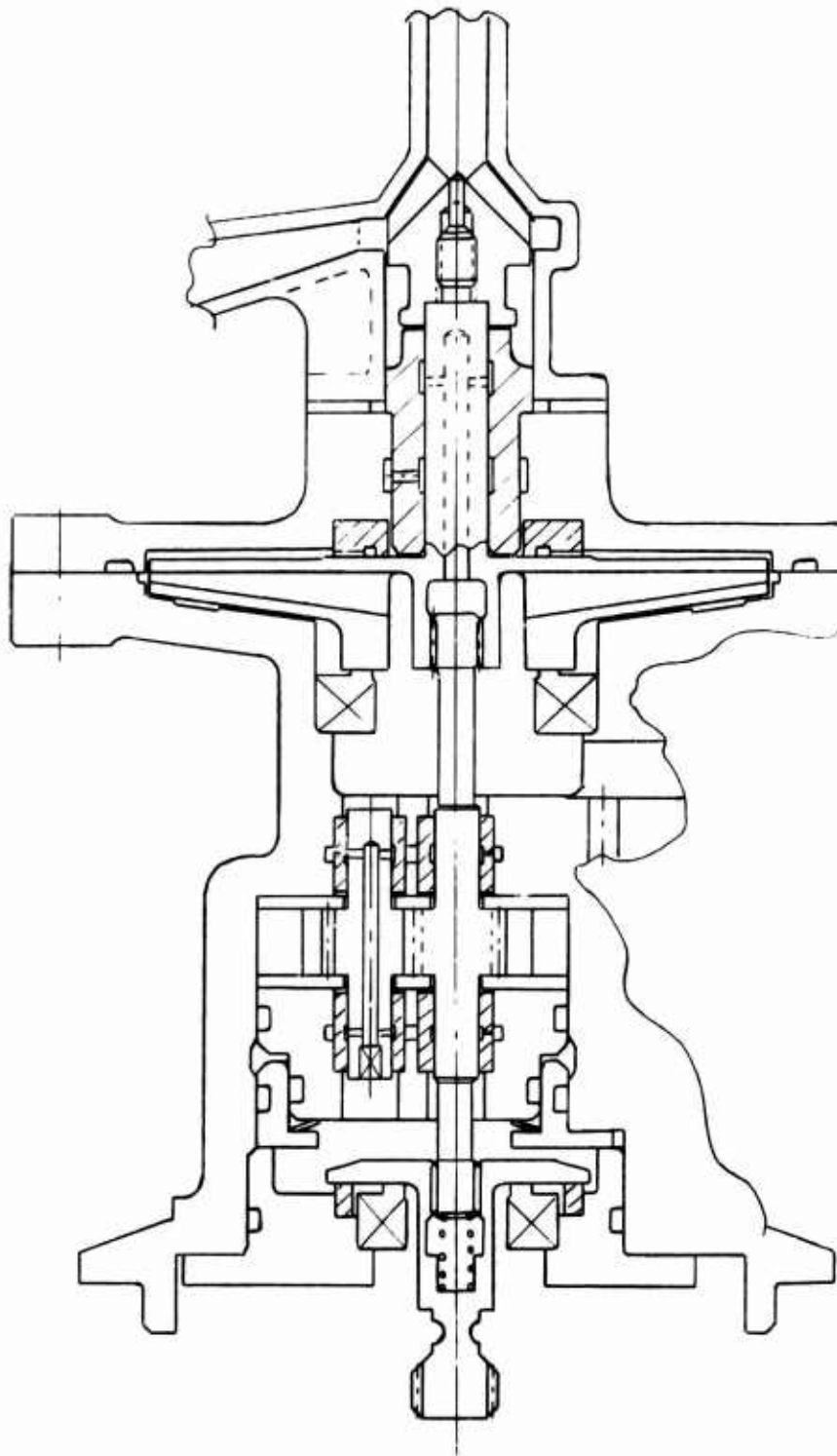
Figure 51.   Baseline Pump Cross-Section.

87

A description of each component including design parameters follows:

Boost Stage

A conical impeller designed to produce 30 psi rise at 37,500 rpm and 450 pph fuel flow is used for the boost stage. The low power requirements of this stage result in low fuel temperature rise. To provide effective electronics cooling, a portion of this relatively cool boost discharge flow is ported to the heat exchanger. The boost stage is located in an insulated housing to prevent main stage discharge heat from increasing cooling flow temperatures. Fuel flow through the heat exchanger is designed to be 20 pph at 2 psi pressure drop. Fuel flow from the boost stage in excess of 20 pph bypasses the heat exchanger and flows into the main stage inlet through a 2-psi bypass valve.

1. Boost Stage Design Parameters

   Type - Conical centrifugal

Cone angle	45°
Outside dia	.586 in.
Inlet dia	.234 in.
Number of vanes	3
Lead	.192 in.
Head coefficient	.4
Material	17-4 steel
Specific speed	1400 rpm

Main Stage

A 2.44 in. dia. radial impeller produces 800 psi at 37,500 rpm, pumping 450 pph fuel flow. Flow from this element is ported to the gear stage inlet. The main stage imparts the head rise into the fuel and is responsible for the input horsepower and fuel temperature rise.

The boost and main stages are mounted on opposite ends of a shaft and supported by a central bearing. Both this journal bearing and the impeller thrust bearings are located in the support housing.

1. Main Stage Design Parameters

   Type - Radial Centrifugal

Outside dia	2.44 in.
Inlet dia	.54 in.
Number of vanes	3
Inlet angle	8°
Discharge angle	25°
Head coefficient	.5
Material	17-4 steel
Specific speed	104

Starting Stage

The unloading gear stage provides 70 pph fuel at 40 psi
rise operating at 3750 rpm. A tungsten carbide sealing
block and side plates are pressure loaded against the
gears for normal starting and operation up to engine idle
speed. At idle speed the main stage pressure rise is
sufficient to actuate the changeover valve which unloads
the gear stage.

1. Starting Stage Design Parameters

Type - Unloading Tip Seal Gear Pump

Gear pitch	40°
Gear O.D.	.400 in
Number of teeth	14
Gear width	.261 in.
Journal diameter	.193 in.
Journal length	.40 in.
Gear material	M-2 Tool Steel

Bearings

The bearing materials used in the pump are as follows:

   Gear pump journal bearings - silver impregnated carbon
   Main stage thrust bearings - silver impregnated carbon
   Main stage journal bearings- Graphitar 39

Insulation

A two-step glass phenolic material (.050 in. thick) is used for a thermal insulator between the main pump housing and the boost pump housing.

Shaft Seal

A standard face seal is used for the shaft seal and also for impeller front shroud seal.

Filtration

To ensure clean fuel for pump bearings and where required in the fluid controller, a barrier type filter is included in the pump package.

Baseline Pump Performance

Boost Stage

Figure 52 is a head-flow calibration of the boost impeller operating with a noncavitating inlet.

V/L testing of this element demonstrated the impeller ability to pump 135°F JP-4 fuel at V/L = .30 with acceptable head degradation. Attempts to run at .45 V/L were not successful because while the impeller was still pumping, it did not produce sufficient head rise to maintain the main element minimum required inlet pressure.

Starting Stage Performance

The starting stage is required for pumping up to approximately 13,000 rpm. Pump performance is shown in Figure 53. During normal operation, the pressure rise across the gear stage is limited to 400 psi by the bypass valve.

Main Stage Performance

Main stage performance from idle to maximum speed is plotted on Figure 54.
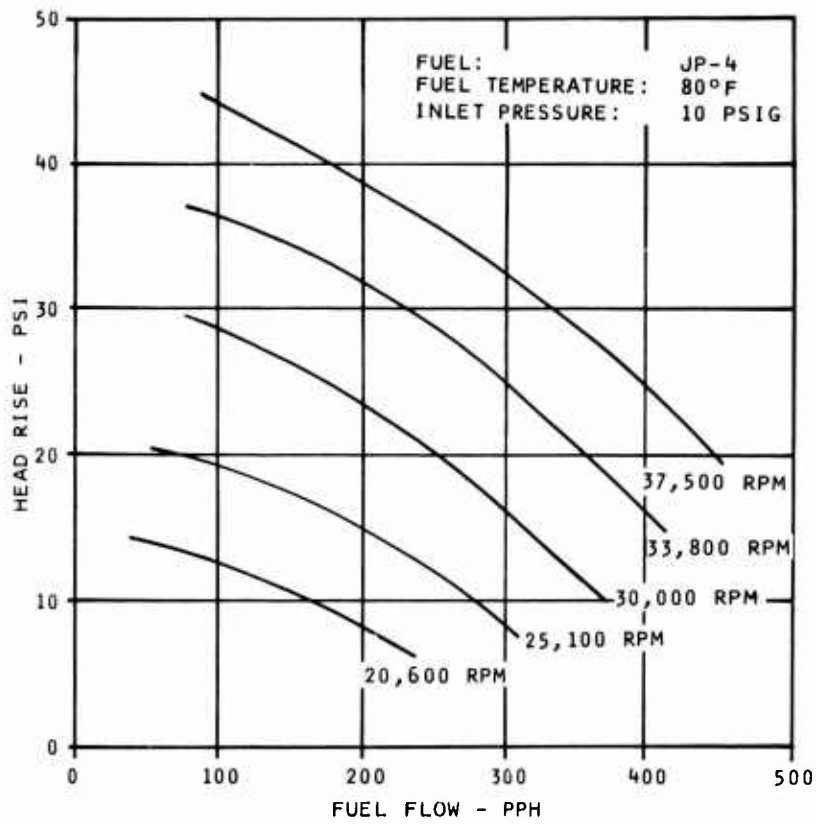
Figure 52. Boost Stage Head Flow Performance.
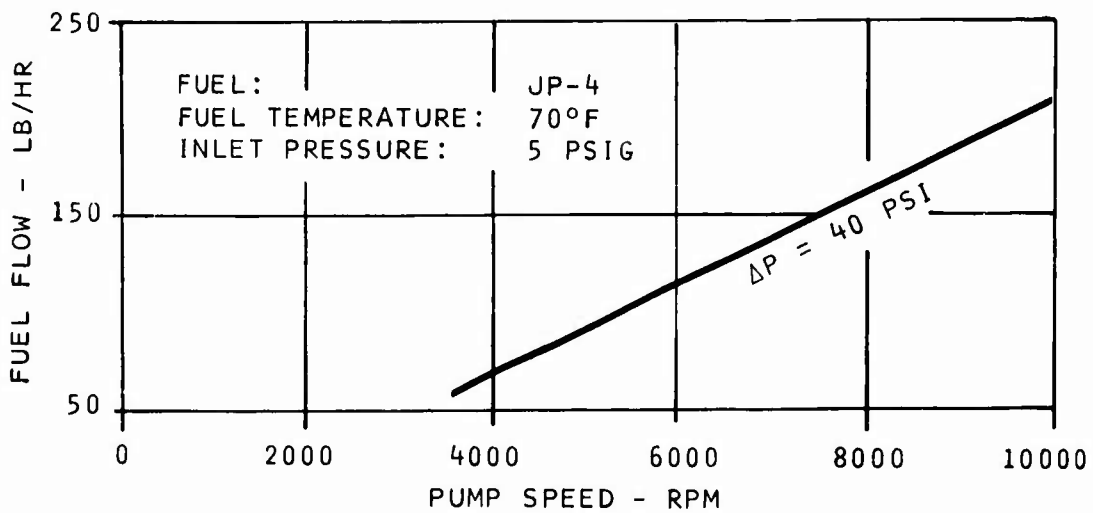
Figure 53. Starting Stage Pump Performance.

91
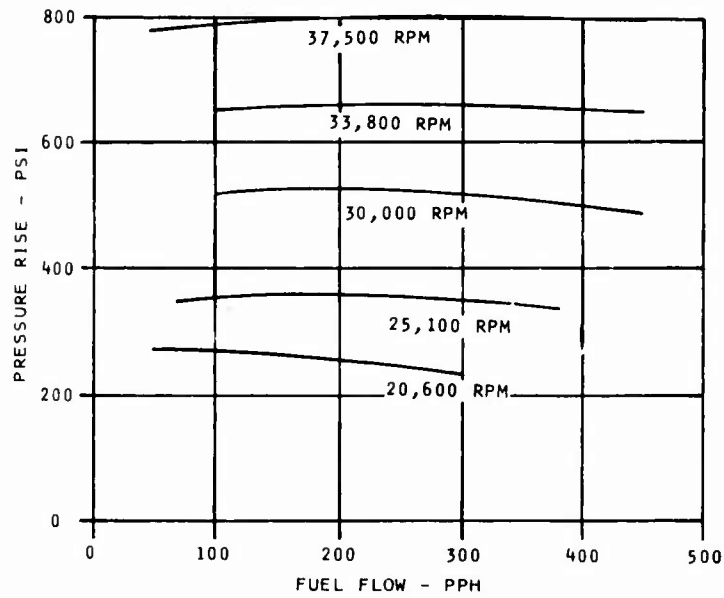
Figure 54. Main Stage Pressure Rise-Flow Performance.
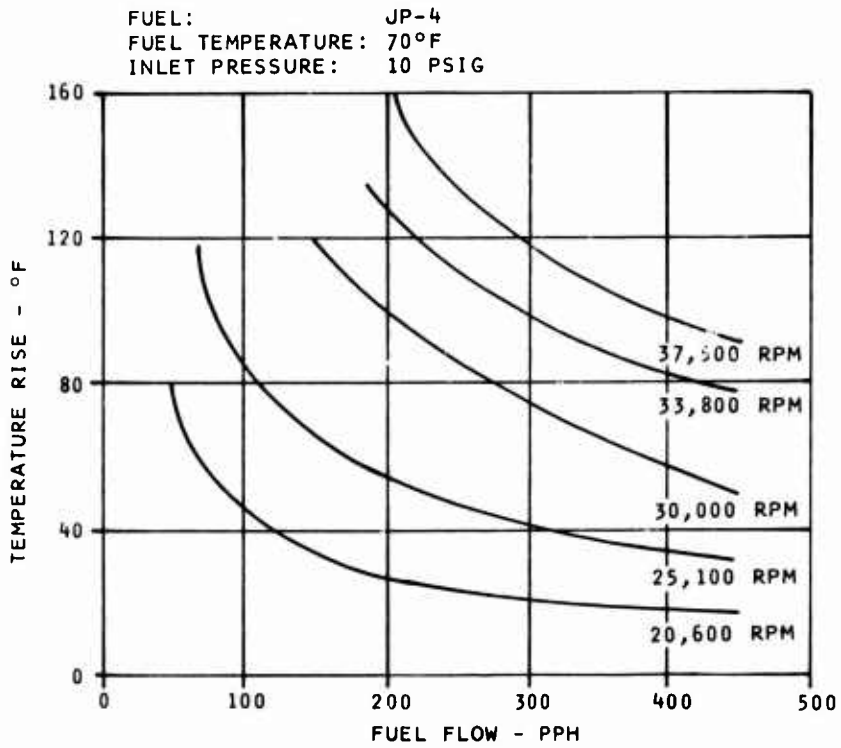
Figure 55. Baseline Pump Temperature Rise.

92

Overall Pump Performance

Temperature rise data is for the combined pumping stages shown in Figure 55. The overall operating efficiency of the pumping element is attributed to high disc friction losses in the main centrifugal stage. These losses were found to exceed values predicted based on the bar-stock pump test results. Subsequent calculations based on work done by J. W. Daily and R. E. Nese (transactions of ASME Vol. 82, Page 217) confirms these findings. Further analytical work indicates selection of a higher pump speed. (55,000 rpm for the 5 lb/sec engine would substantially reduce disc friction losses by reduction of impeller diameter. Disc friction is a function of D^5.) Calculations indicate that increasing pump speed and a radial vaned impeller to increase head coefficient will reduce impeller diameter and, therefore, disc friction losses to reduce input power by approximately 50%.

Figure 56 shows a normalized plot of the main stage head-flow curve. It is apparent from this curve that heat soak from the pump discharge is affecting the inlet flow to this stage and the resulting density decrease is lowering the pressure rise. This is apparent at low flows where high-speed normalized data shows a marked deviation from low-speed data.

A photograph of the disassembled pump is shown in Figure 57.

Endurance Testing

The baseline pump was operated with the control for a total of 277 hours. The pump's performance throughout the tests was recorded and showed no sign of degradation until the contamination tests.

Contamination Testing

The pump and control assembly was tested on contaminated fuel per MIL-E-5007C for 18 hours at 30,000 rpm and 300 pph flow. A reduction in boost pressure caused by a failure of the heat exchange bypass valve caused the main stage to cavitate. Disassembly and inspection of the pump showed that excessive wear had occurred on the gear pump journal and bearings. Apparentl: this is the result of a lack of the proper pressure level to ensure wash flow in the journal area. It was also observed

93
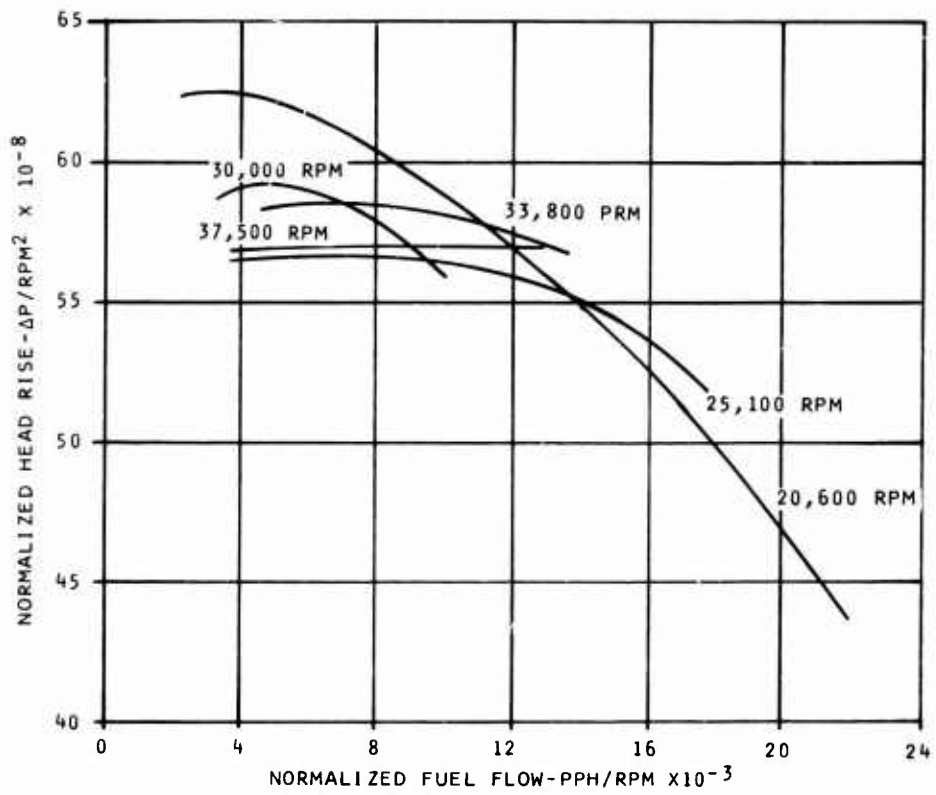
Figure 56. Normalized Main Stage Head-Flow Performance.

94
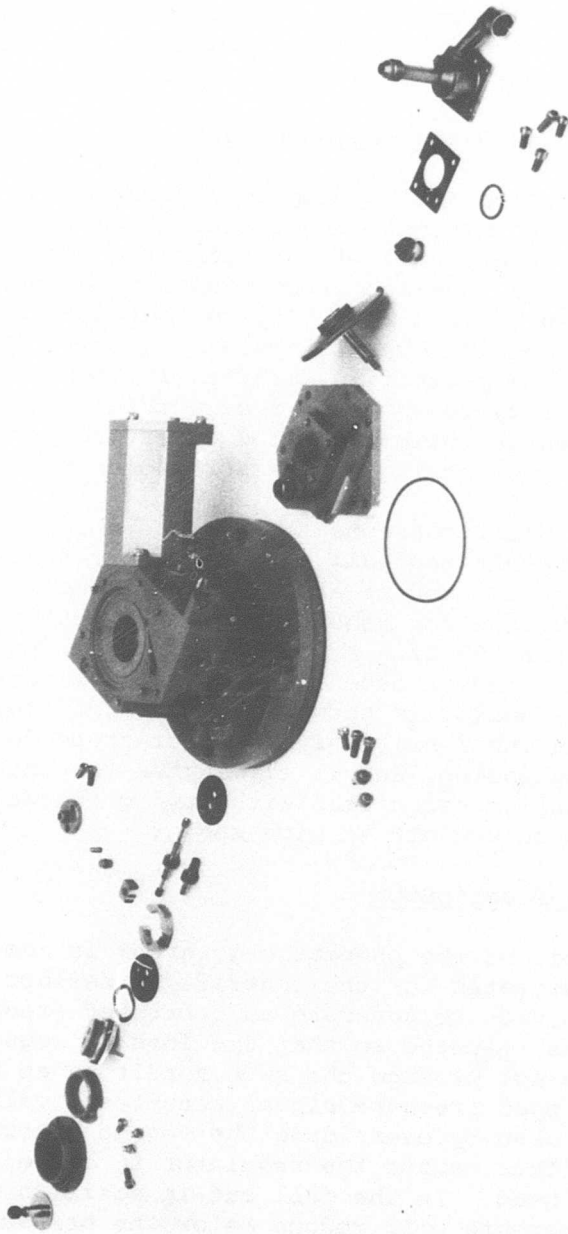
Figure 57. Disassembled Fuel Pump.

95

that the barrier filter showed signs of excessive pressure
drop as the filter convolution area had bulged slightly. A
photograph of the pumping components taken after the contami-
nation test is shown in Figure 58.

Power Turbine Overspeed Governor

The original control system specification required a simple
speed trip to minimize the overspeed caused by a sudden loss
of loa⁻. As a result of surveying the users, it was estab-
lished that a .050-sec proportional redundant overspeed gover-
nor with sufficient authority to shut off fuel would be better
suited to meeting overall system requirements. This concept
offers backup protection for the electronic control; and with
the capability to shut off fuel within 50 ms, it provides
pretty much an optimum control effort to prevent excessive
overspeed (neglecting compressor geometry or bleed control).

Several fluidic concepts for overspeed sensing were reviewd
with the result that all of the simpler schemes were shown to
be response limited at about 150 Hz. These would require a
speed reduction for sensing the power turbine speed which is
specified at 600 Hz. A mechanical speed sensor was therefore
selected, which is essentially a ring of cantilevers. A photo-
graph of a sensor is shown in Figure 59. This speed sensor
concept is inherently easy to manufacture for high-speed
dynamic balancing, and it eliminates the thrust load and mach-
ining problems associated with trying to use conventional fly-
weight speed sensors at high speed.

Operation Description

A schematic of the pneumatic governor is shown in Figure 60.
This illustrates how the centrifugal deflection of the canti-
levers is used to generate an overspeed pressure signal. This
method was selected so that the loss of regulated supply pres-
sure does not produce the same result as an actual overspeed.
The overspeed pressure signal actuates a valve which reduces
metering head by overriding the sensed metering head pressure
signal. This causes the regulator to close and thereby reduce
metering head. In the full cut-in position the control dis-
charge pressure will reduce below the pressurizing valve set-
ting and close. The small flow being metered during this con-
dition will pass through the overspeed valve.

96
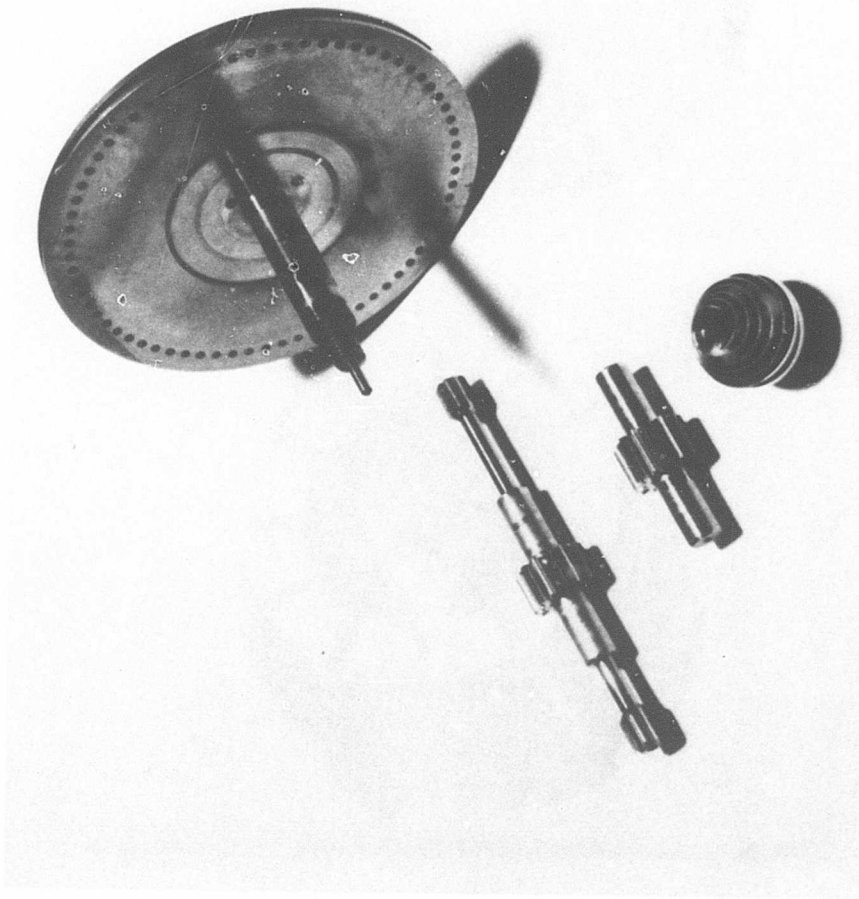
Figure 58.   Pump After Contamination Test.
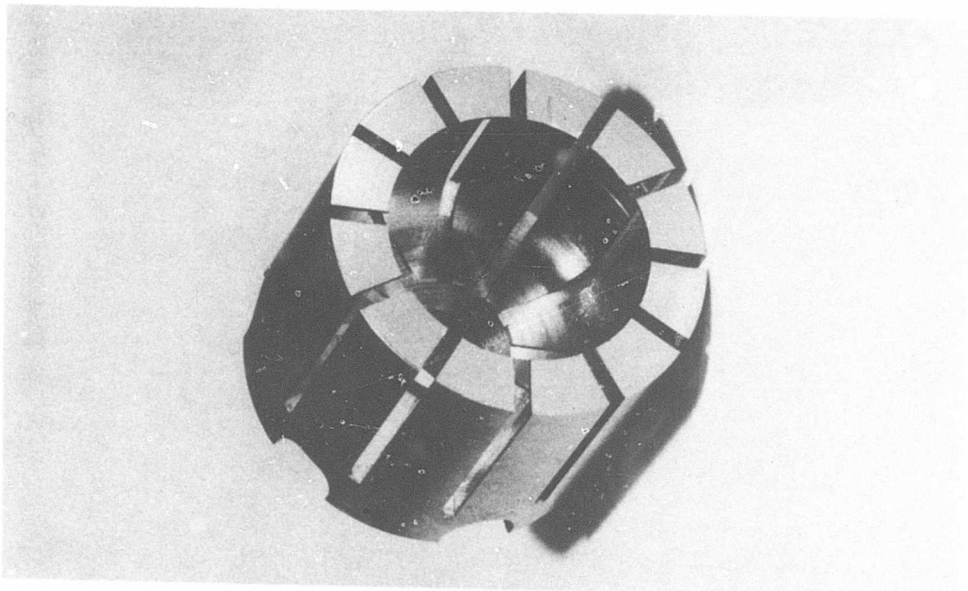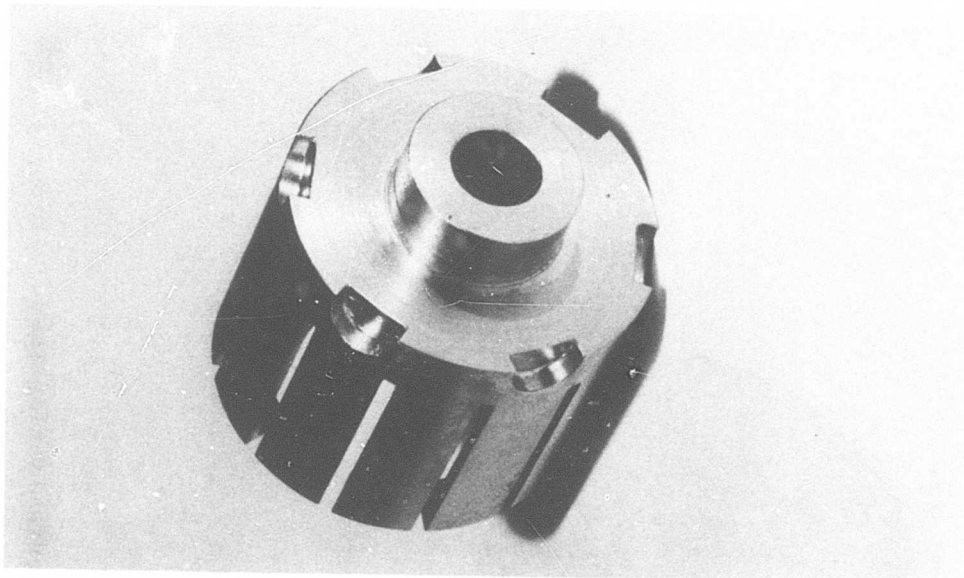
Figure 59.   Turbine Overspeed Sensor.
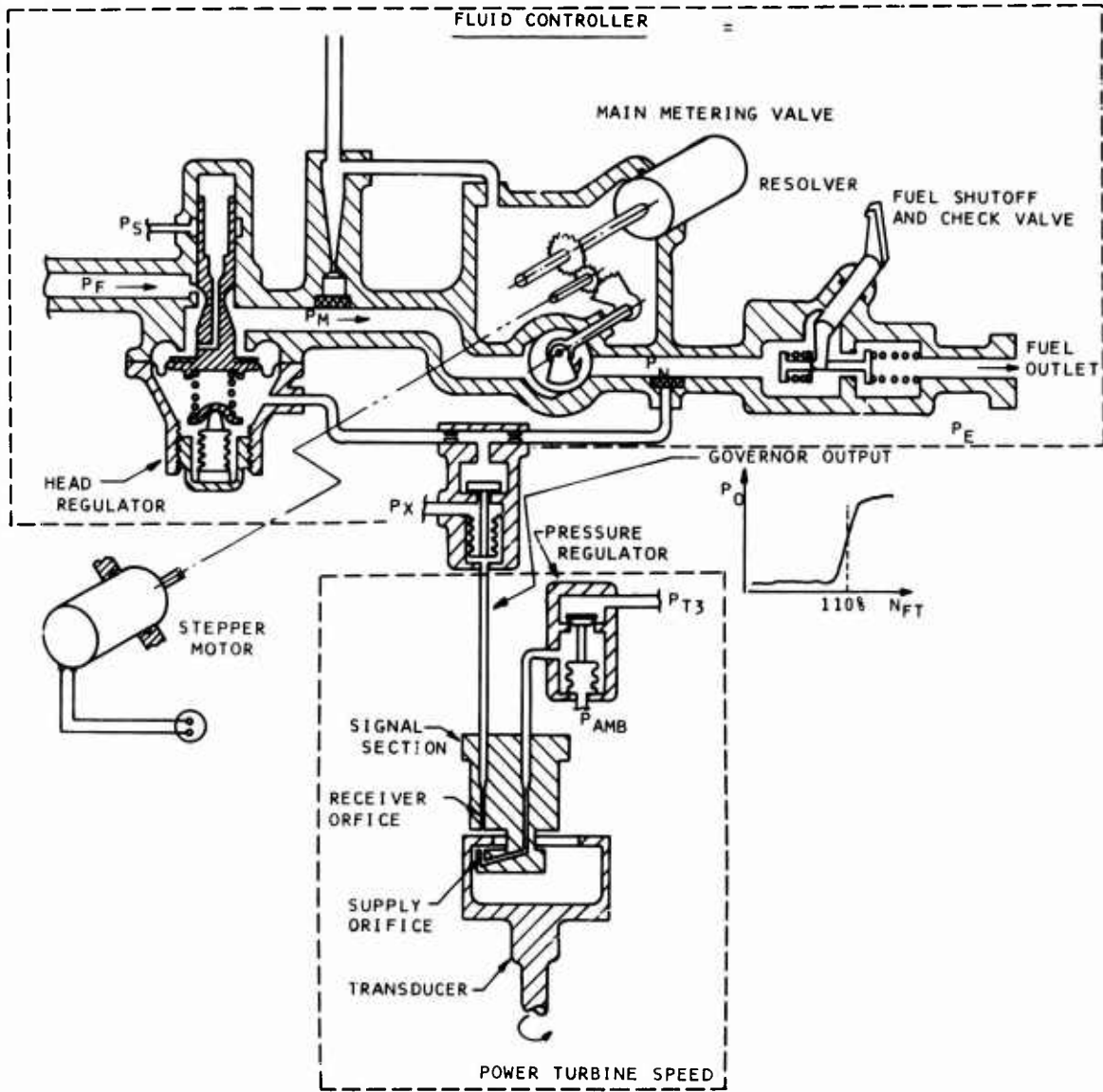
Figure 60.   Turbine Overspeed Governor Schematic.

The feasibility of the design concept has been demonstrated
open looped at speeds of up to 20,000 rpm. The design changes
necessary for the sensor to operate at speeds of up to 50,000
rpm have been determined. Only minor changes in the cantilever
unit sizing and number of segments are necessary for higher
speed requirements.

Closed-loop operation with the pneumatic governor controlling
the fluid controller has been demonstrated using a bypass con-
trol valve in the fuel discharge line.

Speed Sensor Tests

Figure 61 shows the cantilever deflection vs rotational speed
characteristics of the speed transducer unit. The deflection
range of interest is at 20,000 rpm, where supply pressure gets
ported to the receiver. A stroke of approximately .01 in. is
required to saturate the receiver.
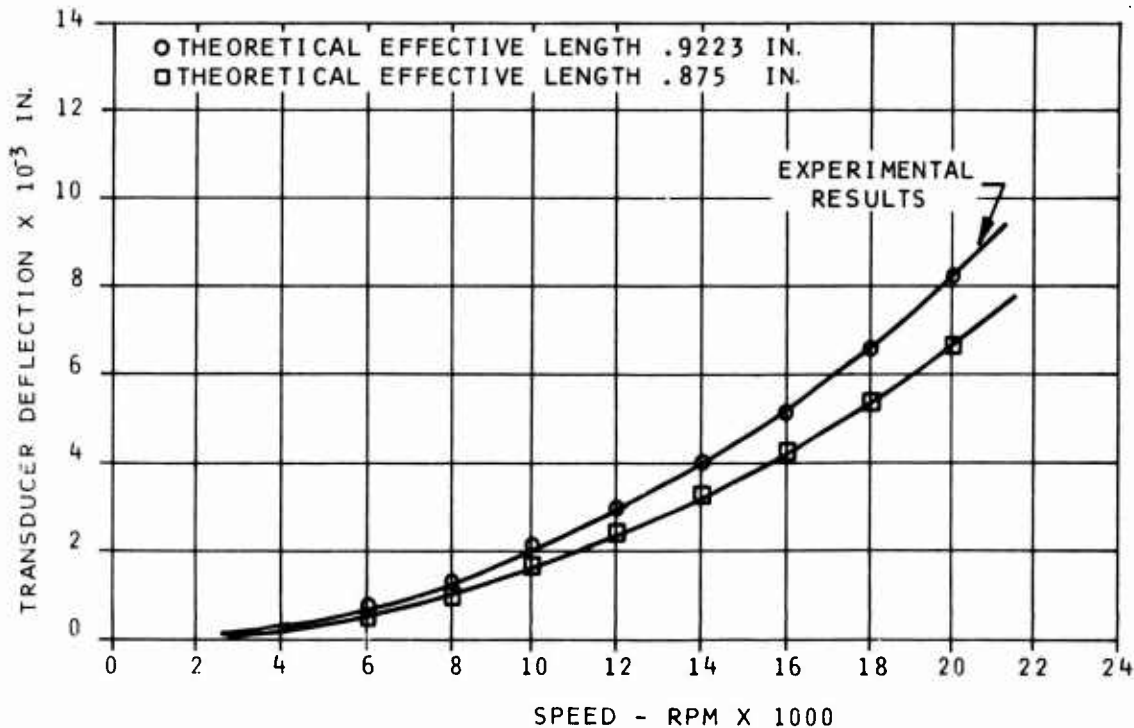
Figure 61. Speed Sensor Deflection.

The speed transducer dimensions required for speeds up to 35,000 rpm were determined by theoretical dynamic stress analysis of the cantilever. Figure 61 shows that good correlation exists between performance calculated theoretically and that obtained by experimental measurement.

Over the governing speed range, the cantilever centrifugal deflection will allow airflow from the supply to the receiver. At saturation, the total pressure recovery of the unit was 8.99 psig for a supply pressure of 15 psig, or 60% recovery. For the orifice area sizing used, compressor bleed requirements would be less than 2×10^{-4} lb/sec, representing .01% of the rated airflow on a 2-lb/sec airflow engine. Figure 62 shows the pressure recovery vs speed characteristics for a supply pressure of 15 psig.
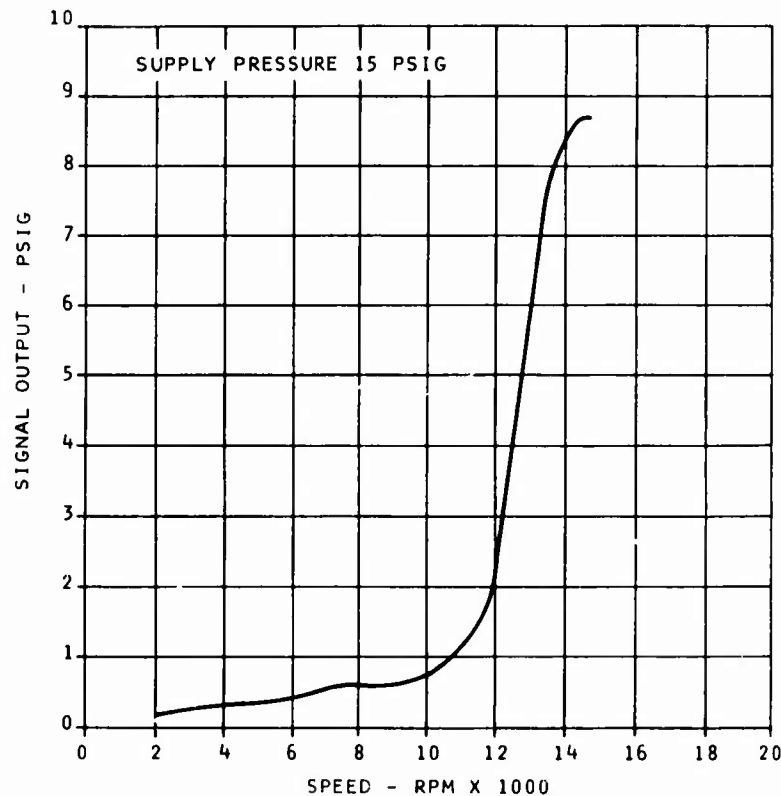
Figure 62. Speed Sensor Pressure Signal.

101

Closed-Loop Operation

The closed-loop performance of the overspeed governor was demonstrated with minimal changes to the prototype fluid controller by allowing the governor to control a fuel discharge bypass valve rather than the metering head bypass as indicated in Figure 60. In both cases the bypass allows pressure dumping to the pump inducer discharge so that performances would be similar. No effort was made to improve the available valve hardware used for the demonstration. As a consequence the system showed hysteresis due to valve stiction. However, the basic concept is well within the state-of-the-art and there is little doubt that the system can be developed.

Summary of Fluid Controller Development

The baseline fluid controller was successful in meeting most of the program objectives.

Flexibility

Flexibility was demonstrated by running the 2-lb/sec engine and 5-lb/sec engine simulators without the need for any adjustments of the fluid controller.

Reliability

A total of 277 hours of running was accumulated. Disassembly of the fluid controller showed that the components were still in good condition. Electronic cooling by fuel from an insulated boost stage was successfully demonstrated.

Size

The estimated weight of the fluid controller was 5.37 lb (without an alternator). The design goal was 4.6 lb. The weight target could be met by changes to the design in the areas of packaging, pump modifications, and PLA linkage. It was found from the survey of requirements that flight idle position was not necessary; elimination of this requirement considerably reduces the size and complexity of the PLA linkage.

102

Operation of a small-high speed pump for an advanced
small engine fuel system has been successfully demon-
strated. Miniaturized pumping elements, both positive
displacement and centrifugal types, proved manufacturable
despite the extremely small tolerances required.

Careful dynamic balancing of all rotating elements is
required to prevent excessive bearing wear. Maximum
unbalance allowed for the program was .0003 in.oz.

Contamination Resistance

Eighteen hours of contamination testing (MIL-E-5007C) were
completed as part of evaluating the endurance of the
control. The pumps and fuel metering system showed
excellent performance. The heat exchanger bypass valve
requires redesign to be more contamination resistant.
It clogged with dirt after 13 hours.

Maintainability

Particular attention was given to maintainability by
designing the control to be modular, and making all
external adjustments and the barrier filter element
accessible from the front of the engine.

Recommendations

To improve overall efficiency and lower the temperature
rise of the main stage, tests should be conducted on
existing bar-stock housing to evaluate a 55,000-rpm
impeller design. The effect of 55,000 rpm on the gear
elements and boost elements should also be evaluated.

Evaluation of the power consumption of the various
elements disclosed that further effort should be expended
to further miniaturize all rotating components to
eliminate disc friction. This would include seal face,
gear diameters, etc.

A higher pressure boost stage must be designed and
fabricated to demonstrate V/L capability in conjunction
with the control and also ensure higher temperature
operation without vapor lock.

High temperature operation of the pump and control demonstrated need for increased boost pressure. Heat transfer from the housing discharge area resulted in occasional vapor lock at the interstage as fuel vapor pressure approached the minimum boost values. Endurance testing was accomplished using inlet pressures of 20-25 psig to avoid this effect. To ensure cavitation-free performance, it is necessary to anticipate interstage fuel temperatures as equal to discharge temperatures and provide pressurization to ensure minimum required NPSH at all conditions.

Provide a new package design to incorporate the alternator, revised pumping system, and simplified PLA input.

SIMULATION AND CONTROL MODE

The engine computer model used for conducting control mode
studies and to determine control system performance require-
ments was established based on data provided by USAAMRDL and
engine manufacturers. This same model was used as an engine
simulator for closed-loop demonstration tests on the complete
system.

Engine and Load Model

The engine and load model described by the block diagram in
Figure 63 is comprised of a single-spool gas generator with
impingement cooled turbine blades and a free turbine driven
helicopter rotor. The model is a fairly simple representation
of the system, but it provides the necessary and sufficient
detail for determining the control system design require-
ments and for demonstrating closed-loop system performance.
For example, the engine stage efficiencies and specific heats
have been held constant over the operating range of the engine
because the amount that they vary has a minor effect on con-
trol requirements. Similarly, variable compressor geometry
and interstage bleed was not simulated because they do not
affect the main control loop when properly scheduled. An engine
model of sufficient detail to determine these requirements
was not considered necessary since engine manufacturers
provide accuracy and dynamic requirements for geometry control
on advanced engines.

Turbine Blade Model

Detailed analytical studies to determine the thermal time
response of a turbine rotor blade are included in the Appendix.
Internal convection, transpiration and inpingement methods
of blade cooling are analyzed. In each case the coolant is
compressor discharge air.

A consensus of opinion among engine manufacturers has led to
a turbine blade model consisting of internal convection cool-
ing with impingement cooling at the leading edge. This
configuration appears the most probable for small advanced
technology gas turbines. The relationship between the turbine
inlet gas temperature and the surface temperature of the
leading edge of the blade model is characterized by a variable
time constant as shown in Figure 64. The steady-state
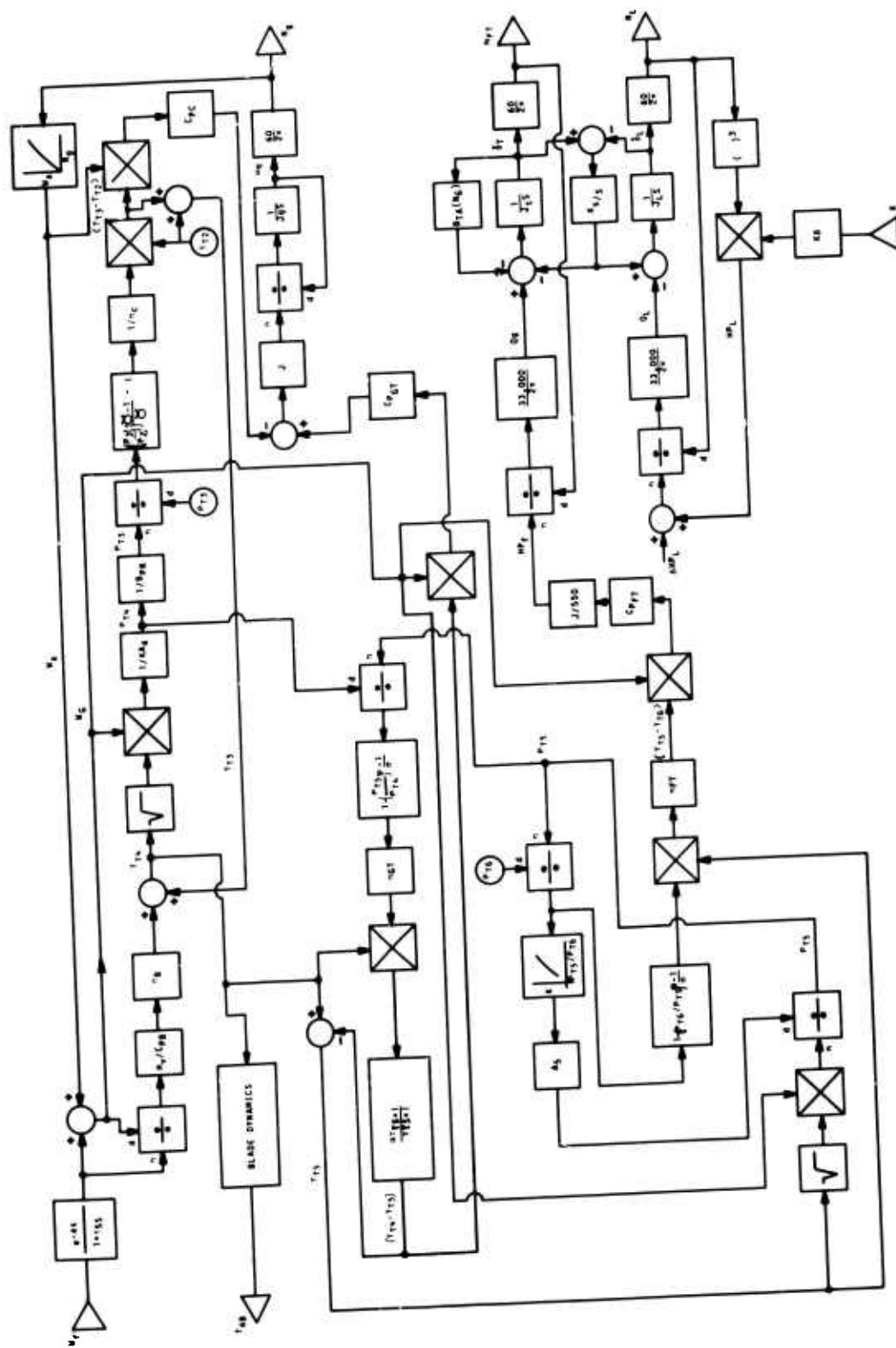
Figure 63. Engine and Load Computer Model.

106
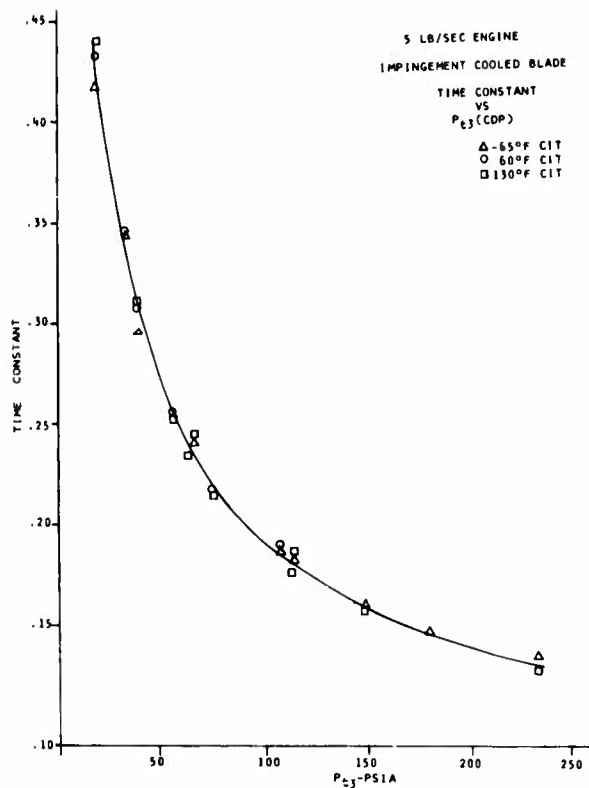
Figure 64.   Turbine Blade Temperature Time Constant.

characteristics are shown in Figure 65. The relationships
can be expressed mathematically by the transfer function from
turbine inlet gas temperature to blade leading edge surface
temperature.

A requirement for the advanced engine control is that turbine
temperature be limited to optimize engine performance and
turbine blade creep life. The inability of known temperature
sensors to meet gas turbine specifications for measuring the
extremely high turbine inlet gas temperature has meant that
the cooled turbine metal or exhaust gas temperature are the
only potential sources to correlate turbine inlet temperature.
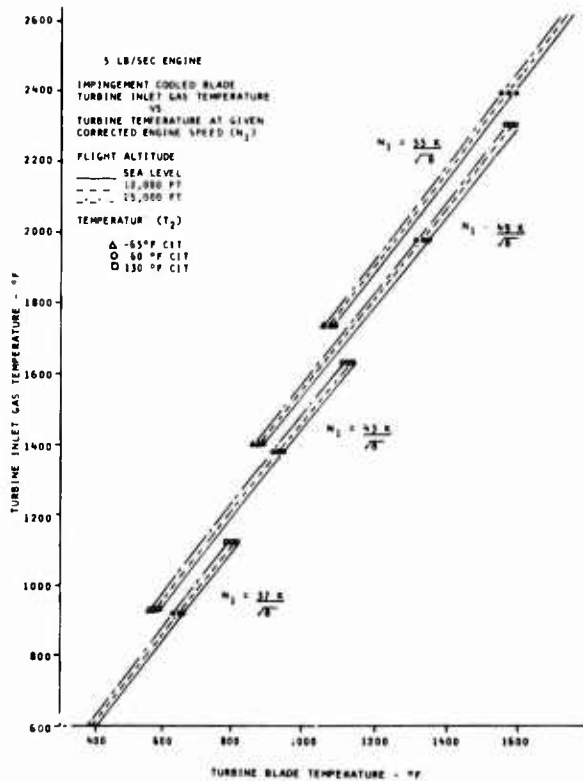
Figure 65. Steady-State Turbine Blade Temperature.

Acceleration Control Mode

In reviewing temperature sensor technology,it is evident that
an acceleration control mode based on a direct measure of the
gas turbine inlet temperature is not practical for engines of
the late seventies. However, because the control system
includes a blade temperature sensor for temperature limiting,
studies were conducted to determine if an acceleration
control could be established using this signal. Simulation
studies evaluating this control mode and comparing it with
a conventional open-loop fuel flow scheduling control are
summarized below.

108

Closed-Loop Temperature Control Acceleration

Closed-loop accelerations are based on prescheduled non-linear curves of maximum allowable turbine inlet gas temperature as a function of gas generator speed and compressor inlet temperature. These schedules are provided by engine manufacturers and are established to avoid surge and overtemperature. The specifications for satisfactory engine acceleration require following the temperature schedule within a maximum error band of ± 100°F. In addition to performance, control complexity and cost are factors which must also be evaluated before an acceptable acceleration control mode is selected.

T_{t4} Control Mode Study

A block diagram of the closed-loop temperature control with a summary of the control modes studied is shown in Figures 66 and 67. The results indicate that a control mode with proportional plus integral plus fuel flow rate feedback compensation can meet the requirements for a closed-loop temperature control. However, an idealized turbine inlet gas temperature sensor has been assumed, $H_B(s) = 1$, and as indicated by Trace (7), gross overtemperature will occur if an uncompensated blade temperature lag of 0.1 second is considered.

Table X compares the temperature control modes with a conventional W_F/P_{t3} acceleration controller. Each mode was optimized by adjusting the control gain until the gas temperature equaled the desired scheduled gas temperature at least once, but never exceeded the schedule, during accelerations from flight idle to 100% speed. A figure of merit was based on minimizing acceleration time and temperature error between the actual and the desired acceleration schedule without overtemperaturing (i.e., minimizing the area between these two curves). As expected, the control mode with the faster acceleration times is closer to the desired schedule. However, the W_F/P_{t3} control gives the fastest acceleration time. Its schedule was established to provide about 100°F of surge margin.
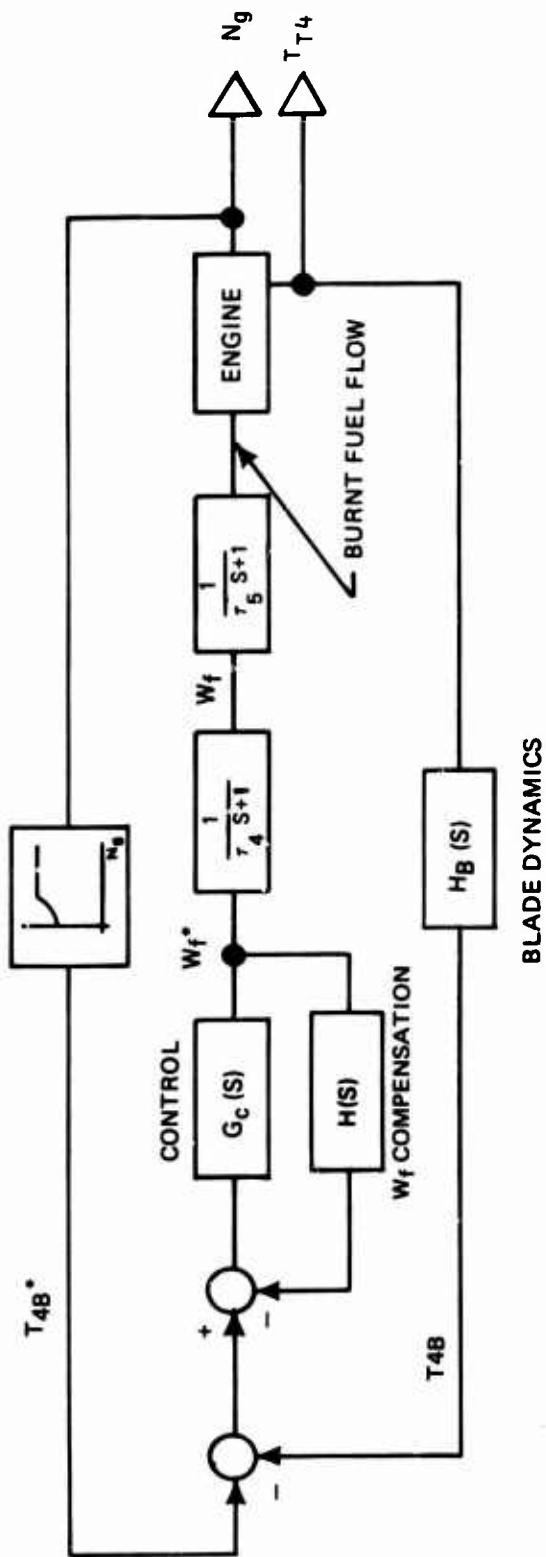
TRACE	$G_c(S)$	$H(S)$	$H_B(S)$	*t 60-95% SECS
4	K_p	0	1	2.6
5	$K_p + K_i/S$	0	1	2.0
6	$K_p + K_i/S$	$\frac{KS}{1+\tau s}$	1	1.9
7	$K_p + K_i/S$	$\frac{KS}{1+\tau s}$	$\frac{1}{0.1S+1}$	2.2

*t = 1.6 sec for $\frac{W_f}{P_{cd}}$ MODE 3

Figure 66. Acceleration Control Mode Studies.
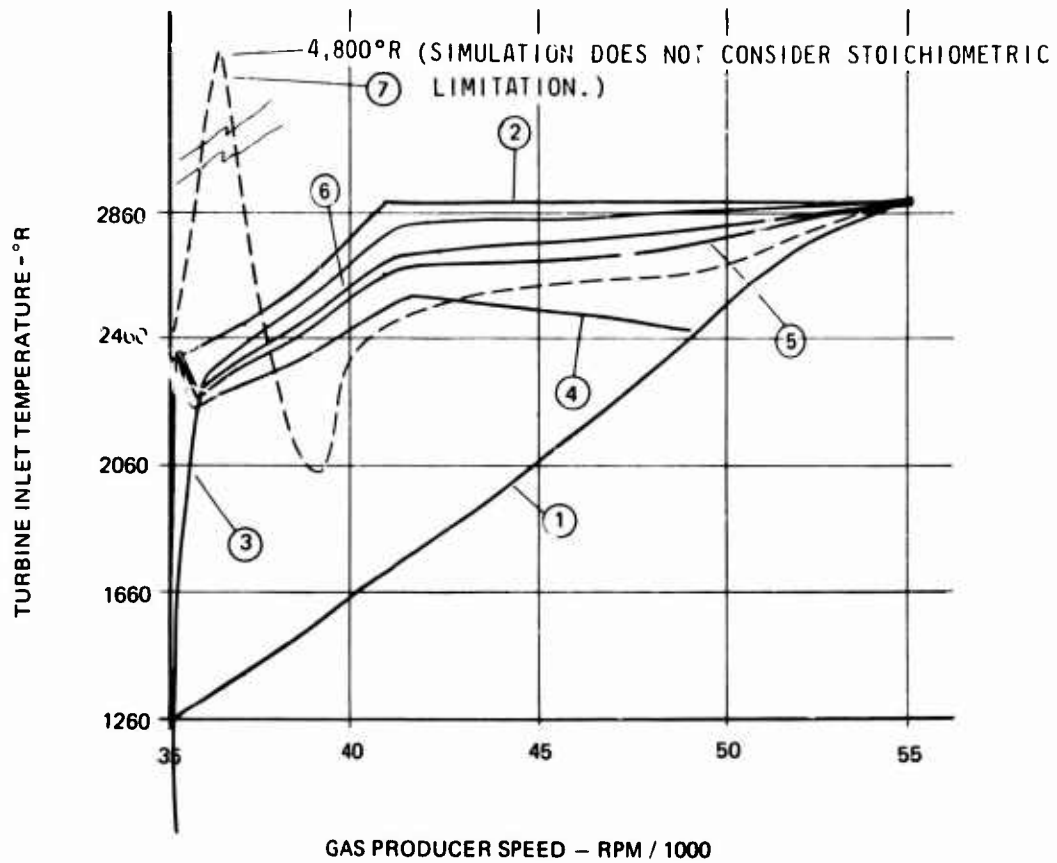
Figure 67.   Acceleration Control Mode Transients.

111

	Performance			Gains		
Mode	$t_{95\%}$ Sec.	t_{ac} $\int_o \Delta T_{t4}\,dt$	Final Offset	Optimum K_p pph/°T_4	$\dfrac{K_p}{K_i}$ Sec	$\dfrac{K_R}{\tau_R}$ SEC
W_F/P_{t3} Schedule	1.6	3.2	–	–	–	
Prop. TIT Closed Loop			8300 rpm	0.64	–	
Prop. + Int. TIT Closed Loop	2.0	8.9	0	0.53	0.565	
Prop. + Int. + Rate Feedback TIT Closed Loop	1.9	5.8	0	1.06	0.565	0.35 0.125

$t_{95\%}$ – Time to reach 95% of final value.

$\int_o^{t_{ac}} \Delta T_{t4}\,dt$ – Error performance criteria (optimized for minimum)

In summarizing these studies the following facts are apparent.

1. Integral action is necessary, as high proportional gain alone will cause excessive overtemperatures immediately following the acceleration request or be unfeasible as shown in Trace 4.

2. Fuel flow rate feedback will further reduce this initial peak in gas temperature, although the improvement is marginal.

3. The temperature controller is extremely sensitive to time lag in the feedback path.

112

4. On performance merit alone, an open-loop W_F/P_{t3} scheduled acceleration is superior to a closed-loop temperature control. However, considerations such as sensitivity to changes in control or engine parameters (through deterioration, battle damage or aging) and fuel heating value must be considered.

Acceleration Control Sensitivity

Control mode sensitivity studies compared and evaluated the W_F/P_{t3} scheduling control with the optimum closed-loop turbine inlet temperature control using sensed blade temperature. The thermodynamic blade model was based on the results of the theoretical study of an impingement cooled turbine blade using compressor discharge air as a coolant (Appendix). A block diagram description of each control mode is shown in Figure 68.

CLOSED-LOOP TEMPERATURE CONTROLLED ACCELERATION

W_F/P_{T3} ACCELERATION SCHEDULE CONTROL
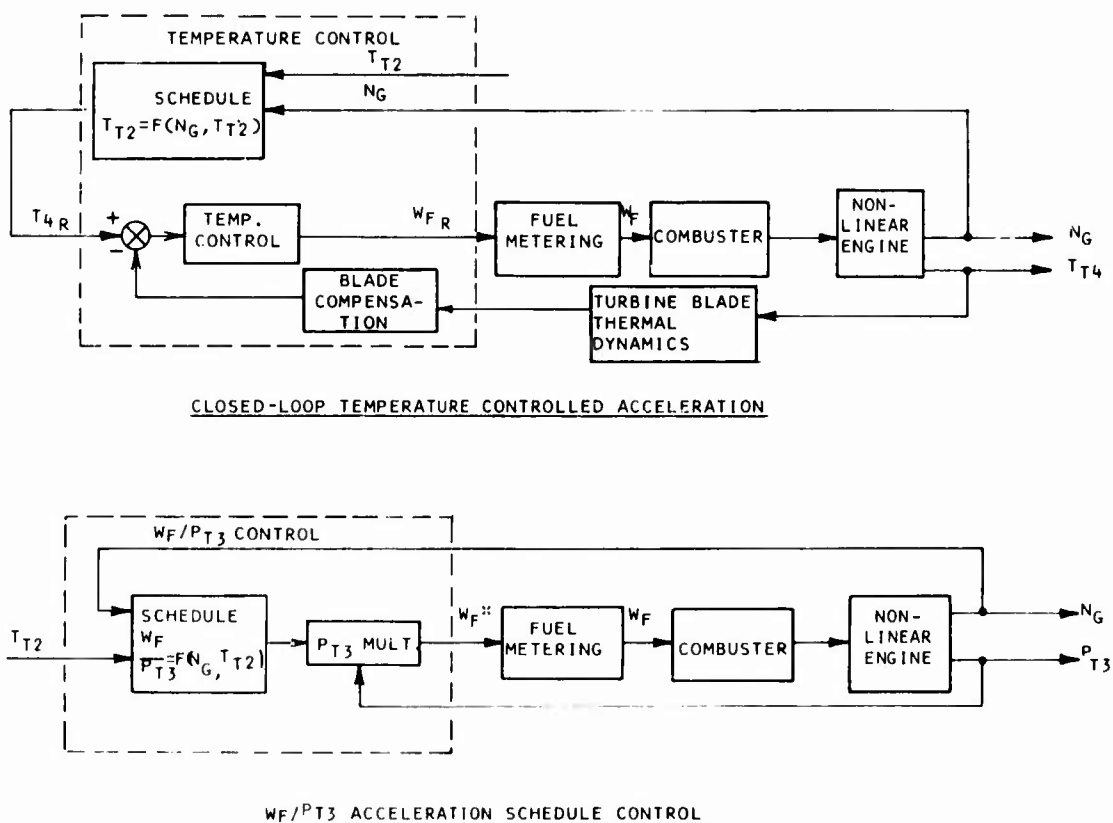
Figure 68. Acceleration Control Block Diagrams.

113

The effects on acceleration performance due to variations in forward loop engine parameters are indicated in Figure 69. These curves show turbine inlet temperature versus gas generator speed during accelerations for 10% variations in airflow and compressor, turbine, and burner efficiencies. As expected, the closed-loop control is practically insensitive to these forward loop variations, whereas gross changes are evident in the W_F/P_{t3} scheduling system. The 10% efficiency changes were used for comparison studies only and are not intended to be typical of actual engine deteriorations.

Figure 70 shows the effect of variations in the feedback loop. For the scheduling control, a 4% variation in W_F/P_{t3} corresponds to (after the initial temperature transient) the allowable 100°F variation in turbine inlet temperature.

The results of these sensitivity studies lead to the following conclusions:

1. Based on acceleration performance alone, no apparent advantage is offered by a closed-loop T_{t4} control as compared to an open-loop W_F/P_{t3} control.

2. Ignoring turbine blade dynamic compensation, a T_{t4} control would still require a bivariate function to schedule T_{t4} as a function of N_g and T_{t2}, plus more complicated dynamic compensation.

3. A T_{t4} control will be slightly affected by variations between engines, engine deterioration, or fuel variations.

4. If turbine blade temperature is used to correlate T_{t4}, the blade time constant (t_B) must be compensated to 10% accuracy.

5. Theoretical studies indicate that an impingement cooled turbine blade thermal time constant is a function of compressor discharge pressure and inlet temperature. However, it can be approximated to a function of P_{t3} alone to an accuracy of about ± 4%.

114
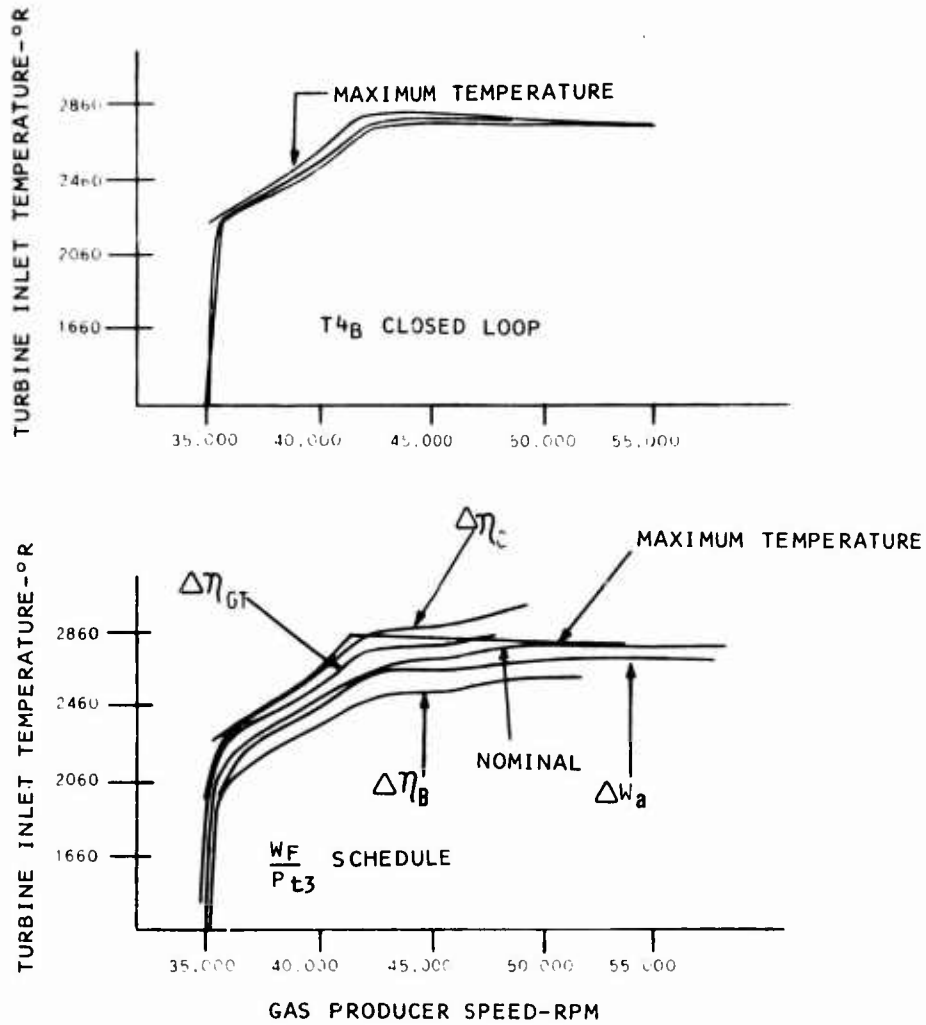
Figure 69.   Acceleration Control Sensitivity
To Forward Loop Variations.

115
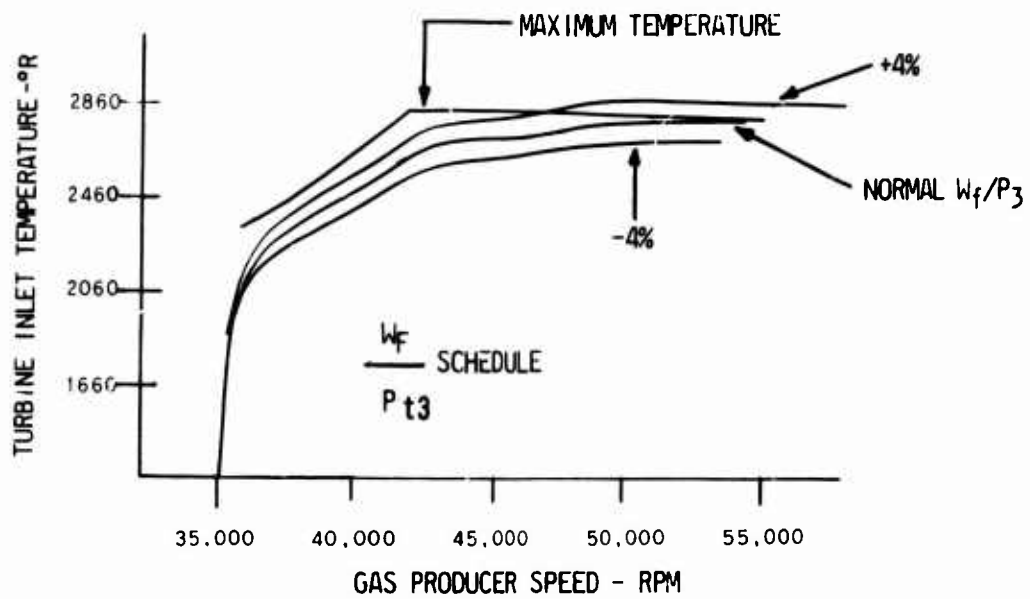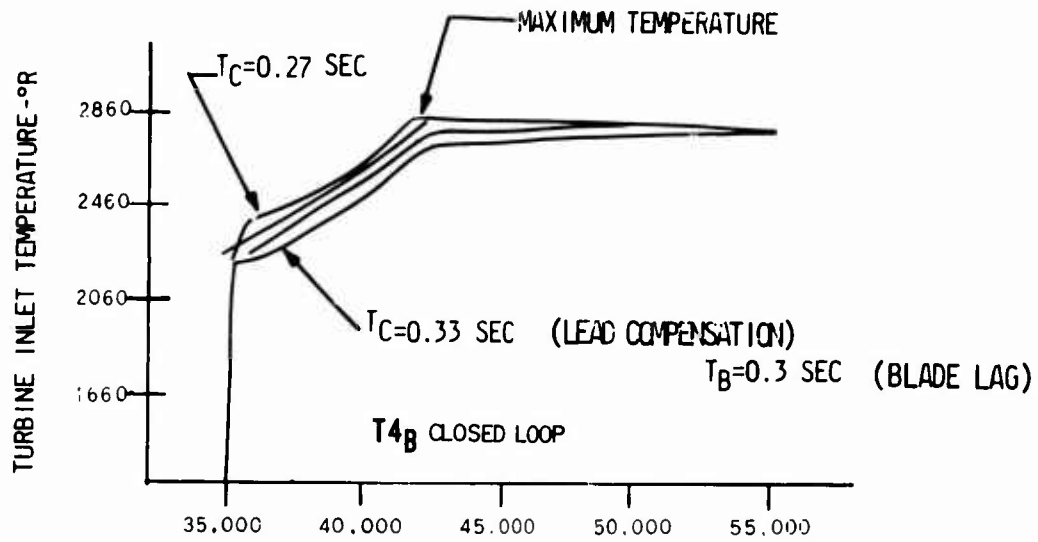
Figure 70. Acceleration Control Sensitivity
To Feedback Loop Variations.

116

The problems imposed in mechanizing a closed-loop T_{t4} control far outweigh any performance advantages such a control may have over the open-loop W_F/P_{t3} scheduling method. The necessity for accurately compensating the turbine blade time constant requires not only complexity in control mechanization but also accurate knowledge of the cooled turbine blade dynamics. Theoretical studies indicate that the blade compensation, at the very least, will require a variable time constant as a function of P_{t3}.

Although the studies conducted have only considered engine operation between idle and 100%, starting schedules must also be considered. Most engine manufacturers felt that starting the engine closed loop on temperature was probably not viable and W_F/P_{t3} start schedules would be required. Having established that a W_F/P_{t3} start control was required, complexity and cost considerations suggest using W_F/P_{t3} for acceleration and deceleration control.

Also, the limited temperature sensing range of any one of the radiation detectors precludes controlling over all of the operating envelope of the engine, without additional complexity of having more than one type detector.

Although engine control theorists have indicated the desirability of a closed-loop turbine inlet temperature acceleration control, these studies have indicated that the proven conventional open-loop scheduling method is either equal to or superior to the closed-loop method in performance, simplicity, and cost.

As a result of the above considerations a W_F/P_{t3} start, acceleration, and deceleration controller was selected and closed-loop temperature limiting will be provided using proportional blade temperature control. Consideration was given to W_F/P_{t1} start and acceleration scheduling, but it was felt that W_F/P_{t3} was more demanding of the control and therefore no problems would be encountered in providing a W_F/P_{t1} control if needed for a particular application.

Control Mode Analysis

Much theoretical groundwork, exploring optimum control modes
for ATECS of the 2- to 5-lb/sec airflow class has been covered
in the past (see references). The control mode philosophy used
herein was based on conclusions from those studies, practical
experience, and results of previous in-house studies. It was
not the intent of this study to explore all possible control
philosophies but rather to refine those already established
into a viable ATEC capable of being physically demonstrated in
the time period of this program.

The control system's functional requirements have been dictated
primarily from user surveys and the selection of an open-loop
acceleration control. Other considerations such as the neces-
sity for integral action, dynamic compensation, functional
nonlinear gains, etc., have been determined in accordance with
additional linear and nonlinear control studies. These studies
were run in conjunction with preliminary control hardware de-
sign, whereby final mode selection was based on trade-offs
between design complexity, hardware cost, and optimum perform-
ance.

Gas Generator Speed Governor Analysis

The selected proportional gas producer governor operates to
maintain the lowest of three reference speeds: PLA request,
maximum allowable speed, or the speed requested to satisfy
the power turbine governor. This mode of control offers
interloop feedback compensation during normal operation,
wherein the control system is working to govern power tur-
bine speed. This is indicated by the transfer function
block diagram shown in Figure 71. The gas producer gover-
nor for this control mode is designed to optimize the
operation of the power turbine governor control loop. This
requires that the governor gain be selected so that its
droop line approximates constant horsepower.

A dynamic analysis of the inner loop from reference gas
producer speed to engine torque was conducted based on the
engine design constants tabulated in Table XI.

118
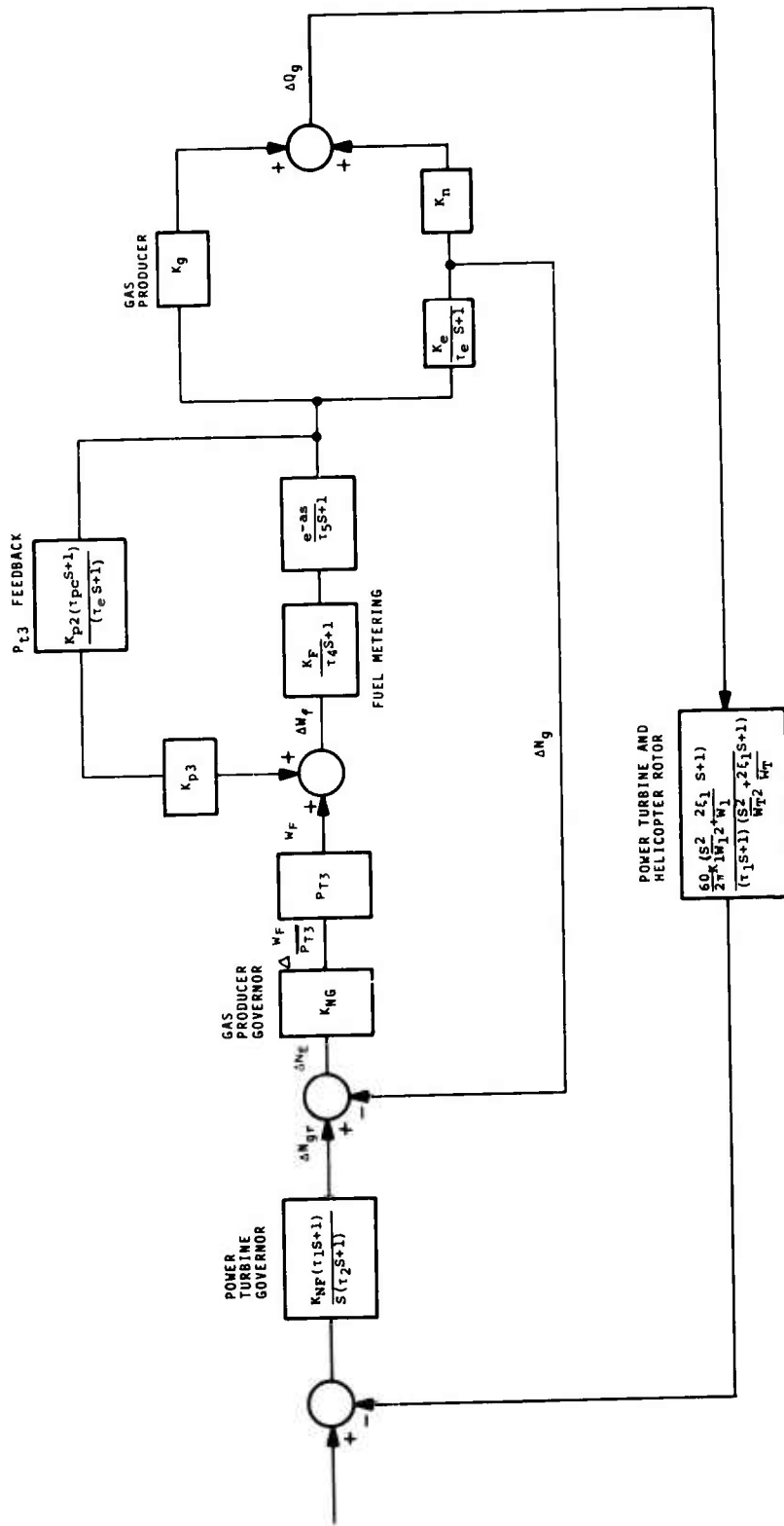
Figure 71. System Transfer Function Block Diagram.

119

TABLE XI.	BASE ENGINE AND LOAD DESIGN CONSTANTS		
Designation	Dimension	75%	90%
K_1	rad/ft-lb sec	55.0	11.0
τ_1	sec	40.0	8.0
W_1	rad/sec	7.0	7.0
ζ_1	rad	0.0015	0.0075
K_g	ft-lb/lb/hr	0.1400	0.281
K_n	ft-lb/rpm	0.0032	0.0052
τ_e	sec	0.500	0.400
τ_5	sec	0.01	0.01
τ_4	sec	0.04	0.04
a	sec	0.00	0.00
K_e	rpm/lb/hr	80.00	31.00
K_{p2}	psia/pph	0.574	.351
τ_{pc}	sec	0.15	0.1993
K_{p3}	pph/psia	1.1	1.7

The results of this analysis are summarized in Figure 72, which shows the optimum gas producer governor gain as a function of speed and altitude for the baseline engine.

The dynamic performance of the overall control/engine/rotor system on power turbine speed control indicated that the improvements in performance obtained with a variable gain gas producer governor did not warrant the added complexity. The reasons for this are that dynamic performance of the engine in the high power range is sufficiently fast to meet control requirement. This allows the gains to be optimized for the low power operating range where performance is normally more sluggish. Also, the system incorporates load anticipation by collective pitch reset

LINEAR METERING VALVE   O SEA LEVEL
                                  □ 25,000 FT

NONLINEAR METERING VALVE   X SEA LEVEL
                                    △ 25,000 FT
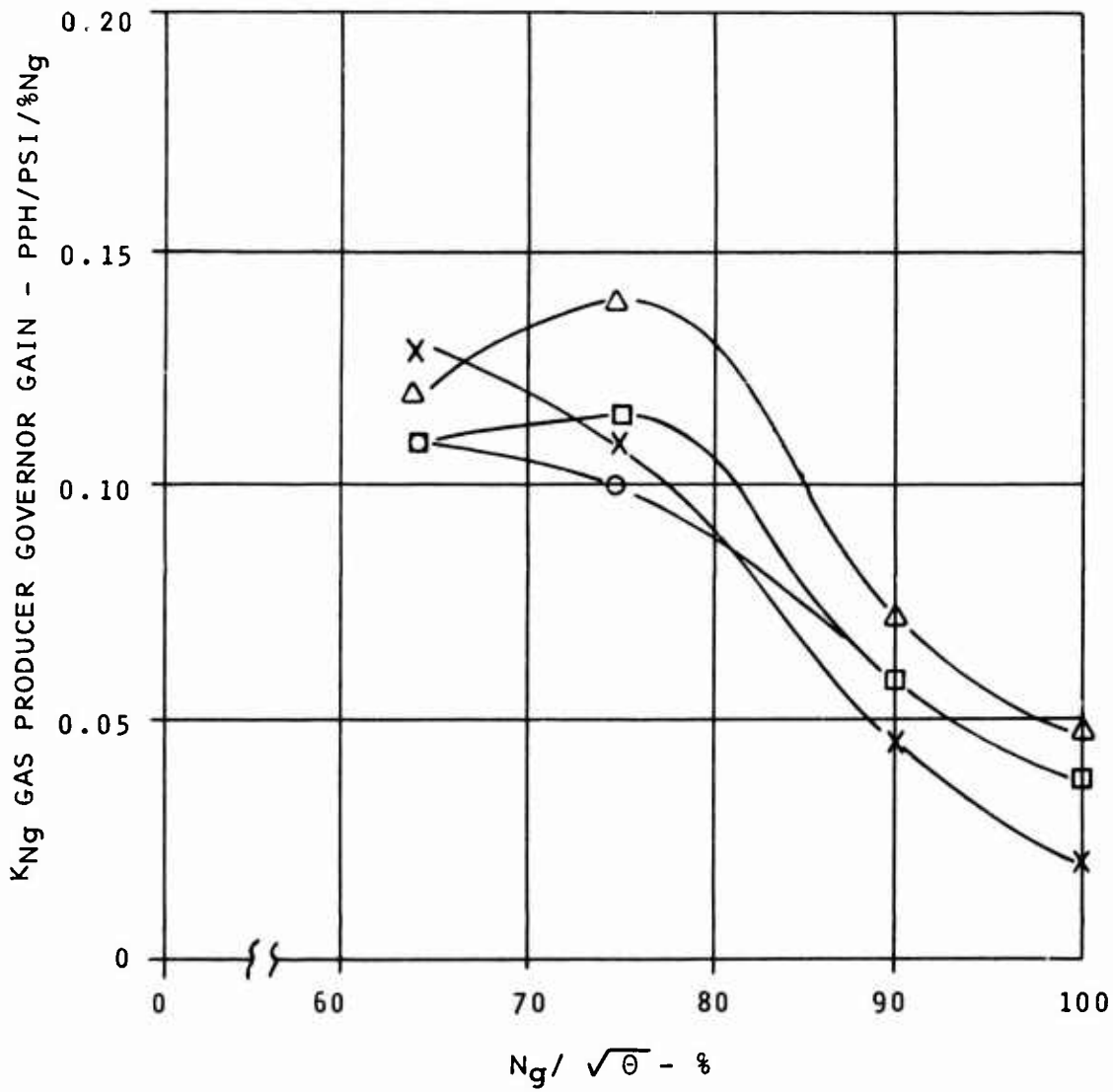
Figure 72. Optimum Gas Producer Governor Gain.

121

of the gas producer governor. This provides improved transient performance by virtue of the resulting lead action.

Power Turbine Speed Governor

The specified steady-state governing accuracy of $\pm$ 1/4% on power turbine speed requires integral control. The dynamic response requirements dictate that proportional control action be included if excessive transient speed errors are to be avoided. The resonant characteristics of helicopter rotors require that the control system provide dynamic compensation to preclude a high frequency limit cycle. For these reasons, a proportional plus integral control with a first order lag for attenuating rotor resonance has been selected.

In view of the wide variation in turbine and rotor dynamic characteristics, studies have been biased towards general control requirements rather than detailed optimization with a specific rotor model. The rotor characteristics defined in the simulation model for use in these control studies are based on actual data for systems in the same power class. With the flexibility in electronics to vary control gains and compensation, a power turbine speed governor that can meet the performance and stability requirements of the chosen models should meet the requirements of all other possible rotor or load configurations. In analyzing the frequency characteristics of a helicopter rotor system it is apparent that the resonance frequency peak typical of helicopter rotor dynamics limits performance, usually between 2.1 to 6 Hz. (See Figure 73.)

Compensation which can attenuate the resonate peak without affecting the primary system time constant (crossover frequency) will enable a higher control gain to be used and result in faster power turbine speed governor performance. In providing a control mode using a first order lag compensator, we are in effect attempting to attenuate the rotor system resonant peak. More sophisticated filtering techniques have been considered, but the complexity and cost of mechanizing them outweighed the performance advantages.
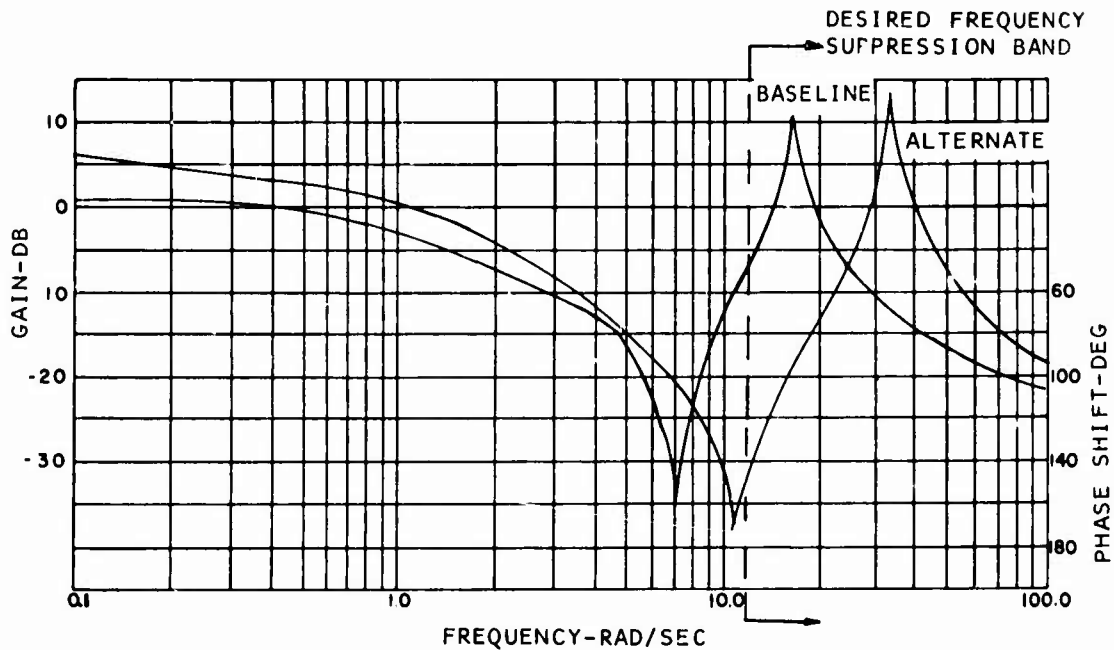
Figure 73. Typical Helicopter Rotor and Free Turbine Characteristics.

1. Governor Design

Linearized studies were conducted to establish the optimum gains and time constant over the operating envelope of the system. The criterion for optimal performance was based on maximizing the crossover frequency and providing as a minimum 6 db gain margin and 45° phase margin. The results of this study showed that both variable gains and time constants were required. Transient performance studies were then conducted to determine how much the variable governor system improved performance over a governor with fixed gains and time constant. The results of this study are summarized in Figure 74, which shows power turbine speed

123

transient for a step change in set speed and a ramp change in
engine load. At the low power conditions (N_g = 70%), the
optimized governor and fixed gain governor have about the same
performance. This was to be expected because the low power
condition requires the lowest gains and longest time constant
and, therefore the variable governor and fixed governor have
approximately the same design values. At the higher power
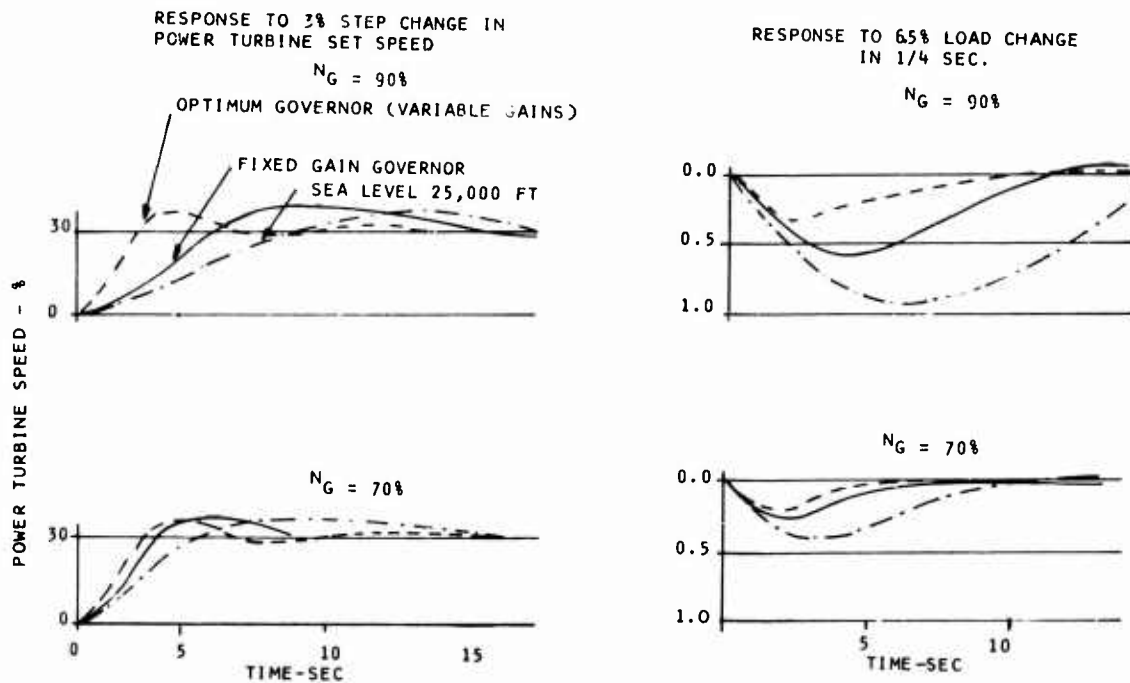
Figure 74. Variable Gain Versus Fixed
Gain Governor Performance.

levels the variable gain governor performance is considerably better. However, because in both cases the system performance is optimized at the critical low power condition and for all operating conditions both governors meet specified requirements, the fixed parameter governor was selected. Furthermore, the system incorporates collective pitch reset which provides load anticipation. This results in a substantial improvement in transient performance as compared to present systems even though the performance is not optimized at high power conditions. The linearized transfer function for the selected design is given by

$$\frac{N_g\%}{N_{fte}\%} = \frac{1.25(2.0\ S+1)}{S(0.75\ S+1)}$$

To preclude limit cycling the governor incorporated dead band stabilization. Also, provisions are included within the control system to reset the integrator to prevent saturation when the power turbine governor is not controlling.

Turbine Blade Temperature Limiting

Excessive metal temperatures within a gas turbine engine will aggrevate such conditions as creep, deformation and drooping. The most prone to these conditions are the 1st-stage turbine blades and stators which receive the direct gas flow from the burners.

The rate of creep in the turbine blades increases drastically above a certain critical metal temperature. Advanced engines will operate at higher gas temperatures for improved performance but this increases the risk of overtemperaturing.

The advanced engine control has a design goal to limit the turbine blade temperature to within $\pm$ 30°F of its critical temperature.

Based on the thermodynamic properties of an impingement cooled turbine blade and the nonlinear temperature versus radiation characteristics of a pyrometer, the control requirements necessary for meeting blade limiting specifications were studied for different steady-state and transient conditions.

125

Control Mode Study

The selected temperature limiting control mode is a proportional reset of W_F/P_{t3}. This mode of control provides the most direct path to fuel flow and thereby to control of temperature. Studies were conducted to establish the temperature limiters performance for both a step loss of cooling air and a step increase in the maximum fuel schedule. The step loss in cooling air results in a more rapid rise in blade temperature than a step increase in fuel flow. This is because the combustor lag in the path between fuel flow and blade temperature provides attenuation. A control mode incorporating a lead compensator to improve dynamic response to blade cooling losses was compared to the uncompensated control mode. Figure 75 indicates the response with lead compensation (Mode 2) and without (Mode 1) to a step loss in cooling efficiency of 10%.
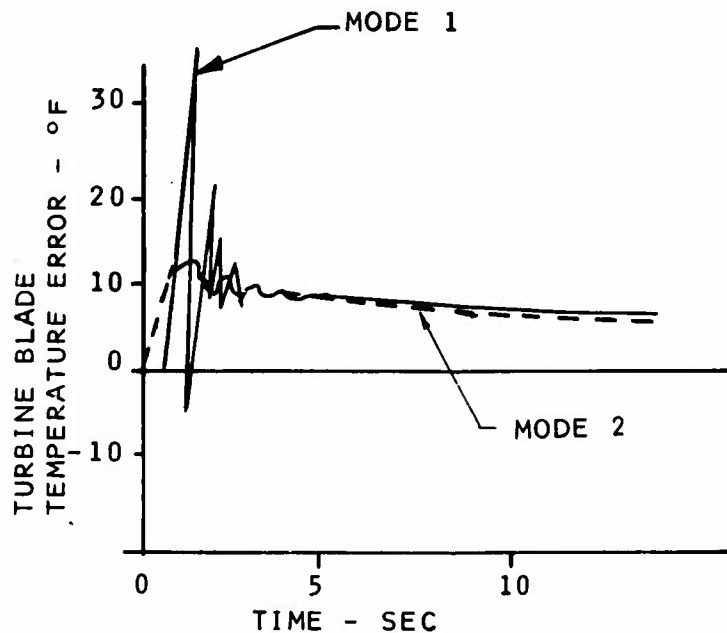
Figure 75. Blade Temperature Response
to Loss of Cooling.

126

Without lead compensation the system 'rings', creating a transient overtemperature spike of 37°F and a steady-state error of 11°F. The lead compensator in Mode 2 reduces the transient overtemperature spike to 13°F and the steady-state error to 9°F. Table XII summarizes a comparison of these two control modes for overtemperatures induced by both cooling inefficiencies and overfueling.

TABLE XII. COMPARISON STUDY – TEMPERATURE LIMITING MODES		
	MODE 1	MODE 2
Control Gain - K_B	0.0055 pph/psi/°R	0.008 pph/psi/°R
Steady-State Blade Overtemperature η_{BT} = 90%	+ 11°F	+9°F
Transient Overtemperature to 4% Step Change in Cooling	+ 37°F	+13°F
Steady-State Resolution for η_{BT} = 100% (Normal)	+ 7.0°F	± 2.0°F
Max Temperature Overshoot for Acceleration from Idle to Max. W_F/P_{t3} Schedule Increased 20% from Nominal	+ 7.0°F	+ 2.0°F
η_{BT} = Blade Cooling Efficiency (Nominally 100%)		

The results of the turbine blade temperature limiting studies indicate that:

1. A simple proportional control mode without compensation will meet the control requirements for all blade over-temperatures induced by a step increase in maximum fuel flow and up to ± 5% step variations in blade cooling.

2. To meet the turbine blade temperature requirements if blade cooling variations are greater than ± 5%, the control will require lead compensation.

3. If the combination of fuel transportation and burner combustion dead times exceeds 50 ms, or the thermal time constant of the blade is less than 0.1 sec, then lead compensation will also be necessary. (The advanced engine model has assumed 20 ms and 0.13 sec respectively.)

A simple proportional W_F/P_{t3} turbine blade temperature limiting control will meet the accuracy specifications over the 2- to 5-lb/sec airflow engines providing that step changes in cooling are within ± 5%. A sudden loss of blade cooling is not likely to be a normal condition, and therefore lead compensation has not been incorporated into the control system. Should this not be the case, or should the engine characteristics differ significantly from those assumed in the model, the lead compensation can be added to improve performance. The design gain required for the turbine blade temperature limiter is .0029 for the alternate engine and .0058 pph/psi/°F for the baseline engine.

Power Turbine Shaft Torque Limiting

The specification for torque control requires steady-state torque limiting to 115 ± 5% of rated shaft torque and a maximum overtorque of 12% for any transient condition. Rated torque is defined as the shaft torque at military rated power and 100% rotor speed.

In synthesizing a torque limiting mode of control, preliminary linearized analysis compared proportional torque control by resetting the gas generator governor with a W_F/P_{t3} control mode. Without dynamic compensation, the gas generator speed

128

reset mode required a low gain for stable operation. As a consequence, response was poor.

Table XIII summarizes the W_F/P_{t3} control mode performance and indicates that the proportional W_F/P_{t3} reset mode will meet the requirements for torque limiting. This control mode meets requirements for both the baseline and alternate engines. The required gains are .03 for the alternate engine and .056 pph/psi/lb-ft for the baseline engine.

Analytically, a W_F/P_{t3} reset torque limiting control satisfies the steady-state and dynamic torque requirements for the advanced technology engine control. The definition of a torque sensor for this control has not been finalized and present indications are that a torque sensor and its relevant signal processing circuits will at best be accurate only to $\pm$ 2.5%.

	Performance		Stability	
Conditions	Steady-State Error	*Transient Torque Error	Gain Margin (D.B.)	Phase Margin (deg)
Sea Level Std. Day (+59°F)	0.0%	+2.0%	8.0	70
Sea Level Cold Day (-65°F)	+2.5%	+5.0%	6.0	45
Sea Level Hot Day (+135°F)	-1.5%	+1.0%	8.0	65
25,000 ft Alt. Std. Day		Low Torque		
Specification	±5%	+12%	6 D.B. (Min.)	45 (Min.)

TABLE XIII. TORQUE LIMITING PERFORMANCE SUMMARY

*Transient following collective pitch increase from 10% to 100% at 70% free turbine governing speed.

129

Twin Engine Load Sharing

The type and frequency of load splits which may occur in multi-engine installations have been covered elsewhere.[10]
The ATEC includes the facility for sharing the load by incorporating a control mode that will uptrim the power turbine set speed demand of the lower power engine in proportion to the load error as shown in Figure 76. As a result of the low torque engine increasing its power output, the coupled power turbines will momentarily overspeed, causing the other engine control to decrease engine power to satisfy its power turbine speed governor requirements. The result will be an integral load sharing control system.
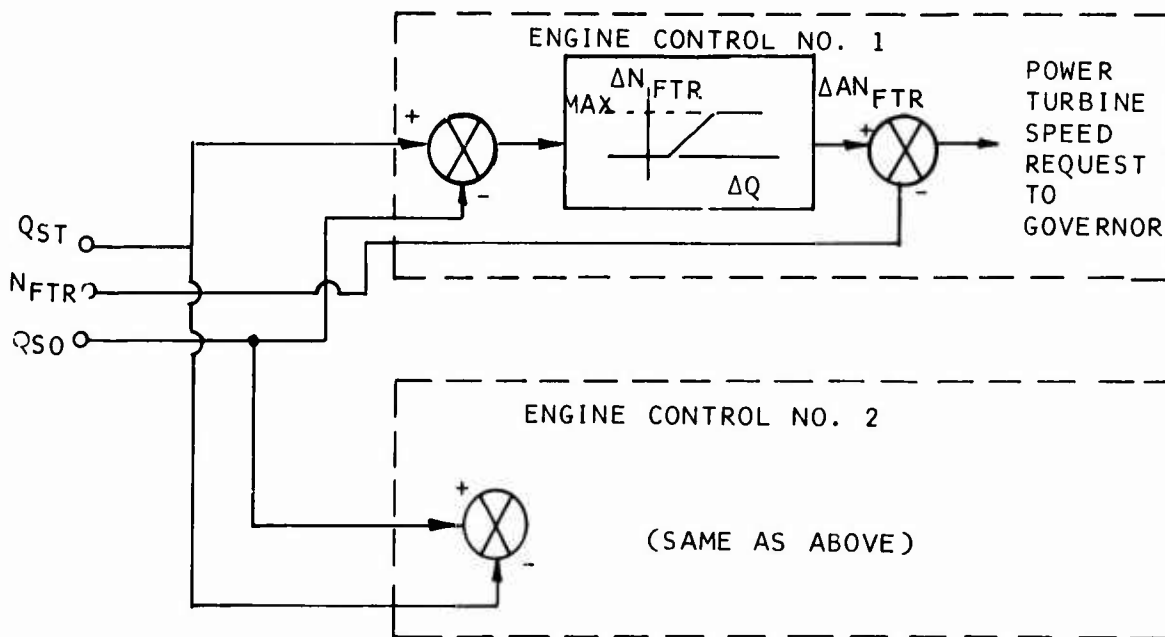
Figure 76. Load Sharing Control Block Diagram.

Studies showed that system performance is maintained with a relatively low control gain ensuring good stability characteristics. The control mode includes a 4% deadband to isolate the torque signals from the steady-state power turbine speed governor control. The amount of deadband required depends on the accuracy of the torque sensor. For this study a 3% torque sensor was assumed.

Also included in the control is a 10% limit on the reset authority of the load sharing control to prevent the possibility of a power turbine overspeed condition (greater than 110%). The gains required are 114 and 490 rpm/lb-ft for the alternate and baseline engines respectively.

The advanced technology engine control, using a power turbine speed trim proportional to the shaft torque error between engines, can meet the requirements for matching loads to ± 5% if a satisfactory torque measuring de ice is available (requiring accuracies to 2% full scale).

Present estimates on available torque sensors indicate that 2.5 to 3.0% accuracies can be obtained. However, these figures may be optimistic unless periodic calibrations and stable temperature conditions are maintained.

Additional Control Studies

Additional nonlinear control mode studies were made to evaluate the impact of integrating all control modes of the system into one functional control system. The more significant results of this study are discussed in the following sections.

Acceleration/Deceleration

Table XIV shows the system acceleration sensitivity to forward loop parameters. The performance is summarized by the time for the engine control to match an acceleration requested fuel flow when operating at steady state along a gas generator speed governor droop line.

Critical dynamics of the fuel metering system are the time lag in the head pressure regulator and the metering valve stepper motor slew rate. The sensitivity to the fuel transportation deadtime is also included in the study summary.

131.

TABLE XIV. ACCELERATION – SENSITIVITY TO CONTROL LAGS				
CONTROL PARAMETERS			ACCELERATION TIME	
Dead Time (ms)	Fuel Metering Lag Time (ms)	Stepper Motor Rate (steps/sec)	$\tau(8\%)$ (sec)	$\tau(4\%)$ (sec)
20	40	500	0.55	0.6
–	–	1000	0.30	0.55
–	–	150	0.25	0.52
–	–·	2000	0.25	0.48
20	0	1500	0.1	0.15
–	10	–	0.12	0.35
–	20	–	0.17	0.40
–	30	–	0.22	0.48
–	40	–	0.25	0.52
0	40	1500	0.18	0.43
10	–	–	0.22	0.45
20	–	–	0.25	0.62
40	–	–	0.45	0.80
0	0	1500	0.06	0.12

Definition: $\tau(8\%)$ = time to reduce error between control demanded W_F/P_{t3} and actual engine W_F/P_{t3} to less than 8%, following gross acceleration demand.

$\tau(4\%)$ = time to reduce error to less than 4%.

Table XV summarizes the acceleration effective time constant for various fuel metering lags and fuel transportation dead times and stepper motor rates.

It is significant that approximately 10% improvement in acceleration time is realized by reducing the metering lag from 40 ms to 20 ms.

132

Fuel Transportation Dead Time (ms)	Fuel Metering Lag Time Constant (ms)	τ (sec)
TABLE XV. ACCELERATION/DECELERATION TIME – SENSITIVITY TO CONTROL SYSTEM LAGS		
Acceleration Idle to Max		
20	40	1.15
20	20	1.05
20	10	1.05
10	40	1.10
Deceleration Max to Idle		
20	40	1.25
20	20	1.20
20	10	1.20
10	40	1.20
0	40	1.20
τ = Time to acceleration/decelerate to 63% of requested speed change. (Effective time constant.)		

Based on these results the dynamic design objectives for the main metering valve system are specified as follows:

1. Main Metering System Dynamic Specification

    Pressure Head Regulator -   Equivalent Lag   25 ms

    Slew Rate (Stepper Motor) - 1000 to 1500 $7.5°$
                               Steps/sec

Integrator Reset

Following a transfer from power turbine governing control to one of the other engine control modes, the governor will continue integrating the speed error open loop and eventually saturate. On return to power turbine governing control, large speed overshoots can occur before the governor can integrate back from this saturated condition.

The control incorporates a means to reset the output of the power turbine governor integrator as a function of the actual control output signal whenever power turbine speed governing is open loop. Also, deadband stabilization is included to prevent limit cycling.

The effect of the integrator reset to prevent large speed overshoots is illustrated in Figure 77. As indicated, the reset scheme eliminates a 6% overshoot for the same condition.
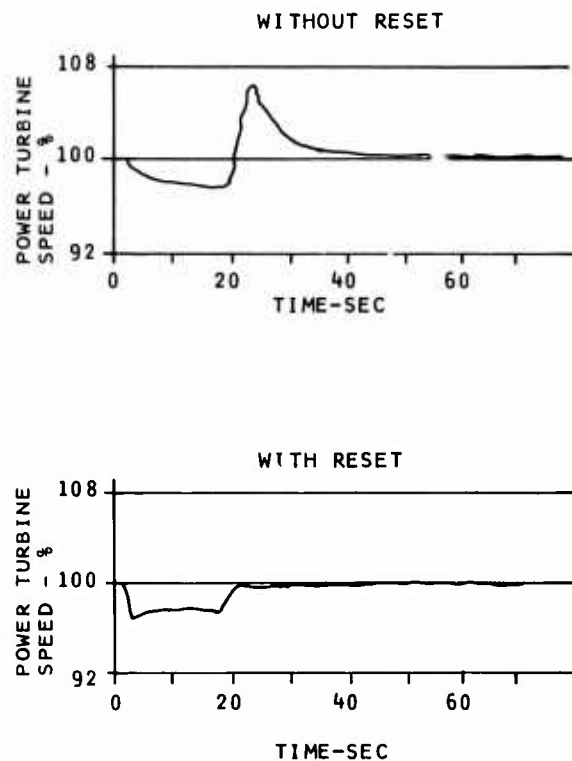
Figure 77. Power Turbine Governor Integrator Reset Performance.

134

SENSORS

The application of electronic computation to advance aircraft
gas turbine fuel controls necessitates the development of
suitable electric transducers to sense input parameters.
These sensors must be compatible with performance and opera-
ting environment, and must also meet size, weight, and cost
constraints. The goal of the sensor development phase of the
program is to evaluate and select the type of sensor which
will be most suitable for sensing compressor discharge pres-
sure, turbine blade temperature, mass fuel flow, and position.

Pressure Transducers

Preliminary Specifications and Evaluation

The first step in the program to select a suitable pressure
transducer for sensing P_{t3} was to generate a preliminary
specification which accurately reflects ATEC requirements.
The pertinent requirements in this specification are:

Pressure range:	8 to 250 psia
Temperature range:	-65°F to +250°F
Accuracy:	Static error not to exceed $\pm$ 1% per point or $\pm$ 0.5 psia, whichever is larger
Response:	Time constant less than 0.01 sec
Warm-up time:	Less than 20 sec to meet full accuracy
Long term-stability:	Less than $\pm$ 0.1% change in output at the calibration temperature during a 6-month period

Letters were sent to 246 manufacturers requesting if they had
an interest in supplying the pressure sensor. This survey re-
sulted in 48 positive replies. These manufacturers were re-
quested to supply a technical proposal and a quote for prices
on prototype quantities and a volume production quantity.

135

Seventeen proposals for pressure transducers were received. These proposals were reviewed and the pertinent data was tabulated for analysis. This analysis determined who were satisfactory suppliers for the pressure transducer. Off-the-shelf pressure transducers were then ordered from these manufacturers for bench testing and evaluation at Chandler Evans.

All of these devices, except for one, were diaphragm type pressure sensors in which some type of strain gage is used to transduce pressure into a proportional voltage. The exception was a capacitive type pressure transducer. Each device was tested over the operating temperature range (-65°F to +250°F) in an environmental chamber. A fused quartz precision pressure test set was used to generate the reference pressure for calibrations. The transducers were tested for linearity, repeatability, hysteresis, thermal drift, etc. The test results are summarized in Tables XVI and XVII.

The evaluation of manufacturer proposals and the results of the test program supports the following conclusions:

1. There is no pressure transducer available at the present time that can accomplish engine-mounted compressor discharge pressure measurements, reliably and economically, within performance specifications. A bulky, remotely mounted, temperature-controlled air data type sensor is necessary to meet the accuracy requirements.

2. The best overall accuracy that can be obtained from any present state-of-the-art pressure transducer, over the specified temperature range, is ± 2.0 psi RSS error at 8 psia, and almost 3.0 psi RSS error at 250 psia. Units that can achieve this accuracy will cost a minimum of $450.00.

136

TABLE XVI. SUMMARY OF PRESSURE SENSOR TEST RESULTS

PARAMETER	DEPOSITED THIN FILM STRAIN GAGE		SEMICONDUCTOR STRAIN GAGE		CAPACITIVE		CHANDLER EVANS SPECIFICATION CE-PS 323A (MODIFIED)
	MEASURED	SPECIFIED	MEASURED	SPECIFIED	MEASURED	SPECIFIED	
END POINT AT 0 PSIA	-.119 TO +.297 MV	-	-.620 +.694 MV	-	46.25 PF 47.35 PF	-	-
END POINT AT 250 PSIA	+36.610 TO +36.054 MV.	-	+130.70 TO +132.63 MV	-	56.45 PF TO 57.90 PF	-	-
ZERO BALANCE	-0.325 TO +0.81% F.S.	<±2% F.S.	-0.467 TO +0.524% F.S.	<±2% F.S.	±1.18%	-	-
FULL SCALE OUTPUT 0-250 PSIA	3.65 $\frac{MV}{V}$	3.67 $\frac{MV}{V}$	31.69 $\frac{MV}{V}$	32.11 $\frac{MV}{V}$	12.66 PF	12 TO 13 PF	-
TERMINAL LINEARITY	+0.125%F.S. 8TO250 PSIA	<±0.3% F.S.	0.14% F.S. 8TO250 PSIA	<0.15% F.S.	-1.33% F.S. WITHOUT COMPENSATION -0.19% F.S. WITH COMP.	±0.1% F.S. CONFORMITY	<±0.1% F.S.S.
HYSTERESIS	0.182% F.S. -65°F TO +250°F	<0.1% F.S.	0.082% F.S. -65°F TO +250°F	<0.05% F.S.	0.04% F.S. +60°F TO +160°F	<0.02% F.S.	<0.02% F.S.
REPEATABILITY	0.14% F.S. -65°F TO +250°F	-	0.10% F.S. -65°F TO +250°F	<0.05% F.S.	0.05% F.S. +60°F TO +160°F	<0.02% F.S.	<0.01% F.S.
THERMAL ZERO SHIFT % F.S. / °F	$\frac{.004\% \text{ F.S.}}{°F}$	$\frac{.005\% \text{ F.S.}}{°F}$	$\frac{.004\% \text{ F.S.}}{°F}$	$\frac{<.01\% \text{ F.S.}}{°F}$	$\frac{.052\% \text{ F.S.}}{°F}$ WITHOUT COMP.	$\frac{<.005\% \text{ F.S.}}{°F}$ +60°F TO +160°F	$\frac{<.01\% \text{ F.S.}}{°F}$ REPEATABLE TO ±.0005% F.S./°F
THERMAL SENSITIVITY SHIFT	$\frac{.005\% \text{ F.S.}}{°F}$	$\frac{<.005\% \text{ F.S.}}{°F}$	$\frac{.004\% \text{ F.S.}}{°F}$	$\frac{<.01\% \text{ F.S.}}{°F}$	$\frac{0.011\% \text{ F.S.}}{°F}$ WITHOUT COMP	$\frac{<.005\% \text{ F.S.}}{°F}$ +60°F TO +160°F	$\frac{<.01\% \text{ F.S.}}{°F}$ REPEATABLE TO ±.0005% F.S./°F
TIME CONSTANT	<6 MILLISEC	-	<6 MILLISEC	-	<25 MILLISEC	<25 MILLISEC	<10 MILLISEC
VIBRATION SENSITIVITY	$\leq 0.004\% \frac{\text{F.S.}}{g}$	$\leq 0.01\% \frac{\text{F.S.}}{g}$	$\leq 0.005\% \frac{\text{F.S.}}{g}$	$\leq 0.006\% \frac{\text{F.S.}}{g}$	$\leq 0.003\% \frac{\text{F.S.}}{g}$	-	$\leq 0.02\% \frac{\text{F.S.}}{g}$

TABLE XVI.-CONTINUED

PARAMETER	DEPOSITED STRAIN GAGE REMOTELY LOCATED		BONDED WIRE STRAIN GAGE		BONDED METAL FOIL STRAIN GAGE		CHANDLER EVANS SPECIFICATION CE-PS 3255
	MEASURED	SPECIFIED	MEASURED	SPECIFIED	MEASURED	SPECIFIED	
END POINT AT 0 PSIA MV/V	0.0225	---	-0.0469	---	+0.0275	---	---
END POINT AT 250 PSIA MV/V	+2.5471	---	+0.9514	---	+2.2312	---	---
ZERO BALANCE % F.S.	+1.3	$<\pm 2.0$	-0.6	1.0	+2.86	<5.0	---
FULL SCALE OUTPUT 0-250 PSIA MV/V	2.5246	+2.5200	+0.9983	+0.9991	2.2037	2.1817	---
LINEARITY % F.S.	+0.14	$<\pm 0.3$	0.10	<0.15	0.2	0.2	$<\pm 0.1$
HYSTERESIS % F.S.	0.18	<0.1	0.14	<0.05	0.25	0.15	<0.02
REPEATABILITY % F.S.	0.05	---	0.	<0.03	0.01	0.02	<0.01
THERMAL ZERO SHIFT % F.S./°F	+0.004	<0.005	+0.005	<0.01	+0.01	0.007	<0.01%F.S./°F REPEATABILITY TO ±0.0005%F.S./°F
THERMAL SENSITIVITY SHIFT % F.S./°F	+0.002	<0.005	+0.005	<0.01	+0.003	0.003	<0.01%F.S./°F REPEATABILITY TO ±0.0005%F.S./°F

3. The greatest source of error in the pressure trans-
ducers are temperature shifts. The zero shift is
random and the temperature coefficient of zero shift
and gain shift are not repeatable from unit to unit.
The temperature gain and zero shift coefficients
can be matched to within 20% but at great expense.

4. Strain gage transducers require several minutes warm-
up before they can measure pressure within their
specified accuracy. This warm-up period is unaccept-
able for engine control.

5. Bonded strain gage transducers exhibit long term
drift characteristics. It does not appear that any
bonded strain gage has less than 0.1% full
scale drift in a six-month period.

Revised Specifications and Sensor Selection

A number of pressure sensor manufacturers were consulted
to determine what improvements in pressure sensor perfor-
mance could be realistically expected in the next five
years. Also, a redistribution of the allocation of errors
in the control was made in order to determine to what extent
we could relax our pressure sensor accuracy requirements.
The results of these efforts are summarized by the graphs
in Figure 78.

The curve labeled Revised ATEC Spec represents the revised
accuracy requirements for the pressure sensor. Although
the reallocation of permissible errors in the control
allowed the pressure sensor accuracy to be relaxed in the
high pressure range (the original specification required a
maximum error of 1% of reading, or 0.5 psi, whichever is
greater), it did not affect the accuracy requirement in the
low pressure range where it is most critical. The curve
labeled 1970 Production Unit is the expected error in a
present day high performance pressure sensor. It obviously
can satisfy the ATEC specification in a limited pressure
range only (between 150 and 250 psia).

139

NOTE: PRESSURE SENSOR ERROR FOR 1970 & 1975
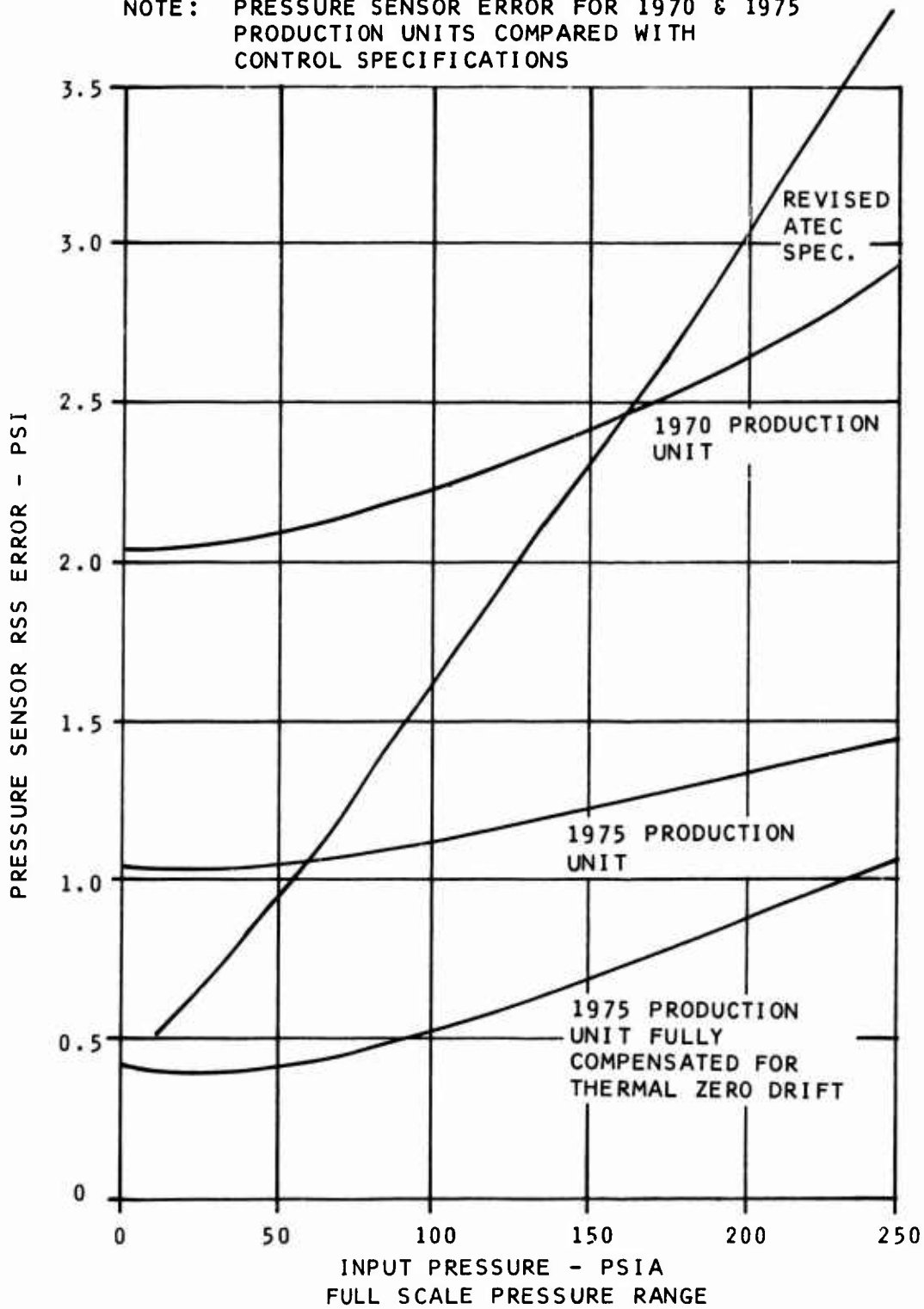PRODUCTION UNITS COMPARED WITH
CONTROL SPECIFICATIONS

Figure 78. Projected Pressure Sensor Accuracy.

140

The expected improvement in the accuracy of pressure sensors
is given by the curve labeled 1975 Production Unit. This
curve indicates that pressure sensor accuracy is expected
to improve by a factor of two in the next five years.
Actually, pressure sensors with accuracy as good as this
are now available, but in small quantity and at high cost.
The best improvement that can be realistically anticipated
is that the production of these higher performance units
can be substantially increased, and their price can be sig-
nificantly reduced. The 1975 production unit meets the
ATEC accuracy requirements over most of the pressure range
except for pressures below 60 psia.

An analysis of the contributing errors indicates that the
primary source of inaccuracy in the low pressure range is
the drift in zero output signal (offset) with temperature.
If it were possible to fully compensate the 1975 production
unit for thermal zero drift, its error would be within
requirements over the entire operating pressure range as
indicated on the graph.

The major problem in implementing this approach is that it
may not be feasible to compensate the pressure sensor for
thermal zero drift beyond what the manufacturer can provide
because of excessively high cost. The extent to which the
thermal zero drift coefficient is repeatable from one
temperature cycle to another and the errors in the compen-
sating elements themselves are the limiting factors in this
approach.

The pressure sensor program was devoted to evaluating the
feasibility of developing a pressure transducer that could
be sufficiently compensated for thermal zero drift to meet
the revised ATEC specification. A variable capacitance
type pressure sensor was selected for this purpose for the
following reasons:

1. Capacitance is a good parameter for controlling
   frequency in an oscillator circuit, and therefore
   it is simple to convert pressure into a frequency
   modulated signal for hybrid computation with this
   type of sensor.

141

2. Warm-up time for a capacitive type pressure sensor is less than 20 sec.

3. Capacitive pressure sensors seem to exhibit less hysteresis, repeatability, and drift errors than strain gage types.

An improved capacitive pressure sensor (mini sensor) capsule for gas turbine applications has been developed. This sensor is greatly reduced in size and weight, and is capable of being used at temperatures up to 600°F. Two prototype capacitive gage pressure sensor capsules were procured from REC (Models 809A1 & 809B1). A schematic of the REC pressure capsule is shown in Figure 79.

REFERENCE-PRESSURE

CABLE TRIAX

CASE 1" DIA. X 1.3" LONG
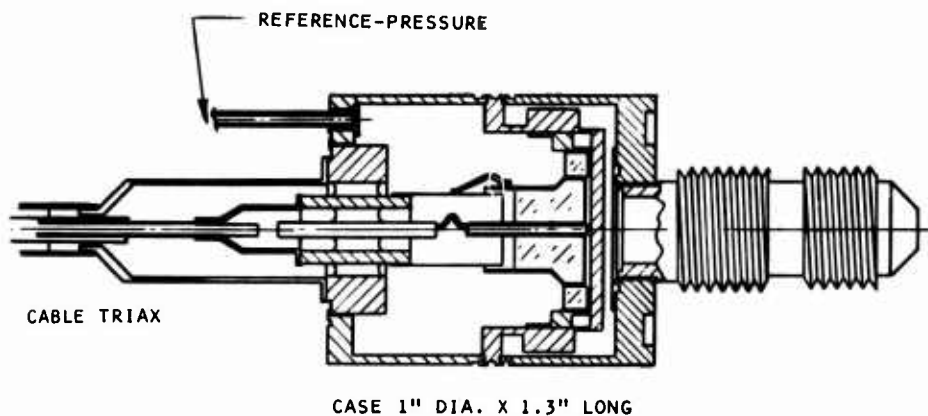
Figure 79. Capacitive Pressure Sensor Capsule.

142

Gage pressure sensors were used since absolute pressure
units were unavailable at the time of procurement. However,
the basic capsule is identical, and performance data obtained
from testing these units will equally apply to the absolute
pressure units. These units were tested for accuracy,
linearity, thermal stability, dynamic response, and vibra-
tion endurance.

We have also developed the electronic signal processing
circuit required to convert the pressure sensor output
capacitance to a signal whose frequency is proportional
to input pressure. The pressure sensor capsule interfaced
with its signal processor provides the pressure transducer
function. The signal processor also provides the pressure
transducer with linearity and temperature drift compensation.

Capacitive Pressure Sensor Specifications

REC specifications for the pressure sensor capsule are given
below. Chandler Evans has confirmed these specifications
through its own test program.

1. Pressure Sensor Static Response

   Sensor output is a capacitance which is a nonlinear
   function of input pressure. The functional relation-
   ship is given by the equation:

   $$C(P) = \left[C_o/1\text{-}KP \right] + C_S$$

where:

$$P = \text{input pressure, 0 to 250 psi}$$
$$C(P) = \text{output capacitance (in pico farads)}$$
$$C_O + C_S = \text{output capacitance at zero input pressure (pico farads)}$$
$$C_S = \text{stray capacitance across the pressure sensor output terminals (pico farads)}$$
$$K = \text{pressure sensitivity factor (psi}^{-1}\text{)}$$

C_O, C_S and K are constants which have the following
values for each sensor.

143

	809A1	809B1	Unit
C_O	6.170076	5.646325	Pico farads
K	0.248224	0.002074	psi^{-1}
C_S	0.002254	0.225275	Pico farads

Both units conform to the above equation to within 0.02% FS error.

2. Hysteresis

The hysteresis error is less than $\pm$ 0.02% FS. The hysteresis in the 809B1 unit was also measured and is less than $\pm$ 0.02% FS.

3. Temperature Drift Characteristics

The temperature drift characteristics for both units are plotted in Figures 80 and 81.

4. Pressure Transducer Static Response

The output frequency of the signal processor is related to pressure sensor capsule capacitance by the equation:

$$f(P) = A/C_O - A/C(P)$$

where
$f(P)$ = output frequency
C_O = capsule capacitance at zero input pressure
$C(P)$ = capsule capacitance at any input pressure
A = scale factor

From this equation and the capacitance versus input pressure function we can derive the equation relating transducer output frequency to input pressure.

If C_S could be made equal to zero, then

$$f(P) = A K P C_O$$

144
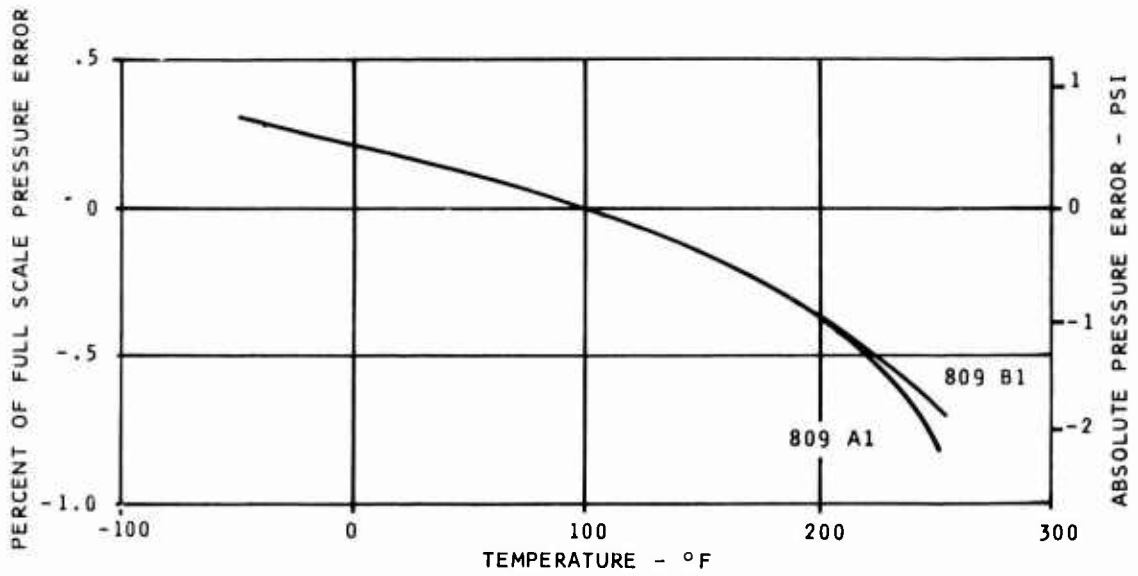
Figure 80.   Pressure Sensor Temperature Sensitivity
at Zero Pressure.
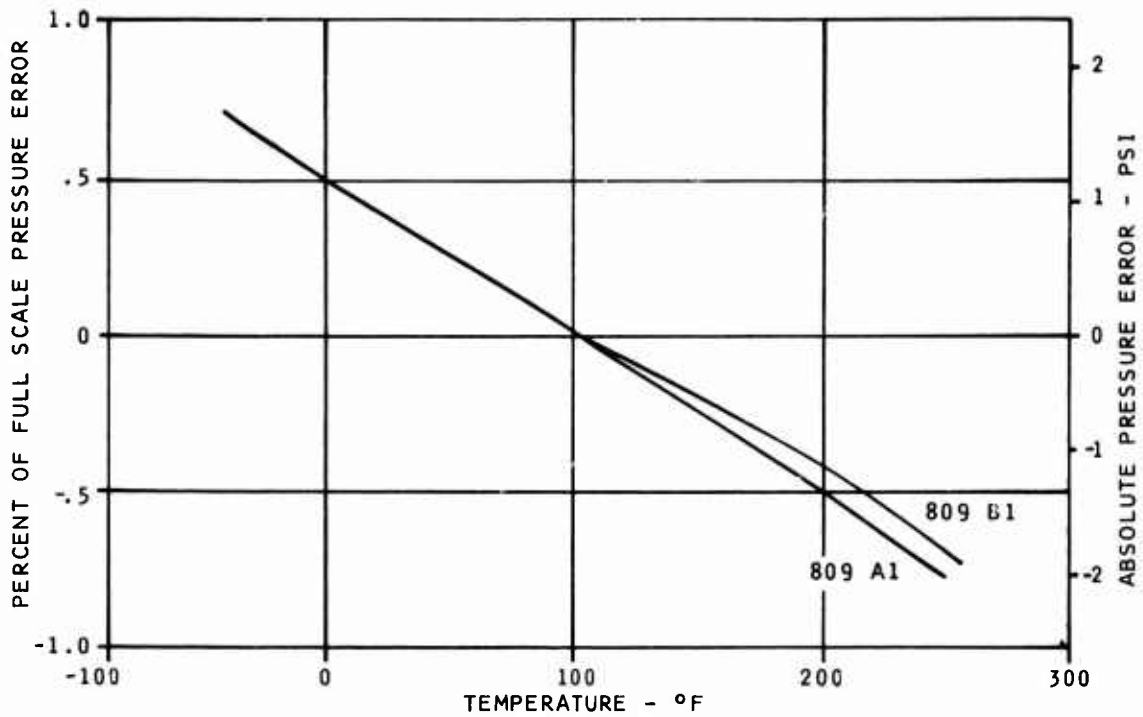
Figure 81.   Pressure Sensor Temperature Sensitivity
at Maximum Pressure.

145

The pressure transducer, developed at Chandler Evans, uses
two capacitive pressure sensors, each provided with its
own signal processing circuit, to generate frequency pro-
portional to pressure. One of the sensor capsules senses
P_{t3} pressure while the other is maintained at zero (vacuum)
pressure. The output frequencies of their signal processing
circuits are subtracted to provide the proportional relation-
ship between pressure and frequency given in the above
equation. Nonlinearity due to stray capacitance is minimized
by use of a compensating capacitor in the electronic signal
conversion circuits. The close match in zero pressure temp-
erature drift characteristics of the two capsules compensates
for zero offset.

Pressure Transducer Tests

The accuracy of the pressure transducer over the operating
temperature range (-65°F to +250°F) was measured in the test
rig illustrated in Figure 82.
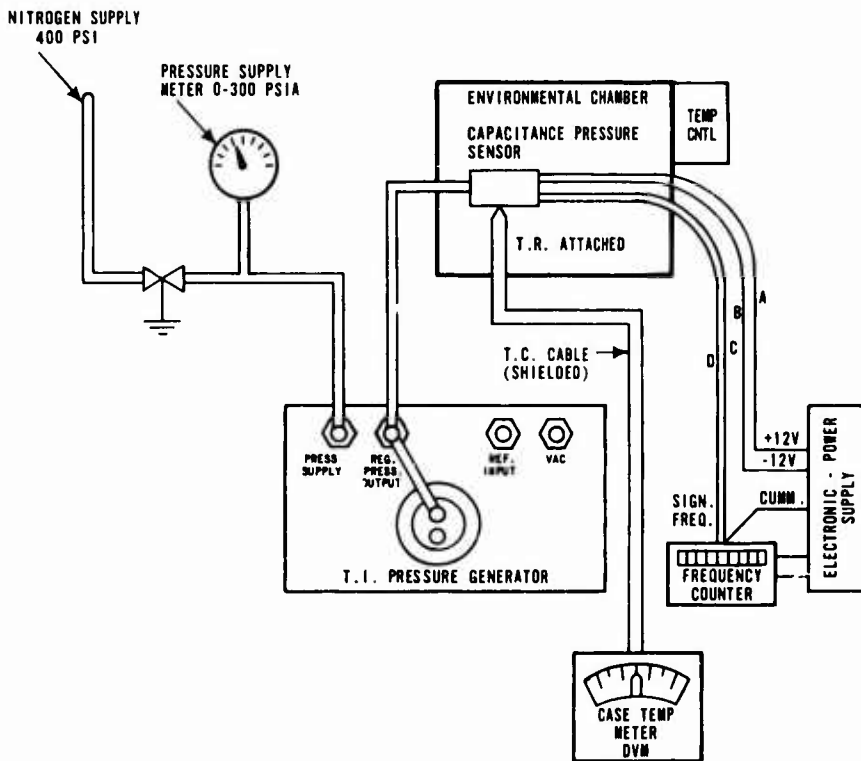
Figure 82. Pressure Sensor Test Rig.

146

Input pressure, accurate to ± 0.004% FS error, is generated by the TI pressure generator, and a high accuracy thermistor is used to measure case temperature within ± 1°F error. The pressure transducer was placed in the environmental chamber and the electronics were modified to attempt to meet the specifications. Due to the low capacitance and output required, it is very difficult to achieve a temperature coefficient with a uniform slope, and it is almost impossible to match the two signal conversion circuits or compensate them to the required specifications over the full -65°F to +250°F range.

It has been proven that nearly all the temperature coefficients of the electronics are due to AC effect on a number of components (stray capacitors, delay time, transition time, etc.). Present-day components, especially operational amplifiers, are not really fast enough for our application, but we feel sure that they will be improved in the future.

Figure 83 represents the best that we can achieve with the limitations of present-day components and in the time allocated for compensation circuit design.

Actually, the main problem was a matter of calibration because of the small capacitances involved. Movement of the board, leads, components and static pickup can all cause errors. This problem should be a bit less severe in the prototype because the boards and leads will be fixed in position. In the production unit, in order to meet our specification, it is imperative that the circuit be mounted inside the transducer and all calibrations and compensations be done with the transducer and then seal the unit.

The test results given in Figure 83 indicate that the pressure transducer is capable of performing within the specified accuracy in the fuel cooled electronic environment (-65 to +200°F). The pressure sensor accuracy problem is, therefore, alleviated by including the transducer in the fuel cooled computer package. Transducer error can be split in half by calibrating at a temperature other than ambient room temperature.

Figure 84 gives pressure sensor error for calibration at +180°. As can be seen, transducer error is well within the allowable limits.

147
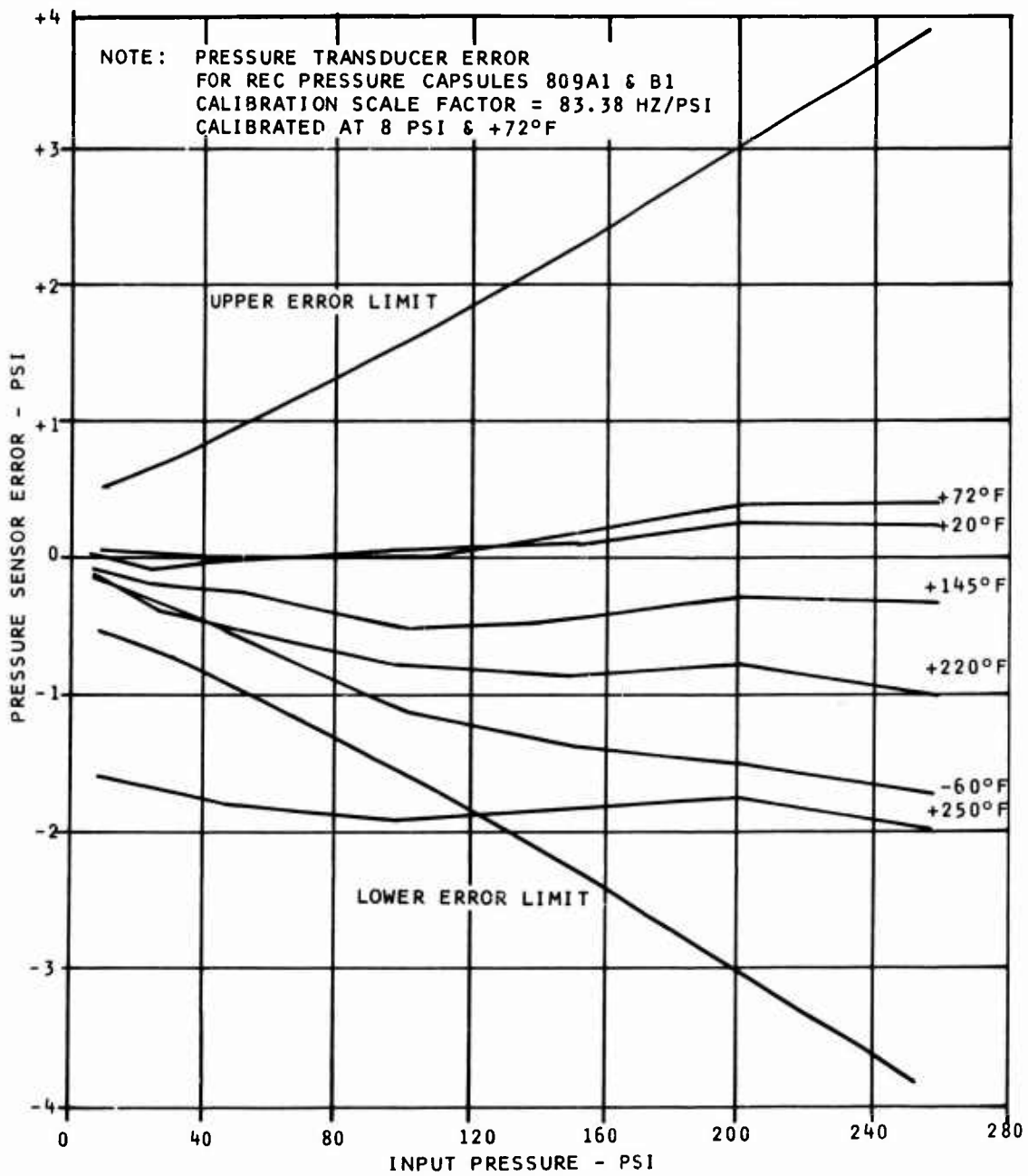
Figure 83. Pressure Transducer Error - Calibrated
at 8 psi and 72°F.

148
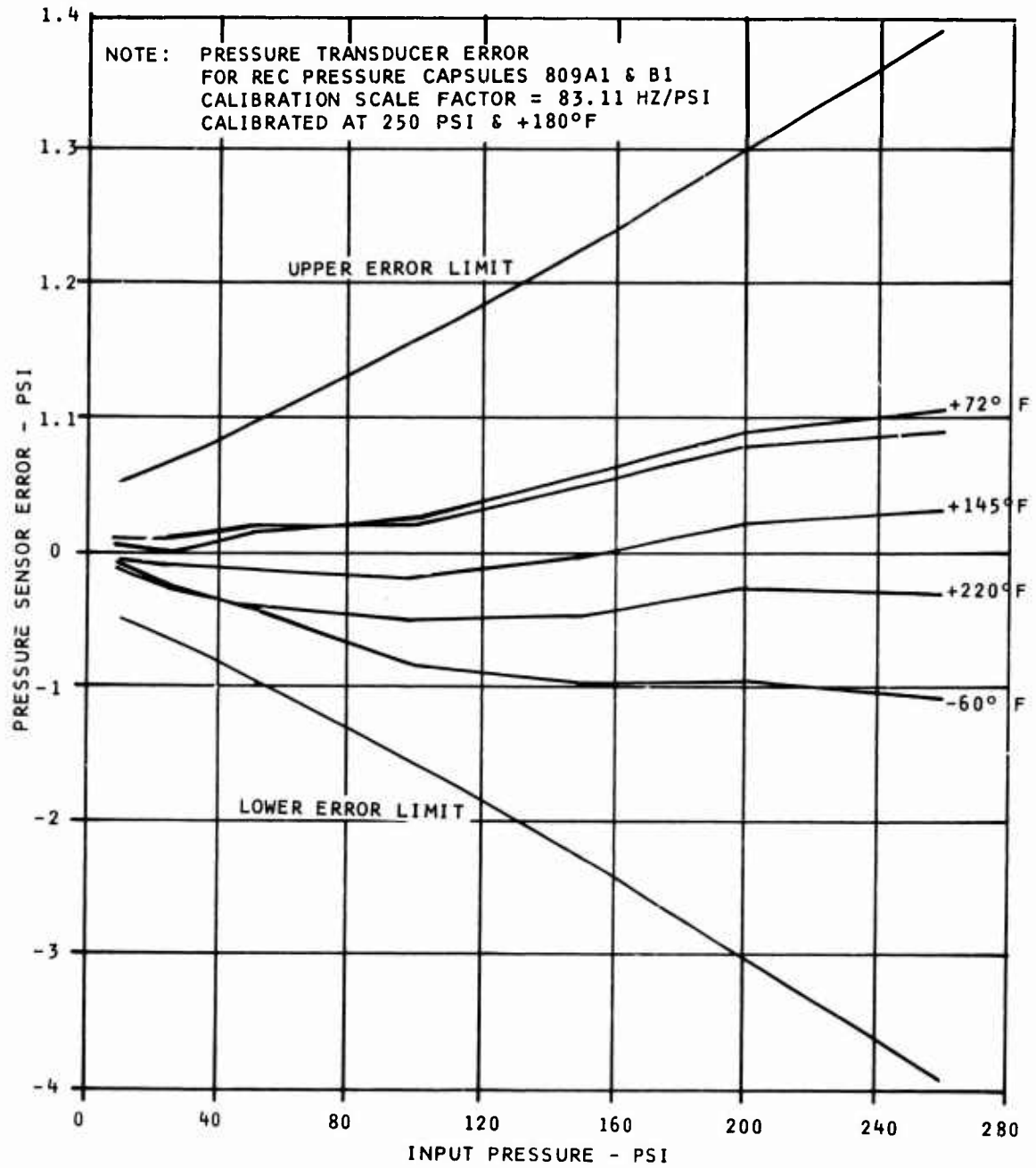
Figure 84.   Pressure Transducer Error - Calibrated
at 250 psi and +180°F.

149

We have also received from REC a development breadboard model of their 831CRI pressure to frequency transducer. This device is an experimental unit which was designed by REC to meet Chandler Evans requirements. It includes both their capacitive pressure sensor capsule and the electronics required to convert capacitance into frequency. The unit is calibrated to provide an output frequency directly proportional to input pressure; i.e.,

$$f = 83.32P$$

where   f = output frequency in Hz
        P = input pressure in psi

The calibration is made at an input pressure of 100 psi with case temperature at +10°F in order to divide the temperature drift errors in half.

This unit was also tested in the environmental chamber for static accuracy over the temperature range of -65°F to +212°F. The results of this test are given in Figure 85 and indicate that the transducer error is within the specified constraints, although its performance is marginal at low pressures.

In addition to the temperature tests, the transducer was also tested at room temperature for hysteresis, repeatibility, and drift. Hysteresis in the transducer static response over the pressure range of 0 to 250 psi is less than 0.05% of full scale, the unit is repeatable to within ± 0.03% of full scale, and drift in the output is negligible.

The change in scale factor from the REC calibrated value of 83.32 to the measured value of 83.50 (Hz/psi) seems to be due largely to differences in test installation and equipment. This difference in scale factor introduces an error in the output of + 0.216% per point which is not critical.

Pressure Capsule Transient Response

The response of the pressure sensor capsule to a step change in input pressure was measured and the results are given in Figure 86.

150

Figure 85.   Pressure Transducer Error - Calibrated
at 100 psi and +10°F.
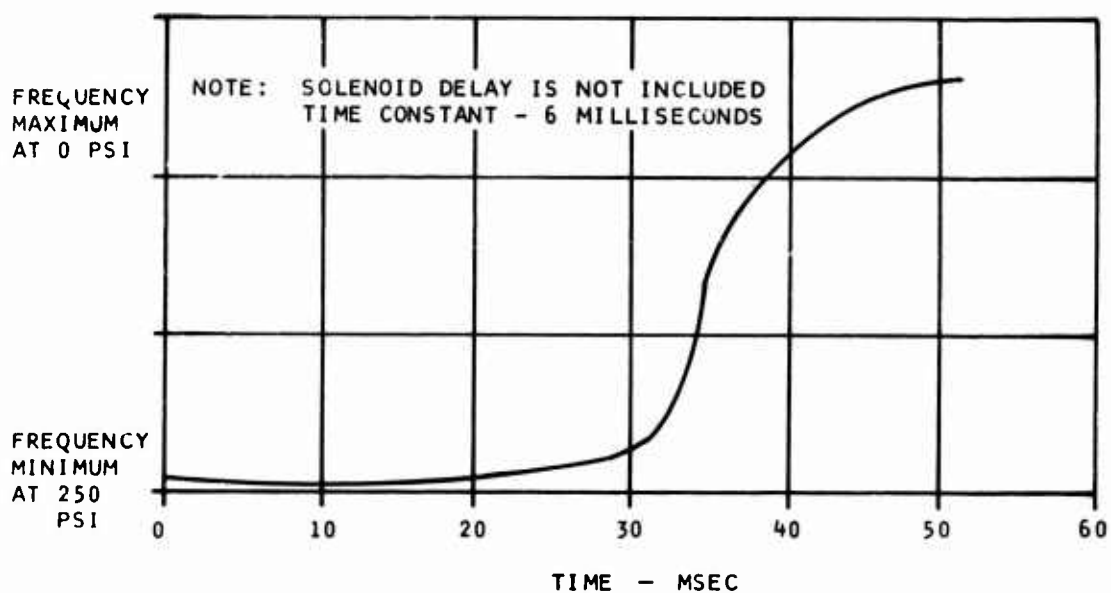
Figure 86. Pressure Capsule Transient Response.

The pressure sensor time constant, obtained from Figure 86, does not exceed 6 ms. This does not include solenoid or electronic delay time. Delay time in the signal processing circuits is negligible. The pressure capsule time constant compares well with that of strain gage pressure sensors previously tested at Chandler Evans. The time constant is primarily due to pneumatic and mechanical lags inherent in the design and construction of most pressure sensor devices.

Pressure Sensor Vibration Testing

The pressure sensor capsule was vibration cycled in accordance with the specifications. The capsule was tested by itself because the signal processor, a breadboard circuit, is not capable of surviving a high vibration environment. The unit was then returned to the test rig and recalibrated. No measurable degradation in transducer response was observed. A shift from the calibrated output did occur; however, its magnitude was less than the error produced by stray capacitance drift. The stray capacitance in the interface wiring changes each time the sensor capsule is reconnected to the signal

processor in the test rig.

Pressure Sensor Evaluation Summary

The pressure sensor development program described in this report demonstrates the inherent capability of the pressure transducer components to provide the required performance when the unit is located in the fuel cooled electronic package. Although the tested units are breadboard constructions and, therefore, do not conform to the ATEC packaging specifications, they are capable of meeting the required envelope constraints with microelectronic components and packaging techniques. The feasibility of providing P_{t3} pressure sensing with sufficient accuracy and response to satisfy the rigorous requirements of specification has therefore been established.

The design and construction of prototype pressure transducers, capable of installation and operation in an engine-mounted fuel control, is justified by the results of this program. A prototype unit is required for demonstration testing on an actual engine. The prospects for a successful engine demonstration test program are good.

Production problems should be investigated after a production prototype unit has been successfully completed. The primary production problems are maintaining the required accuracy over a large production spread and reducing unit cost.

These problems are best solved by working closely with the pressure transducer manufacturer in a pilot production test program.

Flow Sensors

The requirements for an airborne fuel mass flow meter for ATEC applications are contained in Chandler Evans Specification CEPS-326A. The pertinent performance specifications are:

1. Flow rate range: 20 to 700 lb/hr

2. Operating temperature range: -65°F to +200°F

3. Static accuracy: $\pm$ 1.0% of full scale output

4. Terminal linearity: $\pm$ 2.0% of full scale output

153

5. Response: time constant less than 0.010 sec

6. Warm-up time: less than 20 sec to meet full accuracy

7. Long term stability: Less than ± 0.1% change in
                          output at the calibration tempera-
                          ture during a 6-month period.

Letters describing the mass flow meter and its application
together with the above requirements were sent to 119 manufac-
turers to determine if they were able to supply a device meet-
ing these requirements; 17 manufacturers replied in the
affirmative. These manufacturers were given detail specifica-
tions with a request for a proposal and price quotation. Four
proposals were received in response to this effort.

As a result of the analysis of these proposals, the following
conclusions were drawn.

1. There is no practical mass flow meter to date that
    can meet the requirements for small gas turbine
    engine fuel controls.

2. Hot wire anemometer type flow sensors require excessively
    complex electronics and are too costly. In addition,
    they require compensation for changes in fuel thermal
    coefficients and viscosity.

3. Angular momentum devices show promise but their speed
    of response is too low and they are, at present, largely
    restricted to open-loop fuel flow monitoring.

Since the selected baseline system did not require a flow
transducer signal, further effort in this direction was
discontinued.

Pyrometer Development

Specification

It has been established that the specifications for the
radiation pyrometer blade temperature measurement are as
follows:

154

Max blade temperature	1800°F
Max gas temperature	2500°F
Response	.01 sec
Accuracy	± 10°F
Coolant air	up to 1000°F max temp.
	.1% of total engine air mass flow available for purging

Engine Installation

Three types of engines were identified as being likely to occur in the 2-to 5-lb/sec class.

1. Axial combustor with axial turbine

2. Folded back combustor with axial turbine

3. Folded back combustor with radial turbine

Pyrometer installation designs were prepared for all three engine types. These designs showed that the aperture system for a folded back combustor axial flow turbine engine was the most difficult design to execute and a concept with potential for wide application (see Figure 87). Therefore, this concept was selected for detailed development. Other manufacturers are offering lens systems, but no one is known to be developing an aperture system with bends, yet it is the only type of pyrometer that would be of use in a folded back combustor engine.

Having selected the aperture system, it is evident that the silicon detector, being limited to operation below about 300°F, cannot be incorporated closed to the aperture. This generated the need for the three-part design selected as shown in Figure 88.
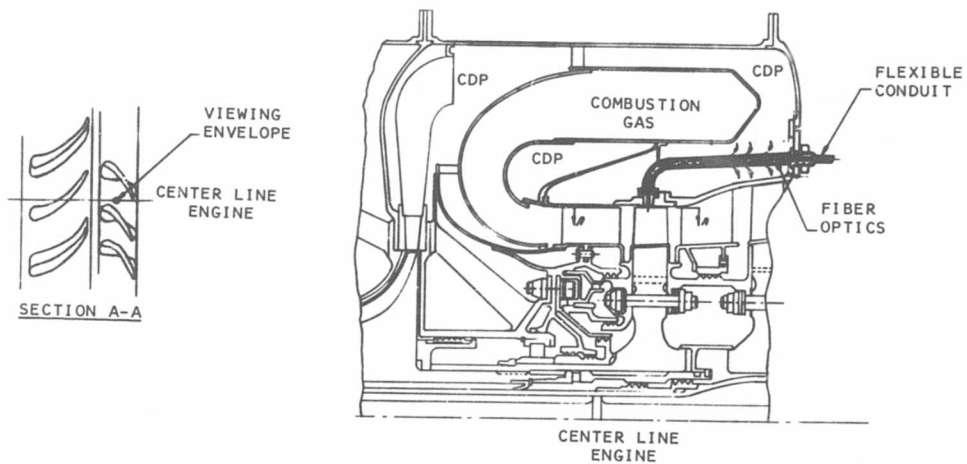
Figure 87.   Aperture Viewing Pyrometer for Folded Combustor.
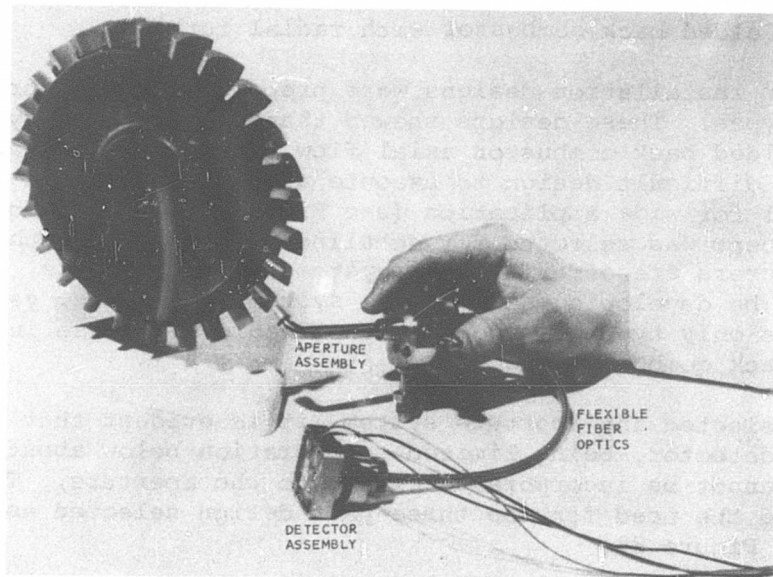
Figure 88.   Pyrometer Assembly.

156

Aperture Assembly

The aperture assembly located within the body of the engine brings the radiation to be measured to the outside of the engine.

Two designs of the aperture assembly were selected for construction: a unit with a 70° bend, and a straight unit.

Installation in an engine will require the use of bent aperture assembly; hence a bent unit was designed. However, this unit cannot be dismantled, and therefore a straight unit was also designed to allow detailed inspection of parts after testing.

A photograph of the parts comprising the 70° bend unit is shown in Figure 89, and a layout drawing is shown in Figure 90.
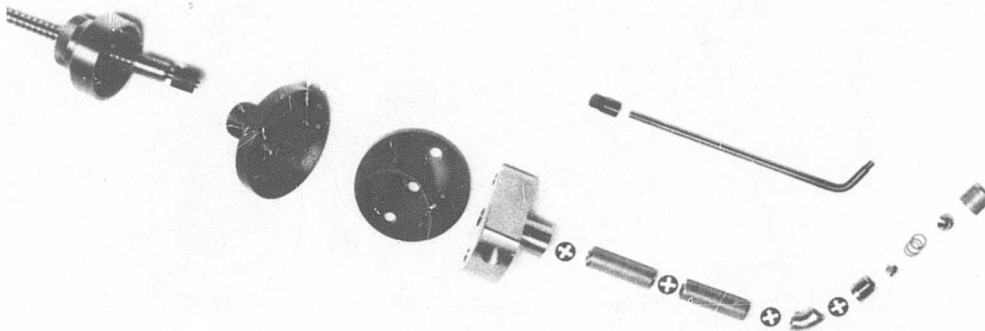
Figure 89. 70° Bend Aperture Assembly.

157
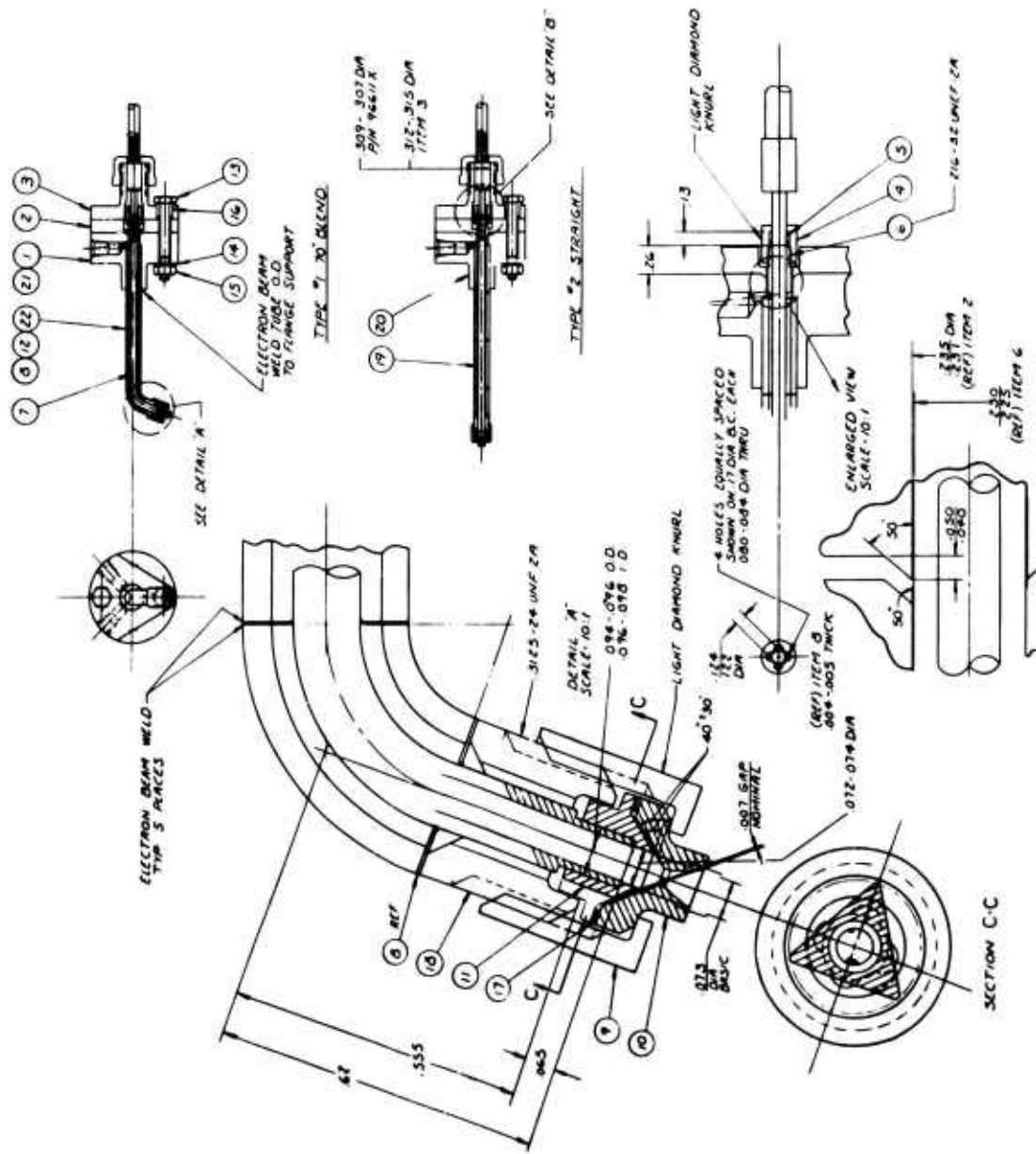
Figure 90. Layout of Aperture Assembly.

158

The aperture assembly includes an image conduit section which is a collection of clad monofibers fused together such that the outer cladding of each fiber forms a continuous matrix. This type of construction is the only system capable of surviving temperatures up to 1000°F and transmitting light around small radii. Single monofibers of the same glass system could be considered for a straight unit.

The image conduit is enclosed and cemented in a steel sheath, which has a coefficient of expansion similar to that of the glass. With this type of construction, it is necessary that both the tubing and the glass be bent simultaneously. This required careful development of the combination tube wall thickness and bending temperature.

The rigid image conduit bundle has to be protected from bending forces and vibration, yet accurately located. Also, it requires thermal isolation from the outer shield, hence it is supported within an outer metal tube by spring steel washers arranged to locate the unit firmly, while minimizing bending forces imparted to the unit and thermal conduction. Purging air flows between the conduit metal sheath and the outer tube.

Thermal isolation of the flexible fiber optic unit from the aperture assembly has been achieved by the use of high temperature plastic (polyimide) insulators.

Flexible Fiber Optics

To provide the optical link between the hot zone aperture assembly and the detector assembly, a flexible fiber optic bundle was selected. A suitable unit has been developed which involves a tri-glass system with fused ends. These ends are secured in steel caps by means of a ceramic cement. Ceramic cement was selected over a conventional epoxy cement to provide better temperature capability where the unit adjoins the image conduit. The development units are sheathed in flexible stainless steel, whereas production units would undoubtedly be sheathed in a rigid steel tubing.

Detector Assembly

The detector assembly is mounted within the fuel cooled
electronics package. This has the advantage of limiting
the temperature excursions to which the detector is sub-
jected. Sealing constraints on the electronics package,
and calibration and interchangeability requirements on the
detector dictated the design of a completely self-contained
unit. A photograph of the unassembled detector hardware is
shown in Figure 91.

An optical glass flat covers the photo diode to prevent the
ingress of dirt when the flexible fiber optic bundle is
removed. This, together with the RTV sealant used for
potting the self-contained first stage of electronics,
makes the unit a rugged device, suitable for engine mount-
ing applications.
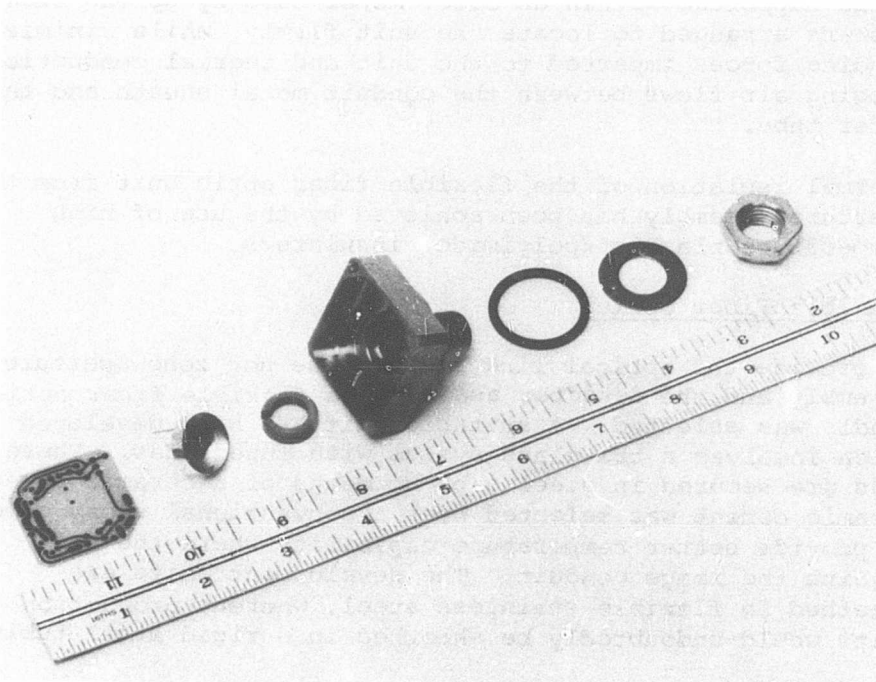
Figure 91.   Radiation Detector Assembly.

160

Pyrometer Bench Testing

The basic components of the pyrometer system were assembled
into a system which was functionally similar to the final
system. This was then tested to evaluate those parameters
listed below which would have an important effect on the over-
all control performance.

1. Repeatability

2. Temperature sensitivity of detector when compensated
    by electronics

3. Response to a single hot blade

4. Frequency response of electronics

5. Purging tests

1. Repeatability

The plot of two calibration runs is shown in Figure 92.
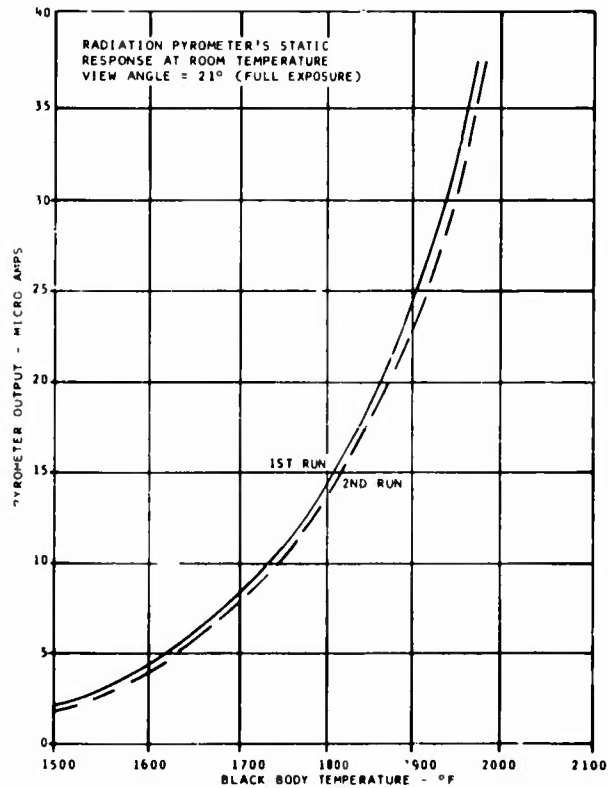
Figure 92. Pyrometer Calibration Test Data.

161

These runs were made some time apart, various other tests having intervened. As can be seen, the repeatability is within 7°F, and this was shown to be the instrumentation limit of repeatability.

2. Temperature Sensitivity

The temperature compensated pyrometer, with integral electronics, was tested at various case temperatures for a fixed target temperature of 1800°F. The result is shown in Figure 93.

It can be seen that when the circuit is tested with the detector for which it was designed (Detector #1), compensation within ± 10°F is achieved. When, however, a different detector is substituted, the performance is not acceptable. This suggests that, unless an entirely different approach to temperature compensation is adopted, each detector will have to be individually tested, and a circuit for each one built.

Temperature compensation can be achieved to any degree desired. The less the variation desired, the more careful the testing and circuit design is required to be. Thus, the final design would have to be based on a careful compromise between accuracy requirements and cost.

3. Response to a Single Hot Blade

The pyrometer was exposed to a radiant metal strip through a chopper disc. Radiation through slots could be attenuated by a wire mesh simulating cool or hot blades. Three test runs were made simulating all cool blades, all hot blades, and one hot blade. The results are shown in Figure 94.

Studies of available published literature, and discussions with engine manufacturers conducted during this program, concluded that the most useful information for limiting temperatures in the engine would be the temperature of the hottest blade. Various other possibilities exist, but since electrically they are simpler to realize, the "hottest blade" strategy was selected for development.

162
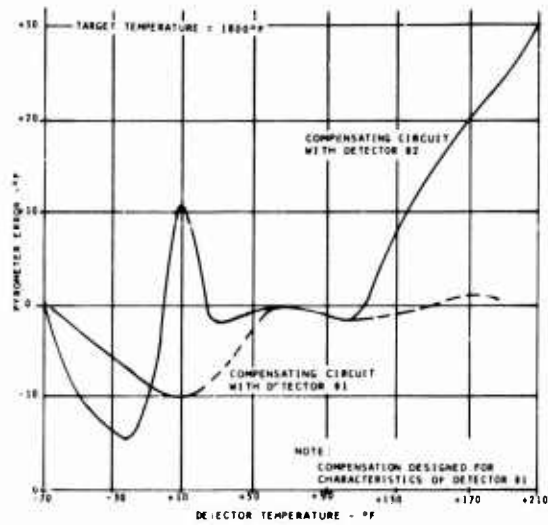
Figure 93.   Temperature Compensated Pyrometer Performance.
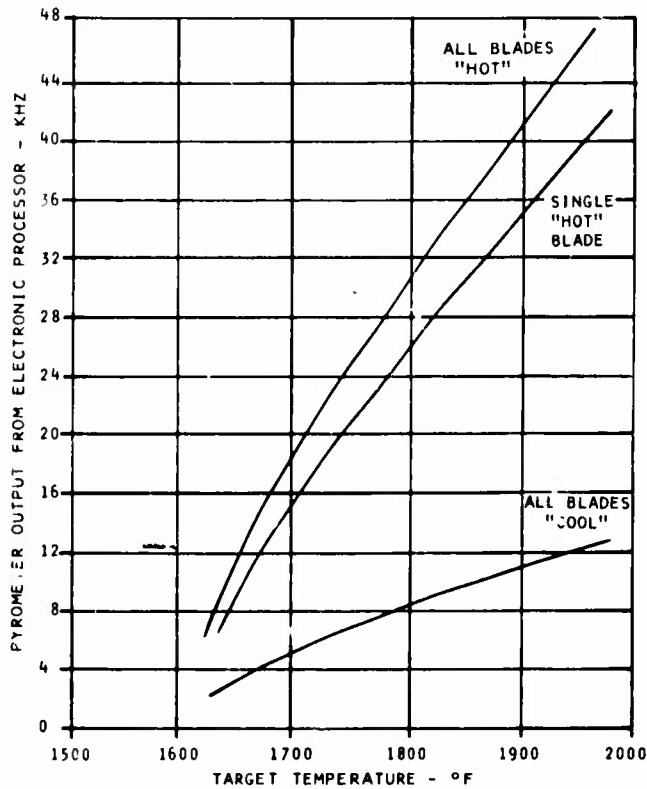
Figure 94.   Pyrometer Simulated Transient Signal.

163

If the strategy is to operate successfully, then the electronic pyrometer processor output should be the same whether one or all the blades are hot. As can be seen from Figure 94, this was almost achieved ($\approx 40°F$ difference). Careful analysis of the test procedure showed that the error was generated entirely by the test setup and procedures. Subsequent measurements have shown that any error that may exist in the pyrometers processing circuitry is less than the experimental accuracy.

4. Frequency Response of Electronic Processor

The frequency response of the sign   sor was measured by substituting a signal g   . in place of the infrared detector. A constant in ut pulse width of 10µS was used. The test resul   are shown in Figure 95.
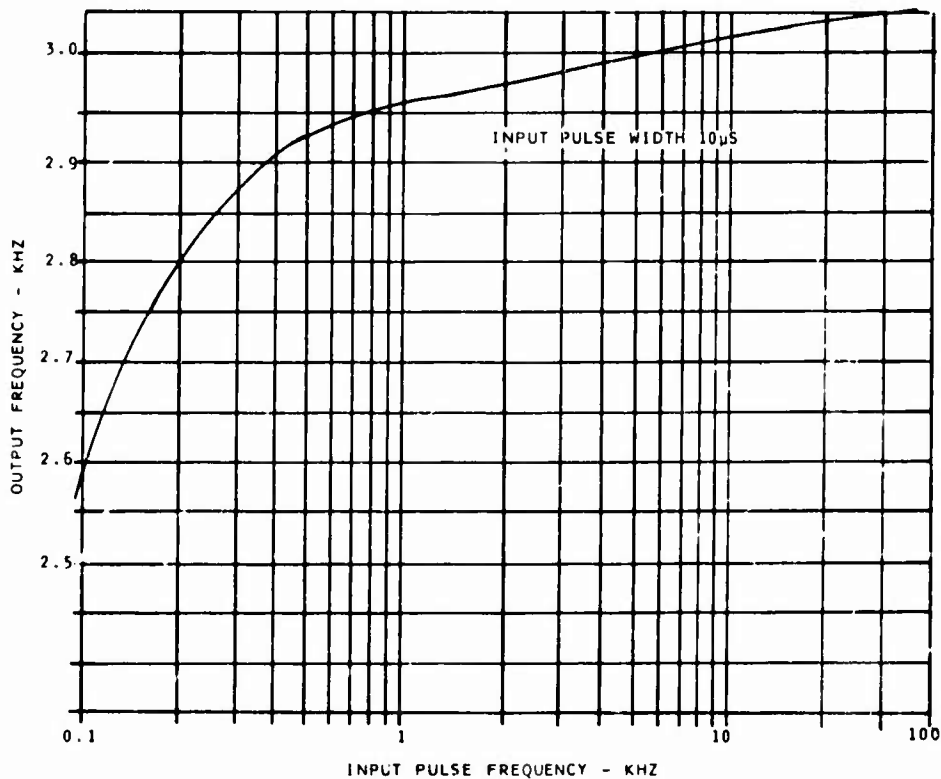
Figure 95. Pyrometry Processor Pulse Frequency Response.

164

If all the blades are equally hot, at 100% speed, then
the circuit has to respond to a 30-KHz signal. However,
with one hot blade at idle speed, the circuit would be
required to handle a 500-Hz signal. An attenuation of
5% is seen to be present over this frequency range.
This is not acceptable and will be corrected in a future
design. The circuit modifications required are simple
and therefore time was not wasted in pursuing this
shortcoming as it would necessitate a printed circuit
layout change.

5. Purging Tests

The bent aperture assembly having been calibrated was
mounted into a purging test fixture which supplied
contaminated purging air to the pyrometer. The test
was run for 50 hrs.

Within 30 minutes of running, leakage of purging gas
between the image conduit glass and metal sheath became
apparent. Despite this, the test was completed.

At the end of the test the aperture end of the assembly
was dismantled and found to be completely clean, and
free of contamination buildup, with the exception of
the image conduit glass face. This had a thick build-
up of contaminant because of the passage of air past
the glass. Study of the design (Figure 90) will show
tha' the shroud on the end of the image conduit creates
a quiet zone at the face of the glass. This feature
had been shown in earlier parts of this test to be very
effective in preventing contaminant buildup. Failure
of the ceramic-cement allowed passage of purge air
through this quiet zone, resulting in the buildup of
contamination. Despite the heavy contamination, the
unit was calibrated after the test. The results are
shown in Figure 96 and indicate that an error of only
65°F with a 1600°F target resulted from the intense
contaminant buildup. It can, therefore, be stated with
a high degree of confidence that solution of the leakage
will bring the unit to within specification.
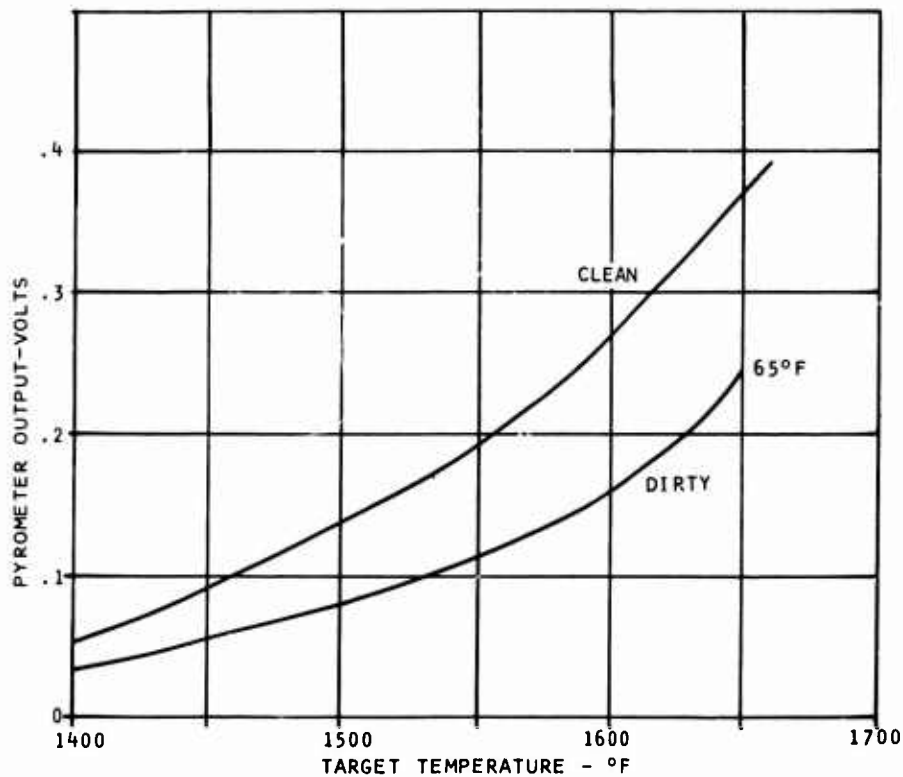
Figure 96. Pyrometer Contamination Test Results.

Development work should continue on:

1. Improving the cementing technique.

2. Not relying on the cement for a total pressure
    seal.

3. Vacuum impregnating the image conduit assembly
    with high temperature epoxy to complete the
    seal.

Burner Rig Tests

The straight aperture assembly was mounted in a burner rig
and subjected to a 100-hr -test at the temperatures, pres-
sures, and velocities simulating an engine installation.
A general view of the burner rig is shown in Figure 97.

The same leakage problem encountered on the bench purging
test was noted in this test. Since this test was aimed at

166
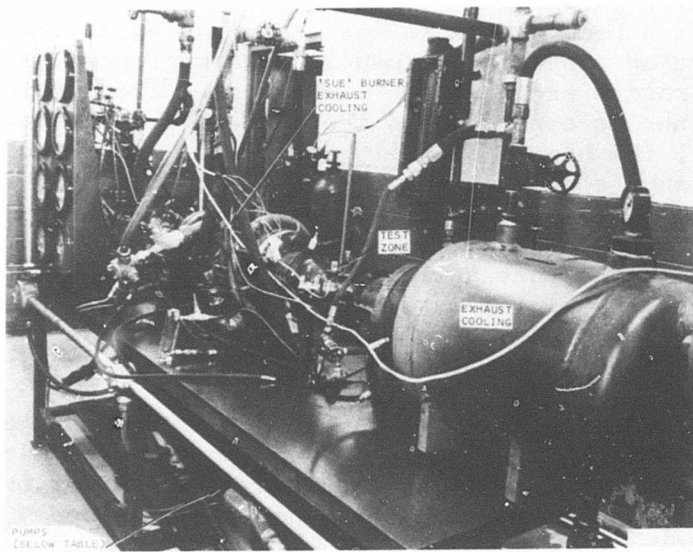
Figure 97.   Burner Rig.

evaluating the ability of the purging scheme to cool the
unit, and to prevent the ingress of combustion products,
this leakage did not interfere with the testing.

At the conclusion of the test the accumulation of dirt from
the leakage was removed. Observation and a calibration
confirmed that the purging had successfully protected the
glass system from any detrimental effects. Temperature
measurements taken on the pyrometer external structure
confirmed that the cooling performance was adequate.

Thermal Testing of Fiber Optics

Thermal testing of the fiber optics was divided into two
phases. Phase one involved the initial screening of pros-
pective glass systems, and phase two was restricted to the
study of the effect of temperature on the transmittance
properties of the system selected in Phase 1. A glass
system was obtained that was capable of transmitting light
after 1000°F exposure in a monofiber or image conduit form.
This system was evaluated further in Phase 2.

167

For installation purposes it is required that the light
pipe negotiate a bend, whose radius is only 2 or 3 diam-
eters, without an appreciable loss in transmittance. Since
the smallest radius around which light can be transmitted
in a glass fiber is dependent on the diameter of the trans-
mitting fiber, the use of one large monofiber was ruled out
in favor of image conduit comprising a large number of small
fibers.

Tests also indicated that a flexible fiber optic system for
use in place of the rigid image conduit capable of operat-
ing at 1000°F was not feasible at this time. Such a flexi-
ble unit would reduce the assembly cost of the pyrometer.

Phase 2 was confined to testing the effect of exposure at
elevated temperatures of 400°F and 700°F on the transmit-
tance properties of this image conduit system. After ex-
posure to 400°F no loss in transmittance was observed
(see Figure 98).
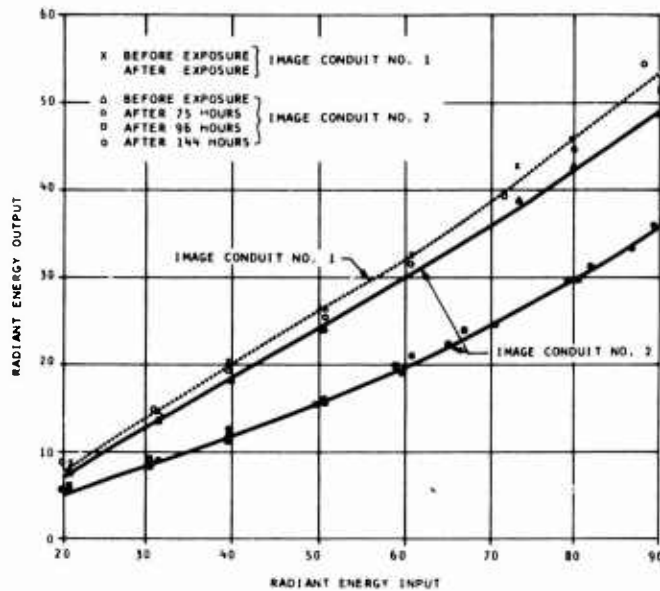
Figure 98.   Temperature Test Results.

After exposure to 700°F, there was some initial loss in transmittance, but further exposure to 700°F produced no further loss. It may be presumed then, that this initial loss is a one time aging effect. Further work is being conducted to investigate this phenomenon.

Vibration Testing of Fiber Optics

Vibration testing was performed on metal sheathed image conduits that were representative of the pyrometer units: one bent unit and one straight. In addition, a flexible fiber optic that will be used to link the hot zone image conduit to the detector assembly was also evaluated.

The vibrating condition was 60 g at 1 KHz for a period of 70 hours, this being more severe than specification requirements. Figure 99 illustrates the effect cf vibration on the transmittance of a straight image conduit, a bent image conduit, and a flexible fiber optic respectively. It will be observed that there is little or no change in transmittance.
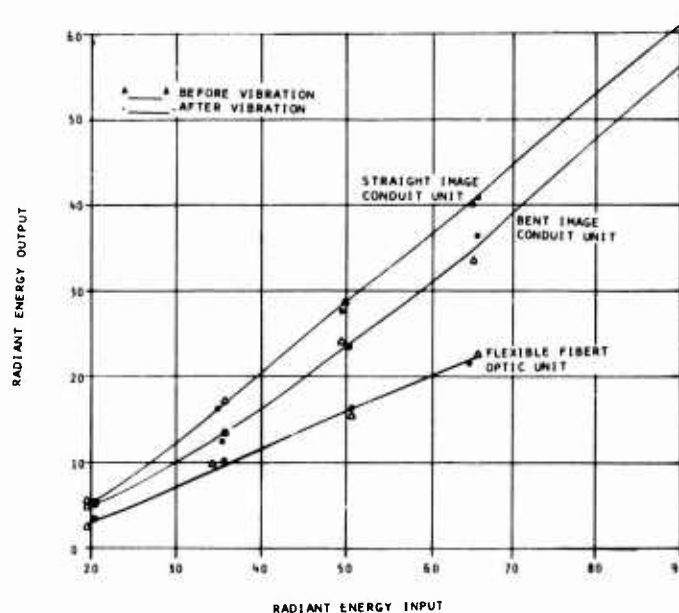
Figure 99. Vibration Test Pesults.

169

Pyrometer Development Summary

The premise was established that it was necessary to demonstrate those features which represented the essence of a good pyrometer by performance and environmental tests. These features include

1. Basic operating concept viability

2. Feasibility of manufacture

3. Purging

4. Cooling

5. Vibration

They were all successfully developed and tested. Problems were resolved which were peculiar to the chosen design, and this work provided valuable experience applicable to the design of a pyrometer. Achievements made in the development effort include

1. Designed a pyrometer suitable for use in a small (2 to 5 lb/sec) engine.

2. Cooled and purged a pyrometer, keeping the air consumption within 0.1% of engine airflow.

3. Temperature compensated the detectors.

4. Developed a high temperature glass system.

5. Developed fabrication techniques including bending image conduits.

The major problem encountered was leakage between the image conduit glass and protective sheath. Future investigation should also consider calibration and interchangeability.

ELECTRONIC COMPUTER

The electronic computer has been developed to satisfy system design goals, and to meet functional requirements and environmental specifications for engine mounting.

The selected hard-wired design philosophy evolved from trade-off studies and development work. A special purpose computer was favored over a programmable computer because for controlling small engines the major portions of the computer are the sensor and interfaces. The spec al purpose computer provides more flexibility for integrati these sensing functions and interfacing with the computer sections of the control. The selected design provides an electrically alterable bivariate function generator (3-D Cam) and adjustable control loop gains. This provides all of the programmability required to meet the flexibility goals fo: the system. The selected hybrid design makes use where po: sible of the advantages offered by digital and analog technologies.

Four operational computers were built and tested during the program. Two were constructed in breadboard form for circuit development and closed-loop demonstration testing. The other two were packaged in a form representative of a production prototype and included provisions for fuel cooling. These were designed for environmental and endurance testing and are referred to as demonstration units. Figure 100 shows a photograph of the demonstrator.

Functional Description

A detailed block diagram showing the functional organization of the electronic computer is shown in Figure 101. The computer provides IGV position control and control of fuel flow through control of the main metering valve (MMV) position. The IGV control schedules the inlet guide vane as a function of corrected speed.

The MMV Control, which schedules engine fuel flow, and is illustrated in Figure 102, may be further divided into six major sections:
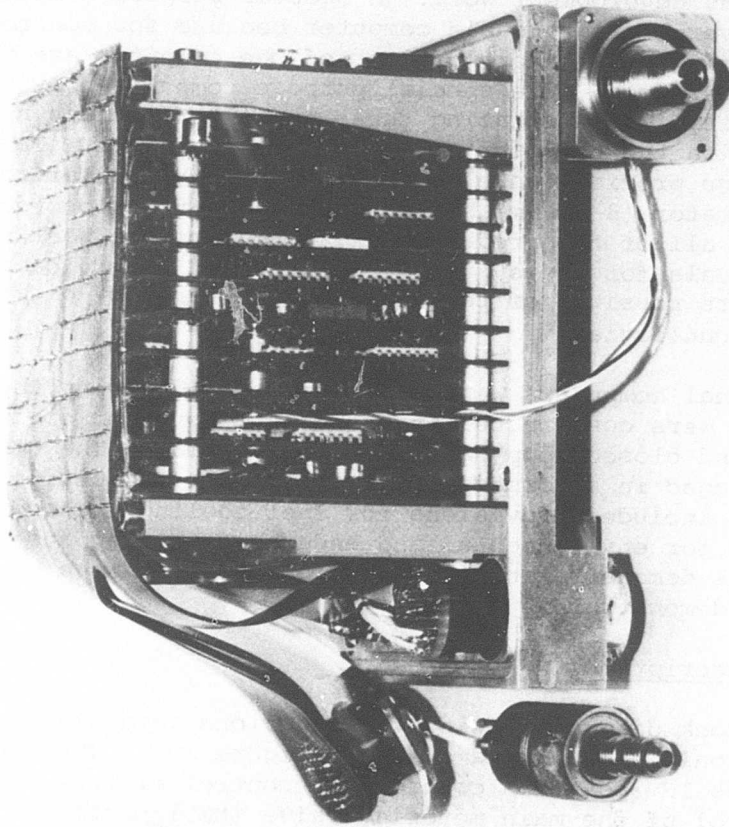
Figure 100. Computer Demonstrator Package.
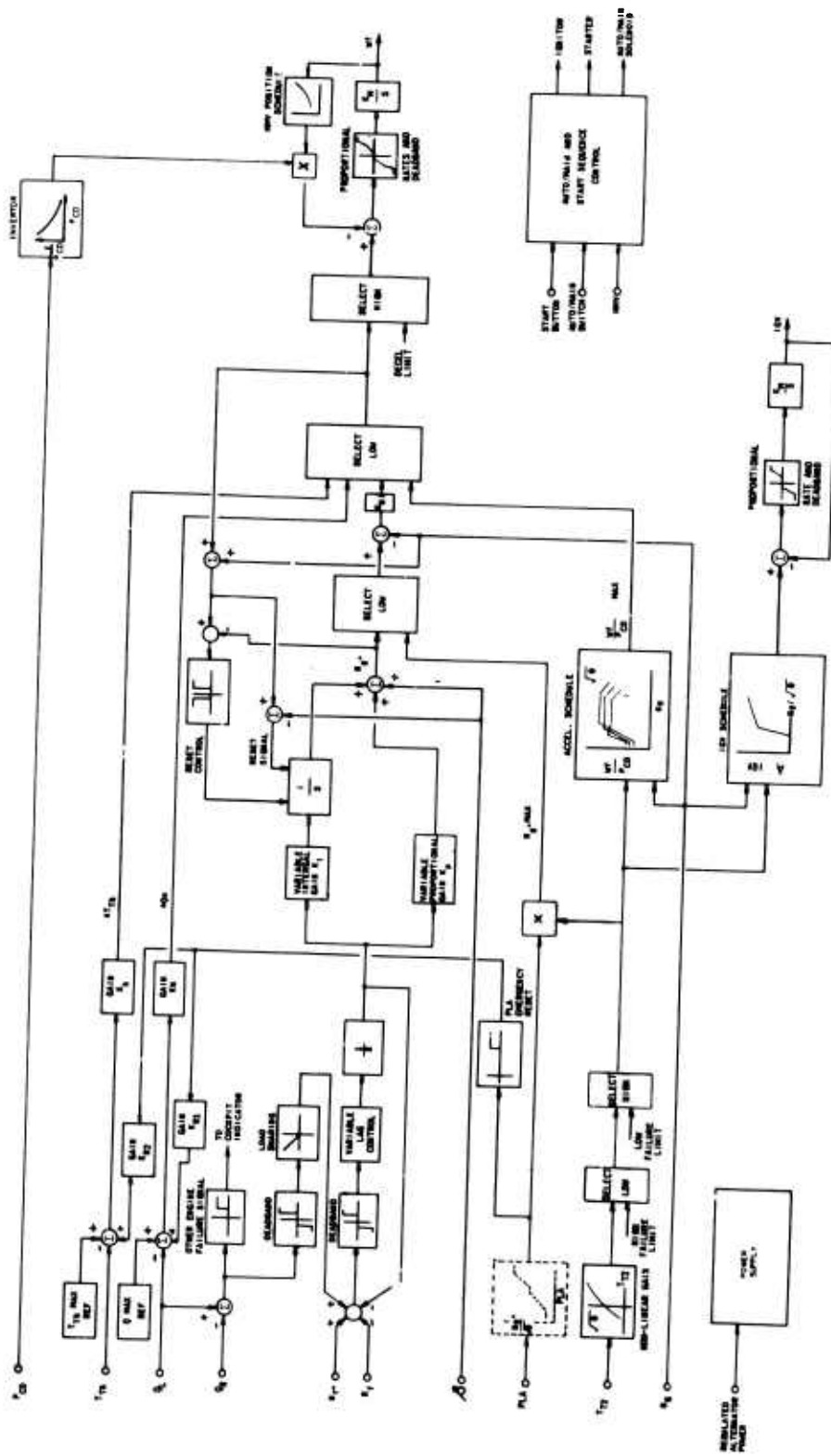
Figure 101. Computer Functional Block Diagram.

173
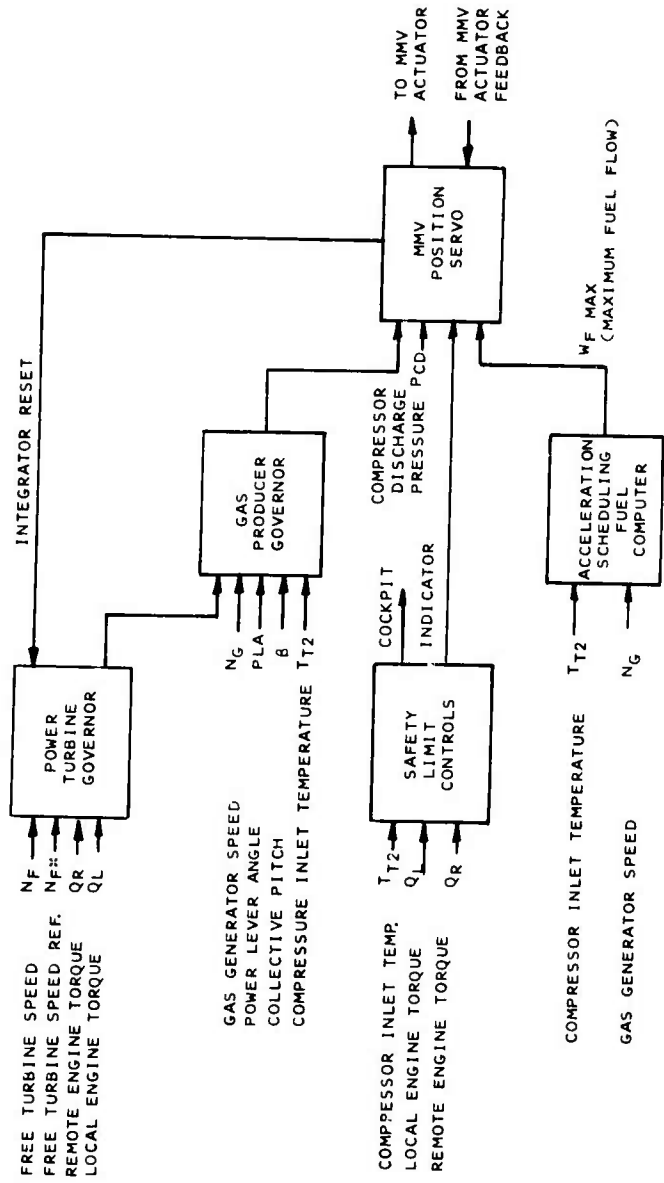
Figure 102. Main Metering Valve Control.

W_F/P_{t3} acceleration and deceleration scheduling.

Proportional gas producer governing

Isochronous power turbine governing

Turbine blade temperature limiting

Torque limiting

Load Sharing

The MMV position servo incorporates compensation for the metering valve nonlinear contour, thereby ensuring the required fuel flow throughout the full dynamic range.

The acceleration scheduling fuel computer schedules maximum fuel flow as a preselected arbitrary function of compressor inlet temperature and gas generator speed.

The gas producer governor schedules fuel flow as a function of:

1. Gas generator speed

2. Power level angle

3. Compressor inlet temperature

4. Collective pitch

5. Power turbine governor demand

The power turbine governor resets the gas producer governor as a proportional plus integral function of power turbine speed error and load sharing error. Circuitry is provided which resets the integrator to avoid large transient errors.

Safety limit controls are incorporated to override fuel flow to prevent turbine blade temperature or torque from exceeding prescribed limits. Cockpit indication of torque failure is also provided.

175

The semiautomatic start sequence allows for pilot manual activation of the ignition system under any operating condition. A further feature provides for automatic shutdown of the start motor when the gas generator has reached self-sustaining speed.

The power supply regulators provide a controlled interface between the fluid controller mounted alternator and the analog and digital circuitry and actuators.

Error Allocation

The anticipated allocation of tolerance among the various system components and computational paths determined in the RSS error analysis is tabulated in Table III (page 23). These provided guidelines for selecting circuit designs.

Signal Processing

The various signal processing methods which were considered include:

DC Analog
Pulse Width Analog
Frequency Analog
Digital

A special purpose control utilizing a monopoly of one of the above processes would be undesirable from many aspects (cost, weight, accuracy, reliability etc.). The control was therefore designed using all the above referenced techniques, with each function utilizing that process which provides the desired requirements with a consideration for the minimization of interface problems.

This philosophy is also advantageous for the following reasons:

1. Computer organization is arranged along functional lines.

2. Processing at all inputs is selected for compatability with the transducer so as to avoid unnecessary demodulations and remodulations.

176

3.   Processing is selected at each point in the
     computer to reflect optimum compatibility
     with adjacent signals with the least hardware
     to perform a given function within the allow-
     able error band.

Component Subassemblies

Several of the computer subassemblies were not readily
available at the onset of this program and, therefore, had
to be developed specifically for this application.

A brief description of these subassemblies is given below:

1.   Speed Network/Error Processor

     The power turbine speed error network is
     implemented by a continuous digital process.
     The speed set digital output network is determined
     by a pilot operated control button. A digital
     representation of actual free turbine speed is
     digitally compared to the set speed resulting
     in a digital error. The accuracy of this circuit
     has been found to be better than 0.1%.

2.   Speed Network Dynamics

     This function, which is basically a first order
     lag, is also implemented by a continuous digital
     process. The lag, which takes the form of closed
     loop system using an integrator with negative
     feedback, processes the power turbine speed error
     signal to the network that generates the integral
     and proportional output signals again in a
     continuous digital manner.

3.   Load Sharing Network

     This network is also implemented by a continuous
     digital process. Digital signals from the local
     and remote engine torque sensors are compared in
     a digital comparator. The resultant error is
     added to the output of the power turbine speed
     network of the low power engine to provide load
     sharing control.

177

4. Function Generators

Figure 103 illustrates the functional implementation of the 2-D schedule utilized to generate the IGV schedule. As can be seen the characteristic is basically a straight line with a breakpoint at an IGV angle of 15°. The specific slope and relationship between IGV angle and N_g are functions of $\sqrt{\theta}$. The initiation of IGV scheduling is defined by multiplying $\sqrt{\theta}$ by an offset feedback signal. The breakpoint change in gain is defined by the comparators and diode network.

The entire schedule is generated by a continuous digital process and the accuracy is better than 0.25%.

Although there are two variables, the requirements can be representated accurately by a 2-D function and multiplier.

Figure 104 presents the functional implementation of the 3-D function generator required for the acceleration schedule. The heart of the system is a 2048 bit Read Only Memory (ROM) organized using 8 bit words. The remainder of the function is implemented mainly as a sample data digital system with a continuous digital output.

During each sampling, a measure of N_g and $\sqrt{\theta}$ is fed into the ROM and a preprogrammed output is provided in accordance with the magnitude of the input functions. This output, which is in binary form, is converted to a continuous signal by a digitally controlled multiplier.

The magnitude of the memory is effectively expanded by the use of interpolation. This takes the form of augmenting the output signal by an increment proportional to the least significant bit measurement of $\sqrt{\theta}$.

178
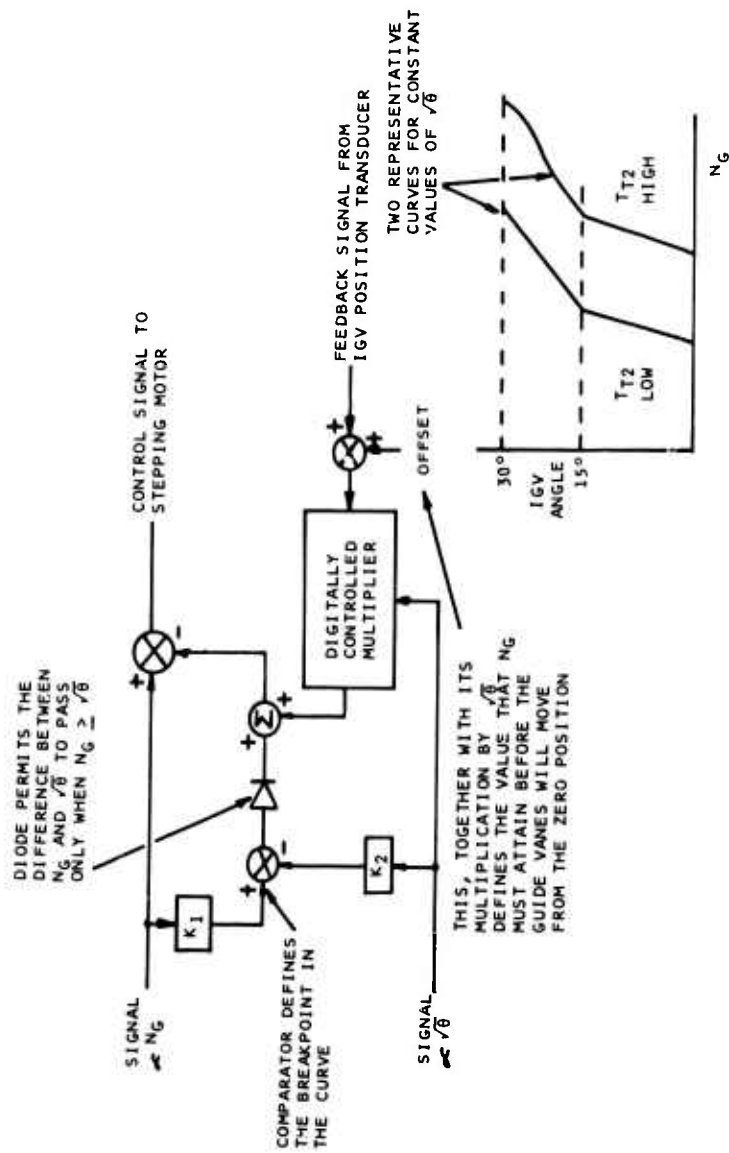
Figure 103. 2-D Function Generator – Functional Implementation for IGV Schedule.

179

TWO OF EIGHT CONSTANT $\sqrt{\theta}$ CURVES

MF/PCD ACELL.

N_G

INTERPOLATION PROVIDES FOUR POINTS BETWEEN ANY $\sqrt{\theta}$ CURVES

SIGNAL $\propto \sqrt{\theta}$

SIGNAL $\propto \sqrt{\theta}$

DIGITAL SIGNAL CONVERTER

DIGITAL SIGNAL CONVERTER

DIGITAL SIGNAL CONVERTER

5 MSB MEASUREMENT OF N_G PROVIDING UP TO 32 SLOPE CHANGES PER CURVE

3 MSB MEASUREMENT OF $\sqrt{\theta}$ DEFINES 8 CURVES WITH $\sqrt{\theta}$ CONSTANT

2 LBS MEASUREMENT

2 LBS OF $\sqrt{\theta}$

2048 BIT READ ONLY MEMORY

8 BIT R.O.M. OUTPUT DEFINING ± 16 SLOPES WITH THE MSB ALSO DEFINING SIGN

DIGITALLY CONTROLLED MULTIPLIER

OUTPUT SIGNAL $\propto$ MF/PCD ACCELERATION

180

Figure 104. 3-D Function Generator – Functional Implementation for Acceleration Schedule.

The three bit $\sqrt{\theta}$ input to the ROM provides 8 constant $\sqrt{\theta}$ curves as a function of N_g. The two interpolation bits enable the definition of 4 points between each $\sqrt{\theta}$ curve. Therefore, with N_g constant and $\sqrt{\theta}$ varying from minimum to maximum, 32 points are provided on the output 3-D surface. With $\sqrt{\theta}$ constant and N_g varying from minimum to maximum, the 8 bit output from the ROM provides 256 points on the surface. Therefore, 32 x 256 = 8,192 points are provided on the output surface over the complete N_g and $\sqrt{\theta}$ range. This provides sufficient accuracy to satisfy starting and acceleration requirements.

5. Signal Selection Networks

Signal selection both for select high and select low together with signal comparison is performed by a continuous digital process that introduces no error over the dynamic operating range.

6. Pressure Sensor Signal Processor

A capacitive pressure transducer consisting of two capacitors, one fixed and one varying with pressure, is used to measure compressor discharge pressure. The two capacitors are inside the same package and are manufactured at the same time to ensure that the temperature coefficients track one another within 1%. The capacitors drive two identical oscillators and their frequency difference represents the pressure.

7. Compressor Inlet Temperature Signal Processor

The relationship between $\sqrt{\theta}$ and T_{t2} is nonlinear over the operating range of inlet temperature. This relationship can be conveniently achieved by a thermistor network. This network consists of resistors and thermistors provided in an arrangement such that the temperature vs resistance characteristics meet the requirements of the computer.

181

8. Radiation Pyrometer Signal Processor

The radiation pyrometer is used to limit the tur-
bine blade temperature to 1800°F. The output sig-
nal from the pyrometer includes both a dc and an
ac component. Unfortunately, the presence of
carbon particles in the turbine inlet introduces
an error in the form of a dc offset coupled with
high frequency noise. The best way to deal with
the problem was to use the ac component of the
signal.

A bandpass filter has been designed to reject all
low and high frequency noise and to block dc. The
signal is precision rectified and amplified. The
output is a dc level representing the blade tem-
perature.

9. Position Sensor Signal Processor

A synchro resolver is used to measure mechanical
position. The brushless resolver has a phase
shift compensation winding which ensures an accu-
racy of ± 0.1% over the temperature range of -55°C
to +125°C. A resolver to digital converter pro-
cesses the resolver position into a 10-bit digital
number. The converter compares an input sinusoidal
waveform with the resolver output sinusoidal wave-
form. The accuracy of the converter is better
than ± 0.1% of FS due to the design feature of
driving the resolver from a crystal controlled
oscillator whose stability is better than ± 0.005%
of FS.

10. Speed Sensor Signal Processor

The speed sensor circuit consists of a magnetic
pickup followed by a differential amplifier. The
differential amplifier is utilized to prevent a
loss in signal should one of the pickup leads be
inadvertently grounded. The amplifier also serves
to convert the magnetic pickup waveform into a
squarewave suitable for processing through digital
logic.

11. Power Supply Rectifiers and Regulators

Figure 105 shows a functional block diagram of the voltage and current regulators. To ensure minimum power dissipation, all the regulators are of the switching type.

The +12V regulator provides a reference to the -12V regulator, enabling these supplies to track. All the voltage regulators have an output ripple of less than 100 mV peak to peak and provide load and line regulation better than 1%.

The current regulators utilize a unique technique whereby the stepping motor winding characteristic is used as a filter in a closed-loop current regulator. The stability of these regulators is better than 5%.

12. Stepping Motors and Drivers/Translators

To comply with system requirements of minimal size and power dissipation, maximum torque, stepping rate and stability, identical size 8, four-phase variable reluctance stepping motors are used to position the MMV and the IGV servovalve.

The translator for the IGV stepping motor is basically a four-phase clock with provision for incrementing the stepping motor at a constant rate or by individual steps in either the forward or the reverse direction. Nominal step size is $15°$ of rotation.

The translator for the MMV stepping motor is similar to that for the IGV function but includes an additional feature. This permits the translator, on command, to issue an eight-phase output, permitting the stepping motor to move in increments of $7.5°$. This provides increased accuracy for metering fuel in the low flow range of operation.
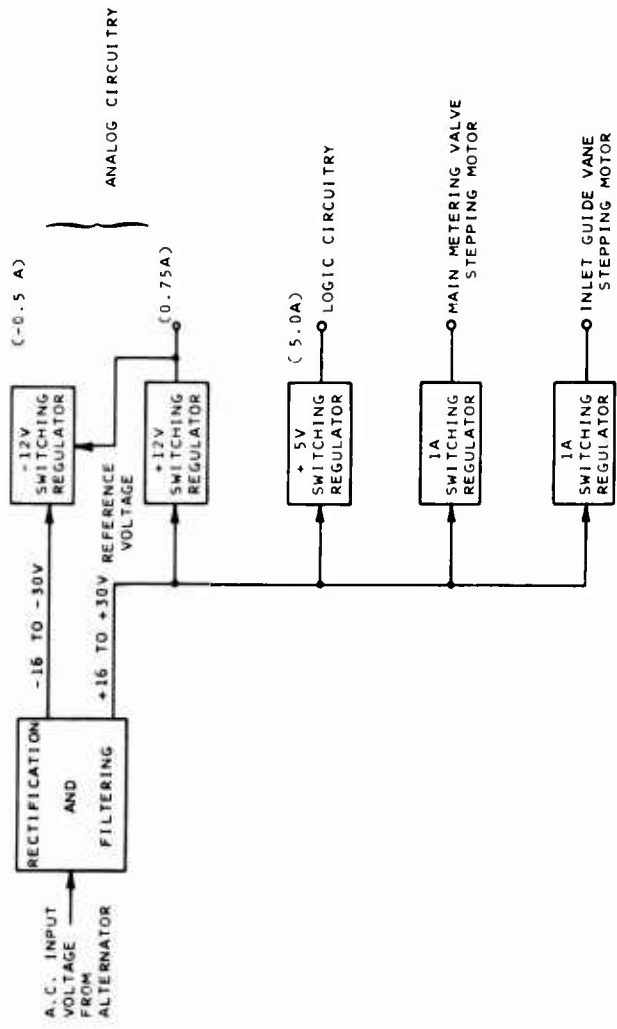
Figure 105. Power Supply Voltage and Current Regulators.

184

For both stepping motors, the drives provide the dual function of sequencing the power to the desired phase and providing the output stage of the current regulator.

Computer Package Design

The two major problems attendant to engine mounted operation are maintaining the integrity of the package, its subassemblies, and connections under vibration conditions of 20g out to 20,000 Hz, and thermal survival.

The demonstration unit was intended to provide a vehicle whereby alternative packaging concepts could be evaluated to demonstrate vibration and temperature integrity. The size and weight of the demonstration unit is considerably larger than the estimated size and weight of the production units.

The demonstration electronic computer is housed within a two-part aluminum case as shown in Figure 106. The compressor discharge pressure and turbine blade radiation detector are also housed within this same case. Both of these transducers and the connector used for signals to and from the airframe are mounted through the cast aluminum cover. The base of the package is a heat exchanger (cold plate) through which fuel flows to cool the electronic package. Aluminum support frames are used to secure the circuit boards to the cold plate.

The intra-control signals pass through a connector in the cold plate. These signals include solenoid, stepping motor, and resolver signals. 'O' ring seals are used to maintain a vapor tight seal necessary in order to retain the dielectric liquid within the package.

1. Structural Design

    The package's internal structure, as shown in Figure 106, is comprised of 13 circuit boards mounted vertically with respect to the cold plate. The boards are located by five through bolts with spacers between each board. The bolts are secured on two webbed "U" brackets shown in Figure 107. The large mounting pad area of these brackets

185
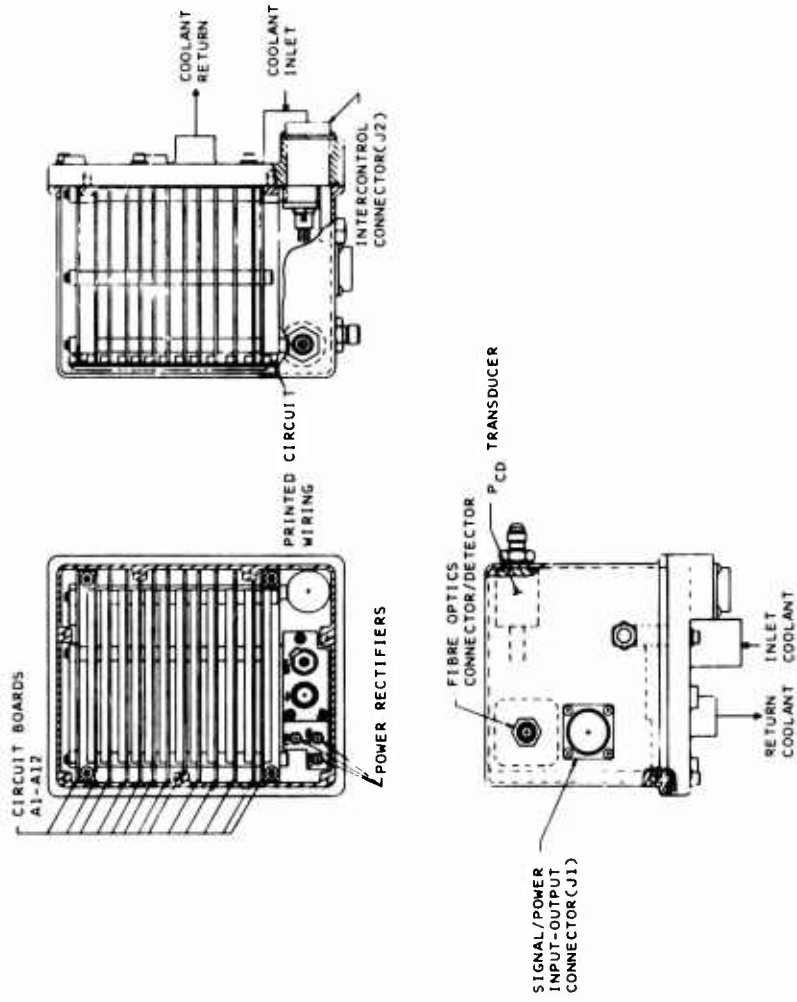
Figure 106. Electronic Computer Demonstrator Layout.

186
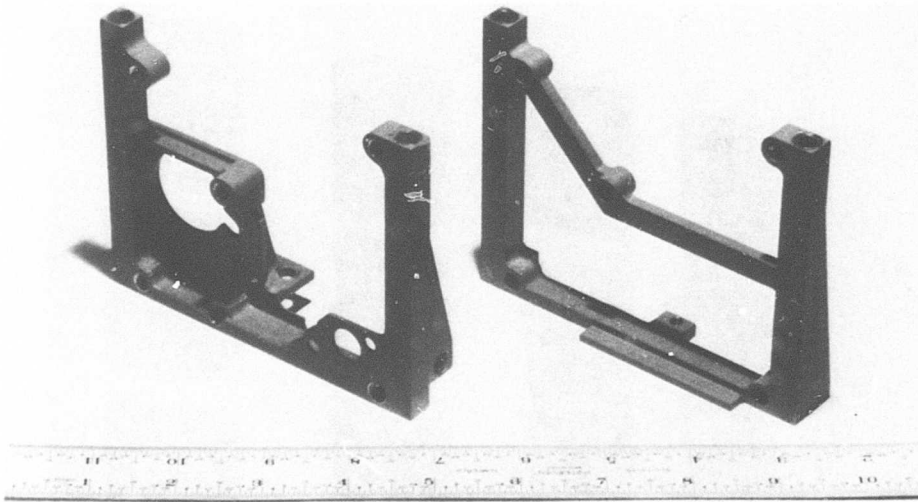
Figure 107. Circuit Board Support Brackets.

combined with several mounting screws ensures suf-
ficient rigidity of the board assembly to withstand
the specified vibration. Interboard connection is
made by means of flexible cabling. This permits
the circuit boards to be fanned out to allow access
for internal testing and modification. A photo-
graph of the disassembled demonstrator is shown in
Figure 108.

2. Cooling System Design

Heat is removed from the package by fuel from the
impeller discharge passing through the cold plate.
This is accomplished in two steps.

The entire package is filled with 3-M Fluorinert
FC-78 inert electronic cooling liquid. Sufficient
vapor space is left unfilled to permit free thermal
expansion of the liquid. 'O' ring seals are pro-
vided at every sealing face to prevent leakage.

187
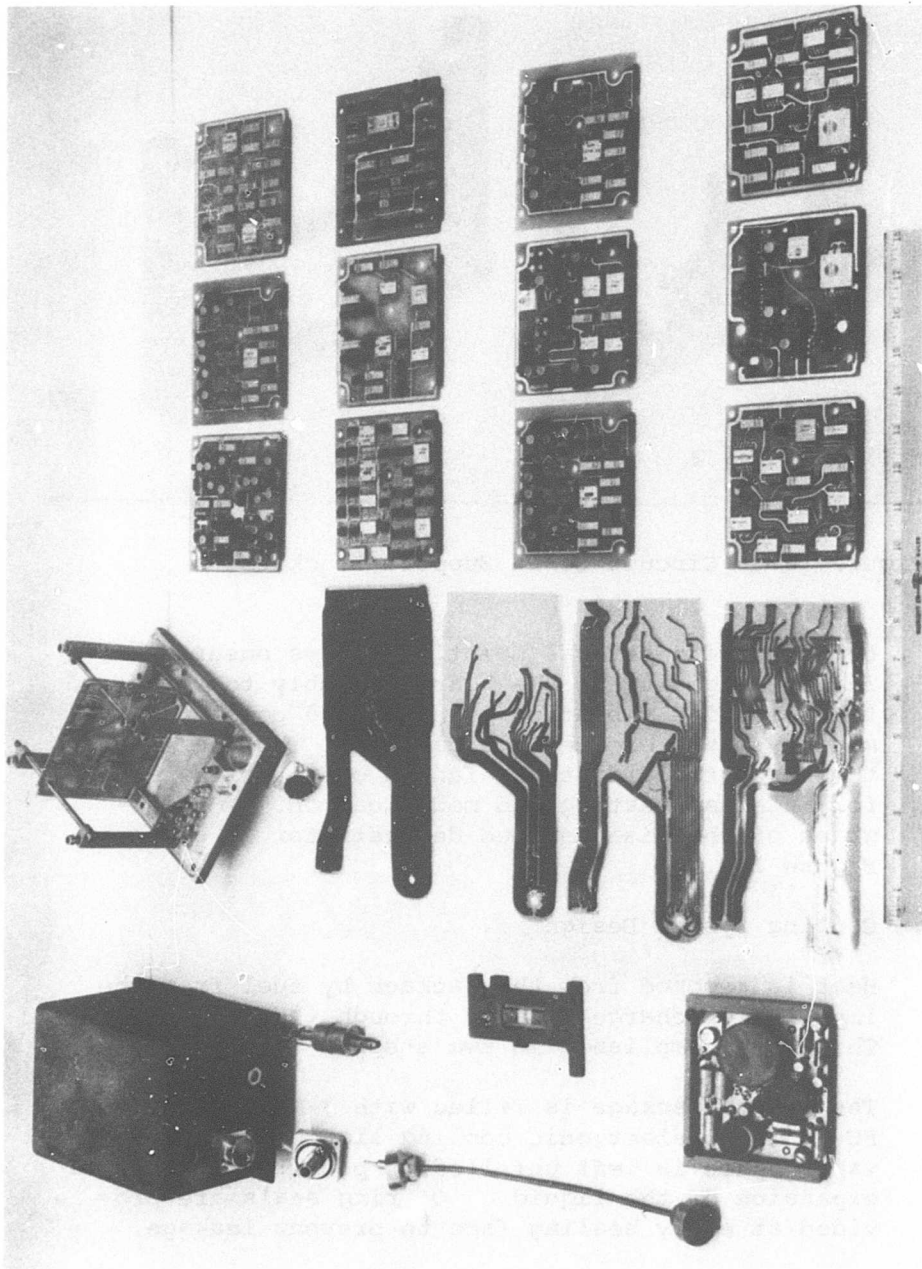
Figure 108. Disassembled Electronic Demonstrator Unit.

188

This technique ensures that all the components are immersed in the fluid, permitting excellent heat flux from the components. No air or other gases are allowed in the package; this ensures saturation conditions which results in maximum heat flux. Since the liquid is in direct contact with the cold plate, the heat is transferred to the cold plate from the bulk of the fluid with the minimum of temperature differential.

Inlet fuel is pumped through the cold plate by a small impeller. This ensures a satisfactory V/L ratio at the inlet to the main pumps. The cold plate is a brazed aluminum assembly utilizing folded fins as the heat exchanger core. The core is arranged within the cold plate to ensure that the maximum possible surface area of the plate is exposed to fuel flowing beneath it. Care has also been taken to ensure that the temperature gradients across the plate are minimized. The plate contains an integral fuel flow bypass path with a pressure relief valve. The relief valve limits the maximum pressure drop across the cold plate assembly to 2 psi.

3. Circuit Boards

There are 13 printed circuit boards (PCB's) on which are mounted the bulk of the electronic components. These boards are epoxy glass cloth (Nemp Grade FR-4) material. Eleven boards are double sided with plated through holes construction. The remaining two are multilayer boards, one with six layers, the other with seven. Conductors on the boards are .014-in. thick copper laminated to epoxy boards. Minimum conductor spacing is maintained at .020 in. Conductor widths and pad (land) areas commensurate with "Institute of Printed Circuits" Design Manual criteria.

Figures 109 and 110 illustrate respectively a completed double sided and multilayer board assembly.
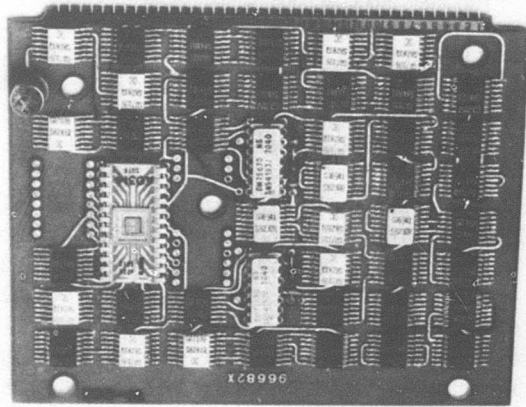
Figure 109.   Double Sided PCB.
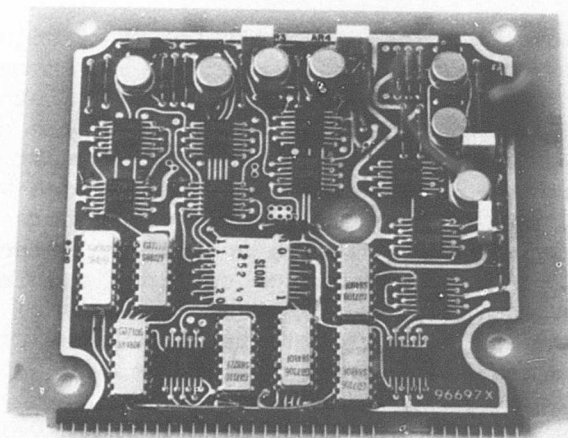
Figure 110.   Multilayer PCB.

190

4. Distribution Boards

    The signal and power distribution between the
    circuit boards is accomplished with four layers
    of flexible printed circuit wiring. This flex-
    ible wiring is fabricated by laminating 1 oz
    copper conductors between layers of Kapton.
    The PCB have pin headers wave soldered to them.
    Distribution cabling is then attached to these
    pin headers.

5. Connectors

    To minimize size, connectors with subminiature
    contacts were selected. Hermetically sealed
    connector MIL-C-38999 units were used in order
    to maintain the vapor tight integrity of the
    electronic housing. A jam nut type was used
    for the airframe interface to facilitate removal
    of the control cover.

6. Microcircuits

    One large-scale integrated (LSI) device was
    used. A metal oxide semiconductor (MOS) read
    only memory (ROM) was employed as part of the
    function generator to store the acceleration
    schedule. This memory device is electrically
    programmable.

    A sizable number of medium scale integrated
    circuits are used throughout the control.
    These include up/down counters, multiplexers,
    binary to octal decoders and various counter/
    storage devices.

    There are about a dozen different types of
    integrated circuits in the electronics. To
    preclude the possibility of component failure
    by moisture contamination, all microcircuit
    devices are purchased in hermetically sealed
    type packages.

191

Five special hybrid circuit designs were used in
this particular system. Three are for digital
signal processing, one for analog signal applica-
tions and one for power switching. All types were
manufactured using thin film techniques except for
one thick film digital device. All devices were
manufactured to specific sections and/or the in-
tent of all sections of MIL-STD-883. Conventional
wire bonding techniques were used to connect the
output leads to the integrated circuit die on the
substrate. Figure 111 illustrates the various
hybrid circuits utilized in the control.

7. Pressure Sensor Installation

The pressure transducer is located within the
electronic package, thereby restricting the maxi-
mum temperature to which it will be exposed to
200°F. Capacitance effects introduced by connectors
are reduced by including the transducer as an
integral part of the package. The inner sealing
face of the transducer includes a preformed packing
'O' ring to prevent coolant fluid leakage.
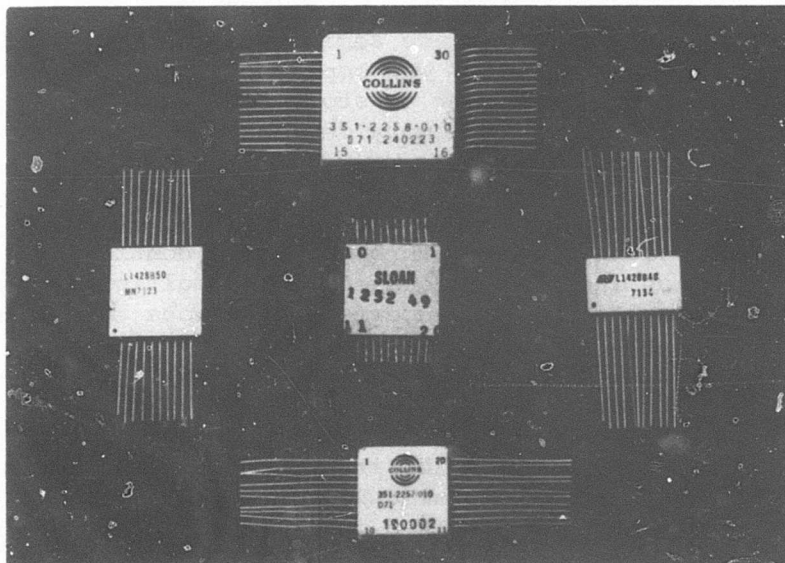
Figure 111. Hybrid Circuits.

192

8. Radiation Detector

The radiation pyrometer detector assembly is
mounted to the package cover in the same manner
and for the same reasons as the pressure trans-
ducer. In the case of the pyrometer however,
use of a standard AN thread size was avoided in
order to eliminate any possibility of erroneous
piping connection.

The pyrometer detector assembly contains
sufficient electronic circuitry to compensate
for temperature changes in the detector itself,
and also to amplify the low level current signal
from the detector.

Design Features and Alternatives

The computer functional design described in the previous
section evolved from a trade-off study on design alternatives.
In some areas, such as the cooling, only one feasible design
concept evolved. In other areas, such as the level of assembly
at which components should be procured, we were able to test
evaluate several design concepts. As a result of these studies
large scale integrated circuits (LSI), medium scale integrated
circuits (MSI), thin and thick film LSI circuits, and discrete
components are all used in this computer package.

It is recognized that the alternate designs considered are by
no means exhaustive. Many others were rejected for being
obviously unsuitable.

At the beginning of the program a basic decision was made to
use digital electronic computation and processing, wherever
possible. This criterion was arrived at for the following
reasons.

1. Digital techniques offer better accuracy and stability
   over its analog counterpart. This is an important
   consideration in the light of the tight tolerances
   that gas turbine engine controls demand and the
   environment in which they operate.

193

2. The 3-D cam which is the heart of the computer is digital and many of the interface functions (speed, stepping motor drive, etc.) are digital in nature, thereby suggesting that their neighboring circuitry should be of the same form to minimize signal conversions.

Alternative Subassembly Designs

1. Speed Signal Networks

   Two methods of signal processing were evaluated to perform these functions and are as follows:

   a. Continuous Digital Process

      This process has the advantages of fast response, high accuracy for minimal hardware and modifications to the design are easy to implement. Its disadvantage is that tight constraints are imposed on the input functions.

   b. Sample Data Digital Process

      This process also offers high accuracy but requires complex hardware and imposes time delay problems which can hurt system accuracy.

      Based on this evaluation, the continuous process was selected for these networks.

2. Function Generator

   a. 2-D

      The alternatives evaluated for this function, which is required to generate the IGV schedule as a function of corrected speed, were a ramp generator and a concept utilizing a read only memory (ROM) for storage of the required information. The former mode was selected to implement this network as it offered the simplest method for the specific requirements of this schedule.

194

b. 3-D

In the light of the complex nature of the
acceleration schedule, it was necessary to use
digital computation, and the best concept to
evolve was based on using the ROM. However,
to utilize the memory in the most efficient
manner, and yet to interface with the input
and output functions accurately and with a
minimum of hardware and time delays, a continu-
ous process was selected over a sampled data
process.

3. Voltage Regulator

Table XVII summarizes the results of evaluating
various methods of voltage regulation in considera-
tion of variations in line voltage, load, and
ambient temperature.

Based on the results of this study the switching
regulator was selected as the optimum mode for
this application.

4. Stepping Motor Regulator

Table XVIII provides a comparison of the stepping
motor power regulators evaluated.

With regard to the requirements of the control and
the data summarized in Table XVIII, the switching
current regulator which utilizes the stepping motor
winding as a filter, was selected as the best method.

5. Stepping Motors and Translators

Table XIX summarizes data on the various types of
stepping motors evaluated.

Based on the results of this evaluation, the four-
phase variable reluctance stepping motor was
selected for both the MMV and IGV requirements.

195

Method	Advantages	Disadvantages
1. Switching	a) High efficiency (low power loss). b) Low power dissipation negates the need for bulky series transistors and heat sinks.	a) Contains a relatively high ripple content in the output. b) Aggravates EMI problems. c) Requires relatively large filtering components.
2. Linear	a) Near zero ripple content in output. b) Tighter regulation possible than with the switching concept.	a) Low efficiency (high power loss). b) Large power dissipation requires elaborate heat sinking at the current levels concerned.
3. Switching + Linear	a) High efficiency (low power loss). b) Low power dissipation. c) Near zero ripple on the output. d) Very close regulation possible.	a) Large component count and expensive.

TABLE XVII. COMPARISON OF METHODS OF VOLTAGE REGULATION EVALUATED

TABLE XVIII. COMPARISON OF STEPPING MOTOR REGULATORS EVALUATED		
Method	Advantages	Disadvantages
1. Voltage Regulators (Switching or linear)		a) As the stepping motor is a current activated device, the desired characteristic cannot be obtained over the environmental temperature range with a voltage source because of changes in stepping motor winding resistance.
2. Switching Current Regulator with the Stepping Motor winding used as a filter.	a) Requires no extra power dissipating components. b) No inductive or capacitive filtering components required. c) Operates at 80% to 90% efficiency.	a) Reduces the inherent damping of stepping motor by approximately 20%.
3. Switching Current Regulator with an L-C filter.	a) No effect on the stepping motors stability. b) Operates at 60% to 70% efficiency.	a) The required L-C filter would have a physical size of approximately 1 inch^3.
4. Linear Current Regulator	a) No effect on the stepping motors stability.	a) Operates at 20% to 60% efficiency.

TABLE XIX.	COMPARISON OF STEPPING MOTORS EVALUATED	
Method	Advantages	Disadvantages
1. 4-Phase Variable Reluctance	a) The selected unit provides approximately 20% safety margin over the required operating characteristic. b) Provides an inherent 40% greater torque over a similar 3-phase unit. c) Fewer resonance problems over its 3-phase counterpart. d) The translater logic is approximately 25% less complex than for a 3-phase unit, as use can be taken directly of binary logic.	a) Requires one more power stage than for a 3-phase unit. b) Requires holding power.
2. 3-Phase Variable Reluctance	a) Requires fewer power stages than for a 4-phase unit. b) Provides less than 5% safety margin over the required operating characteristic.	a) Requires holding power. b) Translator logic is approximately 20% more complex than for 4-phase. c) 3-phase stepping motors are prone to resonance. d) 40% lower output torque than a comparable 4-phase stepping motor.
3. Permanent	a) Does not require holding power.	a) Cannot provide the required torque vs bi-direction operating speed characteristic.

198

6. Compressor Inlet Temperature Sensor and Signal Processor

Table XX provides a comparison of the sensors evaluated to implement this function. Also provided in this table is a listing of the modes of signal processing necessary to interface each sensor with the computer.

With regard to the system accuracy requirements ($\pm$ 0.5%), cost, flexibility, and complexity, the thermistor was selected as the optimum sensor. A further reason for this selection is that a minimal interface circuitry is required to provide the nonlinear transfer function between T_{t2} input and $\sqrt{\theta}$ output. This can be conveniently implemented by a network comprising thermistors and resistors, the total resistance of which varies in proportion to the desired nonlinearity as a function of temperature change.

The mode of signal processing selected for interfacing thermistor network with the computer is an emitter coupled multivibrator that exhibits excellent temperature stability and linearity ($\pm$ 0.25% in each case).

7. Position Sensor and Signal Processor

A program was conducted to test and compare several types of noncontacting position transducers.

The primary design requirement is 0.1% full scale accuracy, and it must operate immersed in fuel over the specified environment.

Three types of noncontacting position transducers were procured and evaluated:

    Linear Variable Differential Transformer
     (LVDT)
    Synchro Resolver
    Magnetic Shaft Position Encoder

199

TABLE XX. COMPARISON OF COMPRESSOR INLET TEMPERATURE SENSORS

Sensor	Linearity	Interchangeability Between Units	Output Change With Temperature	Required Circuitry to Interface With Computer
Crystal The change in crystal frequency with temperature is measured.	± .1%	Best that can be achieved is ± 5% limited by type of crystal cut.	+ 20 ppm/°C.	1. Oscillator 2. Nonlinear function generator
Diode The change in V_{be} with temperature is measured.	Nonlinear above 170°F and below -20°F.	Best that can be achieved is ±10% limited by manufacturing techniques.	-2 mv/°C, large change will yield excellent conversion.	1. Constant current source 2. VCO 3. Nonlinear function generator
Platinum Wire The change in resistance vs temperature is measured.	± .25%	Excellent interchangeability ± 0.05%	+ .25%/°F with a nominal value of 100 Ω at 32°F.	1. Constant current source 2. VCO 3. Nonlinear function generator
Thermistor The change in resistance vs temperature is measured.	± .25%	Interchangeability of ± .25%	Any monotonic resistance vs temperature curve can be obtained. ± .5%	1. Oscillator

Table XXI lists the tests that were performed on the transducers and the results.

The test program revealed the following:

a) Resolver

The accuracy of $\pm$ .1% can be met over the temperature range of -55°C to +125°C, providing an additional compensating winding is used.

The resolver can be packaged in a standard size 8 (.75 inch dia x 1.25 long).

Utilizing the crystal controlled clock in the computer, the resolver to digital converter could be designed to have an accuracy better than $\pm$ .1% over the temperature range of -55°C to +125°C.

b) LVDT

The range of operation is limited to a 1-inch stroke in order to limit the length of the LVDT to 4 inches.

Special electronic circuitry must be designed to compensate for winding temperature errors if the $\pm$ .1% accuracy requirement is to be met.

c) Encoder

In order to process ten bits of information, a disc having ten tracks is required. The means for "reading" each track is a toroidal inductor. When the distance between tracks decreases, the toroidal inductor's output is influenced by adjacent tracks. The number of bits of information that can be processed is limited to seven in a size eight (.75 inch diameter x 1.25 inches long) package due to the interaction between

201

TABLE XXI. COMPARISON OF NONCONTACTING POSITION TRANSDUCERS

Test	Procedure	RESULTS		
		LVDT	Resolver	Encoder
Linear-ity	The transducer's electrical output-position vs mechanical input position was checked for accuracy and re-peatability.	Accuracy within ±.5%. Trans-ducer becomes large (for a ±1" stroke the LVDT length is 4").	Accuracy within ±.1%.	The encoder tested was a 5-bit en-cover. Accuracy was within encoder specification (±3.1%).
Temper-ature	The transducer's mechanical posi-tion was locked in place and its electrical out-put was recorded from -55°C to +125°C.	Accuracy was only ±1% due to changes in wind-ing impedance with tempera-ture.	Accuracy within ±.1%. Requires a compensating winding in order to achieve the accuracy.	The encoder's electrical output dropped to zero for ambient temperatures above 100°C because the magnetic mater-ial's curie point was exceeded.

202

tracks. Consequently, a ten-bit magnetic encoder in a size eight package is not feasible utilizing present-day technology.

Encoders require special "V-Scan" logic circuitry to avoid ambiguities.

The toroidal inductors are ac current operated devices. Each inductor is wound with a primary or interrogation winding and a secondary or output winding. The ac interrogation current required is a 1-amp peak-to-peak sinusoidal waveform. The frequency of the waveform for optimum operation is 200 KHz. This would therefore necessitate the requirement for a complex dc to dc converter in order that the 1-amp peak-to-peak current can be provided into a low impedance load.

With regard to this comparative data, the resolver was selected as the optimum position sensor as the required system accuracy can be provided in the desired package size.

8. Speed Sensor Signal Processor

This function provides an interface between the magnetic speed pickup and the computer. The signal from the pickup is processed through a differential amplifier and a level detector, thereby providing an output frequency proportional to speed and having a waveform commensurate with the signal requirements of the computer. This interface circuit also provides additional features of common mode rejection of inadvertent grounding of any one input lead and the rejection of spurious input noise.

No alternate methods of signal processing were evaluated.
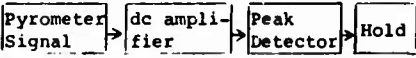
203

9. Radiation Pyrometer Signal Processor
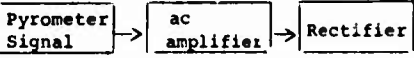
In the design phase, two alternate methods were
investigated for extracting the turbine blade
temperature from the pyrometer signal. The
pyrometer signal variation as a function of each
turbine blade rotation consists of an ac signal
superimposed on a dc level. The first method
investigated involved detecting the peak level
in order to limit the blade temperature to 1800°F.
The second method measured only the peak to peak
or ac signal. Table XXII compares the two methods.

The accuracy of Method II is $\pm$ 1% of FS over the
ambient temperature range of -55°C to +125°C.
Method I can only meet the accuracy of $\pm$ 1% of FS
over a reduced ambient temperature range from 0°C
to +85°C. This is due to the dc offset voltages
caused by ambient temperature changes. In
consequence, the signal processing adopted was
Method II.

10. Pressure Sensor Signal Processor

The extremely low output capacitance from the
pressure transducer imposes rigorous constraints
on the design of the interface circuits with
regard to sensitivity, stability, and rejection
of external effects. With consideration for
these factors, together with regard for the inter-
face requirements of the computer, the output
capacitance of each transducer was used to control
the operating frequency of an oscillator. Sub-
traction of these two frequencies then yields a
signal proportional to P_{t3}. Each oscillator has
a dynamic range of better than 20:1 with linearity
of less than 0.1% and a temperature stability of
0.25%.

No other methods of signal processing were
evaluated.

204

Performance Criteria	METHOD I Processing the Peak Level	METHOD II Processing the Peak-to-Peak Level
Detection Required	In order to detect the peak level, the dc component as well as the ac component of the signal has to be processed.	Only the ac component of the signal has to be processed. The dc component is disregarded.
Signal Level	Pyrometer current varies from $.3 \times 10^{-9}$ amps to 40×10^{-6} amps.	Pyrometer current is the same as in Method I.
Circuitry Required	Pyrometer Signal → dc amplifier → Peak Detector → Hold	Pyrometer Signal → ac amplifier → Rectifier
Effects of Temperature	All amplifiers are affected by temperature. The effect is in the form of a dc drift or offset voltage which results in an offset temperature error. The most stable op. amp readily available is the LM108. When this device is used, the offset voltage caused by temperature is still 10 times more than can be tolerated.	Temperature effects are minimal since temperature only causes a dc offset, and in Method II the dc signal is neglected.
Effects of Carbon Noise	Carbon noise affects the dc level, therefore an error is introduced	Since carbon noise can be filtered out by the ac amplifier its effects are minimized
Response	25×10^{-6} sec	25×10^{-6} sec

TABLE XXII. COMPARISON OF THE PYROMETER INTERFACE CIRCUITS EVALUATED

Package Design Features and Alternatives

The single most critical area in the development of an engine mounted electronic fuel control system is the electronic computer package. To ensure that the system will function reliably, the electronic circuitry must be provided with adequate protection from the severe engine environment. Little work has previously been done in this area, since most electronic systems heretofore developed have been intended for airframe or ground installation.

The primary environmental problems are high temperature and vibration levels. The fuel control must function reliably at fuel housing temperature up to 300°F. Most of the electronic components within the control could not operate satisfactorily at body temperature much in excess of 250°F. In addition, the integrity of the computer package and all electrical connections must be maintained at vibration levels as high as 20g at frequencies of up to 2,000 Hz.

Other package design objectives include the following:

1. To reduce the control area exposed to potential combat damage.

2. To reduce package size and weight to 60 in.^{3} and 3.5 lb.

3. To make the computer readily serviceable.

4. To reduce production cost by simplification of assembly and testing.

Alternative structural designs and cooling system designs were evaluated to determine ways in which these objectives could best be met. This section outlines the results of this evaluation.

External Dimensions

The actual dimensions of the electronic computer production package were dictated by the allowable envelope and the configuration of the fluid controller and alternator.

Component Mounting/Interconnection

Only a few workable alternatives to the use of printed
circuit board could be found. These included conventional
hand wiring and cord wood packaging.

Greater structural strength and rigidity can be realized
by cord wood and other more exotic packaging techniques.
Improved cooling may also be realized by mounting all com-
ponents in proximity to a metallic or other highly con-
ductive heat sink. None of these alternatives were con-
sidered to be acceptable due to their prohibitively high
production costs.

Circuit Board Orientation

Many factors affect the selection of the plane(s) in which
the circuit board will be oriented. The most restrictive
one is the package external dimensional constraints. This
establishes the base about which the other factors must be
considered.

Heat removal is the second most restrictive aspect of the
package design. If metallic conductive paths are provided
for transfer of component heat to the package heat sink,
then the circuit boards must be arranged in a plane paral-
lel with the best heat transfer arrangement for these
conductive paths. If the components are to be submerged
in a liquid coolant, then the circuit boards must be ori-
ented to maximize the convective flow of the coolant
liquid. This orientation would depend on the location of
the cool plate.

Another factor limiting the freedom of circuit board ori-
entation is the effective use of circuit board space. For
example, circuit boards that are long and narrow and which
make connections through either or both of their short
ends will be quite inflexible because of their limited
number of crossovers. Short, wide circuit boards can
utilize the distribution board (often called "mother
board") for their crossovers. This will result in a large
number of interconnections with an attendant reduction in
reliability.

Vibration susceptibility did not influence the selection
of a circuit board orientation significantly. The board
assembly must be designed to minimize resonances in all
three planes. For this reason, no distinct advantage was
found for any particular orientation based on the speci-
fied vibration envelope. However, in a specific installa-
tion one plane may be subjected to more severe vibrations
and for this reason dictate the orientation of circuit
boards.

Other factors influencing circuit board orientation in-
cluded the actual shape of the package interior, acces-
sibility for adjustments, and other special requirements.
Each of these reduces to a matter of economics and engi-
neering judgment.

Circuit Board Interconnection

Commonly accepted means for making connections from one
circuit board to another include cable harnesses, flexible
printed circuit cable, and rigid printed circuit boards.
More exotic means which show promise of greatly increased
package density are presently in the early stages of de-
velopment. However, high cost will restrict using them
for another five years.

Of those interconnection methods available today, we can
quickly eliminate the rigid printed circuit board and the
old fashioned cable harness. The rigid printed circuit
board would require costly tighter manufacturing tolerances
which would otherwise be unnecessary. Rigid printed cir-
cuit board could not be used to pick up leads from connec-
tors or sensors within the package unless they could be
designed to utilize the same wiring plane as the other
printed circuit boards, which is not a likely event.

The use of cable harnesses is just too costly. The manu-
facturing processes required to make and check end connec-
tions is extremely expensive to automate. In addition,
the overall mass of a cable harness requires that it be
securely fastened along its length in order to prevent
connection failures from vibration.

Printed circuit board connectors could not be used. No connector could be found which was free of the multiplicity of reliability problems commonly associated with all connectors. External connectors enjoy an acceptable reliability reputation, but these must depend on their shell structure and housing for close mechanical support. The cost of providing comparable support for printed circuit connectors would be prohibitive.

For the demonstration unit computer we selected the flexible printed circuit cable. This particular flexible cable consisted of 3 layers of printed circuit wiring. Two layers of a flexible ground plane were also used to eliminate signal coupling between layers.

The selection of the flexible PC cable was made primarily to minimize package cost. The thinness of the cable allows great freedom of movement without undue stress at the connection points. Electrical package tolerances may then be relaxed with an attendant cost savings. In addition, strain at the connection points is sharply reduced by this ability of this cable to yield as internal parts make slight movements during vibration. The low mass of the cable further reduces the probability of a vibration failure. Disassembly is also facilitated by the flexibility in that the package can be disassembled without unduly stressing board and connector interconnections.

Types of Printed Circuit Boards

The glass-epoxy printed circuit board common to most military electronic applications has been used. There is no reason to expect problems using these boards in engine mounted electronic applications if they are specified for the temperature environment.

The main question on board selection is whether to use single-sided, double-sided, or multilayer boards. Single-sided boards which have circuitry printed on one side only offer the lowest cost and are the simplest to repair. Multilayer boards offer the greatest packaging density but the cost is higher. Repair and trouble shooting is more difficult. When comparing double-sided boards to multi-layer boards, a 1:3 volume reduction was found to be

209

possible, but at a 4:1 cost increase.

The multilayer board is a laminated piece and offers a much greater rigidity than a single- or double-sided board. As a result, resonant vibration frequencies are higher for the same component weight distribution.

The multilayer board is more expensive to buy and assemble. Components are hand soldered to the outside layers, whereas single- and double-sided boards may be wave soldered, using conventional techniques.

Both double and multilayer boards are used in the demonstration unit.

Circuit Board Support

The main factor dictating the means of support for the circuit boards is vibration resonances. Determining the resonant frequencies establishes the maximum allowable unsupported length of board.

In the demonstration unit package the 4 in. x 4.75 in. circuit boards were supported by bolts in each of the four corners of the board and in the center. Each of the bolts was firmly supported by two structural frame members within the package.

Repairability

Modern solid-state circuitry drastically reduces the possibility of any but factory or Overhaul and Repair Depot service for the electronic computer. Although elaborate test equipment may be developed to isolate failures, someone ultimately has to go inside the electronic computer package and de-solder components and/or other connections to make repairs.

For flight line level maintenance, all that should be done to expedite service is to provide the necessary test instrumentation to enable maintenance to quickly isolate the problem to a replaceable module.

Repairs within the package may be simplified by a design which facilitates disassembly. Unfortunately, this reduces reliability. For example, the use of edge card circuit board connectors would greatly enhance repairability, but the reduction in reliability is too great.

The demonstration unit was designed to take advantage of the flexible cable for connecting the circuit boards. By removal of the circuit board support bolts, all of the circuit boards may be "fanned" about the flex-cable. This allows access to any component and any circuit board for test or replacement.

Another aid to maintenance and repair is to select connectors which can be removed from the computer housing along with the circuit boards. This will enable closer examination of all sides of the circuitry. It will also minimize the probability of further breaks in connections which would result from handling while repairs were being made.

Naturally, the generous use of test points will greatly facilitate troubleshooting. These should be brought out to the edges of the circuit boards to enable measurements to be made before disassembly.

Hybrid Microcircuits

Both thin and thick film hybrid microcircuits were utilized in the demonstration unit computer for evaluations. Five areas of the computer were fabricated in hybrid form. These are listed in Table XXIII along with their associated volume saving.

Contrary to the situation which existed in the late 1960's, fabrication of circuits in hybrid microcircuit form is not excessively expensive. In fact, in production quantities, hybrid microcircuits can seriously challenge the cost of discrete component fabrication.

Results of environmental and endurance testing have shown the hybrids to be comparable to circuits using discrete components. The only problems encountered were with one particular type of hybrid circuit case which used leads

211

TABLE XXIII. HYBRID CIRCUITS PACKAGING SUMMARY

Circuit Designation	Qty Req'd/System	Component Area (in.2)		Board Area (in.2)		Net Board Area Savings (in.2)	Volume Saving (in.3)
		Discrete	Hybrid	Discrete	Hybrid		
Volt to Freq. Converter	2	2.58 (0.26" Height)	1.31 (0.18" Height)	3.43	3.27	0.16	0.25
Frequency Selector	14	14.70	7.00	36.75	17.50	19.25	6.16
Binary Rate Mult.	6	11.04	3.94	27.60	9.85	17.75	5.68
Triple Pulse Syncronizer	4	5.28	2.62	13.20	6.55	6.55	2.13
S.M. Trans. Driver Section	2	6.38 (0.30" Height)	2.80 (0.18" Height)	8.50	7.00	1.50	2.76
TOTALS						45.31 in.2	16.98 in.3

NOTES:
1. Areas shown are for total quantities of "components" required/system.
2. Total board area saved (potential) is approximately equivalent to 3 of the double-sided P.C. boards used in the demonstrator control.
3. Volumetric saving in S.M. translator is significant due to driver transistor's height.

212

0.010 inch thick. These were found to fracture at the case during vibration testing.

In addition to a 1:5 volume reduction, hybrid microcircuits offer other advantages. Reliability surpasses that of equivalent circuits made of discrete devices. This could be partly a result of a more thorough screening of components before assembly. Another contributing factor is the low mass of the components and inter-component wiring within the microcircuit itself.

The hybrid circuit also offers the advantage of tracking in analog circuit design. Here two components may be held at nearly the same temperature because of their proximity. Changes in characteristics of one with temperature will closely follow changes in the other, thereby enabling relatively temperature insensitive differential circuitry to be utilized.

A great difference among hybrid circuit vendors was found. Large differentials in price, perf·.:mance, and quality were noted.

Transducer Location

The compressor discharge pressure and the radiation pyrometer transducers are located within the electronic package. This was done to take advantage of the cooling system. Also, the pressure signal is a very high impedance, capacitance sensitive, high frequency signal. A long lead from the transducer to the electronic processing circuits will deteriorate the signal. The radiation pyrometer signal is an extremely weak current. The first stages of electronic signal processing and amplification are located right on the head of the transducer itself.

Cooling Design Features and Alternatives

The two basic problems in cooling electronic packages include removing the heat from components and then dumping it into a heat sink. Studies in each of the areas were conducted to establish the best overall cooling system for an engine mounte electronic computer.

Removing Heat From Components

Many schemes were considered for transferring heat from the components to the heat sink. However, some of these schemes, while worthy of consideration for future development, would have required development and risks to an extent not considered to be within the scope of this program. Therefore, the criterion for selecting schemes was to utilize currently developed technology or only minor extensions thereof. This reduced the possibilities to the following:

1. Pure conduction.

2. Air convection from untreated circuit boards.

3. Air convection from boards treated with thermally conductive conformal coating.

4. Air convection and conduction from boards conformally coated (as in 3) but with thick copper plating over the coating.

5. Air convection from boards potted in thermally conductive potting compound.

6. Immersion in Silicone dielectric fluid.

7. Immersion in 3-M Fluorinert dielectric fluid.

Performance criteria were established, by which the mechanism could be compared:

1. Convenience of application and cost.

2. Ability to deal with hot spots.

3. Ability to deal with distributed heat load.

4. Ability to conduct heat into cold plate.

5. The effect of package orientation.

6. The repairability of circuit boards.

214

Investigations were undertaken to evaluate the performance
of each mechanism with respect to the criteria listed
above. The results of this study are summarized in
Table XXIV.

The results show the thermally conductive potting compound
and Fluorinert immersion mechanisms to be equally satis-
factory. The potting compound is eliminated because it is
difficult to repair. Therefore, the Fluorinert liquid is
left as the final choice.

The mechanism of cooling in this chosen method is essen-
tially the same as that of a heat pipe. It was suggested
in the proposal for this program that a heat pipe might be
the best cooling mechanism for an engine mounted control
of this power dissipation level. This testing program has
confirmed this to be the case. Any practical deviation
from this cooling scheme would require a large reduction
in power dissipation.

1. Investigation of Cooling Mechanisms

   Of the seven alternate mechanisms considered, the
   last six are all convective. The first mechanism,
   pure conduction, involves the use of a specially
   constructed circuit board, with either exception-
   ally large conductors, an aluminum core, or both.
   Such boards, along with their attendant thermal
   interfaces, were found to be prohibitively ex-
   pensive for this type of control and were dropped
   from further consideration.

2. Convective Heat Transfer Mechanisms

   Convective heat transfer analysis is notoriously
   unreliable, and thus it was felt that any deci-
   sions would have to be based on test data. A
   comparative testing program was therefore con-
   ducted.

   A standard circuit board was designed and con-
   structed (Figure 112). It comprises 28 1 Ω
   resistors mounted on a board whose overall dimen-
   sions approximate those of the circuit boards

215

TABLE XXIV. COMPARISON OF METHODS OF REMOVING HEAT FROM COMPONENTS

|	Photo in Fig. No.	(1) Ease of Application and Use	(2) Ability to Deal with Hot Spots	(3) Ability to Deal with Uniform Heat Load	(4) Ability to Transfer Heat into Cold Plate	(5) Effect of Package Orientation	Conclusion
Test Data (Comparison Curves) Presented in Fig. No.			116	117	118	119	
1. Conduction		Circuit board & interfaces prohibitly expensive: idea dropped.	See Column (1) Abandoned (too costly) ⟶				
2. Air Convection (untreated boards)	112	Easy	85°F temperature rise/1 watt to be dissipated.	15°F temperature rise/1 watt to be dissipated.	6°F temperature rise/1 watt to be dissipated.	Not tested.	Ineffective for hot spots.
3. Air Convection (conductive conformal coat)	113	Easy to apply; difficult to repair boards.	72°F temperature rise/1 watt to be dissipated.	17°F temperature rise/1 watt to be dissipated.	6°F temperature rise/1 watt to be dissipated.	Not tested.	Ineffective for hot spots.
4. Air Convection (conductive conformal coat plated copper heat sink)		Could not find suitable manufacturing technique; idea dropped.	See Column (1) Abandoned (unable to find workable manufacturing process) ⟶				
5. Air Convection (conductive potting) (Figure	114	Fairly easy to apply; impossible to repair.	15°F temperature rise/1 watt to be dissipated.	8°F temperature rise/1 watt to be dissipated.	6°F temperature rise/1 watt to be dissipated.	Not tested.	Works well, not suited to development program.
6. Fluid Convection Silicone Dielectric Fluid		Easy to implement; but residue makes repair soldering impossible; idea dropped	See Column (1) Abandoned (repairs impossible) ⟶				
7. Fluid Convection 3-M Fluorinert Dielectric Fluid		Careful design and assembly required to avoid leaks. No repair problems.	8°F temperature rise/1 watt to be dissipated.	2°F temperature rise/1 watt to be dissipated.	2.5°F temperature rise/1 watt to be dissipated.	20% change in ΔT/watt when rotating best-worst case.	Selected.
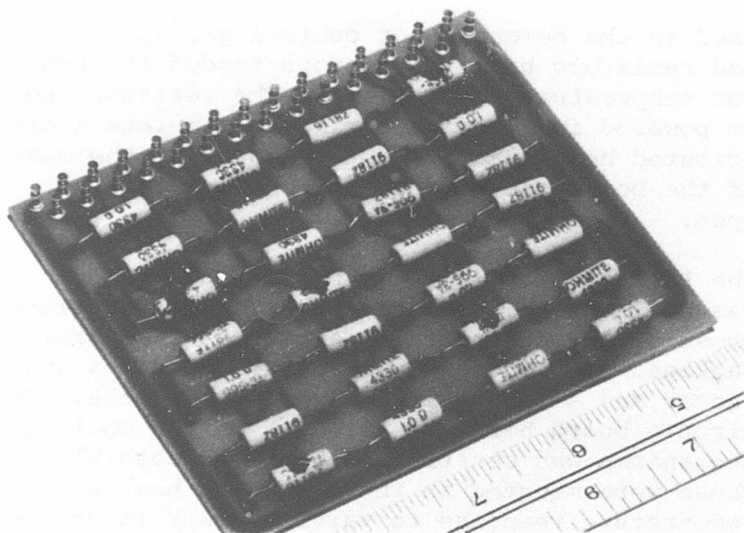
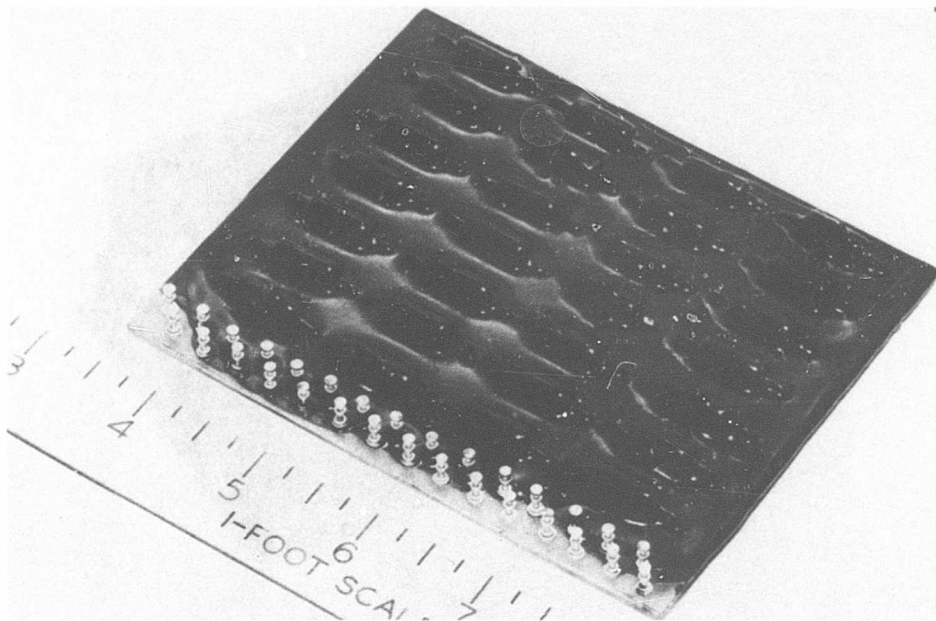Figure 112.   Test Circuit Board - Untreated.

Figure 113.   Test Circuit Board With Thermally
Conductive Coating.

217

used in the demonstrator control package. Selec-
ted resistors have thermistors bonded to them
for temperature measurement. The resistors could
be powered in a series string to simulate a dis-
tributed heat load, or one resistor in the center
of the board can be powered to simulate a hot
spot.

The Plexiglas enclosure shown in Figure 115
was built. Its internal dimensions approximate
those of the demonstrator electronics control
package. The enclosure is provided with a con-
nector and a large aluminum heat sink base. The
circuit board hardware for each of the cooling
mechanisms was constructed wherever possible.
These were mounted in the Plexiglas box, and the
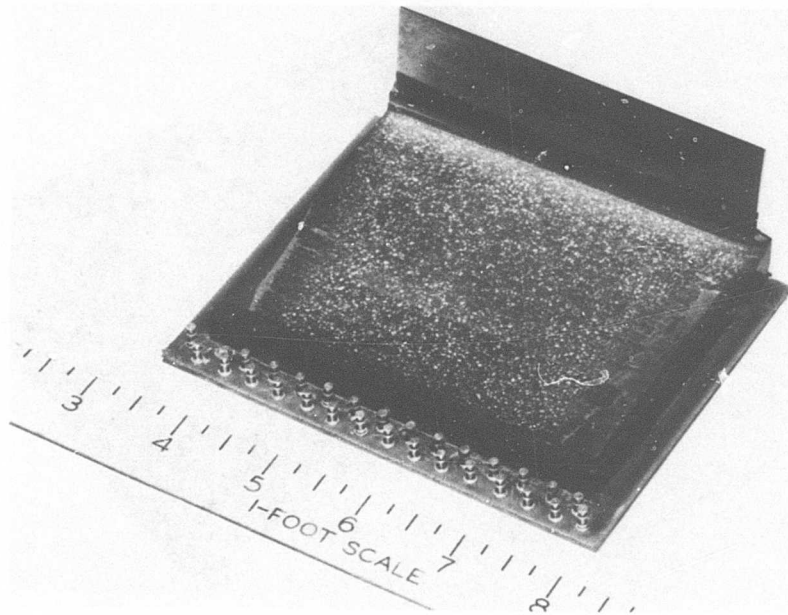temperature response to varying power inputs was
recorded.

Figure 114.   Potted Test Circuit Board
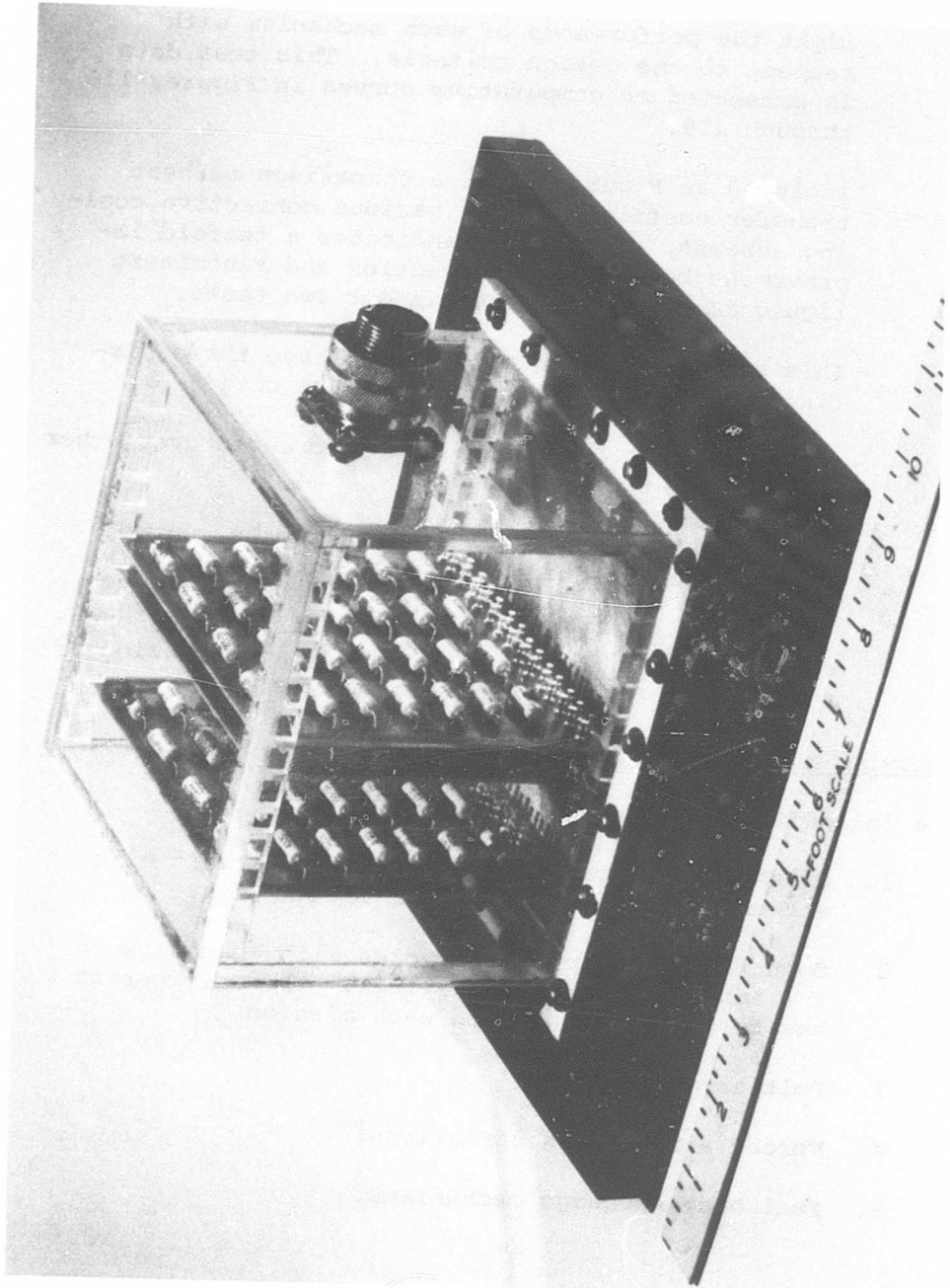With Integral Heat Sink.

218

Figure 115. Electronic Cooling Thermal Test Fixture.

219

This data was carefully reduced in order to high-
light the performance of each mechanism with
respect to the design criteria. This test data
is presented as comparative curves in Figures 116
through 119.

Included as Figure 120 is a comparison of heat
transfer coefficients for various convective cool-
ing schemes. This chart indicates a tenfold im-
provement between air convection and Fluorinert
liquid immersion as noted in our own tests.

This selected mechanization does have three dis-
tinct disadvantages which should be noted:

    a.   Weight is considerably increased over other
        non-fluid methods.

    b.   A leak could result in ultimate control
        failure due to overheating.

    c.   Care must be taken while filling the pack-
        age to ensure that volumetric expansion of
        the fluid will not burst the case.

Removing Heat from Package

The following mechanisms were studied:

    1.   Closed refrigeration type cycles with heat sink
        either to the ambient air or to the fuel.

    2.   Open refrigeration type cycles with heat sink to
        the ambient air or to the fuel. The refrigerant
        has to be replenished on each mission.

    3.   Peltier cooling.

    4.   Forced air cooling variations.
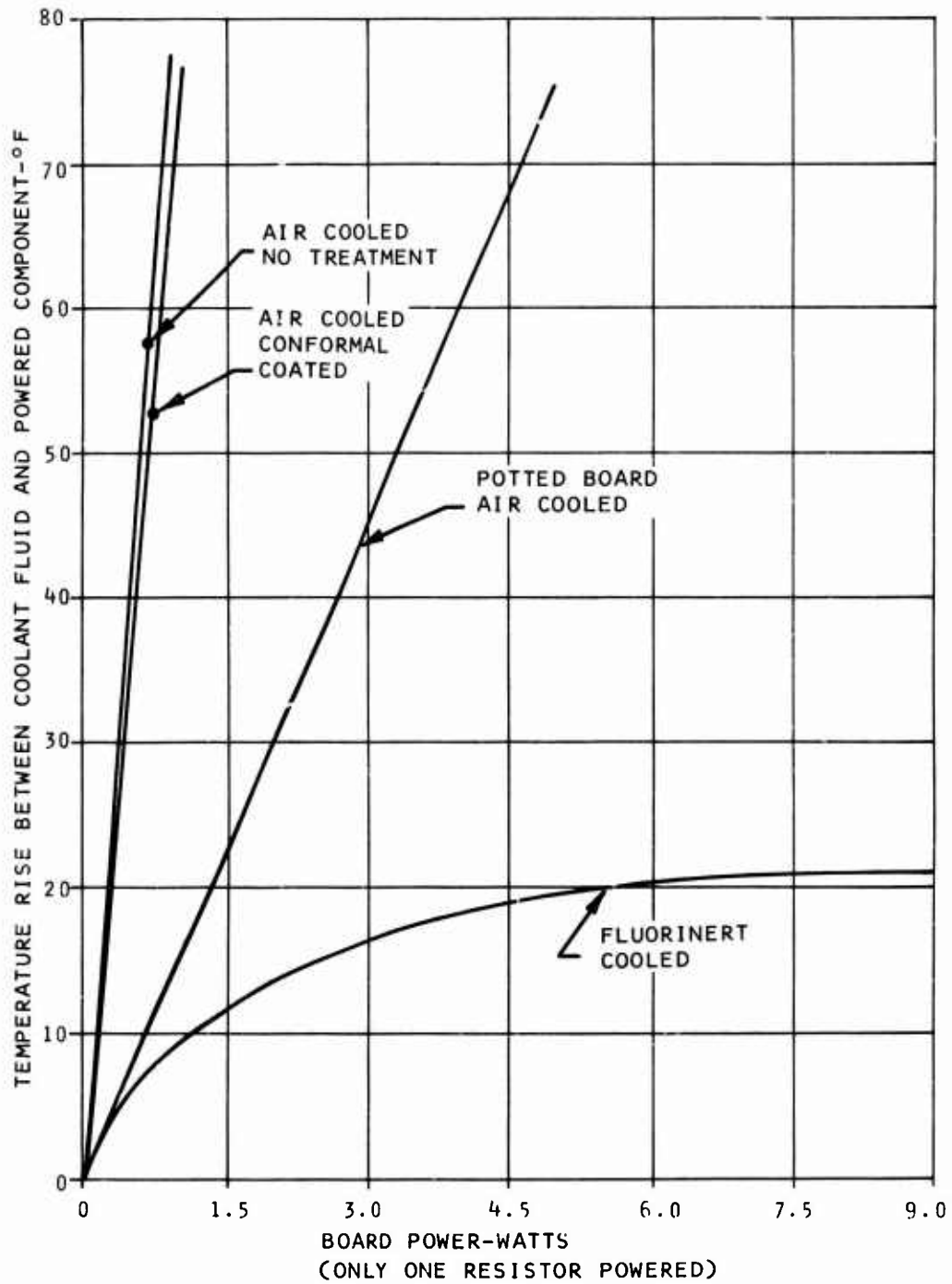
    5.   Fuel heat exchange mechanisms.

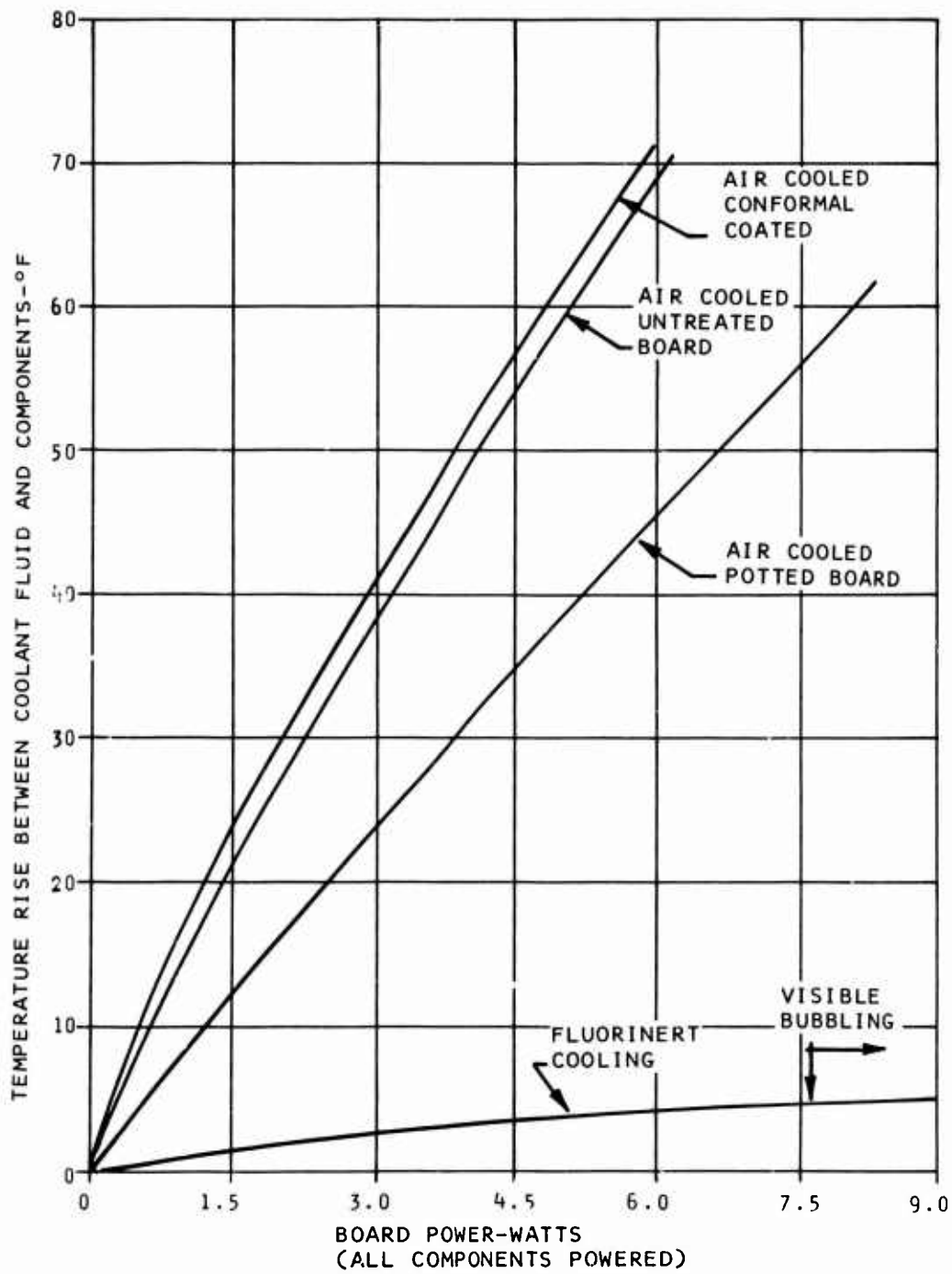Figure 116.   Localized Heat Source Cooling Performance.

Figure 117.   Uniform Heat Load Cooling Performance.
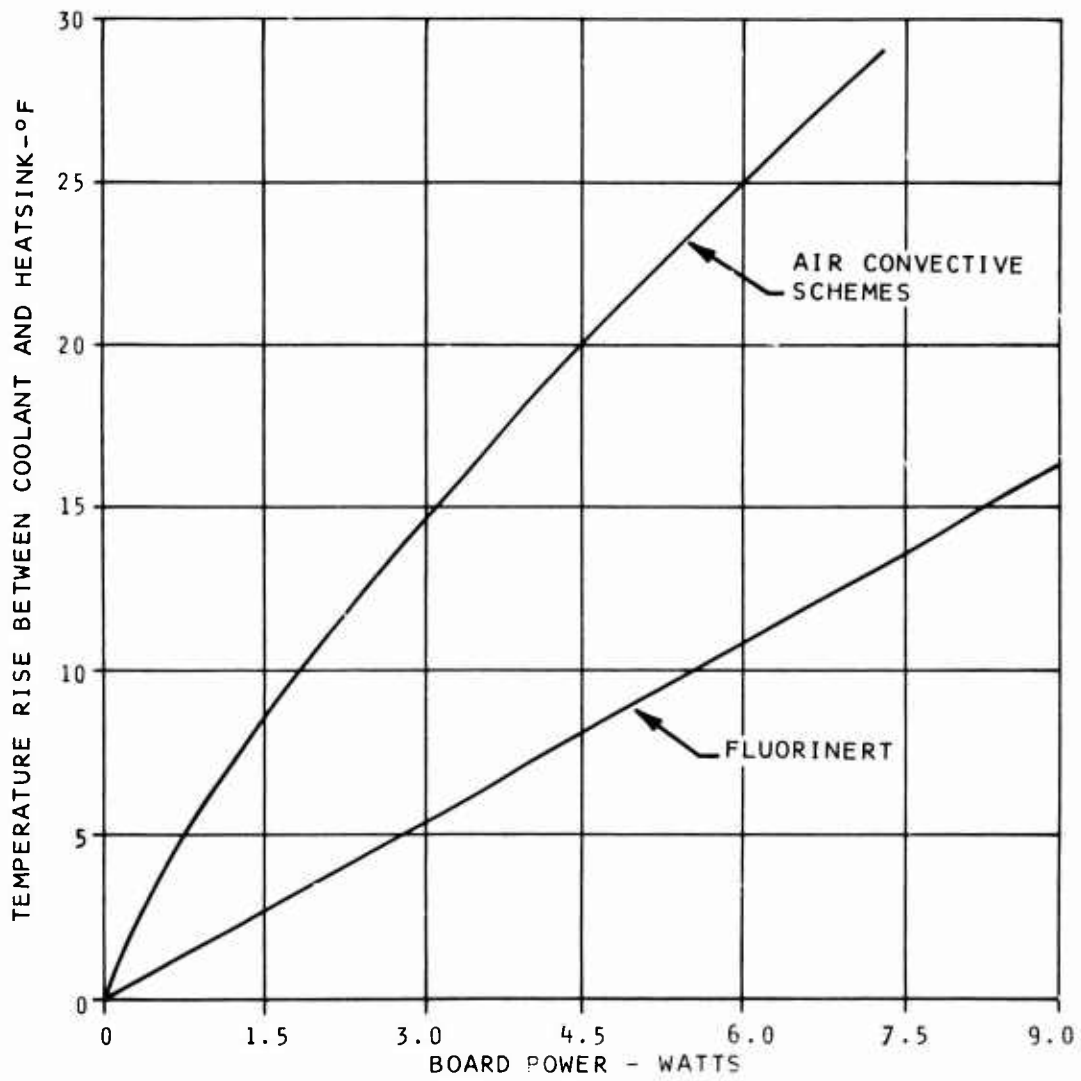
222

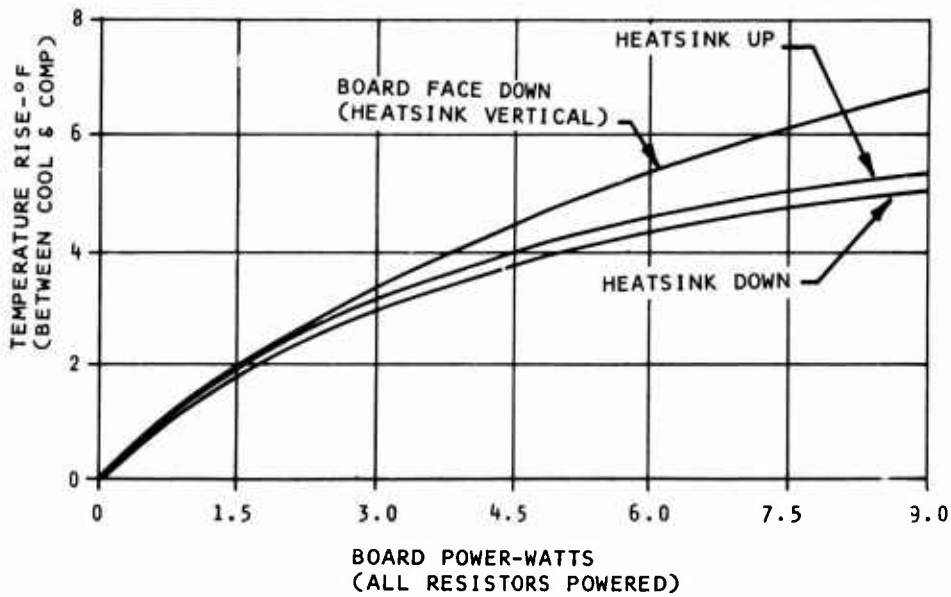Figure 118.   Heat Transfer From Bulk Coolant to Sink.

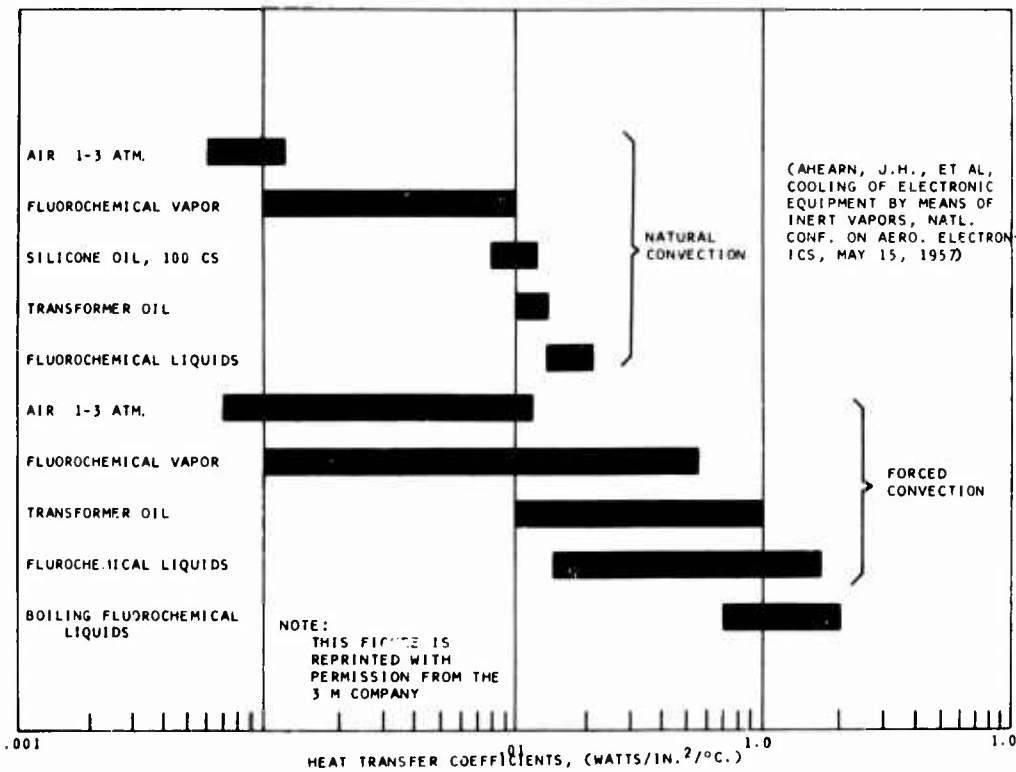Figure 119. Effect of Package Orientation (Fluorinert Cooled).

Figure 120. Heat Transfer Coefficients.

The first three listed mechanisms were found to provide very large temperature differentials, but the power consumption, cost, and complexity of these immediately remove them from consideration on such a control.

The fourth, forced air cooling, requires consumption of more bleed air from the compressor than was considered to be permissible.

The last, while not providing as large a margin of usable temperature differential as the preceding schedmes, is clearly the choice because of the great simplicity and inherent low cost.

Environmental and Functional Testing

Functional and environmental testing comprised a substantial portion of this control development program. Each of the critical component subassemblies developed were individually tested and evaluated. The complete demonstration unit computer was extensively tested by itself before installation with the fluid controller.

This section outlines the results of these tests, and describes test setups and procedures.

Vibration Testing

Figure 121 shows the test setup used for evaluation of the functional performance of the control during exposure to the vibration spectrum illustrated in Figure 122.

The testing procedure adopted (per MIL-E-5272C) entailed vibrating the control in each of three mutually perpendicular axes as defined in Figure 123. For each axis, the vibration frequency range was swept and the four worst resonance points were noted. With the electronic computer in an operational mode, sweep and dwell tests were conducted in accordance with the procedure indicated in Table XXV.
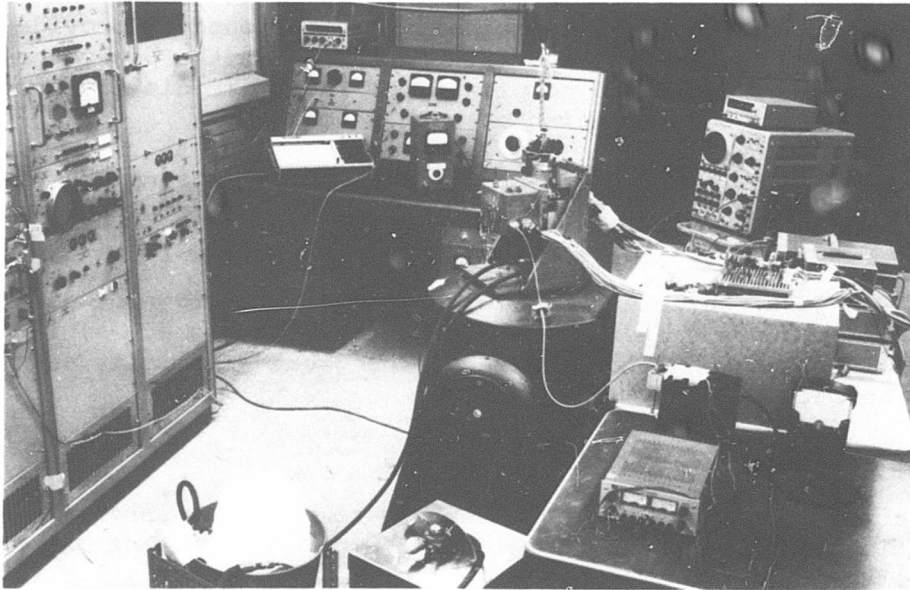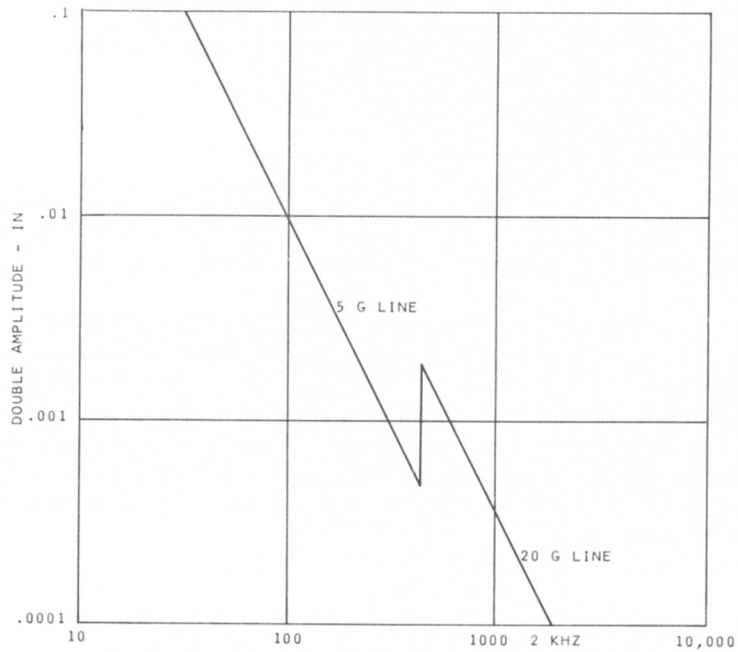
Figure 121.   Vibration Test Equipment.

Figure 122.   Vibration Spectrum.

226

	TABLE XXV. VIBRATION TESTING CONDUCTED	
AXIS	SWEEP TEST	DWELL TEST
X	Sweep for 1 hr from 20 Hz at vibration excitation levels per Figure 124 at a rate of 6 min/cycle.	Dwell for 0.5 hr at each of the following resonance points with a vibration excitation level per Figure 124. 1.948 KHZ 1.595 KHZ 0.956 KHZ 0.592 KHZ
Y	Sweep for 1 hr from 20 Hz to 2 KHZ at vibration excitation levels per Figure 125 at a rate of 6 min/cycle.	Dwell for 0.5 hr at each of the following resonance points with a vibration excitation level per Figure 125. 1.264 KHZ 0.980 KHZ 0.820 KHZ 0.480 KHZ
Z	Sweep for 1 hr from 20 Hz to 2 KHZ at vibration excitation levels per Figure 126 at a rate of 6 min/cycle.	Dwell for 0.5 hr at each of the following resonance points with a vibration excitation level per Figure 126. 1.60 KHZ 1.20 KHZ 0.80 KHZ 0.65 KHZ
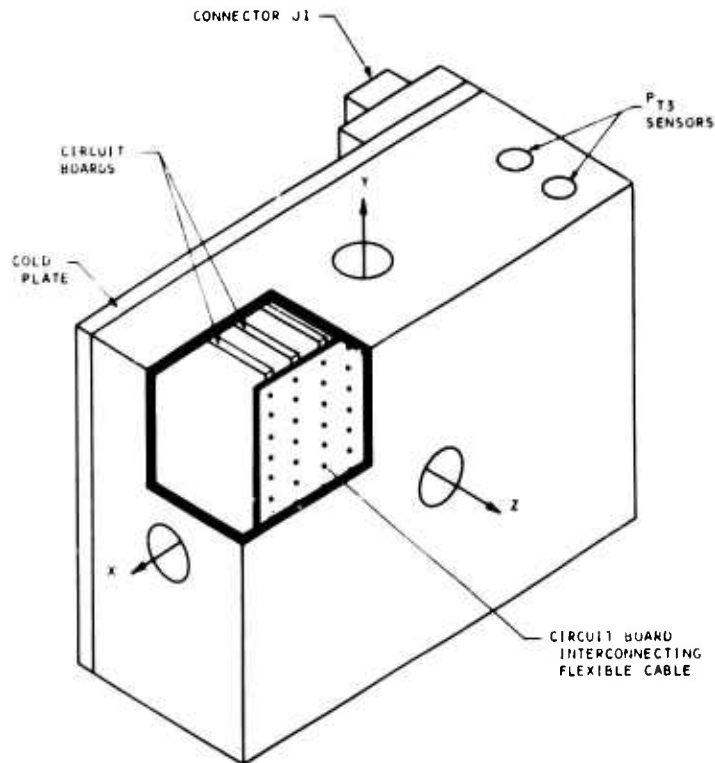
Figure 123. Control Vibration Axis.

Figures 124 through 126 illustrate the vibration levels experienced by the control as measured by an accelerometer positioned in the center of the control cover in the plane of vibration. Vibration levels in excess of 100g were recorded. However, it is not known what levels the circuit boards felt.

The above test procedure was conducted on two separate occasions. The first testing revealed that components were inadequately bonded to the printed circuit boards and insufficient support was provided in mounting the printed circuit boards.

The effect of these problem areas was amplified by an inadequate test fixture that allowed "g" forces well in excess of the specified excitation levels.

Figure 124.   Vibration Test - Axis X.

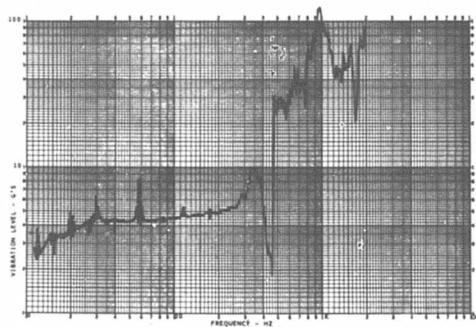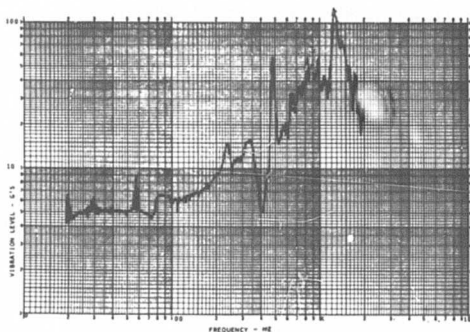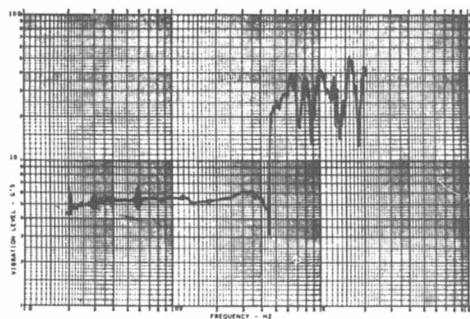Figure 125.   Vibration Test - Axis Y.

Figure 126.   Vibration Test - Axis Z.

229

After modifications to the control and test fixture, to eliminate the above problems, vibration tests were repeated.

The results indicate that the majority of the control is capable of performing normally in the vibration environment. The exceptions to this are as follows:

1. The main computer timing oscillator failed at an early stage in the vibration test.

2. The outer shield of the P_{t3} transducer output lead fractured.

3. The base-emitter junction of a signal transistor in the -12v regulator became open circuited.

4. Three solder connections developed an open circuit.

Temperature Testing

1. ### Demonstrator System

   Figure 127 illustrates the setup used for evaluation of the functional performance of the control over the environmental temperature extremes.

   The demonstrator unit filled with the fluorinert dielectric fluid was placed in the environmental box, and external function generators and signal simulators (potentiometers, etc.) were used to provide input functions to the computer. Temperature controlled silicone was pumped through the cold plate to simulate fuel flow.

   The procedure adopted for the testing at 77°F and 257°F was to allow the control to stabilize at the specific temperature while operational. The silicone fluid was maintained at a temperature of 135°F. A calibration was then performed.

230
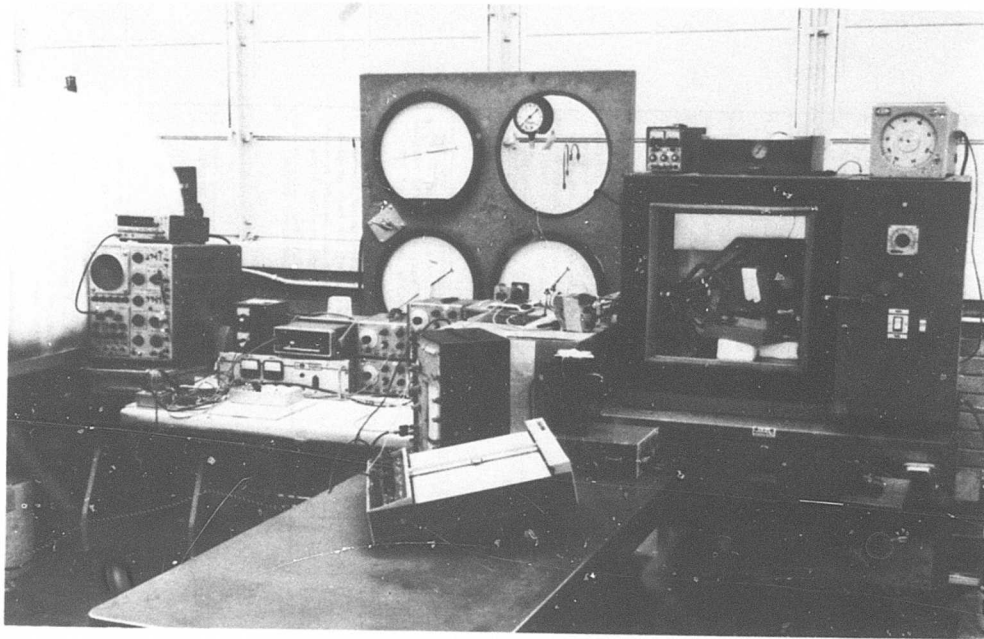
Figure 127.   Temperature Test Equipment.

For the tests at -67°F the control was allowed to
soak nonoperational at -67°F and then turned on
for short intervals to perform a small portion of
the calibration test, thereby negating the effects
of component self-heating.

Table XXVI presents a list of the tests performed
and the results obtained, together with pertinent
comments on the data.

It should be noted that for all system testing the
integrator was disconnected and the proportional
path gain was modified to maintain the required
system signal limits. This modification was imple-
mented to allow stable open-loop testing of the
system to be performed.

TABLE XXVI. TEMPERATURE TEST DATA - DEMONSTRATOR SYSTEM

| DESCRIPTION TEST	SETTINGS	CALIBRATION DATA AT $T_{AMB} = -55°C$	CALIBRATION DATA AT $T_{AMB} = 25°C$	CALIBRATION DATA AT $T_{AMB} = 125°C$	COMMENTS
1. To measure the N_{ft} lag output in response to specific N_{ft} and N_{ftr} signals.	$N_{ft}=52.3\%(N_{ft})$ $N_{ftr}=58.1\%(N_{ft})$	$\Delta N_{ft}=5.82\%(N_{ft})$	$\Delta N_{ft}=5.81\%(N_{ft})$	$\Delta N_{ft}=5.82\%(N_{ft})$	The maximum variation from the room ambient setting is 0.01% (N_{ft}) which is well within the maximum permissible deviation of ±0.05% (N_{ft})
2. To measure the N_{ft} lag output with the N_{ftr} signal augmented by a specific load sharing signal.	Settings as #1. $Q_{ao}=29\%(N_{ft})$ $Q_{at}=26.16\%(N_{ft})$	$\Delta N_{ft}=8.72\%(N_{ft})$	$\Delta N_{ft}=8.71\%(N_{ft})$	$\Delta N_{ft}=8.72\%(N_{ft})$	The maximum variation from the room ambient setting is 0.01% (N_{ft}) which is well within the maximum permissible deviation of ±0.1% (N_{ft})
3. To measure the N_{gr} signal as provided by a specific output from the N_{ft} path and β.	Settings as #2. $\beta = 30\%$ (β). PLA = Emergency.	$N_{gr}=85.1\%$ (N_g)	$N_{gr}=84.7\%$ (N_g)	$N_{gr}=85.1\%$ (N_g)	The maximum variation from the room ambient setting is 0.4% (N_g) which is within the maximum permissible deviation of ±0.5% (N_g)
4. To measure the N_f/P_{t3} command signal provided by the acceleration schedule with specific N_g and T_{t2} input signals.	Settings as #3. $N_g = 31\%$ (N_g) $T_{t2} = 60°F$	$N_f/P_{t3}=97.3\%$ (N_f/P_{t3})	$N_f/P_{t3}=97.9\%$ (N_f/P_{t3})	$N_f/P_{t3}=104\%$ (N_f/P_{t3})	The maximum variation from the room ambient value is 6.1%. This is well in excess of the ± 2.0% (N_f/P_{t3}) change permitted. The reason for this discrepancy is the large variation of the $\sqrt{\theta}$ output signal.
5. To measure the output of the $\sqrt{\theta}$ circuit in response to a specific T_{t2} input.	$T_{t2} = 60°F$	$\sqrt{\theta} = 98.8\%$ (Setting)	$\sqrt{\theta} = 100\%$ (Setting)	$\sqrt{\theta} = 103.5\%$ (Setting)	The maximum variation from the room ambient value is 3.5% (setting) which is well in excess of the ±0.5% (setting) permissible. The specific reason for this deviation is unknown but has been isolated to the circuitry interface.
6. To measure the specific difference between the two torque signals (local and remote) necessary to activate the engine failure indicator.	$Q_{so} = 29.1\%$ (N_{ft})	$Q_{at} = 44.0\%$ (N_f)	$Q_{at} = 43.9\%$ (N_f)	$Q_{at} = 44.0\%$ (N_f)	The maximum variation from the room ambient setting is 0.1% (N_{ft}) which is well within the maximum permissible deviation of ± 2% (N_{ft}).
7. To measure the N_g speed level necessary to activate the start motor inhibit signal.	Settings as #3	$N_g = 21.3\%$ (N_g)	$N_g = 22.1\%$ (N_g)	$N_g = 24.1\%$ (N_g)	The maximum variation from the room ambient setting is 2% (N_g) which is well within the maximum permissible deviation of ±5% (N_g)
8. To measure the N_f/P_{t3} command signal provided by the T_{4B} loop responding to a specific T_{4B} input.	Settings as #3 except $N_{ft}=40\%$ (N_{ft})	Not operational	Not operational	Not operational	The T_{4B} circuit was found to be non-operational prior to the initiation of the test program. Post testing evaluation revealed that the light sensing diode was open circuited.
9. To verify that the M.M.V. stepping motor responds proportionally to a variation in the overtorque signal, when this mode of control is selected.	Settings as #6	O.K.	O.K.	O.K.	Desired proportional control ensued.
10. To verify that the M.M.V. stepping motor responds proportionally to a variation in the P.I.A. angular position, when this mode of control is selected.	Settings as #6	O.K.	O.K.	O.K.	Desired proportional control ensued.
11. To verify that the voltage regulators perform correctly with switch-on after soaking at -55°C.	Line voltage varied 16-30V	O.K.	N/A	N/A	All voltage levels were normal with switch-on after soaking at -55°C.
12. To verify that the I.G.V. stepping motor responds proportionally to either a variation of N_g or T_{t2}.	N_g and T_{t2} varied.	O.K.	O.K.	O.K.	Desired proportional control ensured with change of both variables.

232

2. Voltage Controlled Oscillator (VCO)

This function, which was used in the collective pitch and blade temperature circuits, was tested initially to evaluate its linearity over the operating input voltage range at room temperature. Table XXVII presents the data from this testing.

(VCO)

Input (voltage) ⟶ | K (KHZ/volt) | ⟶ Output (Frequency)
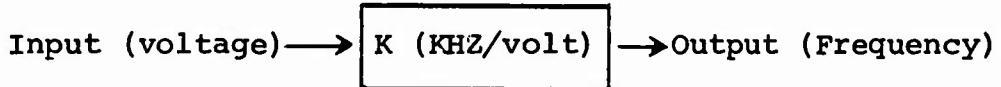
TABLE XXVII. VCO TEST DATA		
Input Voltage (volts)	Output Frequency (HZ)	K(KHZ/volt)
1	0.626	0.626
2	1.251	0.625
3	1.875	0.625
4	2.497	0.624
5	3.112	0.622
6	3.740	0.623
7	4.357	0.622
8	4.973	0.621
9	5.585	0.620
10	6.199	0.620

The results indicate that the maximum linearity deviation = 0.0967% compared to the ± 0.5% maximum permissible deviation. Figure 128 illustrates the performance of the VCO over the full environmental temperature range. As can be seen, the output frequency variation from -55°C to +125°C is 0.5%, which is within the required accuracy of ± 0.35%.
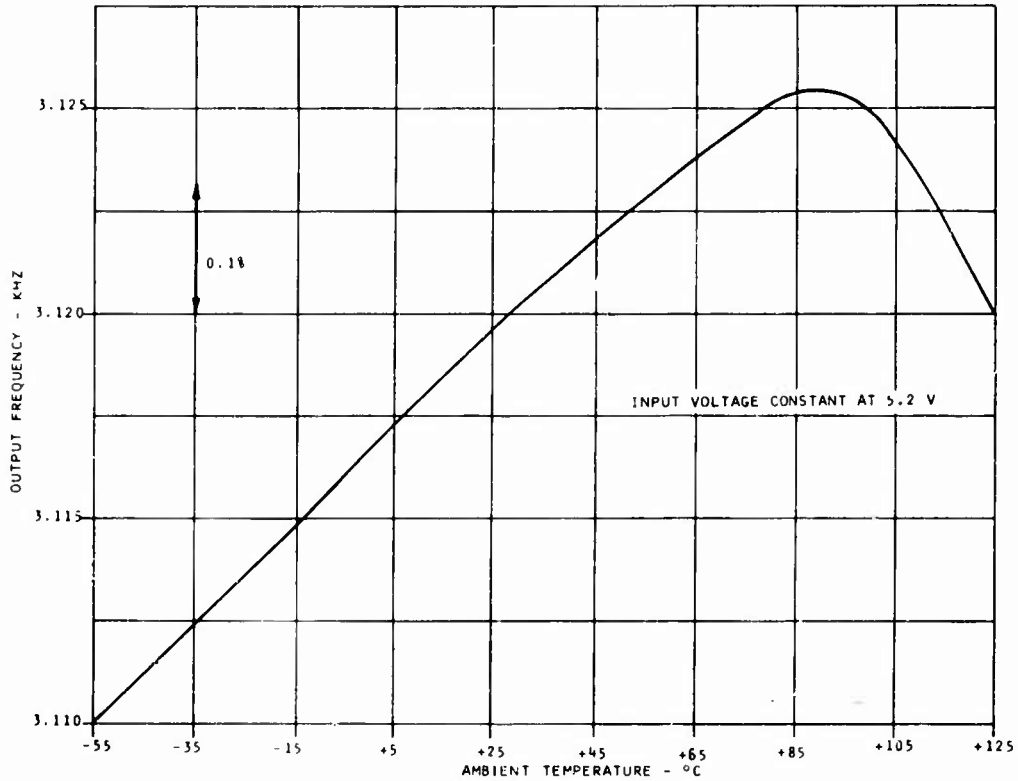
233

Figure 128. VCO Temperature Characteristics.

3. T_{t2} to$\sqrt{\theta}$ Converter

This function, which converts the T_{t2} temperature
measured by a thermistor into an output frequency pro-
portional to $\sqrt{\theta}$, was tested to compare the actual per-
formance versus the desired characteristics. The data
from this test is presented in Table XXVIII.

234

TABLE XXVIII. $\sqrt{\theta}$ GENERATOR TEST DATA		
Inlet Temperature (°C) (T_{t2})	Theoretical Output Frequency (KHZ) ($f\theta$)	Measured Output Frequency (KHZ) ($\sqrt{\theta}$)
-54.0	178.496	178.098
-51.0	179.734	179.293
-37.0	184.692	184.286
-25.5	189.648	189.178
-12.3	194.604	194.278
+ 1.0	199.562	199.011
+15.0	204.518	204.430
+29.0	209.476	209.403
+43.5	214.432	214.720
+54.5	218.150	218.191

Comparison between theoretical and measured data reveals a maximum deviation within the requirement of ± 0.5%. Figure 129 provides the results of testing the performance of the circuit over the environmental temperature range. As can be seen, the stability is within ±.5%.

4. P_{t3} Interface Circuit

This function receives its input signals from the reference and variable pressure transducers and processes an output frequency signal in proportion to P_{t3}; the circuit was evaluated over the temperature range -55°C to +125°C. The variable and reference signals were held constant at a level such that the P_{t3} output signal was approximately mid range. Figure 130 presents the results of this testing and as can be seen, the variation in the output is +0.6 to -0.05%. Subsequent testing revealed that this variation remained approximately constant throughout the total P_{t3} operating range. The magnitude of this variation is within the maximum limits for pressure in excess of 50 psia. However, for pressure in the range 8 psia to 50 psia, the above referenced signal variation represents a deviation from requirements.
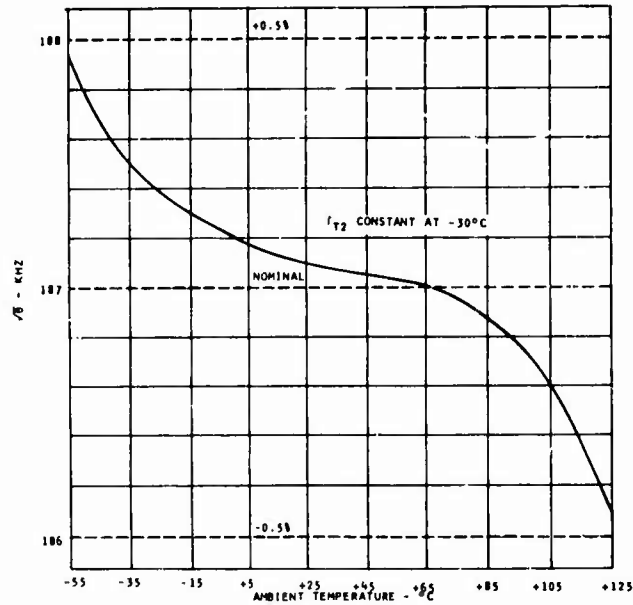
235

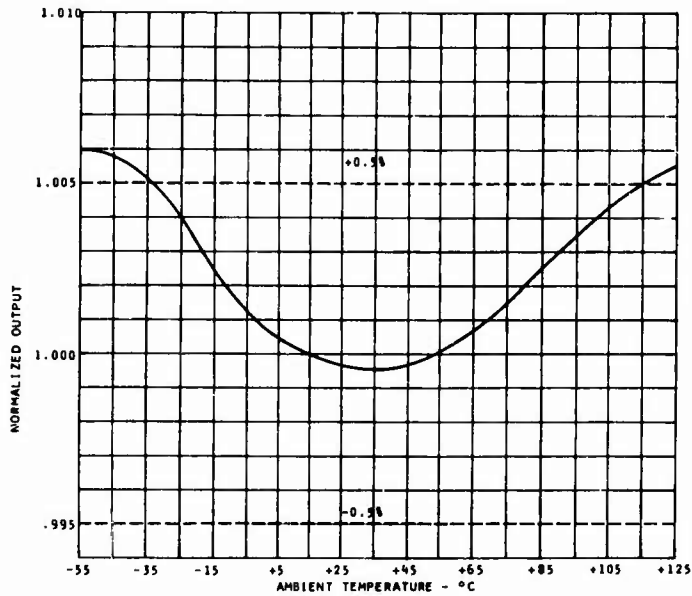Figure 129. T_{t2} to $\sqrt{\theta}$ Converter - Temperature Characteristics.

Figure 130. P_{t3} Interface Circuit - Temperature Characteristics.

236

5. Voltage Regulators

Figures 131 and 132 illustrate respectively the line and load regulation of the +12V regulator over the environmental temperature range. As can be seen, the performance is within the accuracy requirement of ±1%.

Figures 133 and 134 present the results of testing of the 5V regulator to evaluate the line and load regulation. As the data indicates, the performance is per requirements except for the line regulation at 125°C, where a slight deviation from the + 1% boundary exists. Testing of the -12V regulator indicated that its output magnitude tracked the output from the +12V regulator to within ± 0.2%.

6. Current Regulators

Figure 135 illustrates the line and load regulation of the stepping motor current regulator over the environmental temperature range. As can be seen, the regulator performance is within the desired limits of ± 5% for either one-or two-phase excitation. Figure 136 illustrates the efficiency of the regulator with variation in line voltage.

7. 3-D Function Generator (Acceleration Schedule)

Figures 137 and 138 illustrate respectively the theoretical and circuit generated acceleration schedule output signals in response to a variation of N_g and T_{t2}. The eight curves on each figure are constant T_{t2} characteristics.

A detailed comparison between the two figures indicated that the theoretical and circuit generated results are identical to within ± 2%.

Development Achievements

Development of the electronic computer has allowed advances to be made both in circuit design and in electronic package design. Circuit design improvements center on accuracy of measurement of engine variables and electronic implementation of

237

Figure 131. +12V Regulator - Line Regulation.

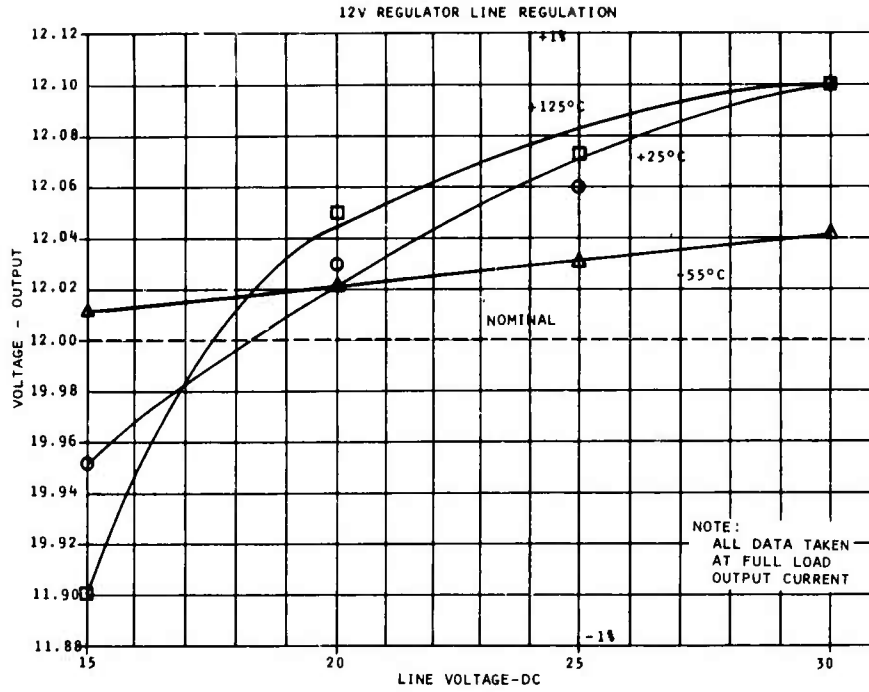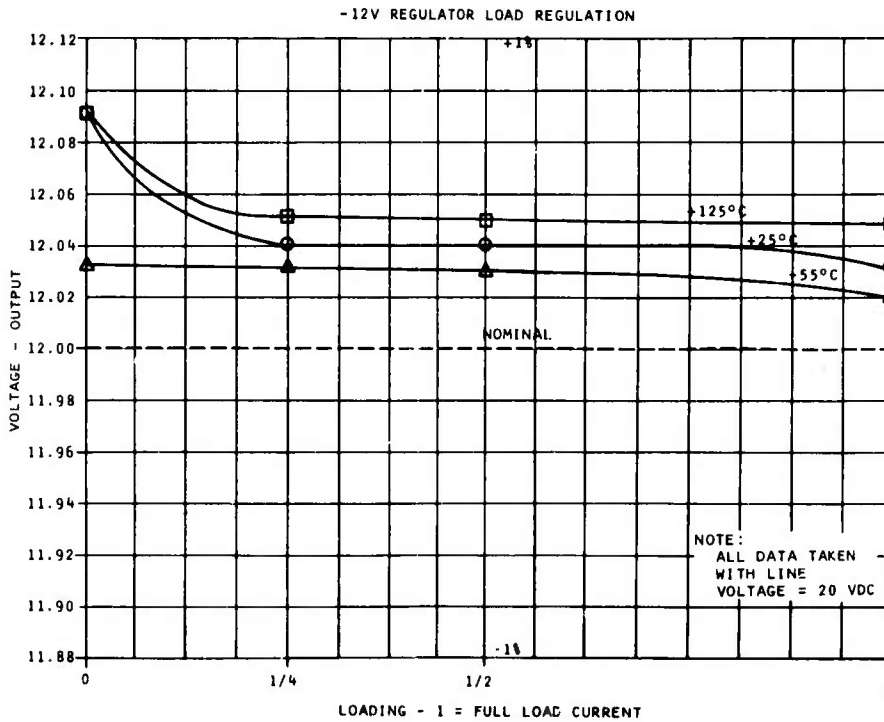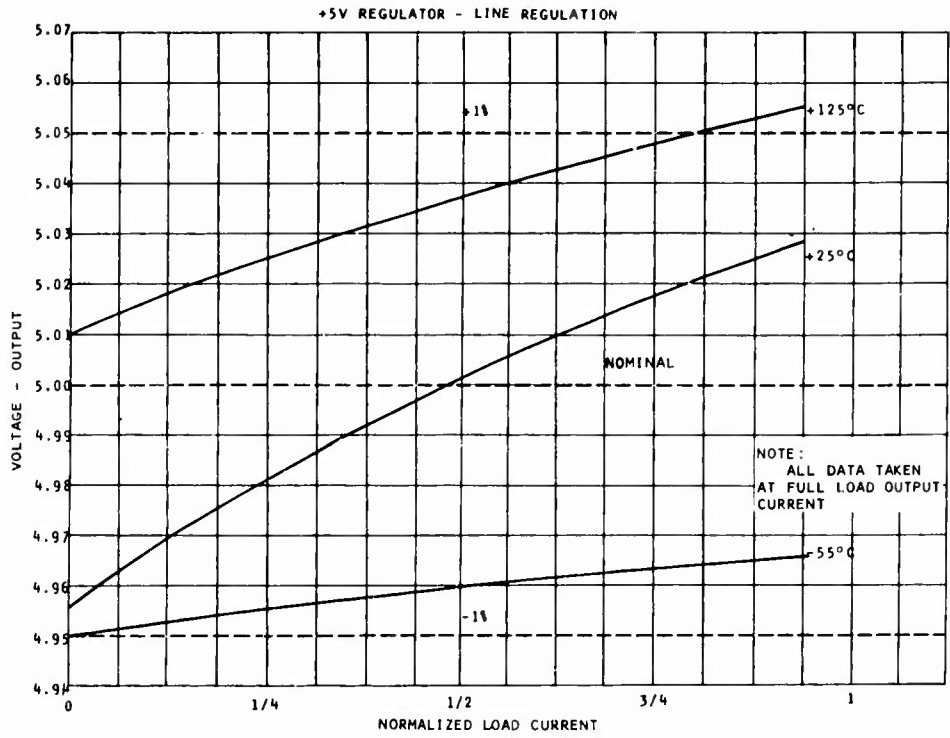**Figure 132. +12V Regulator - Load Regulation.**

238

Figure 133. +5V Regulator - Line Regulation.
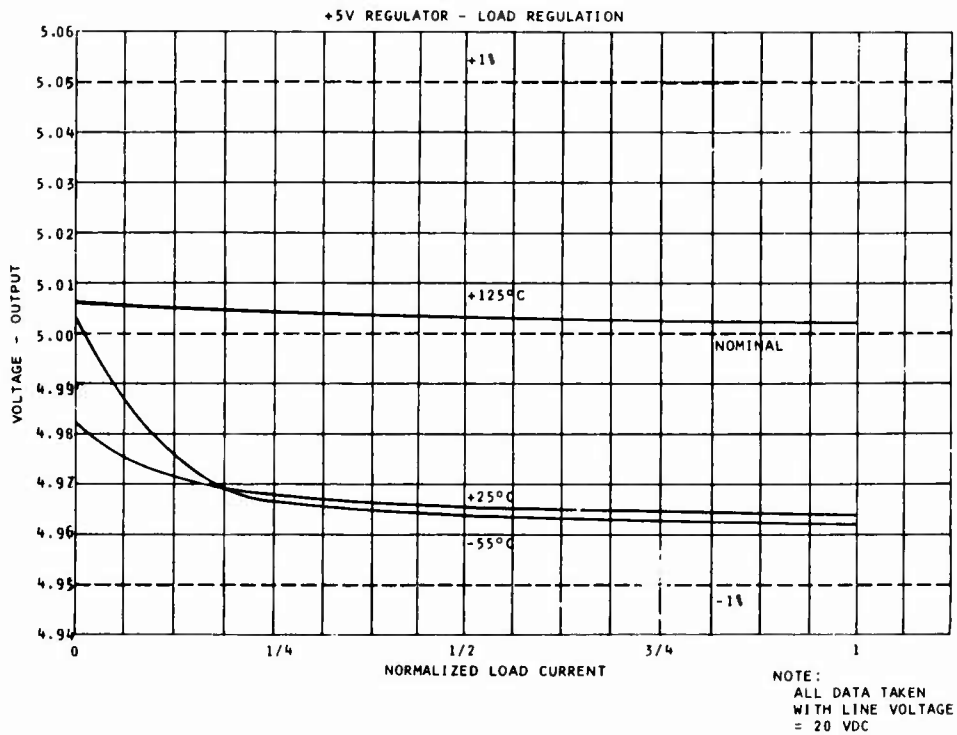

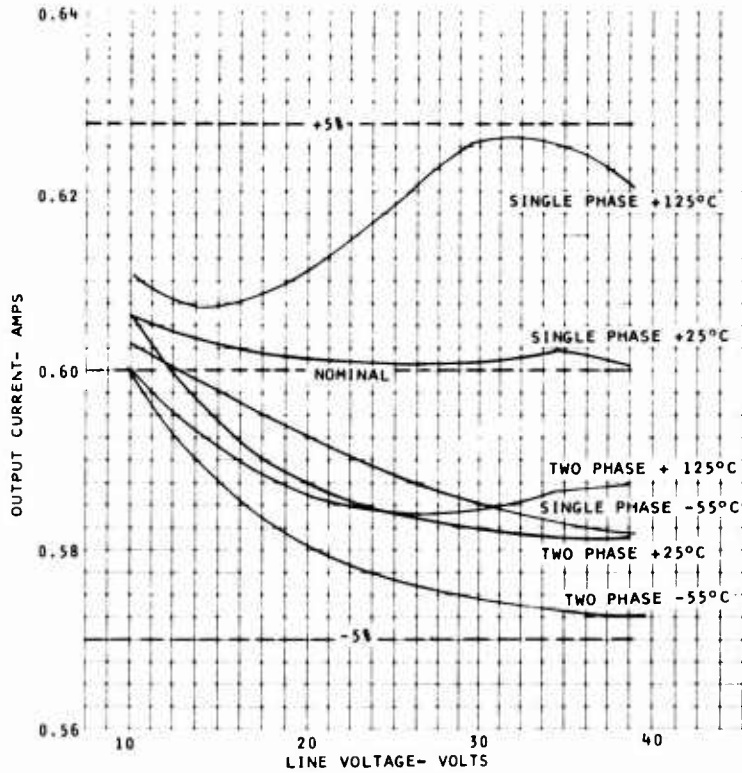Figure 134. +5V Regulator - Load Regulation.

239

Figure 135.   Current Regulation - Line and Load
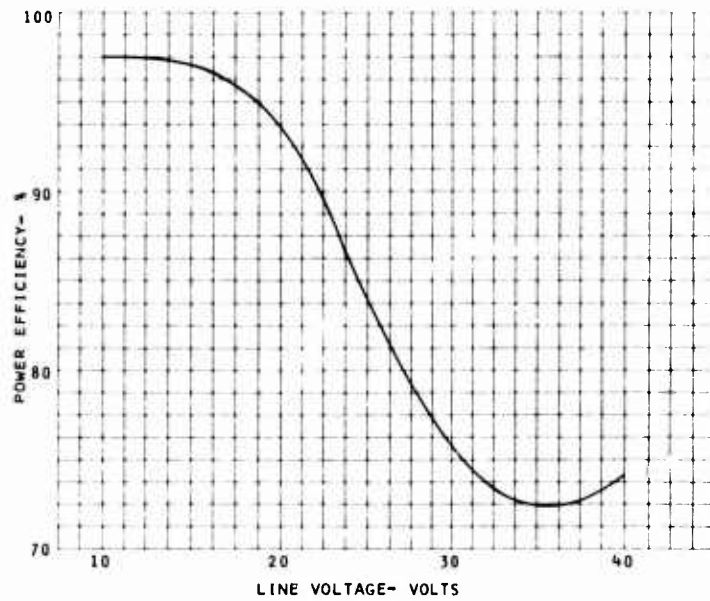Regulation Curves.

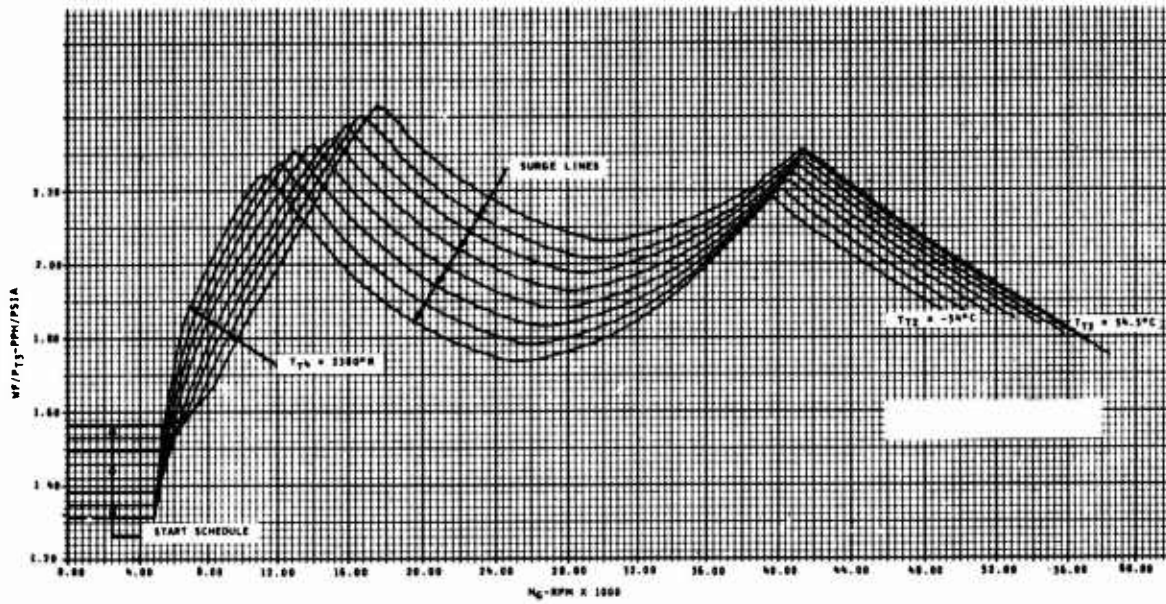Figure 136.   Current Regulator - Efficiency.

240

Figure 137.   3-D Acceleration Schedule - Theoretical Curves.
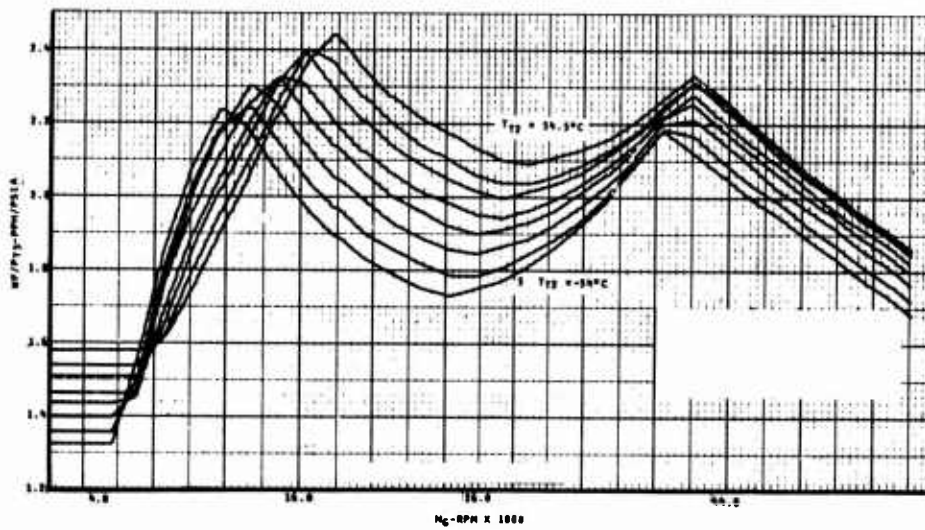

Figure 138.   3-D Acceleration Schedule - Circuit
Generated Curves.

241

cams. Package design innovations are primarily those new aspects of this design which allow the package to survive in an engine environment.

Electronic Cams

An all electronic digital device capable of generating two-dimensional and three-dimensional schedules has been fabricated and tested. These units are the electronic counterpart of two-and three-dimensional cams of the hydro-mechanical control. The functions generated by the electronic cams are readily altered to accommodate new scheduling requirements, yet they are cost compatible with other common devices which cannot be changed.

These function generators use programmable read-only memories (ROM) to "remember" the contour of the cam surface. A sharp reduction in cost of ROMs has been experienced since the fall of 1969 when this development work was initiated. Previously, it was felt that ROMs were incompatible with the cost objectives.

It is presently possible to provide an accuracy of better than 1% over the entire range of fuel control functions utilizing a single 2048 bit ROM. Devices with larger capacities, presently being developed, will allow accuracies considerably better than this, although it is not considered to be necessary for this application.

Improved Pressure Sensing Accuracy

Pressure sensing accuracy of better than 2 psi out of 250 has been demonstrated using a capacitive pressure transducer. Test data supporting this accuracy was taken while both the transducer and the interfacing electronics were varied in temperature from −55°C to +110°C.

Pressure sensing systems available in 1969, which would have been utilized for this type of application, could achieve no better accuracy than ± 3 psi over this range.

Improved Maintainability

Potential control system maintainability has been improved in two ways. First, the ease with which problems are diagnosed may be improved through the use of electronic diagnostic equipment. Second, the need for periodic computer adjustment and calibration is virtually eliminated.

As part of its function of controlling an engine, the electronic computer must measure continually several engine operating variables. Since each of these signals must be converted to an electrical format, they are readily available for use by engine/control diagnostic equipment. Results of intermediate computations within the control computer are also available for use by a diagnostic unit.

Cockpit engine instruments may also avail themselves of these signals. This would eliminate the need for a second set of transducers.

The need for periodic adjustments to the electronic computer is drastically reduced by the nature of the signal handling. Electronic computation networks are not subject to loss of accuracy or misadjustment due to wear or contamination. The pulse and digital information is not subject to deterioration with changing component values or variations in environmental conditions. This makes possible a form of "designed" calibration.

Semiautomatic Start Sequencing

Logic required to provide semiautomatic start has been built into the fuel control computer.

By incorporating these logic networks within the computer, we have realized both a reliability improvement and a cost saving. By locating this hardware on the engine adjacent to its power source, the probability of cable and connector failure is minimized. Since it shares a case, cooling mechanism, and power supply with the computer, the cost and weight are minimized.

Temperature Sensor

A radiation pyrometer temperature unit was developed to operate within the computer package.

At the beginning of this program, the only hardware available was laboratory equipment. This was incapable of meeting size, weight, or dynamic requirements and was not suited for survival in an engine environment.

The sensor developed as part of this program meets all of these requirements. The silicon photocell is housed along with the first-stage electronic amplification circuitry in the cooled electronic computer package. Both the sensor and its ancillary electronics have been tested satisfactorily throughout an ambient temperature range of from -55°C to +125°C. Response time has been found to be better than 30 microseconds.

Package Improvements

The most critical of the needs for fuel control computer development is in the area of the electronic package. The need for the fuel control computer to be engine mounted is apparent. However, the vast majority of electronic package development work in the past has been oriented toward airframe installation of equipment. A substantial effort in this program has been devoted to evaluating solutions to the problems of survival in the engine environment.

The capability to cool engine mounted electronics has been demonstrated.

Electronic components are usually limited to applications where they can operate at a temperature of lower than 250°F while dissipating power. The problem is further aggravated by the package size requirements which continually press for higher component densities. In this case, the control is mounted on an engine housing which reaches operating temperatures as high as 350°F. No cooling air is available.

A computer developed here utilizes the incoming fuel as a coolant. The fuel is passed through a heat exchanger in the base of the electronics package before it reaches the high pressure fuel pump. Heat is led from the individual components to this heat exchanger through a dielectric fluid in which all of the electronic components are immersed. This permits a uniform maximum temperature to be maintained inside the package with point to point variations of not more than a few degrees Fahrenheit.

This package has been subjected to extensive testing both at $-65°F$ and at $+250°F$. The test results have demonstrated that continuous operation of the electronic computer is possible at ambient temperatures as high as $+250°F$ and incoming fuel temperatures of $135°F$.

Although specific problems have been encountered during vibration, it has been shown that electronics can be packaged to survive engine vibration. The vibration problems which have been identified do not require major changes in packaging philosophy.

Recent experience has shown vibration levels on engines presently being developed to be as high as 20 g's at frequencies up to 2,000 Hz. This exceeds the requirements of current military specifications which dictate the tolerance level to be 20 g's at frequencies up to 500 Hz.

Vibration testing conducted on the computer package has shown the new higher requirements to be within the range of tolerance of electronic packages.

System Improvements

The extensive use of electronic computation has established the potential for cost and size improvements in post 1975 production. Advances in components occurring during the past two-year period alone have allowed for a marked improvement in flexibility through the development of electrically alterable cams. As more and more engine control functions can be integrated within the computer package, further cost reductions may be realized, since a common power supply and package can be shared by all electronic functions.

Summary and Recommendations

The computer development effort demonstrated that engine mounted electronic packages are practical for production in the mid-seventies. No problem was encountered which could be considered to be an insurmountable barrier to the detail development of such a unit. The demonstration unit computer has successfully endured operational tests at ambient temperatures of 250°F at the maximum specified fuel inlet temperature of 135°F.

Vibration failures were experienced. However, the causes are evident, and several possible solutions are available. Component cooling is a risk area, since undesirable measures must be taken in order to assure proper operation at the high temperatures specified. Sensitivity of interface circuitry to variations in temperature and supply voltage have been minimized, but at the expense of costlier components and component matching.

By using a dielectric fluid filled case, a workable method of removing component heat was demonstrated but at a penalty in weight and vulnerability. The fluid itself would weigh about 1.0 pound in the production package and a loss of fluid resulting from combat damage or a leak could result in a malfunction.

Vibration susceptibility is another problem area. A design must be demonstrated which will withstand excessive vibration levels, and not add unduly to the package weight and cost.

Failure modes, fault isolation and maintainability must be considered further before a production unit is developed. Presently impeding progress in this area is the lack of a good assessment criterion for evaluating alternate design concepts. In this area of design, costs can rise exorbitantly, and therefore a close liaison between the developer and the user is required to reach a workable solution.

It is recommended that future development work on the electronic computer be concentrated on upgrading the circuits and packaging designs to improve reliability and reduce complexity and cost, and eliminate the vibration problems. The use of new very low power dissipating electronic components should be investigated to reduce the power and voltage regulation requirements. This may make it possible to eliminate the need for the dielectric fluid.

ALTERNATOR POWER SUPPLY

The electronic fuel control computer as well as the engine ignition systems must have a reliable source of power. The power supply for each should be free of voltage transients, and effects of excessive electro magnetic interference (EMI). Traditional obstacles are met whenever we attempt to obtain this power from an engine source or from the airframe. Should airframe power be used, any loss in this source due to combat damage, cable failure, or overload by another system, could result in the loss of the engine control and ignition functions. Airframe power is subject to transients in excess of $2\frac{1}{2}$ times the rated supply voltage. This, together with stringent EMI requirements, would impose severe design criteria for the fuel control.

The major problem with the engine driven alternator is its 10:1 operating speed range. The alternator must be sized to provide adequate power for both ignition and the fuel control computer when the engine is cranking at 10% speed. At 100% speed, the power requirements are about the same, yet most alternators will supply ten times the nominal output voltage or 100 times the rated power.

Preliminary investigations were made to answer such questions as:

1. Is it better to use airframe electrical power for the fuel control or should the engine generate its own?

2. Should the alternator be mounted on the engine drive shaft, on the engine's accessory gear box, or within the fuel control itself?

3. Would an alternator with the capability of preregulating its output be advantageous?

These questions were evaluated and this resulted in the selection of a fuel control mounted, preregulated alternator as the optimum power source.

As a consequence of this investigation, a "breadboard" alternator was developed in accordance with the electrical requirements of the electronic computer and with regard to the mechani-

247

cal constraints of an alternator mounted in the fuel controller and running at pump speed. The major goal in the development of this alternator was to demonstrate an efficient alternator preregulation concept when operated over representative and load ranges.

The specification for the alternator is summarized as follows:

1. Operating Speed

   Controlled electrical parameters are required over the speed range of 3,410 rpm (10% speed) to 40,910 rpm (120% speed).

2. Power Requirements, Winding #1 (Fuel Control Power)

   Speed 10% to 35% (3,410 rpm to 11,935 rpm)
   Rectified output voltage to be held within 15 V.dc to 30 V. dc with a permissible load variation of 5.2 A. dc to 2.6 A. dc.

   Speed 35% to 120% (11,935 rpm to 40,920 rpm)
   Rectified output voltage to be held within 15 V. dc to 30 V. dc with a permissible load variation of 8.0 A. dc to 5.2 A dc.

3. Power Requirements, Windings #2 and 3 (Power for two ignition exciters)

   A minimum output of 2.5 watts into a 40 ohm resistive load from 5% to 120% speed (1,705 rpm to 40,920 rpm).

4. Regulation

   The design to be such as to require a maximum of 0.5 A. dc control winding current.

5. Size

   For interfacing with the pump the stator and rotor sections are not to exceed a combination size of 3.25 inches diameter and 3.00 inches long.

248

Alternator System Design

1.   Alternator

The alternator as described in Figure 139 is a three-phase synchronous machine with a rotating permanent magnet field. The rotor is a four-pole component manufactured from Alnico 6 permanent magnet material. The stator assembly comprises a three-phase output winding and a single-phase control winding. Regulation is achieved by the pulsing of direct current through the control winding in one direction to increase the alternator output and in the reverse direction to reduce the output. Although not included in this unit, provision has been made in the design for two ignition exciter power windings.

2.   Alternator Regulator

Figure 139 includes a functional block diagram of the regulator. The rectified dc output voltage from the alternator is compared to a voltage proportional to the desired alternator output. The resultant error is passed through lead/lag compensation and a deadband section. This activates a switching current regulator to either "boost" or "buck" the alternator output, depending on whether the alternator output is lower or higher than required.

Open-loop testing of the alternator defined the required input current into the control winding to effect the desired regulation. This characteristic, which has been designed into the regulator, is illustrated in Figure 140.

Design Features and Alternatives

In selecting the fuel control mounted regulated alternator as the optimum power source, the following points were considered:
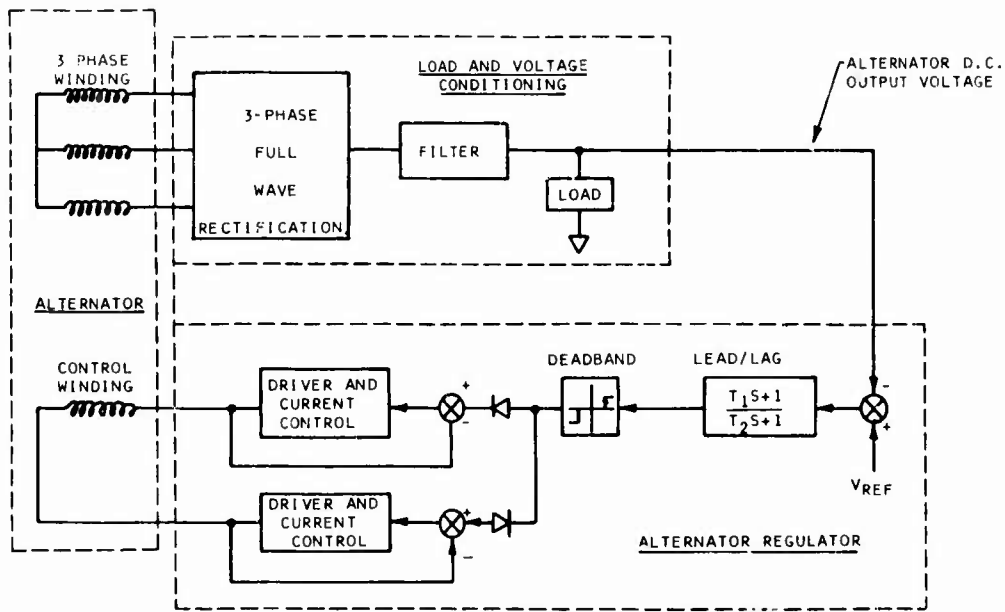
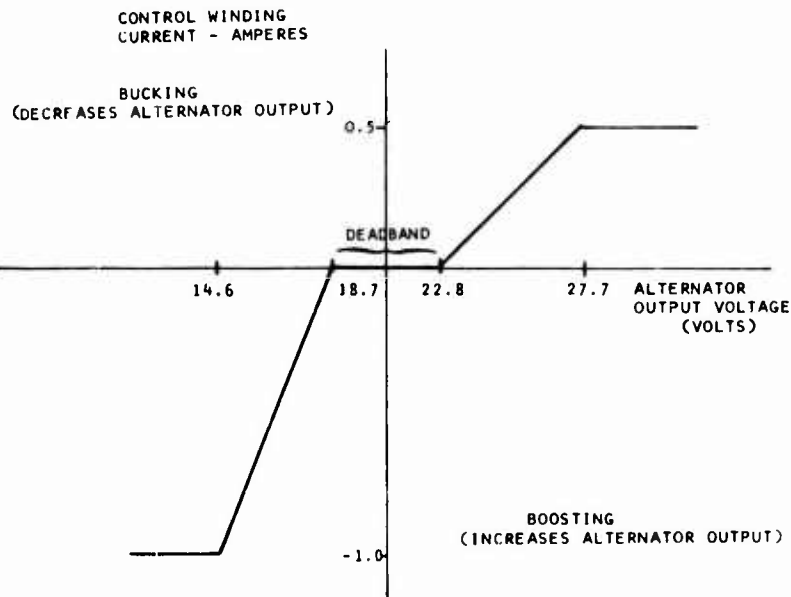Figure 139.   Alternator and Regulator Functional
Block Diagram.

Figure 140.   Alternator Control Winding -
Current Characteristics.

250

1. Problems in using the aircraft +28V dc supply.

   a. The ±600V transient possible on the line warrants careful design of the interface to the voltage regulators within the control.

   b. The +80V surge possible on the line with its inherent low source impedance requires the incorporation of expensive components in the interface to the voltage regulators.

   c. The direct connection of the fuel control to the airframe supply demands the implementation of stringent EMI requirements.

   d. An inverter is required to provide the negative supply required by analog circuitry.

   e. It is possible that a number of potential applications where a +28V dc supply is not available.

   f. There are possible periods when the dc supply can fall to zero. Although operation isn't required for these periods, the disadvantage is obvious.

   g. The variation in line voltage and surge levels demands that the voltage regulators accept an 8:1 variation in line voltage.

2. Problems in Using the Aircraft 110V, 400 Hz Supply

   a. The comments mentioned in 1.c and 1.f above are also applicable here.

   b. The input voltage level demands the use of a 400 Hz step down transformer. For the current levels required by the control this would be prohibitively large (in excess of 15 cubic inches).

3. Advantage in Using a Voltage Controlled Alternator

   a. The engine would form a self contained unit, integral with its own power source and accessories.

   b. Isolation of the ignition exciters and fuel control from the airframe supply will reduce the EMI effects between the engine and remainder of the aircraft electrical/electronic equipment.

   c. By controlling the alternator output voltage, the circuiting necessary to interface with the computer voltage regulators is minimal, allowing the use of low cost components and keeping power dissipation low.

4. Alternator Installation Considerations

   a. Alternator Integral With Fuel Control vs Engine Shaft Mounted Alternator

     Many free turbine engines have the power turbine shaft passing through the center of the gas generator shaft and out of the front of the engine. To mount the alternator on the gas generator shaft with this engine design would result in the alternator rotor diameter being determined by the gas generator shaft and not by the electrical requirements. Hence, the alternator rotor would be excessively large with high centrifugal stresses.

     If the alternator is mounted on the engine shaft the harness is longer, since it has to be routed out of the engine to the fuel control and engine igniters.

   b. Alternator Integral With the Fuel Control vs Engine Accessory Mounting

     The accessory gearbox on the engine typically provides mounting for the engine starter, fuel control, oil pump, and alternator drives. Each component is gear driven or shares a drive, has oil

lubricated ball or roller bearings, and is sealed from ambient. The design for integrating the alternator with the fuel control is shown on Figure 141.

The alternator is driven at the same speed as the fuel pumps and shares the same carbon bearings, which are wash flowed with clean fuel. The size required of the pumps and alternator decreases as the drive speed increases. The estimated weight saving for the design shown in Figure 141 compared to an accessory mounted alternator is 5 lb. This includes an allowance for elimination of a drive gear and shaft, Marman clamp, reduced size bearings, housing and rotor.

c. Alternator Packaging Study

Design studies have been performed to consider the mechanical aspects of the alternator and its integration into the control package. The first consideration was whether to run the rotor in fuel or dry. Running in fuel has the advantage of eliminating the need for seals. The problem with running the rotor in fuel is that fluid churning adds heat to the fuel and also wastes power. The estimated power loss for running the rotor in fuel is 2.4 hp (at 37,500 rpm). This was considered to be excessive, in comparison to the dry requirements (0.25 hp). It was decided, therefore, to run the rotor dry.

Many alternatives for mounting the alternator were considered and included series or parallel mounting with the pump drive shaft separetely mounted on the engine or in the space between the engine and the control mount. The design selected mounts the alternator integral with the fluid controller on the pump drive shaft. This design requires the minimum number of bearings for the total system.

The bearings are carbon for high-speed rotation, wash flow lubricated with clean fuel from a barrier filter. The components on the pump drive
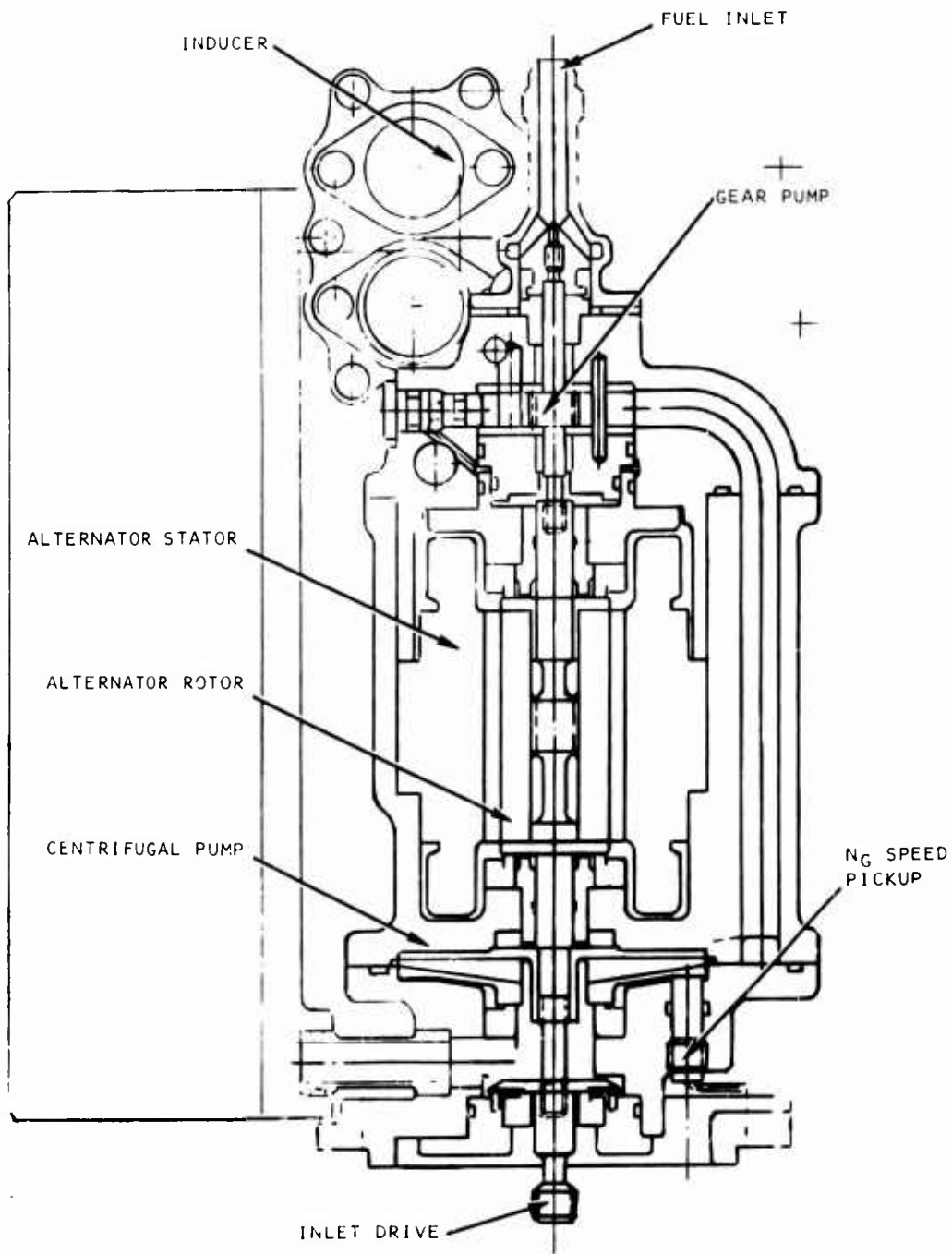
253

Figure 141. Integrated Alternator and Pump Package.

254

shaft are arranged to be in decreasing power
requirement from the control input drive spline.
They are also arranged in order of importance to
continued operation of the engine for any single
failure along the shaft drive line. The centri-
fugal pump, being of prime importance, is first,
followed by the alternator, and then the gear pump,
which is required only during engine starting,
and last is the inducer.

The alternator design integrated into the control
package is shown in Figure 142. It is evident
from these photographs that the incorporation of
the alternator into the control package has very
little effect on the overall dimensions of the
control.

5. Alternator Design Concepts

a. Alternator

In arriving at the decision to utilize a rotating
permanent magnet alternator, the points summarized
in Table XXIX were considered.

TABLE XXIX. COMPARISON OF ALTERNATOR CONCEPTS		
	Advantages	Disadvantages
Wound Rotor	Easy to regulate efficiently.	Requires brushes.
Flux Switch	Magnets do not ro-tate; thereby, stress is reduced on the components.	Large leakage losses and difficult to efficiently regu-late.
Permanent Magnet Rotor	Efficient to regu-late. Most eco-nominal concept for the power and speed considered.	Design consideration required for the stresses on the per-manent magnets.

255
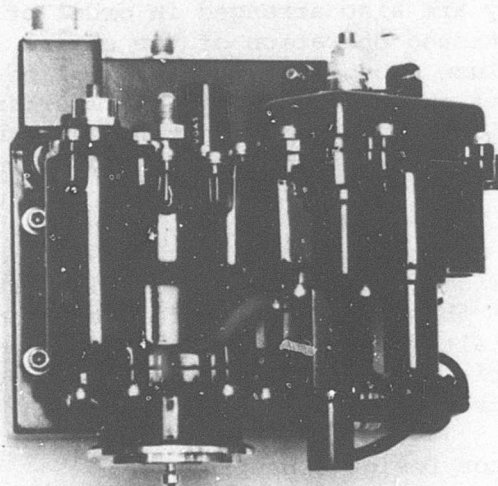
CONTROL SYSTEM MOCK-UP WITHOUT ALTERNATOR
LOOKING RADIALLY OUTWARD FROM ENGINE
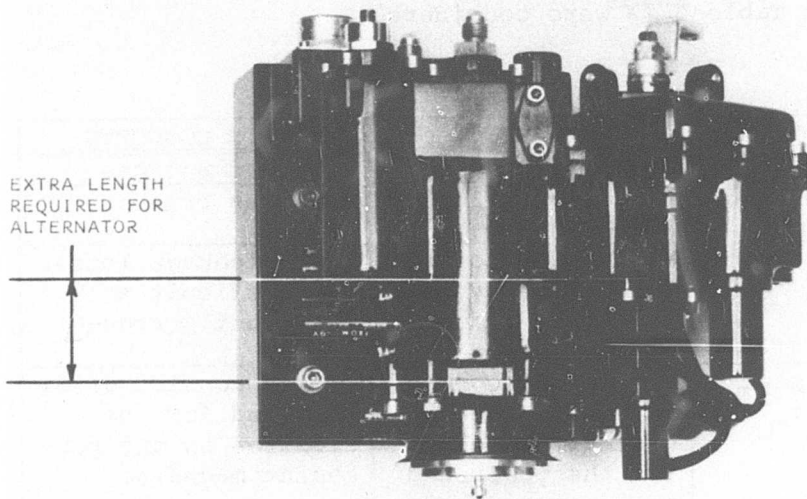
EXTRA LENGTH
REQUIRED FOR
ALTERNATOR

Figure 142. Mock-Up With and Without Alternator.

256

b. Alternator Regulator

A proportional continuous current field control and
a proportional switching philosophy were considered
for this function. Although the number of compo-
nents required by a continuous regulator is gener-
ally low in comparison to its switching counter-
part, the variation in ambient temperature and
alternator loading would cause a continuous regu-
lator to dissipate a prohibitively high amount of
power. In consequence, a switching regulator was
selected. In this mode the field coil lag provides
filtering of the switched input current.

Test Data

After separate open-loop tests on the alternator and regulator,
the two were connected together and closed-loop testing was
performed.

Figure 139 illustrates the block diagram of the test circuitry
and Figures 143 and 144 illustrate the test setup.

The alternator/regulator configuration was tested over rated
speed and load variations at room temperature. The test results
are illustrated in Figures 145 and 146.

From an examination of Figure 145 it can be seen that above
11,500 rpm the alternator performs as required although the
load regulation is poor in relation to the regulation as a func-
tion of speed. Below 11,500 rpm there is a rapid drop-off in
the output to a degree that load currents in excess of 2.6 A.dc
would cause the output voltage to fall below 15 V.dc for
speeds below 11,500 rpm.

Figure 146 illustrates the control winding current necessary
to achieve the characteristics shown in Figure 140 . As can be
seen, the control current is in excess of the 0.5 A.dc maxi.
mum at low speeds, and at high speeds the control winding
appears to saturate; i.e., the control current does not fall
away with increase of speed.

A summary of the above problem areas and the required correc-
tive action is presented in Table XXX.

257

ALTERNATOR

HYDRAULIC
DRIVE MOTOR
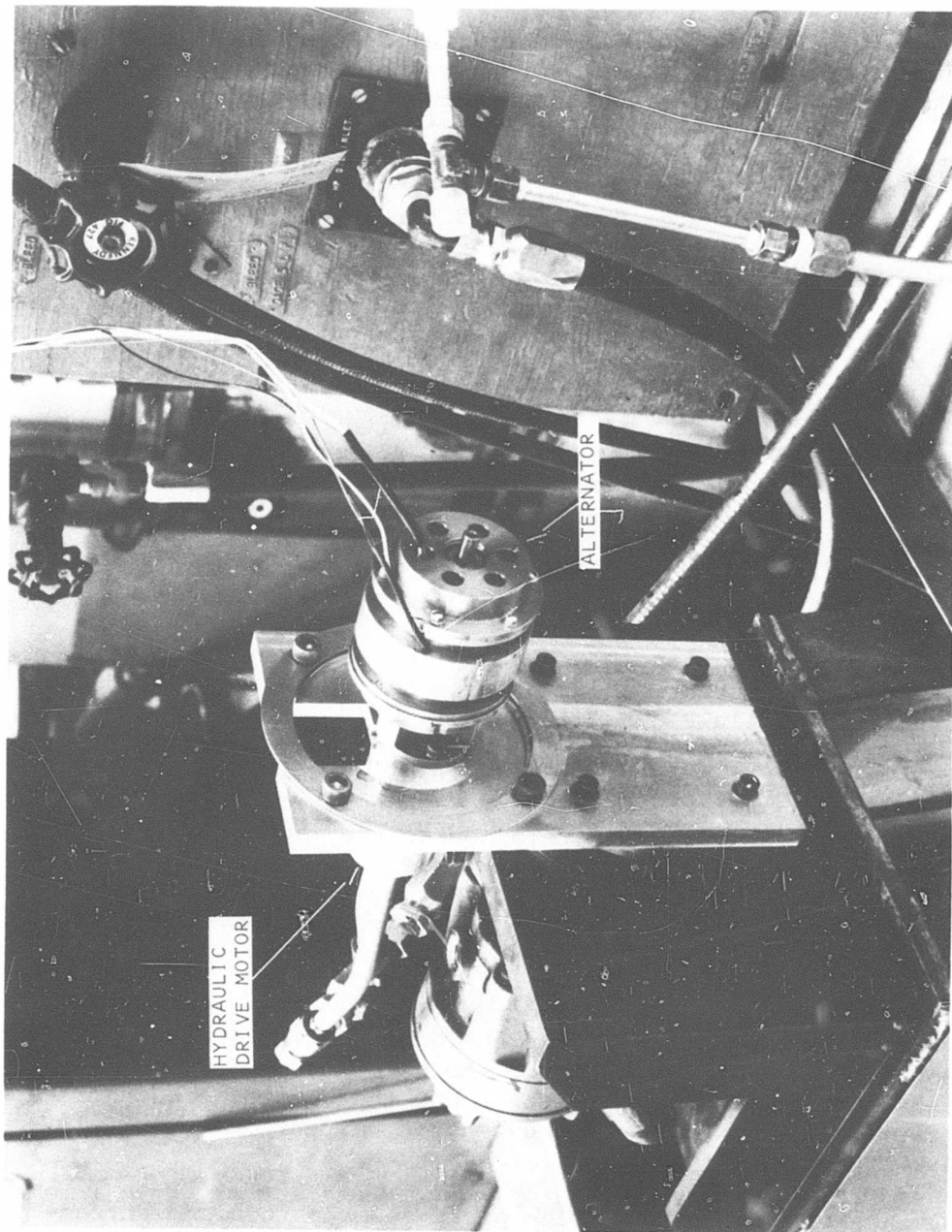
Figure 143. Alternator Test Fixture.

258

ALTERNATOR TEST
EQUIPMENT AND
REGULATOR

HYDRAULIC
TEST STAND

ALTERNATOR AND
HYDRAULIC
DRIVE MOTOR
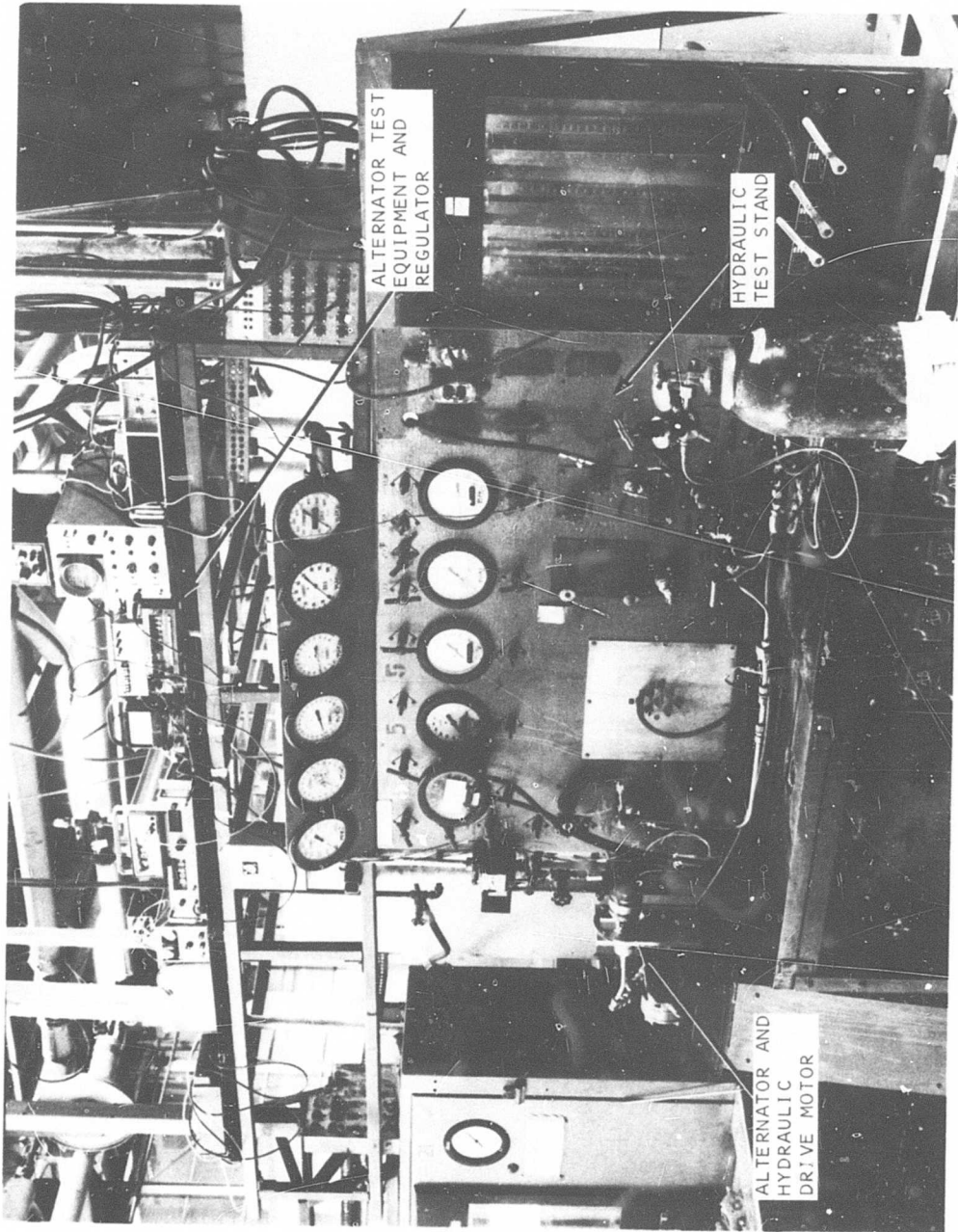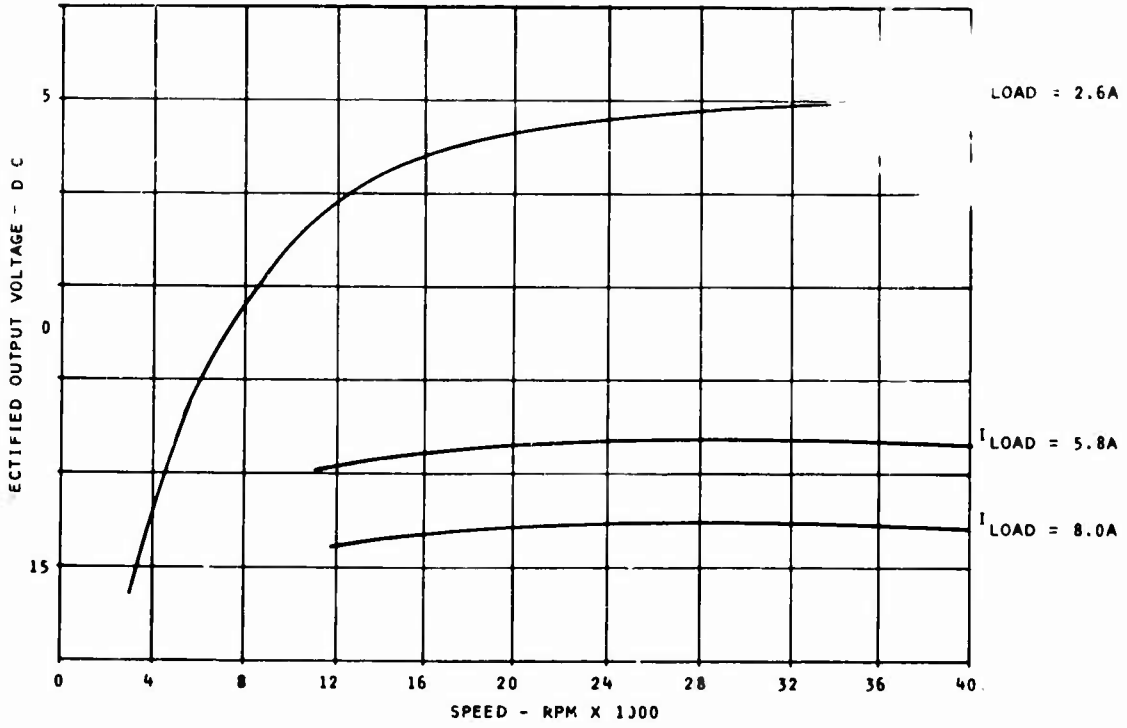
Figure 144. Alternator Test Fixture.

259

Figure 145. Alternator Regulating Characteristics.

260
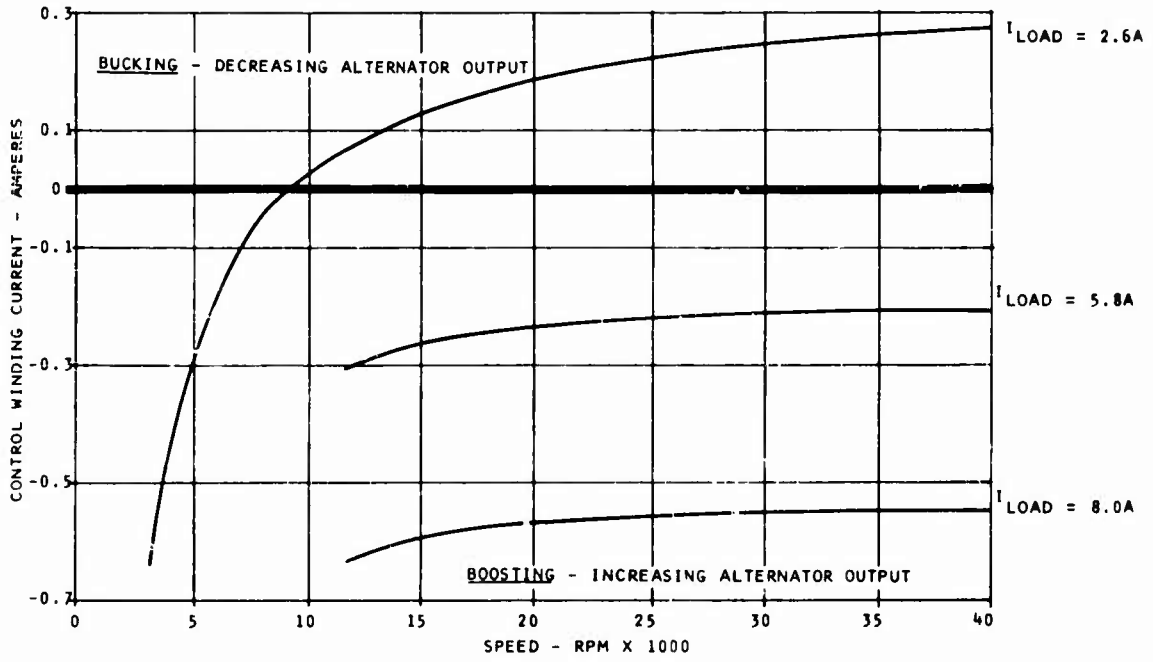
Figure 146. Alternator Regulating Characteristics.

261

TABLE XXX.	DISCUSSION OF ALTERNATOR PROBLEM AREAS	
Problem	Cause	Corrective Action
Fall-away in output below the 15V dc minimum requirements at speeds less than 11,500 rpm.	Excessive leakage flux from the control winding, resulting in the required control current to be prohibitively high at low speeds.	Relocate the control winding to the inner stator dia. This would virtually eliminate leakage flux and reduce the ohmic resistance per turn of the control winding, thereby reducing the power requirements of this winding.
Although well within requirements, the load regulation is not as good as the speed regulation.	The present design is based on the regulator responding to the alternator peak voltage. Therefore, load changes cause changes in the ripple factor and hence variations in the dc level.	Improve the filtering of the input voltage to the regulator such that it responds to the average voltage instead of the peak.
Relatively high level of control current required at high speeds while providing heavy load; i.e., 0.6 amp required 0.1 amp designed	Excessive armature reaction and inductive reactance losses.	Redesign the stator rotor to increase the reluctance to minor flux paths. Modify the stator winding turns/wire diameter in order that the alternator can be optimized to the load requirements.

Evaluation of Rare Earth Magnet Materials

Within the past five years a number of magnetic alloys have been developed that offer peak energy products many times greater than the conventional Alnico magnetic material. These newly developed alloys, termed "Rare Earth Magnet Materials", have the potential of drastically increasing the power to weight ratio of permanent magnet alternators of the type developed in this program. Therefore, as a part of this program, the properties of these alloys were evaluated to ascertain their applicability.

The results of this research effort indicate that samarium cobalt is the most promising material. However, its high energy product (5 to 8 times that of Alnico) is offset by the following disadvantages:

a. The tensile strength of samarium cobalt is only 75% of that of Alnico. With our present design philosophy, the magnets would not be able to withstand the centrifugal forces at our high operating speeds (50,000 rpm) without the inclusion of expensive magnet retention hardware.

b. The cost of samarium cobalt is at present four times greater than the conventional Alnico materials, which is already a significant percent of the cost of the alternator.

c. The new materials are extremely hard to demagnetize, making machining extremely difficult and expensive.

Goals Achieved in the Program

1. Demonstrated an efficient preregulated permanent magnet alternator.

2. Evaluated advanced magnet materials applicable to alternator designs.

3. Demonstrated a unique bidirectional switching current regulator that uses the control winding characteristics as a filter.

Summary and Recommendations

This program has demonstrated an efficient permanent magnet pre-regulated alternator suitable for providing power to gas turbine engine fuel controls.

The performance is within requirements except for low output at low speed, and saturation at high speed. However, these problems can be eliminated by the relocation of the control winding to the inner stator diameter, thereby reducing leakage flux, and the redesigning of the stator core slots and the main output winding. These changes will eliminate minor flux paths and provide a better impedance match to the load.

Apart from the aforementioned modifications, further work in other areas could yield useful results. The present implementation uses bidirectional control winding current for regulation. However, a scheme using unidirectional control current would effect a 75% reduction in the regulation circuitry.

The new magnet materials evaluated have not sufficient tensile strength to allow for an economical design based on the present regulated alternator concepts. However, the development of a different philosophy that allows for the economical use of permanent magnets in a regulating alternator, whereby the stresses are low, would be an obvious advantage.

CONCLUSIONS AND RECOMMENDATIONS

The development effort during this program has put together
the technology for an advanced electronic fuel control for
small gas turbine engines. This control system makes possible
significant improvements in the overall engine/control system
through electronic accuracy and flexibility, integration of
accessories, improved diagnostics capabilities, and the devel-
opment of a high-speed pump, electromechanical geometry act-
uator for precise geometry position control, and radiation
pyrometer turbine blade temperature sensor for temperature
limiting.

Closed-loop demonstration testing was successfully completed.
The same breadboard hardware was used to control an analog
computer simulator of both a 2- and 5-lb/sec airflow free tur-
bine engine and helicopter rotor system.

The weight and size goals for a production configuration control
system package were demonstrated. A flight package version of
the complete control system was designed and three mock-ups were
fabricated. One mock-up of the main control, which comprises
the fuel cooled electronic computer and fluid controller, one
of the remotely mounted electrohydromechanical IGV actuator,
and a second mock-up of the main control which includes a
built-in regulated alternator to provide weight savings and
improved performance through accessories integration. The
control system provides more functions and is less than half
the size of the Chandler Evans TA-2 fuel control presently in
use on the Lycoming T-53 free turbine helicopter engine.

The system design and performance compliance was proven through
a comprehensive test program. The control system successfully
completed three simulated hot fuel-hot cay missions of 3 hours
each, 30 hours cyclic operation at room temperature, 50 hour
cycling at 250°F ambient, 20 hours of cycling at -65°F fuel
and ambient, and 18 hours running on contaminated fuel.

A feasible concept for sensing turbine blade temperature using
a radiation detector located in the cooled electronic package
and compressor air to purge the aperture and cool the glass
optical circuit was built and tested. The sensor was designed
for viewing the tips of axial turbine blades on an engine which
has a folded back annular combustor can. The sensor is fast
enough to detect a single "hot blade" exceeding the maximum

265

allowable temperature. A small amount of development effort is required to eliminate the gas seal problem in the glass conduit. It should then be possible to build a unit for demonstration on an engine.

Control mode studies showed that it was not practical to use the blade temperature signal for controlling engine starting or acceleration. Starting and acceleration schedules for closed-loop temperature control still require a 3-D cam, and in addition a much more complicated control is needed than for the conventional W_f/P_{t3} start and acceleration control. The only advantage closed-loop temperature control has is that its operation is independent of fuel heating value.

A comprehensive test evaluation of available pressure transducers was conducted. A variable capacitance type was selected. It offers a viable concept for satisfying engine mounted accuracy requirements through continued development.

Several possible methods of actuating compressor geometry were studied. The selected electrohydromechanical system was shown to be best for meeting load and accuracy requirements. Pneumatic (P_{t3}) actuators have problems handling the load and engine manufacturers generally oppose using P_{t3} air because of dirt and temperature problems. Also, bleeding the compressor hurts engine performance.

At 37,500 rpm combination lifting tip seal gear pump for starting and centrifugal pump for steady-state running was successfully developed. The manufacturability of these very small high-speed components was also demonstrated. However, the efficiency of the centrifugal pump must be improved to eliminate excessive fuel temperature rise, particularly for application on the 2-lb/sec engine. The major problem is disc friction losses which can be substantially reduced by decreasing the disc diameter and running the pump at 50,000 rpm. This higher shaft speed will also reduce the size of the alternator. The integrated alternator and pump mechanical design, bearing, and seals should be demonstrated at this higher speed.

Comprehensive vibration and environmental temperature testing on prototype fuel cooled electronic computer demonstrator packages proved that engine mounted electronic controls can be developed for the 1970's. Through the gamut of tests that were conducted, specific areas of technical risk were identified

266

which would prevent using this control technology without further development. The vibration and temperature integrity of the electronics package and its level of sensitivity to noise and supply voltage variations require improvements. This can be done with the use of newly developed lower power dissipating electronic components which offer low sensitivity to noise and voltage variations and significant reduction in heat generation. This will also make redesigning for mechanical stability and heat transfer that much easier, particularly because it may be possible to eliminate the dielectric fluid.

LITERATURE CITED

1. Daily, J. W., and Nece, R. E., FLOW PHENOMENA OF PARTIALLY ENCLOSED ROTATING DISKS, Transactions of the ASME, Vol. 82, February 1960.

2. Eckert and Drake, HEAT AND MASS TRANSFER, 2nd Ed., New York, McGraw-Hill, 1959.

3. Kays, W. M., CONVECTION HEAT AND MASS TRANSFER, New York, McGraw-Hill, 1966.

4. Chupp and Helms, EVALUATION OF INTERNAL HEAT TRANSFER COEFFICIENTS FOR IMPINGEMENT COOLED TURBINE AIRFOIL, AIAA 4th Propulsion Joint Specialist Conference, No. 68-654, June 1968.

5. Metzger, S., IMPINGEMENT COOLING OF CONCAVE SURFACES WITH LINES OF CIRCULAR AIR JETS, Transactions of the ASME, July 1969.

6. Widlar, R. J., AN IMPROVED POSITIVE REGULATOR, I. C. Application Bulletin, No. AN-23.

7. Soule, Thomas L., Anschultz, Donald E., Perkins, Melvin L., STUDY OF AN ADVANCED CONTROL SYSTEM FOR SMALL FREE-TURBINE ENGINES, USAAVLABS Technical Report 69-41, U.S. Army Aviation Materiel Laboratories, Fort Eustis, Virginia, June 1969, AD 860 679.

8. Karol, Joseph, and Hatch, Robert, ADVANCED ENGINE CONTROL SYSTEM STUDY, USAAVLABS Technical Report 69-53, U.S. Army Aviation Materiel Laboratories, Fort Eustis, Virginia, August 1969, AD 862 599.

9. Swick, R. M., Skarvan, C. A., INVESTIGATION OF COORDINATED FREE TURBINE ENGINE CONTROL SYSTEMS FOR MULTIENGINE HELI-COPTERS, USAAVLABS Technical Report 67-73, U.S. Army Aviation Materiel Laboratories, Fort Eustis, Virginia, December 1967, AD 666 796.

268

10. Chestnutt, David, and Bartek, L. R., CH-54A SKYCRANE ENGINE LOAD SHARING, USAAVLABS Technical Report 66-47, U.S. Army Aviation Materiel Laboratories, Fort Eustis, Virginia, May 1966, AD 634 503.

11. Richardson, Harry L., Tommasini, Rocco M., ADVANCEMENT OF SMALL GAS TURBINE ENGINE ACCESSORY TECHNOLOGY, USAAVLABS Technical Report 67-13, U.S. Army Aviation Material Laboratories, Fort Eustis, Virginia, April 1967, AD 652 896.

12. ELECTRONIC INTERFERENCE CHARACTERISTICS REQUIREMENTS FOR EQUIPMENT, MIL-STD-461A, 1 May 1970.

13. VIBRATION REQUIREMENTS FOR EQUIPMENT, MIL-E-5272C, 13 April 1959.

14. ENGINES, AIRCRAFT, TURBOJET AND TURBOFAN, TESTS FOR, MIL-E-5009D, 13 November 1967.

15. FLUIDS, CALIBRATION FOR AIRCRAFT FUEL SYSTEM COMPONENTS, MIL-F-7024A, 19 May 1969.

16. ENGINES, AIRCRAFT, TURBOJET, TURBOFAN, GENERAL SPEC. FOR, MIL-E-5007C, 30 December 1965.

17. JET FUEL, GRADES JP4, JP5, MIL-T-5624G-1, 30 October 1970.

18. SPECIFICATIONS AND STANDARDS APPLICABLE TO AIRCRAFT ENGINES AND PROPELLERS, ANA Bulletin 343V, 1 July 1968.

19. AIRBORNE ELECTRONIC & ASSOCIATED EQUIPMENT, APPLICABLE DOCUMENTS, ANA Bulletin 400U, 5 November 1964.

20. ELECTRONIC EQUIPMENT STANDARDS, MIL-STD-454C, 15 October 1970.

21. UTILIZATION OF AIRFRAME POWER, MIL-STD-704A, 9 August 1966.

22. ENVIRONMENTAL TEST METHODS, MIL-E-810, 21 September 1970.

23. ENVIRONMENTAL TESTING AERONAUTICAL EQUIPMENT, MIL-E-5257.

24. TURBO PROP ENGINES QUALITY TEST SPEC., MIL-E-8595, 3 September 1954.

25. SYSTEM DESIGN REQUIREMENTS, PSM-1035A, 18 November 1969.

26. FLUID CONTROLLER SPECIFICATIONS, PSM-1070A, 17 July 1970.

27. QUALIFICATION TEST SPEC. – TA-2T, QTS 1515.5516, 4 March 1966.

APPENDIX
TRANSIENT TURBINE BLADE TEMPERATURE ANALYSIS

This appendix presents a theoretical study of the transient thermal relationship in a gas turbine between gas temperature and the leading edge of an internally cooled turbine blade.

This study includes the following cooling configurations: (a) internal convection cooling, (b) internal impingement cooling, and (c) transpiration cooling. Complete mathematical analyses are presented for cases (a) and (b). A closed form solution is obtained through a simplified physical model. For case (c), the cooling process is analyzed based on the simplified Couette flow model. The time constant obtained for cases (a) and (b) agress in order of magnitude with the results given by General Electric (theoretical) and Solar (empirical).

The surface temperature of the turbine blade will be measured by a radiation pyrometer. This measurement will be used as a controlling parameter in a gas turbine control system. It will be used to ensure that the blade temperature is maintained within structural limits and to determine gas temperature which is controlled during acceleration and deceleration.

The turbine blade is immersed in a flow of hot gas. The physical characteristics of this gas environment are a function of engine speed and flight altitude. Cooling air flow is directed from the compressor to the interior of the blade. The cooling characteristics are a function of the internal geometry of the blade. Three different cooling configurations are covered in this report: internal convection cooling, impingement cooling, and transpiration cooling. A dynamic simulation of flight operation of an impingement cooled blade is also considered. The geometry of this blade is the best estimate of what will be used on future 5-lb/sec engines.

INTERNAL CONVECTION COOLING

A typical blade configuration is shown in Figure 147.. Hot gas impinges on the blade leading edge and the coolant is directed from the compressor through the cooling passages and vented into the main stream.
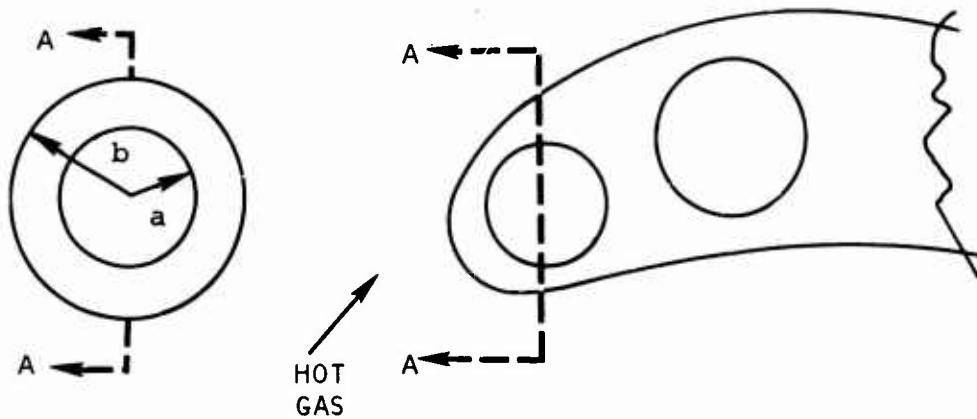
271

Figure 147. Typical Turbine Blade Configuration.

The thermal energy transport phenomena are due to the combined effects of forced convection (gas to blade) and thermal conduction of the blade. The film coefficients for convection heat transfer in general are a function of the Reynolds and Prandtl numbers of the gas. Conduction of heat is governed by the thermal diffusivity $\alpha = k/\rho c$ of the material.

Simplified Model for the Leading Edge of the Blade

If the gas temperature and film coefficient variation is not great in the vicinity of the leading edge, no substantial temperature gradient is expected across the plane A-A. Assume this temperature gradient is zero, then the time dependent diffussion equation can be written as:

$$\frac{\partial T}{\partial t} = \frac{k}{\rho c} \left(\frac{\partial^2 T}{\partial r^2} + \frac{1}{r} \frac{\partial T}{\partial r} \right) \tag{5}$$

with the boundary conditions and initial condition

$$r = b \qquad hg\left(T_{t4} - T_{4B}\right) = k\left.\frac{\partial T}{\partial r}\right]\ r = b \tag{6}$$

$$r = a \qquad h_a\left(T_a - T_c\right) = k\left.\frac{\partial T}{\partial r}\right]\ r = a \tag{7}$$

$$t = o \qquad T = T(\ln r/a,\ \ln r/b) \tag{8}$$

Equations (5) to (8) are "eigen value" problems. For mathematical simplicity, the initial value is assumed to be constant. The assumption will not affect either the final steady-state temperature or the transient characteristics.

The solution of the above equation is

$$T(r,t) = T_1(r) - \sum_{n=1}^{\infty} e^{-\alpha\lambda_n^2 t}\ T_2(r) \tag{9}$$

where $T_1(r)$ = steady-state value

λ_n = Nth eigen value

The validity of (9) can be verified by letting $h\ell/k \rightarrow o$

where ℓ = characteristic of the blade dimension.

Where the energy balance equation is reduced to

$$h_gA_g\ (T_{t4} - T_m) - h_aA_a\ (T_m - T_c) = \rho cV_g\frac{dT_m}{dt} \tag{10}$$

The solution is a simple exponential function of time, and time constant for equation (10) is

$$\rho cV / (h_gA_g + h_aA_a).$$

273

Film Coefficient

The empirical data of film coefficient around a cylinder in a flow of gas normal to its axis can be approximated by

$$(N_u)_g = \sqrt{R_{eg}} \quad \text{(Ref. 2)} \tag{11}$$

The internal film coefficient is

$$(N_u)_c = 0.02 \; P_r^{0.6} \; R_{ec}^{0.8} \quad \text{(Ref. 3)} \tag{12}$$

for flow parallel to the cylindrical axis.

$(N_u)_c$ is calculated for the maximum blade temperature, then $(N_u)_c = 0.02 \; P_r^{0.6} \; R_{ec}^{0.8}$ is used to calculate the required coolant mass flow rate.

INTERNAL IMPINGEMENT COOLING

The aim of internal impingement cooling is to save coolant flow and to provide equivalent cooling effectiveness as considered in the previous section. The general geometric configuration is shown in Figure 148.
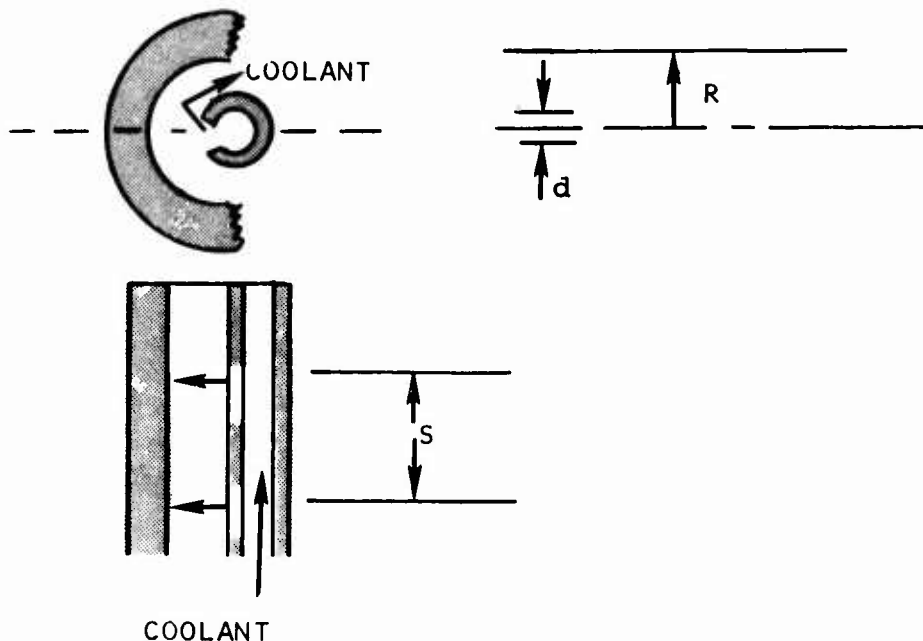

Figure 148. Internal Impingement Blade Cooling Geometry.

The coolant is vented at the trailing edge of the blade to provide film cooling in that region.

Internal Film Coefficient

According to Ref. 4 , the Nusselt number for impingement cooling is (empirical)

$$Nu = 0.44\ Re^{0.7}\ (\frac{d}{s})^{0.8}\ e^{-0.85}\ (\frac{\ell}{s})\ (\frac{d}{D})^{0.4} \tag{13}$$

$$Nu = hd/k, \quad Re = 4w/\pi\mu d.$$

The governing differential equation for transient temperature is the same as equations (5) to (8).

TRANSPIRATION COOLING

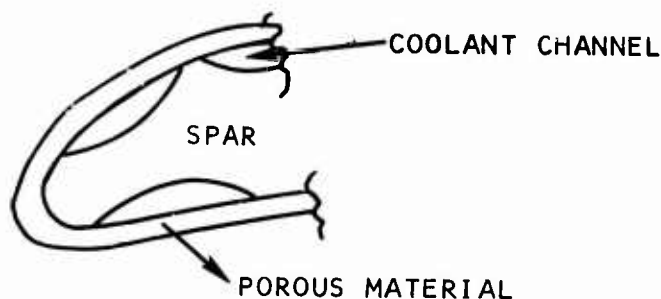The general configuration is shown in Figure 149.

Figure 149.   Transpiration Blade Cooling Geometry.

Coolant diffuses through the porous material and provides a nearly isolated thermal layer for the blade. The effectiveness of cooling can be estimated from the Couette flow model

$$\frac{h_{tr}}{h_o} = \frac{P_r \, R_e}{e^{P_r R_e} - 1} \tag{14}$$

where h_{tr}/h_o is the ratio of film coefficient of transpiration cooling to one without, and

$$R_e = \rho \frac{V_s \delta}{\mu} \tag{15}$$

is defined by the coolant diffusing velocity and the main stream boundary layer momentum thickness. For $P_r \approx 0.7$ and $R_e \approx 5.0$, $h_{tr}/h_o \approx 0.1$. For $R_e \approx 10$, $h_{tr}/h_o \approx 3 \times 10^{-3}$.

The effectiveness of reducing the film coefficient by increasing the coolant diffusion rate appears very attractive for constant blade temperature design. This is desirable for very high turbine inlet temperature operation.

Transpiration Cooling and Blade Surface Temperature Control Mode

If surface temperature of the blade is considered as the parameter for control mode, design of the coolant mass flow rate becomes critical. Over usage of the coolant will not only increase the response time (due to large thermal resistance) but also cause immunity of blade temperature from the variation of hot gas temperature. Numerical solution for transpiration cooling was provided by Curtiss Wright Co. for Chandler Evans. Their final report includes transient study at four different engine speeds operating at ground conditions.

276

SIMULATION FOR FLIGHT OPERATION

Dynamic simulation was carried out using a fixed internal impingement cooling geometry and a fixed acceleration schedule. Engine gas state conditions were derived from specified engine data. The blade to gas time constant and steady-state blade surface temperature were calculated for various combinations of altitude, compressor inlet temperature, and engine speed.

The results plotted in Figures 64 and 65 indicate that:

1. A nearly unique function defines time constant as a function of the compressor discharge pressure (Figure 64).

2. The steady-state blade temperature is between 63% and 67% of the gas temperature at different operating conditions (Figure 65).